ProQuest LLC.
789 East Eisenhower Parkway
P.O. Box 1346
Ann Arbor, MI 48106 – 1346

Active Sites in the Acylation of Anisole with Acetic Anhydride over Zeolite Beta

G. S. PAINE

A thesis submitted in partial fulfilment of the requirements of
The Nottingham Trent University for the degree of Doctor of Philosophy

October 2002

There is a peculiar affinity between the oxides of aluminium and silicon.

-Iler, The Chemistry of Silica, 1976

Abstract

Acylation is a key step in the manufacture of aromatic ketones used as intermediates in the fine chemical and pharmaceutical industry. The conventional method, and at the present time, the most widely applied method of preparation of these ketones is the homogeneous Freidel Crafts acylation of aromatics with carboxylic acid derivatives using Lewis acid anhydrous metal halides as catalysts, most notably $AlCl_3$. However, recently, the first industrial process has been introduced for the acylation of anisole and veratrole using zeolite Beta and zeolite Y respectively. Such a process overcomes the environmental problems associated with using metal halides, the latter are required in more than stoichiometric amounts and lead to a significant amount of inorganic by-product.
The effect of hydrothermal, thermal, chemical modification, ion exchange, and oxidative regeneration on the acidic properties of zeolite Beta is probed using a combination of FTIR, MAS NMR, and XRD studies. The acidic properties of ZSM-5, zeolite Y, mordenite, and mesoporous MCM-41 are also considered briefly. It was found that the catalytic activity of the entire range of zeolite Beta samples is related to the concentration of framework tetrahedral atoms, and to their partial positive charge. On active zeolite Beta samples, the reversible transformation of framework tetrahedral aluminium to framework octahedral aluminium was observed upon adsorption of the acylating agent, acetic anhydride. Only limited transformation was observed on the inactive Na-Beta. A mechanism is proposed for the acylation of anisole with acetic anhydride over zeolite Beta. It is a modified Eley-Rideal type mechanism whereby acetic anhydride interacts with framework tetrahedral aluminium (which acts as a Lewis acceptor), forming an octahedral complex. This polarises the anhydride molecule, forming the active electrophilic cation intermediate. A molecule of aromatic substrate (anisole) impinges from the liquid phase, reacting with the acylium cation and forming a Wheland intermediate. The decomposition of the Wheland intermediate to p-methoxyacetophenone (p-MAP) and acetic acid completes the

process. The desired product, p-MAP, is rapidly and selectively formed on all zeolite Beta samples. The exclusive products of the reaction, p-MAP and acetic acid were found to be the main contributors of catalyst deactivation. The catalytic activity of ZSM-5, zeolite Y, mordenite, and mesoporous MCM-41 was significantly lower than on zeolite Beta samples. Catalytic data would suggest that pore size and acidic strength play no major role in the activity of the different materials tested. The much higher catalytic activity observed over zeolite Beta samples may be related to the unusual flexibility of framework tetrahedral aluminium exhibited by this material, allowing it to adopt higher coordination environments.

Acknowledgements

I would like to thank the following people for their contribution to the investigation, by providing knowledge, encouragement, and friendship.

Dr. M. Stockenhuber
Prof. R. W. Joyner
Dr. J. S. J. Hargreaves
Dr. G. Fuller
Dr. I. Burton
Mr. G. Burgess
Mrs. J. Dixon
Mr. M. J. Duggan
Mr. Ing. M. W. E. Van Den Berg
Dr. G. Grubert
Dr. A. Kogelbauer
Dr. D.C. Apperley

Contents

Chapter 1. Introduction

Chapter 2. Experimental

Chapter 3. Results and Discussion

Chapter 1. Introduction

1.1 Scope of the thesis

The use of zeolites in the acylation of aromatics has received great attention over recent years; such extensive investigation has led to the development of the first industrial application of zeolites for the acylation of anisole and veratrole. Zeolite Beta was found to be the most promising candidate for further investigation, particularly in the acylation of anisole with acetic anhydride.

The thesis describes the effects of ion exchange, calcination procedure, chemical modification, and regeneration primarily on the acidic properties of Zeolite Beta, however faujasite, ZSM-5, mordenite, and the mesoporous MCM-41 are also studied briefly. The acidic properties of these materials are related to their catalytic activity. The model reaction used throughout the investigation is the acylation of anisole with acetic anhydride in the liquid phase. The effect of changing the substrate and acylating agent, substrate/acylating agent ratio, mass and particle size of the catalyst, and temperature effects are also investigated. An extensive study of adsorption of reactants and products on zeolite BETA are observed using a combination of FTIR, and MAS NMR, in order to probe the interactions occurring at the active sites.

By evaluating such extensive data it is possible to substantiate and contribute to existing knowledge in this field, and look more deeply at what is occurring at the active site during catalytic reaction, giving further insight into the mechanism of reaction, and the causes of deactivation, which are the aims of this investigation.

1.2 Acylation of aromatics (Conventional procedure)

An acyl group, -COR is introduced onto the ring when an aromatic compound reacts with a carboxylic acid chloride, RCOCl, in the presence of $AlCl_3$. For example, the reaction of benzene with acetyl chloride yields the ketone, acetophenone.

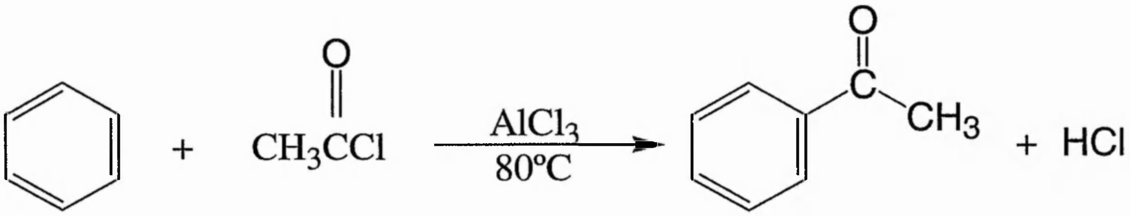

Figure 1.2.1 Reaction of benzene with acetyl chloride to yield acetophenone.

The reactive intermediate in Friedel Crafts acylation is a resonance stabilized acyl cation, generated by reaction between the acyl chloride and $AlCl_3$. An acyl cation is stabilized by interaction of the vacant orbital on carbon with a lone pair orbital of the neighbouring oxygen. Once formed, the acyl cation does not rearrange; rather, it is attacked by an aromatic ring to give unrearranged substitution product [1].

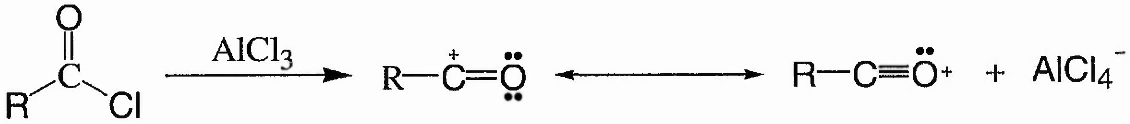

Figure 1.2.2 Resonance structures showing stabilization of the acyl cation [1].

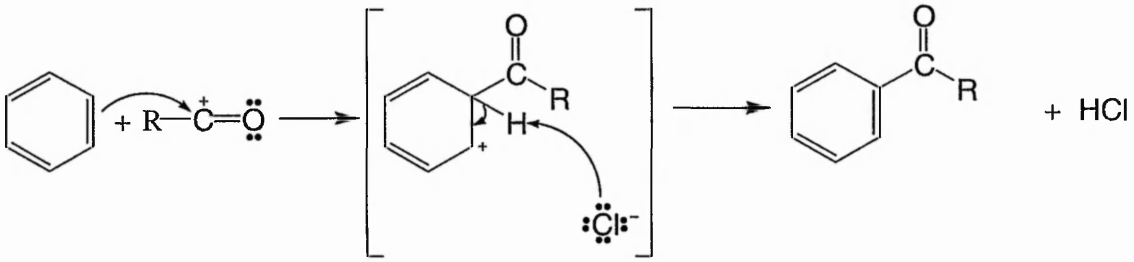

Figure 1.2.3 Mechanism of the Friedel Crafts acylation reaction [1].

1.3 Zeolites – A definition

Zeolites are a class of metastable, crystalline aluminosilicates comprising silicon and aluminium atoms linked in tetrahedral coordination by oxygen atoms. Zeolites are unique in that they exhibit microporous character with unique, uniform pore dimensions, allowing certain hydrocarbon molecules to enter while rejecting others on too large a molecular size.

1.4 Zeolite structure

Structurally, the zeolite is a crystalline aluminosilicate with a framework based on an extensive three-dimensional network of oxygen ions. Situated within the tetrahedral sites formed by the oxygen can be either a Si^{+4} or Al^{+3} ion. The AlO_4 tetrahedra in the structure determine the framework charge. This is balanced by cations that occupy nonframework positions. A representative empirical formula for a zeolite is written as:

$$M_{2/n}O \cdot Al_2O_3 \cdot xSiO_2 \cdot yH_2O$$

M represents the exchangeable cations, generally from the group I or II ions, and n represents the cation valence. The value of x is equal to or greater than 2 because Al^{3+} does not occupy adjacent tetrahedral sites. The crystalline framework structure contains voids and channels of discrete size. The pore or channel openings range from 3 Å to 8 Å, depending on the structure. Water molecules present are located in these channels and cavities, as are the cations that neutralize the negative charge created by the AlO_4 tetrahedra in the structure. Understanding zeolite materials on the basis of a specific set of structural elements can range from one extreme, that of simply identifying the size of the pore openings, to the completely opposite case, where a detailed visualization is needed of the sequences of building blocks that form the regular pattern characteristics of a given zeolite. In order to compare the large number of complex zeolite structures, structural building units were developed. These units are used to understand the way that individual structures form from the complex mixtures used in their synthesis.

1.4.1 Structural building units

The primary building unit of a zeolite is the individual TO_4 unit, where T is either Si or Al. A secondary building unit (SBU) consists of selected geometric groupings of those tetrahedra. There are nine such building units, which can be used to describe all of the known zeolite structures; these are shown in **Figure 1.4.1.1**. These secondary building units consist of 4, 6, and 8 member single rings, 4-4, 6-6, and 8-8 member double rings, and 4-1, 5-1, and 4-4-1 branched rings. Most zeolite frameworks can be generated from several different SBU's. The secondary building unit provides a convenient method of topologically describing and relating different zeolites [2].

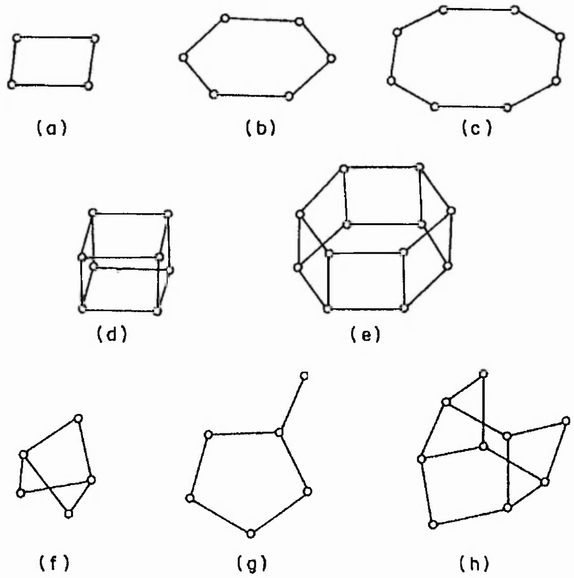

Figure 1.4.1.1 Secondary building units (SBU's) found in zeolite structures [2].

1.4.2 Pore size, dimensionality and shape

All zeolites that are significant for catalytic and adsorbent applications can be classified by the number of T atoms, where T = Si or Al, that define the pore opening. The three main pore openings that are of practical interest for catalytic applications are descriptively referred to as the 8, 10, and 12 ring openings. Zeolites containing these pore openings may also be referred to as small (8-member ring), medium (10-member ring), and large (12-member ring) pore zeolites. However in this simple classification, no indication is given as to the exact dimension of the pore openings or whether the zeolite contains a one, two, or three dimensional system of interconnected pores.

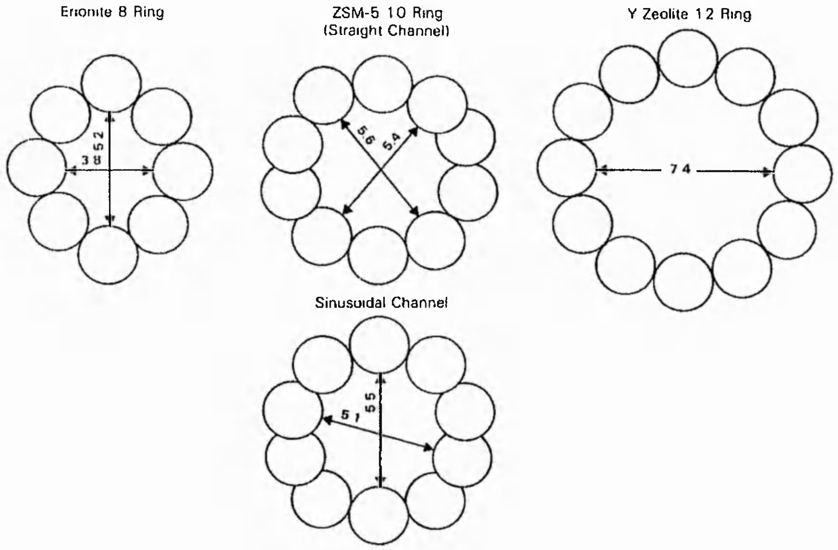

Figure 1.4.2.1 Examples of three types of pore openings in the zeolite molecular sieves. Erionite contains an 8-ring pore opening; ZSM-5, two 10-ring systems differing in the shape of the opening; and faujasite, a 12-ring pore system [2].

In addition to pore size of the zeolite, it sometimes becomes important to also consider the fine details of the channel system, such as the number of dimensions those pores encompass and the pore mouth shape. As the free diameter of the windows increases in the 8, 10, and 12 ring systems, the adsorbed, reacting, or reacted species move more or less readily from one void to the next, and the cage like character of the voids diminishes progressively. Therefore, instead of visualizing a zeolite in terms of the interconnection of voids by their 8, 10, and 12-ring pore openings, the structures can be viewed as a series of one, two, or three dimensional tubes or channels. For example, both ZSM-5 and ZSM-11 contain intersecting three-dimensional 10-ring channel systems. The ZSM-5 zeolite contains a zigzag channel system intersecting a straight 10-ring channel to produce the three-dimensional pore system. The ZSM-11 structure contains two 10-ring intersecting straight channels that form the three-dimensional pore system.

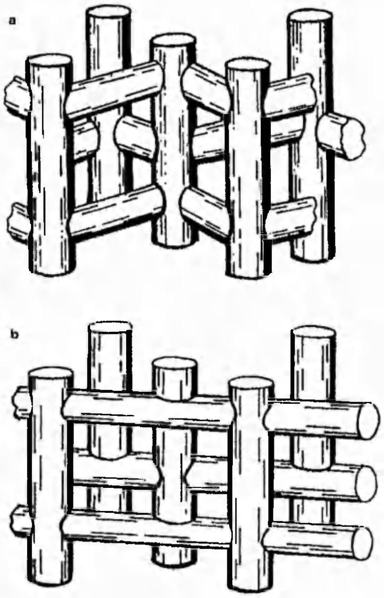

Figure 1.4.2.2 “Hollow tube” representation of ZSM-5 (a) and ZSM-11 (b), both 10-ring zeolites [2].

The shape of the pore opening is categorized primarily by the number of T atoms forming the pore mouth opening. However, other factors are important in determining the size and shape of the pore opening such as:

1) Configuration of the T and O atoms relative to each other.
2) Silica / alumina ratio.
3) Size of the cation.
4) Location of the cation.
5) Temperature.

For the ideal planar configuration using 2.7 Å as the diameter of the oxygen atoms, an 8-member ring opening is 4.4 Å, and the 10 and 12-membered rings would be 6.0 and 7.7 Å, respectively. The actual opening, however, deviates from these values. It is the structure of the zeolite that shapes the pore mouth. For example, zeolite A and erionite are both small pore (8 ring) zeolites, zeolite A has a pore dimension estimated from its structure to be 4.1 Å, and erionite has a pore diameter of 5.2 × 3.2 Å, reflecting the elongated nature of the erionite channel system. Though the structure dictates the shape of the pore opening, this opening can be further modified. The number of cations in the channels and cavities, and their size will also contribute to the final size of the pore opening. Since the Si/Al ratio governs the number of cations required to achieve a neutral structure, this too, will influence the size of the pore opening. The location of the cation can also effect the size of the pore opening. Zeolite A, containing Na^+ cations, has an effective pore dimension less than would be expected for its 8-member ring framework opening. This is due to sodium ion occupancy of sites where it will partially block the 8-ring window. Temperature can also cause changes in the size of pore openings. A variation in the amplitude of vibration of 0.1 to 0.2 Å is expected upon changing the temperature from 80 to 300 K, which is sufficient to alter the adsorption capabilities of a given zeolite [2].

1.5 Zeolite synthesis [3]

As zeolite structures are built from SiO_4^{4-} and AlO_4^{5-} tetrahedra these primary building blocks must also be present in the synthesis mixture and, because aluminate ions are only stable at high pH values, zeolite synthesis almost exclusively takes place from basic solutions. An important factor determining the synthesis conditions is the Si/Al ratio of the zeolite to be synthesized. The higher the Si/Al ratio and so the lower the Al content the more difficult is the synthesis and the more severe the conditions that are needed. There are a number of subsequent events that occur in the course of a zeolite synthesis. Generally the first step is the preparation of the reaction mixture at low temperature (< 333 K). The different ingredients are mixed in this step, which in most cases results in the formation of the so-called synthesis gel. In this gel silicate and aluminate monomers and oligomers in solution are in equilibrium with condensed silicate and aluminate units in the gel phase. In some cases a digestion period is necessary to reach this equilibrium. In the second step the temperature of the synthesis mixture is raised to the crystallization temperature (generally between

100 and 200ºC). During this process continued dissociation of silicate and aluminate oligomers occurs, resulting in an increasing concentration of monomeric silicate and aluminate species in solution. Once the high crystallization temperature is reached, zeolite crystallization will start after an induction period. During this induction period the dissolution of the gel phase continues, leading to the formation of clusters of polysilicates or aluminosilicates that become stable above a certain critical dimension (e.g. about 10 Å for zeolite A and about 20 Å for zeolite ZSM-5), and crystallization commences. The course of nucleation and crystallization of zeolites can generally be described by a characteristic S-shaped crystallization curve, in which the amount of crystalline material is plotted against crystallization time. Depending on the type of zeolite, crystallization will be completed after several hours to several days. The crystals must then be separated from the mother liquor by decantation, filtration or centrifugation, followed by washing with water. The final step in zeolite preparation is the drying and calcination procedure, after which the zeolite void volume is free for the different applications. To illustrate the different aspects of zeolite synthesis, the preparation of faujasite (Si/Al = 2.5) and ZSM-5 (Si/Al = 12) are described. For the synthesis of faujasite it is necessary to add extra SiO_2 in the form of reactive silica gel or silica sol to the synthesis mixture [4] to obtain the right composition. A typical gel composition in this case is:

Mol ratio
$Na_2O : Al_2O : SiO_2 : H_2O = 4.00 : 1.00 : 10.0 : 160$

The synthesis of ZSM-5 and other (very) high silica zeolites becomes possible when, instead of alkali hydroxides, tetraalkylammonium hydroxides are used to obtain the high PH necessary for zeolite synthesis. In the case of ZSM-5 tetrapropylammonium hydroxide must be used [5]. A typical gel composition is:

Mol ratio
$Na_2O : Al_2O_3 : SiO_2 : TPAOH : H_2O = 1.25 : 1.00 : 30 : 18 : 800$

The synthesis of low silica mordenite is possible from alkaline mixtures, but in order to obtain high silica mordenite with a chemical composition of $Na_2O.Al_2O_3.10SiO_2$ it is necessary to add an organic modifier. Because of the low Al content, the zeolite framework loses its polar properties and can no longer be stabilised by the adsorption of hydrated alkali ions. Instead, positively charged organic molecules are needed which, besides charge compensation, also have nonpolar interactions with the zeolite framework. Amines are often used for this purpose, and for mordenite synthesis diethylamine (DEA) is used in particular. A typical gel composition is:

Mol ratio
$Na_2O : Al_2O_3 : SiO_2 : DEA : H_2O = 4.00 : 1.00 : 1.00 : 6.60 : 20 : 300$

Zeolite Beta can be synthesised from an aluminosilicate gel having the nominal composition: (where TEAOH stands for tetraethylammonium hydroxide)

Mol ratio
$Na_2O : Al_2O_3 : SiO_2 : TEAOH : H_2O = 0.9 : 1.00 : 30 : 3 : 250$

1.6 Zeolite shape selectivity

Shape selectivity plays a very important role in molecular sieve catalysis [6]. Highly crystalline and regular channel structures are among the principal features that molecular sieves used as catalysts offer over other materials. The difference in products observed in the acid-catalysed transalkylation of 1-methyl-2-ethylbenzene using non-zeolitic acid catalysts and using the acid form of zeolitic mordenite is a prime example of shape selectivity. This example highlights the selectivity of the zeolite-based catalyst for the desired transalkylated products rather than the undesirable tri-substituted product obtained when non-zeolitic catalysts are used. The shape selective properties of the 10-ring zeolite ZSM-5 have been exploited in the following processes: M-forming, dewaxing, lube production, xylene isomerisation, methanol to gasoline conversion, and ethylbenzene production [7]. Shape selectivity operates in the above processes by reactant shape selectivity, product shape selectivity, or transition-state shape selectivity [2]. Reactant shape selectivity results from the limited diffusivity of some of the reactants, which cannot effectively enter and diffuse inside the crystal. For example, the distillate dewaxing process is a reactant shape-selective process in which only the straight-chain or slightly branched paraffins present in the distillate are able to enter the ZSM-5 pore, where they crack to lighter products; this yields a less waxy overall product with a lower pour point [8]. Product shape selectivity occurs when slowly diffusing product molecules cannot rapidly escape from the crystal, and undergo secondary reactions. The alkylation of toluene with methanol to form p-xylene is a good example of product selectivity. The various possible alkyl aromatic products have markedly different diffusivities in ZSM-5. For example, the diffusion coefficients of p-xylene and o-xylene in ZSM-5 at 588 K are, respectively, 10^{-7} and 10^{-10} cm^2 s^{-1}. Thus, even though the equilibrium distribution of p-, m-, and o-xylenes is 23:51:26, a ZSM-5 catalyst for the reaction can result in a product distribution of 46:36:18 [9]. Restricted transition-state selectivity is a kinetic effect arising from the local environment around the active site: the rate constant for a certain reaction mechanism is reduced if the necessary transition state is too bulky to form readily [7]. For example, the steric strain of the larger transition state complex required to crack 3-methylpentane in zeolite ZSM-5 is the proposed cause of its lower reactivity than that of n-hexane [2]. The methanol-to-gasoline (MTG) conversion is another good example of transition-state shape selectivity, where the available space in the cavities of zeolite ZSM-5 determines the largest bimolecular reaction complexes that can form. Hence, all products have fewer than 11 carbon atoms, with xylenes predominating [10]. **Figure 1.6.1** shows the three types of selectivity: reactant, product, and transition-state shape selectivity.

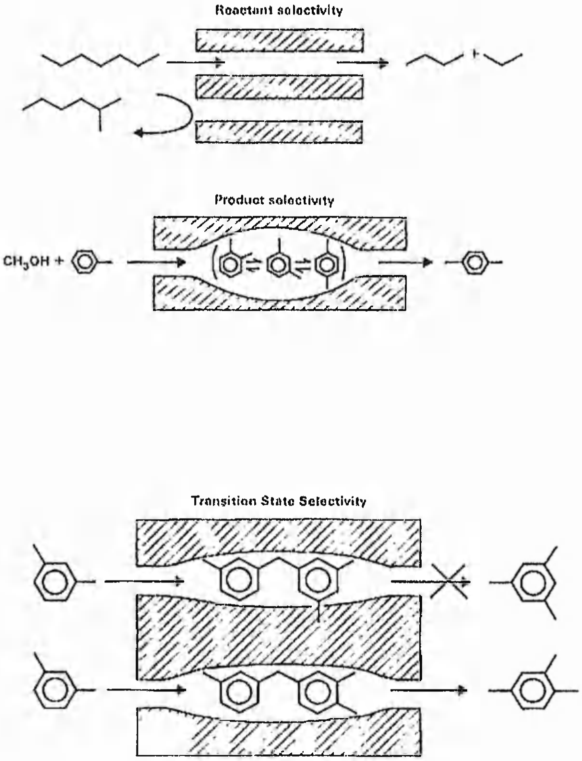

Figure 1.6.1 Reactant, product, and transition-state shape selectivity [6].

1.7 Zeolite acidity

The reactivity and the selectivity of zeolites as catalysts are determined by an imbalance of charge created by the tetrahedrally coordinated Al atoms that introduce a negative charge into the zeolite lattice. This negative charge is balanced by the presence of cations. Brønsted and Lewis acid models of acidity have been used to classify the active sites in zeolites. Brønsted acidity is proton donor acidity; this occurs in the zeolites when the cations balancing the framework anionic charge are protons. Lewis acidity is electron pair acceptor acidity; a trigonally coordinated aluminium atom, for example, is electron deficient and can accept an electron pair, and thus behaves as a Lewis acid [11]. For example, as depicted in **Figure 1.7.3**, when a hydrogen form of a zeolite is heated to high temperature, water is given off and coordinatively unsaturated Al^{3+} ions are formed, and these act as strong Lewis acids. In this process, one

Lewis site is formed from two Brønsted acid sites. **Figure 1.7.1** shows the hydrogen form of a zeolite. To simplify the representation, the SiO_4 and AlO_4 tetrahedra are strung out, with a loss in the depiction of the three dimensional geometry. Also, it should be recognized that the proton is mobile within the structure.

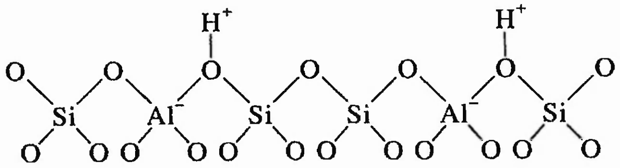

Figure 1.7.1 Hydrogen form of a zeolite [11].

Figure 1.7.2 shows a segment of a zeolite in the sodium form and calcium form. The exchangeable cations are placed near AlO_4 tetrahedra, because the negative charges are predominantly located there. In the calcium form, the single Ca^{2+} ion balances the charge of two AlO_4^- tetrahedra. In the actual zeolite, the negative charge is not localized on one or two tetrahedra but is distributed over the framework of oxygen ions.

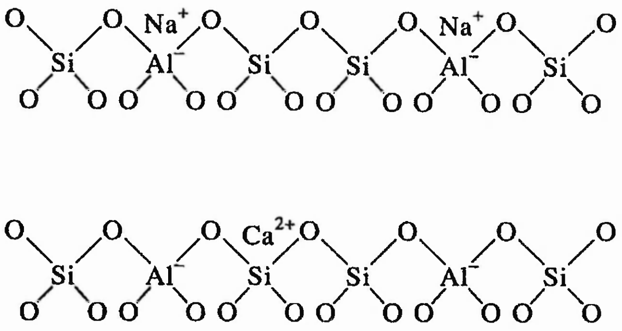

Figure 1.7.2 The sodium and calcium forms of a zeolite [11].

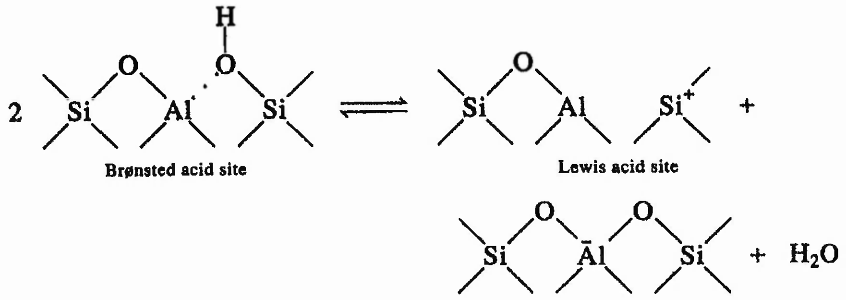

Figure 1.7.3 Formation of Lewis acid sites from 2 Brønsted acid sites after treatment to high temperature [11].

Zeolites with high concentrations of protons are hydrophilic, having strong affinities for polar molecules small enough to enter the pores. Zeolites with low proton concentrations are hydrophobic, taking up organic compounds from water–organic mixtures; the transition normally, but by no means always, occurs at a Si/Al ratio near 10. The total acidity of a zeolite may be considered to be a contribution of both an extensive factor representative of the number of acid sites and an intensive factor representative of the strength of individual sites [12], [13]. For structurally pure hydrogen zeolites, the nature of acid sites is conceptually well defined. In this case Brønsted acidity is associated with the labile protons in the neighbourhood of tetrahedrally coordinated lattice aluminium sites [14]. Thus, the extensive factor of acidity is simply the number of protons held by the lattice aluminium per unit volume. Already in 1965 it was recognized that the intensive factor could be greatly enhanced by the simple process of dehydroxylation, which reduces the extensive factor. In high silica zeolites the lattice aluminium atoms are far apart from each other, and thus it may be expected that all protons would have about the same environment and thus have equal acidic strength. There are many factors, which may affect the intensive factor of the acidity of zeolites. For example, it has been well documented that an optimum aluminium concentration exists in zeolites which corresponds to maximum acidic strength [15-22]. Although further increasing the lattice aluminium concentration results in an increase in the extensive factor, the intensive factor is reduced due to delocalization of the negative charge density on the lattice. Zeolite acidity can be drastically altered by hydrothermal, thermal, and chemical modifications. Hydrothermal modifications (or steaming) occur because of careless catalyst preparation, deliberate catalyst treatment, and reactions occurring on the catalyst. Both steaming and dehydroxylation can occur during the preparation of the active proton-exchanged catalyst unless adequate precautions are taken to avoid moisture and excessive heat. Both effects are accompanied by the loss of aluminium from the crystal lattice. The acid sites on molecular sieves have been studied extensively with both physical and catalytic characterization techniques [23-29]. These include infrared spectroscopy, measurements of the adsorption/desorption properties of probe molecules such as ammonia and pyridine, and acid-catalysed reactions including selected cracking and isomerisation of organic molecules. These methods give information regarding the nature, number, strength, and location of the active sites.

1.8 Zeolites used: Structure and acidity

1.8.1 Zeolite Beta

The three-dimensional, highly siliceous, large pore zeolite Beta (BEA) is developing into a major catalyst in organic chemicals conversions, contributing to low waste technology. Examples of successful applications of zeolite Beta include aromatic alkylation [30], aromatic acylation [31], indole synthesis [32], aromatic nitration [33], and aliphatic alkylation [34]. Zeolite Beta has a three-dimensional intersecting channel system. Two mutually perpendicular straight channels, each with a cross section of 0.76 × 0.64 nm, run in the a- and b-direction. A sinusoidal channel of 0.55 × 0.55 nm runs parallel to the c-direction. **Figure 1.8.1.1** shows the three-dimensional channel system of zeolite Beta.

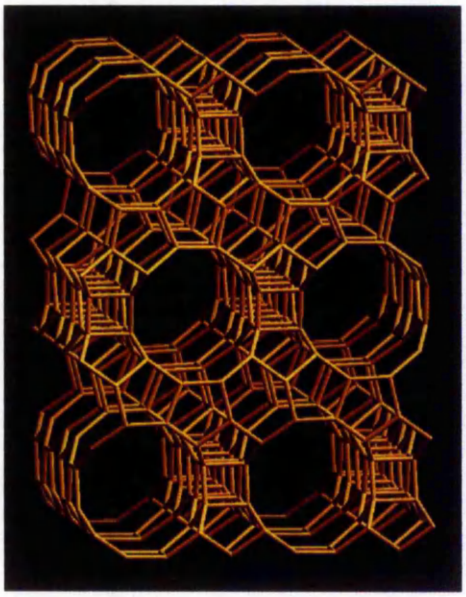

Figure 1.8.1.1 Three-dimensional channel system of zeolite Beta (100 plane).

Zeolite Beta possesses unique acid properties, which are related to local defects. These defects are generated when a tertiary building unit (TBU) is rotated 90° around the c-direction with respect to the neighbouring TBU's in the same layer. The rotated TBU cannot connect properly with the adjacent layers. This results in T atoms that are not fully coordinated to the framework, thereby creating potential Lewis acid sites [35]. Thus the large numbers of local defects in zeolite Beta result in a high proportion of partially coordinated aluminium atoms which give rise to Lewis acidity. **Figure 1.8.1.2** shows the tertiary building units for zeolite Beta.

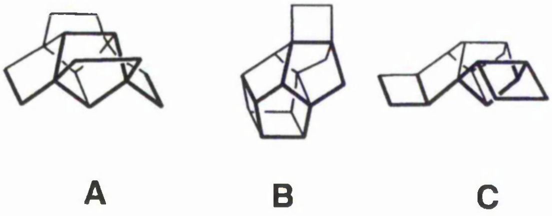

Figure 1.8.1.2 Tertiary building units for zeolite Beta [35].

The aluminium atoms in zeolite Beta can produce Brønsted as well as Lewis acidity. The first type of acidity is introduced by aluminium atoms that are tetrahedrally coordinated in a locally perfect framework. Al-sites located at the external surface, probably terminated by hydroxyl groups, also require a charge-compensating proton, thus also producing Brønsted acidity [35]. It is thought that Brønsted acidity is present on both the internal and external surface. As already mentioned, local defects comprise partially coordinated aluminium atoms giving rise to Lewis acidity. These aluminium atoms are always located between two neighbouring TBU's, and thus Lewis sites are predominantly present on the internal surface [35].

1.8.2 ZSM-5

ZSM-5 has a three-dimensional intersecting channel system. The secondary building units of the MFI structure are built up by 5 membered- rings. The straight channels of ZSM-5 consist of 10 membered- rings with an opening of 0.56 × 0.53 nm, which run parallel to the a-axis. The straight channels are connected by sinusoidal channels, which have a diameter of 0.55 × 0.51 nm and run parallel to the b-axis. Molecules can also move in the c-direction by alternately using both channels. Although the channels of ZSM-5 are relatively small in comparison with those of large pore zeolites such as faujasite and mordenite, it is still possible to adsorb naphthalene molecules which have a kinetic diameter of 0.74 nm, this can be explained by the flexibility of the 10-ring apertures [36]. **Figure 1.8.2.1** shows the three-dimensional channel system of ZSM-5.

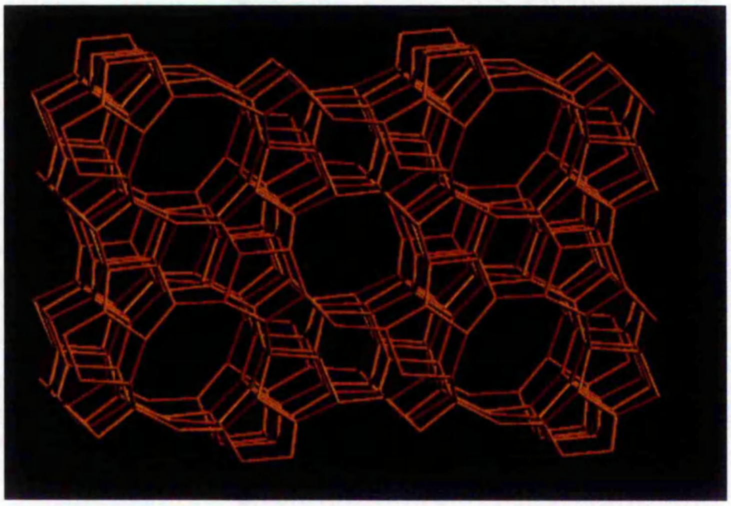

Figure 1.8.2.1 Three-dimensional channel system of ZSM-5 (010 plane).

The aluminium atom concentration in ZSM-5 is very low and continuously variable over many orders of magnitude. As the concentration of aluminium in ZSM-5 is increased, the number of acid sites increases, however the acid sites tend to remain in a state of high dilution because of the high proportion of silica present. The Brønsted acid sites in ZSM-5 are therefore considered to be highly ionised [37].

1.8.3 Mordenite

Mordenite has a two-dimensional channel system. The secondary building units of mordenite are built up by four and five-membered rings. Parallel straight channels, which are built up by 12-membered rings and have a diameter of 0.70 × 0.65 nm perpendicularly intersect smaller channels, which are built up by 8 membered rings and have a diameter of 0.57 × 0.26 nm. For practical applications, mordenite is normally considered to be a uni-dimensional, large pore zeolite with side pockets, since the 8-membered ring openings constrain the diffusion of molecules. **Figure 1.8.3.1** shows the two-dimensional channel system of mordenite.

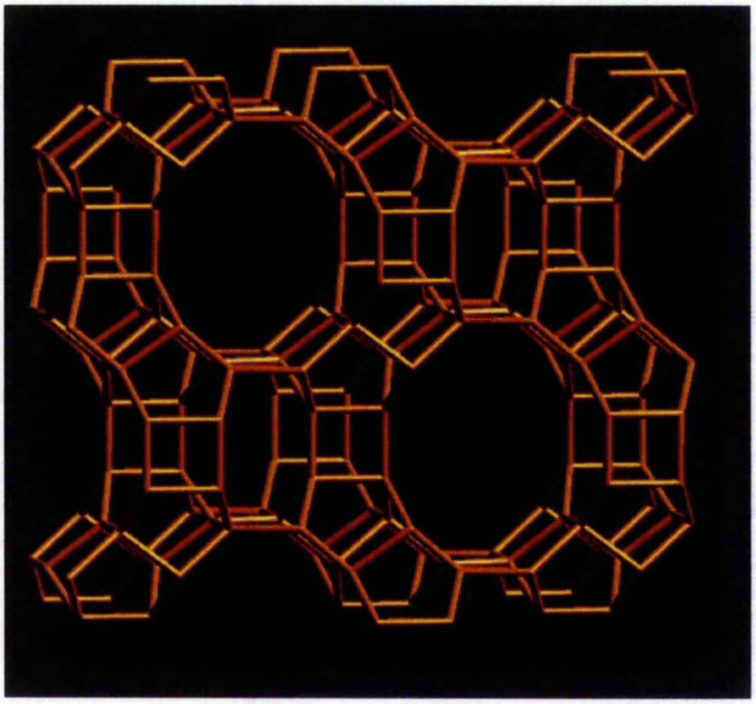

Figure 1.8.3.1 Two-dimensional channel system of mordenite (001 plane).

Mordenite is a strong acid, the Si/Al ratio of which can be easily changed from 5 to higher values using a variety of techniques including steaming of ammonia ion-exchanged materials and direct acid treatment.

1.8.4 Faujasite (zeolite Y)

Faujasite has a three-dimensional pore system. The secondary building units of faujasite are built up by six and four-membered rings. The supercages or α-cages of the structure are 1.20 nm in diameter and are interconnected by 12-ring openings, which have a diameter of 0.74 nm. The supercages are surrounded by the smaller sodalite cages or β-cages, which can be accessed by 6-ring openings with a diameter of 0.24 nm. The sodalite cages are connected via four hexagonal prisms, the third type of cages in the structure, the γ-cages. **Figure 1.8.4.1** shows the three-dimensional channel system of faujasite.

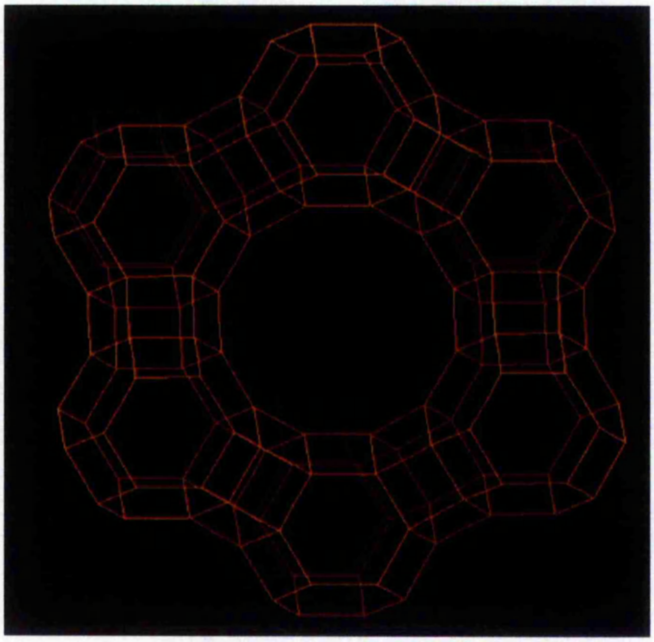

Figure 1.8.4.1 Three-dimensional channel system of faujasite (111 plane).

Faujasite is a low silica containing molecular sieve, it contains so many aluminium sites that its overall acidity actually increases as aluminium is removed, either by dealumination [38], or by increasing the Si/Al ratio [39]. Faujasite prepared by the process of dealumination, whereby a reactant such as $SiCl_4$ extracts Al from the framework, or by treatment with steam, is called ultrastable Y (USY). The high proton donor strength of USY means it acts as a superacid, which at high temperatures is able to protonate even paraffins, thereby initiating catalytic cracking.

1.8.5 MCM-41

MCM-41 is a novel mesoporous silicate material discovered by Mobil researchers. The dimensions of the straight parallel channels vary from 2 to 10 nm, depending on the template micelle dimensions. These materials close the gap between microporous zeolites and macroporous materials. **Figure 1.8.5.1** shows the mesoporous parallel channels of MCM-41.

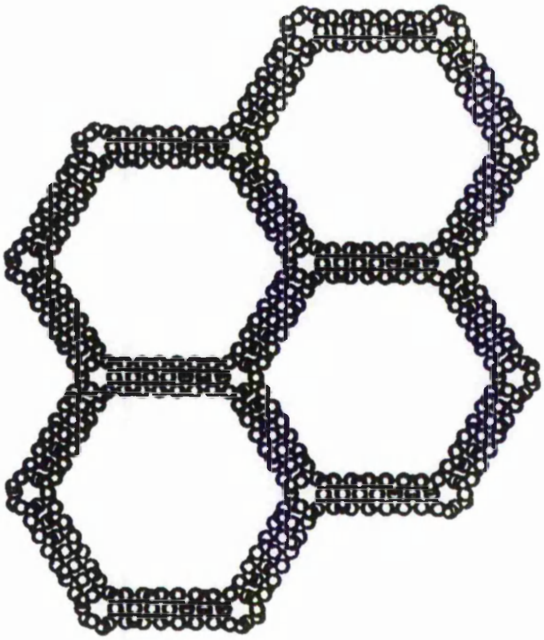

Figure 1.8.5.1 Mesoporous parallel channels of MCM-41.

MCM-41 might be a catalyst component for the reaction of high molecular weight hydrocarbons, which should be able to penetrate large pores. A precondition for catalytic use of purely siliceous MCM-41 is its modification by incorporation of Al and transition metal elements into the silica framework in order to increase the acidity, ion-exchange capacity and catalytic activity. There are many reports of the synthesis and characterization of Al-MCM-41 with different Si/Al ratios, prepared by adding Al sources prior to calcination [40]. In a study by Kosslick *et al.*, [41] the acid properties of Al-, Ga-, and Fe-substituted MCM-41 was investigated. The addition of trivalent metal sources to the MCM-41 synthesis gel led to the incorporation of a fraction of these elements into tetrahedrally coordinated framework positions, this was proven by the appearance of Brønsted acidity. These workers observed weak, medium, and strong Brønsted acid sites, depending on the degree of substitution and the type of element used. It was also suggested that Lewis acid sites, formed by extraframework metal species, may exhibit varying degrees of acidic strength.

These authors concluded that MCM-41 modified by such methods may be applied in acid catalysis.

1.9 Acylation of Aromatics – The use of zeolite catalysts

Progress towards environmentally responsible processing is marked by the elimination of waste and by-product generation and reduced dependence on hazardous chemicals. The key to both is often provided by catalytic as alternatives to stoichiometric processes [42]. The acylation of aromatics is of great importance throughout the chemical industry, most notably for its participation in the manufacture of many pharmaceuticals, e.g. the production of Ibuprofen and (S)-Naproxen involve an aromatic acylation step [43]. In addition many synthetic fragrances of the musk type contain an acetyl group [43], [44]. The conventional method of preparation of these aromatic ketones is the homogeneous Friedel Crafts acylation of aromatic compounds using acid chlorides or anhydrides over metal chloride catalysts as dealt with in **1.2**. However this procedure requires more than stoichiometric amounts of catalyst, this is due to the formation of a complex between the product and the catalyst, the hydrolysis of which leads to the loss of catalyst and the formation of a large amount of inorganic by-products which cause considerable environmental problems [45]. The problems associated with traditional homogeneous catalysts have lead to a great deal of activity in the search for alternative catalysts, in particular reusable heterogeneous catalysts such as zeolites. Zeolites are not only more resourceful, and more environmentally friendly than their more conventional homogeneous counterparts, but they offer another advantage in that selectivity is not only determined by the characteristics of the acid sites but also can be orientated towards the desired product by their pore system. The use of zeolites in aromatic acylation has been well documented [46-48].

1.9.1 Aromatic acylation studies over zeolite catalysts

Zeolites are currently being widely studied for their application in the synthesis of organic and fine chemicals. In conventional Friedel Crafts acylation, an acyl group is attached to the aromatic substrate using homogeneous Lewis acid catalysts such as $AlCl_3$ and BF_3 [49]. Other highly active metallic halides recommended for use with acyl halides include $FeCl_3$, $FeBr_3$, $SbCl_5$, $TiCl_4$, and $ZrCl_4$ [45]. These catalysts are required in more than stoichiometric amounts and lead to the possibility of undesirable side reactions. For these reasons, other catalysts such as iron sulphate [50], iron oxide [51], trifluoromethanesulphonic acid [52], and more recently the solid acid catalyst, lanthanide trifluoromethane sulphonate, have been produced for the acylation of substituted benzenes [53]. Solid superacids, sulfated zirconia and alumina (SO_4/ZrO_2 and SO_4/Al_2O_3) have been successfully used for the benzoylation of toluene with benzoyl chloride and benzoic anhydride [54]. Tungsten oxide supported on zirconia (WO_3/ZrO_2) was also found to be active in acylation [55]. Solid acids derived from montmorillonite, a class of smectite clay naturally available, by the process of exchange with different metal ions and impregnation with the salts of the metals were explored as catalysts for Friedel Crafts acylation reactions [56]. The catalytic activity of cation exchanged mesoporous clays for the Friedel Crafts acylation of aromatic ethers has been reported in good yields [57]. However, the most appealing and promising candidates for the future production of aromatic ketones are heterogeneous catalysts, in particular zeolites [58], [59]. Medium and large pore zeolites have been presented as ideal catalysts for the future industrial production of aromatic ketones [60]. H-ZSM-5 has been used in the acylation of less substituted aromatic molecules such as benzene, phenol and toluene [61-63], while zeolites with larger pores such as zeolite H-Beta and HY have been used extensively in the acylation of arylethers such as anisole and polysubstituted aromatics such as xylenes and mesitylenes [64-67]. Recently, zeolite Al-ITQ-7, a tri-directional zeolite has been shown to be active in the aromatic acylation of 2-methoxynaphthalene with acetic anhydride [68]. A relatively new zeolite, Al-

ITQ-7 has a slightly smaller pore diameter than zeolite beta, and gives improved selectivity to the desired product in this reaction, 2-acetyl-6-methoxynaphthalene. A commercial process for the acylation of anisole and veratrole with acetic anhydride using zeolite Beta and faujasite, respectively, was recently developed by Rhône Poulenc [69], [70]. Bulkier molecules such as 2-methoxynaphthalene have also been efficiently acylated using large pore zeolites such as zeolite Beta and faujasite [46], [71], [72]. The possibility of using zeolites as catalysts for the acylation of various aromatics, using acetic anhydride as the acylating agent, has been well demonstrated [46-48]. In particular zeolite Beta was found to be a selective catalyst for the synthesis of p-methoxyacetophenone by acetylation of anisole [73], and faujsite for the synthesis of 3,4-dimethoxyacetophenone by veratrole acetylation [73]. Friedel Crafts acylation of anisole with acetic anhydride using H-Beta and HY zeolites was described by Harvey *et al.*, [74]. In this study H-Beta was consistently found to be the most active catalyst for acylation reactions compared with USY and ZSM-5. Similarly, Freese *et al.*, [67] found zeolite Beta to be the most active catalyst for acylation using anisole as substrate and acetic anhydride as acylating agent compared to faujasite and ZSM-5. In both the above studies the reactions were carried out in the liquid phase in a batch reactor. A number of gas phase acylation studies have also been reported in the literature. Selective gas phase acylation of heteroaromatics such as thiophene, furan, and pyrrole with acetic anhydride using zeolite catalysts was reported by Hölderich *et al.*, [75]. Rohan *et al.*, [76] studied the acylation of anisole with acetic anhydride over zeolite H-Beta, and determined its deactivation behaviour in the gas and liquid phase. The gas phase catalytic acylation of a series of aromatic compounds including benzene, toluene, xylenes, mesitylenes, isopropylbenzene and N,N-dimethylanaline using medium and large pore zeolites as catalysts, and acetic acid or acetyl chloride as acylating agents was carried out by Pandey *et al.*, [61]. A substantial proportion of the literature related to the acylation of aromatics over zeolite catalysts state the importance of choosing a particular substrate and acylating agent for a specific reaction. Highly activated aromatic rings such as anisole are preferred as opposed to less activated aromatic molecules such as toluene which give low yields [77]. The choice of substrate also becomes important when using different zeolites, a study carried out by Spagnol *et al.*, [78] found that zeolite Beta was more active than zeolite Y when anisole was used as substrate, upon changing the substrate to veratrole zeolite Y becomes far more active than zeolite Beta. The explanation for this effect is that the acylated intermediate formed during veratrole acylation cannot be formed in the pores of zeolite Beta. This problem is not encountered in the case of zeolite Y because the supercages of this structure are very large and the intermediate can be accommodated very easily. Similarly, Richard *et al.*, [79] found that zeolite Beta was more active than zeolite Y in the acylation of benzofuran using acetic anhydride as acylating agent, upon changing the substrate to 2-methylbenzofuran zeolite Y became the most active catalyst. These workers concluded that the access of 2-methylbenzofuran to the active centres is probably easier in the case of zeolite Y than in the case of zeolite Beta, and that the pore size of the zeolite and the substrate chosen for reaction are critical parameters in order to ensure good reactivity. The nature and structure of the acylating agent are also essential in order to obtain maximum activity. Much of the older literature refers primarily to the use of carboxylic acids and acid chlorides as acylating agents in the acylation of aromatic substrates over zeolite catalysts. The acylation of anisole with acid chlorides and carboxylic acids over acid zeolites was studied by Corma *et al.*, [65]. The acylation of less activated substrates such as toluene and butylbenzene was found to be slow over carboxylic acids [80]. When anisole was used as substrate, acylation over zeolite Beta was readily catalysed by carboxylic acids and acid anhydrides. These workers concluded that acid anhydrides were more suitable acylating agents due to the absence of side reactions, which were observed with carboxylic acids. Gunnewegh *et al.*, [80] found that the acylation of anisole with long chain acids such as octanoic acid proceeds more readily than with the short chain acetic acid, and a similar phenomenon was found with the acylation of toluene [64]. More recently, acetic anhydride has consistently found to be the most active acylating agent over zeolite catalysts [81-83].

1.9.2 Acidity studies over zeolite catalysts

The acidity of zeolites governs their activity, explaining why many studies have been devoted to the determination of the nature, the number, and the strength of acid sites [84]. Many of the reaction patterns for the conversion of organics over acidic zeolite catalysts show a marked resemblance to those observed over strong 'classical' protonic acids such as 98% H_2SO_4, Lewis acids promoted with proton donors, and macroreticular sulfonated polystyrene ion-exchange resins [85-91]. The acidic properties of zeolites are intimately linked to the quantity, nature and distribution of the aluminium atoms attached or trapped in the three dimensional network of pores and cavities. The subject of 'activity/acidity' in zeolites is complex and the literature is extensive [92-95]. The ability of solid acids to act as catalysts is a consequence of the presence of different types of acid sites. In general, solid acids may exhibit Brønsted as well as Lewis acid sites. If a reaction is catalysed by one of these species the catalytic activity is determined by (1) the concentration, (2) the strength of acidity (and its distribution) and (3) accessibility of the corresponding sites provided that the reaction is not diffusion controlled [96]. The determination of these three parameters is a main topic of spectroscopic investigation on solid acids. A number of Nuclear Magnetic Resonance, Infrared, Electron Paramagnetic Resonance, X-ray Diffraction and X-ray Photoelectron Spectroscopic methods for the characterization of acid sites in solids have been developed over past years [25-29], [97-101]. Knowledge of the acidic properties of zeolites has been shown to be very valuable in explaining and predicting their behaviour as catalysts for particular reactions. The essential step in determining the acidic properties of a zeolite is the modification of the as-synthesized material by various treatments. Dealumination, the removal of framework aluminium without destroying the micropore structure is one of the most useful and widely used modifications. It can be achieved by hydrolysis of the Al-O- Si bonds by acid leaching combined with steaming, by complexation of the aluminium by oxalic acid [102] and by direct replacement of aluminium by silicon with gaseous silicon tetrachloride [103] or the bulkier $(NH_4)_2SiF_6$ [104].

Dealumination also promotes formation of a mesoporous system [105], [106]. In general four types of hydroxyl groups may exist in zeolites: (1) terminal, non-acidic OH groups on the outer surface of the crystals, (2) bridging OH (acidic) connected to the framework (strictly tetrahedral Al coordination), (3) OH groups bound to extralattice aluminium species (generally considered to be non-acidic) and (4) SiOH groups in lattice defects [107]. In the ideal case of a defect free crystal the first two types of hydroxyls are exclusively present with well-defined molecular surroundings [108]. Types 3 and 4 hydroxyls may form with dealumination or during synthesis. Dealumination by steaming generally results in the generation of extralattice aluminium species and framework defect sites filled with hydroxyl groups. In a study by Kiricsi *et al.*, [108], zeolite Beta was prepared with different Si/Al ratios by a hydrothermal method and dealuminated by leaching with dilute HCl. Samples of zeolite Beta from the various stages of H-Beta synthesis, and after leaching, were characterized by FTIR. These workers found that all samples exhibited both Lewis and Brønsted acidities. The type of OH groups present, and also their distribution were greatly affected by sample treatment. Five types of hydroxyl IR absorptions were found; those from strongly acidic bridging hydroxyls (3605 cm^{-1}); OH groups bonded to extralattice aluminium (3660-3680 cm^{-1}); internal SiOH at framework defects (3730 cm^{-1}); terminal SiOH groups (3745 cm^{-1}); and a very high frequency absorption (3782 cm^{-1}). The very high frequency absorption was assigned to OH groups connected to aluminium, which is leaving the framework. On the basis of band shifts during the adsorption of probe molecules, these workers concluded that the hydroxyl groups could be ranked in order of decreasing acidity, (1) bridging OH groups, (2) hydroxyls associated with extraframework aluminium, (3) hydroxyls responsible for the very high frequency band, (4) internal SiOH, and (5) non acidic terminal SiOH. In this study the very high frequency OH group was found to be moderately acidic, not strongly acidic, or non acidic as concluded by others [109], [110]. A similar study was carried out by Heinichen *et al.*, [111], and they found similar results after modification of zeolite Beta by acid treatment and calcination with high heating rate. In this investigation, an additional broad IR band was found between 3300 cm^{-1} and 3700 cm^{-1} and this was assigned to hydroxyl nests created by imperfections of the zeolite lattice [108], [109], [112]. Other FTIR investigations probing the effect of various dealumination techniques on the hydroxyl groups in zeolite Beta are in full agreement with the above workers [113], [114].

In addition to FTIR studies, ^{27}Al MAS NMR studies are also very useful in the study of zeolite acidity [115-119]. ^{27}Al MAS NMR studies are potentially very helpful for probing the quantity, coordination and location of aluminium atoms in aluminosilicates. It has been accepted that the 0 ppm peak, (from $Al(H_2O)_6^{3+}$ as a reference), is assigned to octahedral aluminium, and that at 50-60 ppm to tetrahedral framework aluminium. Heavy distortion of the tetrahedral or octahedral symmetry around the aluminium atoms causes a strong electric field gradient at the site of the nucleus. It strongly broadens the ^{27}Al NMR signal and therefore leads to some ^{27}Al NMR invisible peaks [115]. Loss of signal can be attributed to the quadrupolar nature of the ^{27}Al nucleus. In a low symmetry environment the second order interactions between the asymmetrical electric field gradient at the nucleus and the quadrupolar moment broadens the NMR signal beyond detection in a simple MAS experiment. Campbell *et al.*, [120] studied the effect of calcination and hydrothermal treatment on the dealumination of HZSM-5 zeolites. They found that treatment of the zeolite, whether dry heating or steaming, led to loss of ^{27}Al NMR signal intensity, despite findings that the aluminium content of the zeolite, as measured by chemical analysis, had remained unchanged. A similar decrease was observed in other studies concerning the steam treatment of HZSM-5 [118], [121], [122]. These workers concluded that calcination or hydrothermal treatment resulted in loss of tetrahedral aluminium species, the more severe the treatment, the greater the loss of total NMR visible aluminium. Following deammonation of the HZSM-5 a signal of small intensity appeared at 2 ppm, which was attributed to aluminium with octahedral symmetry and arises from aluminium removed from the zeolite lattice during activation. Upon further calcination or hydrothermal treatment, the intensity of this octahedral signal remained the same or decreased, suggesting that while the most easily removed aluminium in the lattice formed octahedral species, further treatment led to formation of alternative aluminium species of low symmetry. These workers also found a broad signal at approximately 30-40 ppm, which was observed in spectra of more severely treated samples. A similar signal was reported in studies of dealuminated Y [123], [124]. This signal can be attributed to aluminium in a distorted tetrahedral environment or 5-coordinate aluminium [125]. A study by Engelhardt *et al.*, [126] also reported that a small broad band in the 25-30 ppm region appeared in their ^{27}Al MAS NMR spectrum and could be due to penta-coordinated Al. An interesting study carried out by Kuehl *et al.*, [127] on zeolite Beta found that two types of octahedral species could be formed during steam treatment. On moderate steaming octahedral aluminium species created by partial hydrolysis of framework Si-O-Al bonds are formed, and upon severe steaming, a substantial proportion of the framework aluminium is completely hydrolyzed, and non-framework aluminium species are generated. The octahedral aluminium observed in the former case could convert reversibly to tetrahedral aluminium sites upon aqueous NH_4^+ exchange or reaction with NH_3 gas. A similar phenomenon was found by Bourgeat-Lami *et al.*, [109], they proposed that a fraction of the aluminium in the framework can reversibly change coordination from tetrahedral to octahedral without leaving its framework site. The same workers found that the preparation of protonic zeolite Beta by thermal decomposition of the ammonium form, or by exchange of alkali cations with dilute nitric acid, yielded a material that contained NMR invisible and octahedrally coordinated aluminium atoms. In infrared spectra, in addition to structural bridging hydroxyls and silanols, OH signals at 3665, 3680 and 3780 cm^{-1} were observed. Upon adsorption of pyridine at room temperature, or ammonia at 373 K, all the aluminium atoms recover a tetrahedral symmetry. In addition, exchange of the protons by ammonium, sodium and potassium cations by reaction of the zeolite with aqueous salt solutions at 353 K retransforms 6-coordinated aluminium into 4-coordinate aluminium. It was concluded by these workers that the introduction of protons into the lattice of zeolite Beta severely disturbs the coordination of some framework aluminium atoms. In the presence of water the distorted sites may feature an octahedral symmetry or undergo hydrolysis of the Al-O bonds. Partially hydrolyzed aluminium sites would account for the various hydroxylated species evidenced by infrared spectroscopy and for the NMR invisible aluminium.

The composition and Si/Al ordering of zeolite frameworks can be deduced by ^{29}Si MAS NMR studies. Using this technique it is possible to distinguish all five possible Si(nAl) building units, where Si(nAl) represents an SiO_4 tetrahedron linked to $nAlO_4$ tetrahedra and to (4-n) other SiO_4 tetrahedra. Kunkeler *et al.*, [114], and other workers [112], [128] assigned these five possible building units to the following chemical shift positions, -98 ppm $Si(OSi)_2(OAl)_2$, -105 ppm $Si(OSi)_3(OAl)$ or $Si(OSi)_3(OH)$, -111 ppm and –115 ppm (both attributed to $Si(OSi)_4$. The ratio of tetrahedral silicon and aluminium atoms in the zeolite framework can be directly calculated from the Si(nAl) peak intensities in a ^{29}Si MAS NMR spectrum according to Engelhardt *et al.*, [126]. The resulting $Si/Al_{Si\ NMR}$ ratio, however, does not correspond to the real Si/Al_{fw} ratio when defect sites (SiOH) are present in the framework, because the peaks due to Si(nAl) and Si(nOH) overlap in the ^{29}Si spectrum. Thus, the $Si/Al_{Si\ NMR}$ ratio is always lower than the actual Si/Al_{fw} ratio [129]. An ^{29}Si MAS NMR study by Campbell *et al.*, [120] concerning the dealumination of H-ZSM-5 found loss of signal intensity for the Si(1Al) component following calcination or hydrothermal treatment of the zeolite samples which indicates that Si-O-Al bonds in the zeolite lattice are breaking. A narrowing of the Si(0Al) signal and changes in its profile was also observed and are indicative of loss of aluminium from the lattice [122].

^{1}H MAS NMR can also be used as a non-invasive method of determining the acidity of zeolites. Müller *et al.*, [129] studied the dealumination of zeolite Beta, Mordenite and ZSM-5 by thermal treatment, leaching with oxalic acid and treatment with $SiCl_4$, and used a combination of ^{1}H, ^{29}Si and ^{27}Al MAS NMR studies to determine the effect on acidity. Three signals were found to be present in the ^{1}H NMR spectrum, at 1.8, 4.4, and 3-7 ppm. On the basis of literature [130] the peak at 1.8 ppm is due to non-acidic OH groups attached to Si in the framework, the component at 4.4 ppm was due to bridged acidic OH (Si(OH)Al) groups, and the broad component between 3 and 7 ppm was due to hydrogen bonded silanols and/or bridged Brønsted groups. The ^{1}H MAS NMR carried out by Müller *et al.*, [129] showed that the extent of dealumination in zeolites increased with the number of Brønsted acid sites interacting with the zeolite framework.

The use of XRD has also been successfully applied by some workers to determine if dealumination of a zeolite sample has occurred. Line broadening in powder XRD is related to both the size of coherent crystalline domains and to lattice imperfections or strains [131]. Zeolite Beta produces sharp ($h = 3n$, $k = 3n$) and broad peaks in XRD patterns, consistent with faulting by a/3 and b/3 displacements on (001) planes. Thus, as a first approximation, the width of sharp (3n,3n,l) reflections will be mainly determined by the crystal size, while that of the broad reflections is related to faultings. In a study on nanocrystalline Beta, Camblor *et al.*, [132] reported an increased peak broadening and a shift to lower 2θ values as the Al content of their nanocrystalline Beta increased. These authors suggested that this could be taken as an indication of the isomorphous substitution of Si by Al in the framework. A study by Trombetta *et al.*, [113] concerning surface acidity modifications induced by thermal treatments and acid leaching on microcrystalline H-Beta found a similar phenomenon. These workers found that there was no loss in crystallinity after calcination and acid treatments, however their XRD profiles showed that the position of the peak shifts towards higher 2θ values as the amount of aluminium inside the framework decreases. The peak moved from 22.43 to 22.48 2θ values when the treatment temperature increases from 773 to 923 K, confirming that thermal treatment caused progressive dealumination. When the thermal treatment at 923 K was followed by an acid washing, the 2θ value increased further up to 22.62. However, if the sample is washed once again, a shift towards lower 2θ values (22.53) was observed. This may indicate that, under these conditions, a partial realumination of the surface occurred [109].

The acidic strength of both Brønsted and Lewis acid sites can be deduced from Temperature Programmed Desorption of ammonia (TPDA) studies [133], [134], or TPD of pyridine [135-137]. A study by Camiloti *et al.*, [134] investigated the acidity of zeolite Beta as determined by TPD of ammonia. In this study the acidity of zeolite Beta samples with Si/Al ratios ranging from 18 to 33 was determined using appropriate temperature programmed desorption of ammonia conditions. Samples with greater Si/Al ratios presented higher acid strength by retaining ammonia at higher temperatures. These results indicate that as the aluminium content in zeolite Beta is reduced, the strength of the associated acid sites increases.

The acidic properties of zeolite catalysts can also be modified by ion exchange with different metals. Fe-zeolites have recently seen renewed interest due to their ability to catalyze selective reactions in various fields. Mauvezin *et al.*, [138] investigated the identification of iron species in Fe-Beta zeolite. In this study a series of Fe-zeolite Beta samples were prepared either by exchanging parent Beta (Si/Al = 12.5) with $Fe(NO_3)_3$ or by impregnation. The identification of Fe species in Fe-Beta was carried out by temperature-programmed reduction with H_2 or CO, and Mössbauer and DRIFT spectroscopies after various pretreatments. The pretreatment consisted of the calcination by O_2, the reduction by H_2, and the calcination by N_2O of the pre-reduced sample. After calcination in O_2, Fe_2O_3 aggregates were only present when the exchange level exceeded 100%. At an exchange level lower than 100%, Fe would mainly be present as binuclear oxocations of the type $\{(OH)FeOFe(OH)\}^{2+}$, with the proportion decreasing as Fe content decreased. There were some un-reducible Fe atoms, possibly in tetrahedral coordination in the zeolite framework. After the calcination in N_2O of pre-reduced Fe-Beta, the great difference was in the formation of different Fe oxocations, much more easily reducible than those formed upon calcination in O_2. It was postulated that these specific oxocations would be composed of mononuclear Fe species. A study by Joyner *et al.*, [139] investigated the preparation, characterization, and performance of Fe-ZSM-5 catalysts. In this study a number of Fe-ZSM-5 catalysts were prepared and characterized by various techniques. Iron was introduced by aqueous exchange, by a novel method proposed by Feng *et al.*, [140], by exchange from a rigorously dried methanolic solution accompanied by agitation with ultrasound, and by a method intended to promote solid state exchange. The degree of interaction with the zeolite framework was probed by examining the effect on the zeolite proton OH band in the infrared spectrum. Less than 30% of the protons were exchanged from aqueous solution, but almost 80% exchange was achieved using ultrasound, as well as the method reported by Feng et al. Initially, both methods exhibited mainly isolated metal ions; however, calcination of the samples prepared according to Feng *et al.*, [140] exhibited rather large oxide clusters. After aqueous exchange and activation, most of the iron present was in the form of small oxygen containing nanoclusters within the zeolite matrix, with EXAFS measurements indicating an average composition of Fe_4O_4. Depending on the preparation methods, isolated cationic species within the zeolite matrix were also found. The small Fe_4O_4 type clusters could not be reduced to the metallic state, even by hydrogen at 1100 K, although inter-conversion between Fe(II) and Fe(III) was easy. Correlations between catalytic activity in the selective catalytic reduction of NO_x by propene in oxygen/helium and the infrared spectroscopy results for adsorbed NO indicated that nanoclusters were more active (per iron atom) than isolated cations.

1.9.3 Studies probing the relationship between active sites and activity

Many studies contained in the extensive literature in this field have related the acidity of modified zeolite structures to their catalytic activity in a model reaction. Gaare *et al.*, [141] investigated modified zeolites as catalysts in Friedel Crafts acylation. Modified zeolites were found to be active catalysts in Friedel Crafts acylation of anisole by acetyl chloride and acetic anhydride. The effect of two different modifications of the zeolites were tested; lanthanum exchange and varying the Si/Al ratio. For the rare earth modified zeolites, the activity was found to be dependent on the lanthanum content, and the yield increased with the level of lanthanum even up to 93% exchange. Dealuminated faujasite was also found to be very active, and an almost linear increase in the yield with decreasing aluminium fraction was found. This was attributed to the increased hydrophobicity of the dealuminated zeolites. In contrast with a study carried out by Freese *et al.*, [67], who studied the acylation of aromatic compounds on H-Beta zeolites. These workers studied the Friedel Crafts acylation of anisole by acetic anhydride and the Fries rearrangement of phenyl acetate in the liquid phase using the H form of various zeolites. Comparing the activity of NH_4-Y with that of H-Y zeolite it was found that the presence of Brønsted acidic sites was a necessary prerequisite for the catalytic activity. However, dealumination of H-Beta zeolite, i.e. the reduction in the number of Brønsted acidic sites, did not favour a further increase in catalytic activity. These results were found to be in agreement with data published by Harvey *et al.*, [74] who studied the same reaction on several zeolites. However, H-Beta and H-Beta (dealuminated) zeolites were found to differ in their kinetic behaviour. The dealuminated H-Beta zeolite showed a higher activity in the initial period compared to H-Beta zeolite. They assumed that this phenomenon was due to the improved diffusion in the dealuminated sample caused by changes in pore distribution. Ma *et al.*, [142] studied the Friedel Crafts acylation of anisole over zeolite catalysts. They investigated the liquid phase acylation of anisole with alkanoic acids, anhydrides and substituted benzoic acids. When carboxylic acids were used as acylating agents, the activity of faujasite increased with its Lewis acidity, showing that Lewis acid sites were more active than the Brønsted acid sites. Spagnol *et al.*, [78] in a similar investigation found that Brønsted acids activate more strongly acetic anhydride than Lewis acids do, and Lewis acids exhibit a higher complexation affinity with acylchloride compared with Brønsted acid sites. Bhattacharya *et al.*, [143] studied the selective benzoylation of naphthalene to 2-benzoylnaphthalene using H-Beta catalysts. The liquid phase benzoylation of naphthalene was investigated in the temperature range 333 - 358 K using benzoyl chloride as the benzoylating agent. H-Beta was found to catalyze the reaction efficiently and selectively to 2-benzoylnaphthalene and was found to be superior to the other zeolite catalysts and $AlCl_3$. The conversion of benzoyl chloride to the products largely depends upon the reaction conditions and the acidity of the zeolite. It was concluded that the presence of strong Brønsted acid sites in the zeolite catalysts appears to be very important for the polarization of benzoyl chloride into an electrophile ($C_6H_5CO^+$) which then attacks the naphthalene ring resulting in the formation of benzoyl naphthalenes. Quaschning *et al.*, [144] studied the properties of modified zirconia as a Friedel Crafts acylation catalyst. Both precipitated and aerogel synthesized zirconia were modified employing gaseous and solid compounds, respectively, as well as concentrated mineral acids. It was found that zirconia prepared with solid ammonia sulfate or ammonia sulphite generates very high Brønsted acidity at the zirconia surface after a certain calcination procedure. Increased acidity can be achieved using aerogel techniques for the synthesis of sulfated zirconia, in this case a comparatively large BET surface area, combined with a high concentration of Brønsted acid sites was obtained. These workers concluded that, under the conditions applied, that the benzoylation of anisole occurs exclusively on Brønsted acid sites. In contrast, solid Lewis acids showed little or no conversion of the benzoylation agents into the desired aromatic ketones. Choudary *et al.*, [57] studied the acylation of aromatic ethers with acid anhydrides in the presence of cation-exchanged clays. The best results were obtained when Fe^{3+} and Zn^{2+} exchanged clays were employed as catalysts. The higher activities obtained using Fe^{3+} and Zn^{2+} exchanged montmorillonites were attributed to the synergistic effect of Brønsted and Lewis acidities. Singh *et al.*, [145] found that acidic zeolites are active in the benzoylation of toluene with benzoyl chloride. The results of this study showed that zeolite H-Beta was the most active and selective zeolite catalyst. $AlCl_3$ gave lower conversion of benzoyl chloride compared to the H-Beta at 18h reaction time. The total acidity of the zeolites did not show any correlation between acidity and catalytic activity; however, strong acid sites of H-Beta and Re^{3+}-exchanged faujasite enhanced the benzoyl chloride conversion considerably. These workers also found that an increase in the Si/Al ratio of the

H-Beta resulted in a decrease in the formation of methylbenzophenones. Isaev *et al.*, [146] studied the liquid phase thiophene acylation by butyryl chloride using zeolites. HZSM-5, H-mordenite and USY (ultrastable Y) with various framework Si/Al ratios, various numbers of Brønsted and Lewis acid sites, and various amounts of nonframework aluminium were employed. The number of Brønsted and Lewis acid sites was obtained by FTIR using chemisorbed ammonia. These workers found a correlation between the initial rates of reaction and the number of Lewis acid sites, whereas there was no correlation between initial rates and the number of Brønsted sites. This conclusion on the overwhelming role of Lewis acidity in acylation contradicts the opinion of Corma *et al.*, [65] who by a series of experiments using faujasite and HZSM-5 concluded that the active sites are the Brønsted sites. Heinichen *et al.*, [111] studied the effect of modification of zeolite Beta on its catalytic behaviour in the acylation of aromatics. They found that zeolite Beta with different Si/Al ratios dealuminated by acid treatment showed enhanced catalytic activity in the acylation of anisole compared to the untreated material. However the Si/Al ratio was found to have no influence on the catalytic results. It was presumed that acid centres – silanol groups – in the micropores, not linked to framework aluminium, are the catalytic active species. A severe calcination of zeolite H-Beta resulted in a more profound increase of catalytic activity in the acylation of anisole. This was assumed to be caused by acid groups of the formed extraframework alumina, possibly migrated on the outer surface. The activity of the severe calcined sample was reduced by acid treatment; this was due to the removal of extraframework aluminium. Haouas *et al.*, [147] studied the effect of flexible lattice aluminium in zeolite Beta during the nitration of toluene with nitric acid and acetic anhydride. These workers found that the framework aluminium in H-Beta plays a critical role during the nitration reaction. They observed the reversible transformation of the coordination environment of the tetrahedral lattice aluminium into an octahedral coordination upon interaction with nitric acid, acetylnitrate and acetic acid. The ability of H-Beta to accommodate such a coordination state transformation was found to be consistent with the high degree of lattice flexibility of this zeolite and makes it unique for this type of reaction. The narrow width of the ^{27}Al NMR signal of the aluminium complexes formed when nitrate ions interact with the zeolite wall suggested the necessity of the opening of the Si-O-Al bond in the lattice to accommodate a very high symmetry environment. The dynamic character of those aluminium atoms, which are only partially connected to the framework, were thought to play a key role in the catalytic activity and selectivity. Nitration occurs through surface bonded acetylnitrate as the reactive nitrating species, and since classical shape selectivity concepts do not account for the observed selectivity patterns with this large pore zeolite, they concluded that the product selectivity was dictated by steric hindrance during the formation of the Wheland intermediate which is induced by adsorption on the zeolite surface. These workers concluded that the reason for the high para-selectivity was the presence of a surface bonded nitrating species which forms the sterically less demanding Wheland intermediate in which the methyl group points towards the main channel. A proposal along the same lines was made by Nagy *et al.*, [148] for the nitration of substituted aromatics over HZSM-11 without specifying the nature of the active site that could cause such action. Haouas *et al.*, [147] stated that the possibility that nitronium ions fixed to the oxide matrix of the zeolite on the Brønsted acid site and becoming a nitrate-like moiety could not be completely discarded, however this was thought to be unlikely since this type of interaction would be unlikely to lead to a change in the coordination symmetry.

1.9.4 Studies concerning catalytic aging/deactivation

Catalyst aging or deactivation is a time dependent decay of catalyst activity and/or selectivity that can ultimately be caused by a change in the number, nature, or accessibility of the catalyst sites. While rapid declines in conversion are experimentally quite obvious, some selectivity changes may be more subtle, reflecting differences in steric, electronic, dielectric, or mass transport/diffusion properties of the catalyst. If decay rates are rapid, measurement of accurate kinetic parameters can also be challenging [149]. A diversity of factors can lead to aging. Strong adsorption of even small amounts of impurities that can have a strong affinity for catalytic active sites can lead to severe poisoning effects. Commercial feedstocks frequently contain appreciable quantities of such poisons, although some are process generated. Build-up of higher molecular weight organic polymer not only block active sites, but can ultimately occlude pores with coke. Zeolitic 'coke' in its most general sense is a term used to describe a variety of higher molecular weight materials formed within zeolite pores or on the external surface [85], [150], [151]. Coke may range in nature from simple olefin oligomers or other species with low diffusivities that are strongly chemisorbed at acid sites all the way to highly aromatic, hydrogen deficient carbonaceous material that may be the end result of hydrogen transfer processes and high temperature reactions, and which can be removed only by oxidative regeneration or other severe processes. Karge *et al.*, [151] gives an excellent account on coke formation in zeolites, including its characterization and mechanism of formation. In addition to coke, adsorption of organometallic poisons, e.g. V or Ni complexes, can cause selectivity deterioration (e.g. gas and coke from Ni) or ultimately zeolite lattice damage (from V). The presence of water, either as reactant or product, in a zeolite catalyst system may not be harmful or may even be beneficial [152] under certain circumstances. On the other hand, prolonged or multiple-cycle exposure of the zeolite to steam (e.g. in oxidative regeneration), particularly at high temperatures, can result in loss of tetrahedral aluminium sites or other structural damage [153]. Rohan *et al.*, [76] studied the acetylation of anisole by acetic anhydride over H-Beta zeolite and aimed to determine the origin of deactivation of the catalyst. The liquid phase acetylation over H-Beta zeolite of anisole with acetic anhydride in equimolar amounts was carried out in a batch reactor at 333 K. It was found that p-methoxyacetophenone (p-MAP) was selectively and rapidly formed on the fresh catalyst. However, a rapid deactivation occurred which was attributed to a large extent to the pronounced inhibiting effect that p-MAP has on the acetylation. In a flow reactor and at higher temperature (363 K), the catalyst deactivation was much slower particularly when an anisole rich (anisole/acetic anhydride molar ratio of 5) was used as reactant. Catalyst samples were recovered after various times on stream and the organic material, which was retained in significant amounts on the zeolite, was analysed by GC and GC/MS. The major part of this material, which consisted of p-MAP, could be recovered by soxhlet extraction in methylene chloride. Due to its high polarity, this reaction product was strongly retained in the large mesoporous volume of the H-Beta zeolite. The minor part could only be recovered after dissolution of the zeolite in a hydrofluoric acid solution. It consisted mainly of di- and tri-acetylated anisole entrapped in the zeolite micropores. As these workers showed by nitrogen adsorption, these compounds cause pore blockage. The latter was responsible for part of the catalyst deactivation, the other part being due to p-MAP located in the mesopores. The use of an excess of anisole enhanced catalytic activity as it limited both the retention of p-MAP and the formation of poly-acetylated anisoles. Derouane *et al.*, [154] also studied catalyst deactivation in the acetylation of anisole. In this study the liquid phase acetylation of anisole by acetic anhydride (anisole:acetic anhydride in a molar ratio of 2:1) using zeolite H-Beta (Si/Al=11) as catalyst was carried out in a batch reactor at 363 K, without and with addition of the product, p-MAP. As was expected, acetic acid and p-MAP were produced in equal amounts during the initial stages of the reaction but acetic acid was consumed at long reaction time and high conversion. Partial zeolite dealumination of the used catalyst was evidenced by ^{27}Al MAS NMR spectroscopy and the regenerated catalyst showed a lower activity agreeing with its reduced Al content, i.e., acidity. Without added p-MAP, acetylation occurs rapidly at low conversion but deactivation becomes important as conversion increases. The reaction rate is largely decreased when p-MAP is added to the reaction mixture, indicating inhibition of the reaction by p-MAP. A detailed kinetic analysis using a Langmuir-Hinshelwood model was performed to quantify the nature and extent of the reaction inhibition by p-MAP. It showed that the adsorption equilibrium constant for p-MAP exceeds by a factor of at least 6 the adsorption equilibrium constant for any of the reactants, and that the occupancy of the intracrystalline volume of the zeolite by p-MAP increases rapidly with conversion, thereby reducing the access of the reactants to the catalytic sites. It was concluded that the deactivation of the catalyst as conversion increases was mainly due to product inhibition, i.e. the competitive adsorption of the reactants and products in the zeolite intracrystalline volume, which could be rationalized in terms of the zeolite acting as a solid solvent. Moreau *et al.*, [155] studied the acetylation of dimethoxybenzenes with acetic anhydride in the presence of acidic zeolites. These workers found, in contrast to Derouane *et al.*, [154], that the use of regenerated catalyst (zeolite washed and reactivated at 823 K to eliminate organic products) resulted in the same activity and initial rate as the fresh catalyst. Similarly Smith *et al.*, [66] studied the synthesis of aromatic ketones by acylation of aryl ethers with carboxylic acids in the presence of H-Beta. These workers also found that the zeolite could be recovered, regenerated and reused to give almost the same yield as the fresh zeolite. However, in agreement with Derouane *et al.*, [154], Bhattacharya *et al.*, [143] studied the benzoylation of naphthalene to 2-benzoylnaphthalene using zeolite H-Beta. These workers found that H-Beta, recycled four times, resulted in a slight decrease in benzoyl chloride conversion after each cycle, this was attributed to the minor dealumination of the zeolite catalyst by HCl formed during the reaction. Similarly Jacob *et al.*, [156] studied the benzoylation of o-xylene to 3,4-dimethylbenzophenone using various zeolite catalysts. The spent H-Beta catalyst was recycled three times without loss of product selectivity but with a decline in the catalytic activity. In this case, the catalyst was removed from the reaction mixture by filtration, washed thoroughly with acetone, calcined at 773 K for 16 h in the presence of air and characterised for its chemical composition (Si/Al) and crystallinity. In order to check the structure and crystallinity of the catalyst after reaction, X-ray powder diffraction patterns were recorded. XRD measurement indicated that the catalyst retains the H-Beta structure and the crystallinity was found to be 71.4% (after third recycle) when compared to the parent catalyst (100% crystallinity). It was concluded that the HCl liberated during the reaction promotes the extraction of aluminium to some extent from the framework positions of zeolite H-Beta. Such types of extractions and a little decrease in the crystallinity of H-Beta may be responsible for the decrease in catalytic activity after each cycle. Freese *et al.*, [67] studied the acylation of aromatic compounds on H-Beta zeolites. These workers observed a change in the colour of the catalyst from white to dark brown and took this as an indication of coking. To study the influence of coke formation, the spent catalyst was exposed to a fresh reaction mixture. They found that the catalyst was still active, i.e. the loss in activity of the activated H-Beta zeolite was probably caused by the deposition of higher molecular weight compounds ('coke'). The fresh reaction mixture added was able to extract these compounds, the desorption of which was hindered. In addition, after a typical reaction run, the coked catalyst was ex situ extracted with dichloromethane and used in a second run, and they demonstrated that the activity was further improved. When used catalyst was regenerated in air at 770 K for 4 h, the initial activity was completely restored, i.e. the non-extractable coke forming compounds were removed by oxidation. They concluded that two types of coke exist in the channel system and/or on the external surface: (1) extractable ('reversible'), and (2) non-extractable ('irreversible') coke.

1.9.5 Studies investigating competitive adsorption effects in zeolite catalysis

Derouane *et al.*, [157] studied the competitive adsorption of reactants and products in the Friedel Crafts acetylation of anisole and toluene. The liquid phase acetylation of anisole by acetic anhydride and isopropenyl acetate, and that of toluene by acetic anhydride, using zeolites H-Beta, HMFI, and HFAU as catalysts was studied. Evidence was obtained for competitive adsorption effects of the reactants resulting from differences in their adsorption equilibrium constants (AEC). Estimated values of the AEC show that preferential adsorption is in the order toluene < acetic anhydride < anisole < isopropenyl acetate. In all cases, the acetylation products were adsorbed more strongly than the reactants, but the competitive adsorption of acetic acid and acetone appeared to be negligible when acetic anhydride and isopropenyl acetate were used as acylating agents. The effect of dealumination was investigated for the acetylation of toluene by acetic anhydride, using H-Beta as catalyst. Both the initial and the quasi-stationary state reaction rates were proportional to Al content, i.e., the number of Brønsted sites at low Al content. The rates decreased at high aluminium content, indicating that competitive adsorption effects were enhanced due to increased zeolite polarity and polarisability. These workers concluded that competitive adsorption effects, involving both reactants and products, need to be controlled in order to achieve maximum catalytic performance when zeolites are used as catalysts in the liquid phase. Moreau *et al.*, [155] studied the acetylation of dimethoxybenzenes with acetic anhydride in the presence of acidic zeolites. They evidenced the competitive adsorption of both reactants and products, and they concluded that the deactivation of the catalyst was due to a partial adsorption of the reaction product, 3-4-dimethoxyacetophenone, and acetic acid formed during the reaction.

1.9.6 Studies probing the mechanism of acylation on zeolite catalysts

Electrophilic aromatic substitution involves attack of an electron deficient species, E^+, on an aromatic, ArH, to form a larger aromatic product, Ar-E. In ‘classical’ organic chemistry, the first phase of this process may sometimes be interaction of the approaching electrophile with the π orbitals of the aromatic to form a π complex. The next stage involves localized attack of the electrophile on a ring carbon atom to form a carbocation, often termed a σ complex or arenium ion, in which the positive charge is delocalised over the five remaining nuclear carbon atoms, and the H atom and E group are in a plane perpendicular to that of the ring carbocation. The formation of the arenium ion is frequently but by no means always the rate-determining step, depending on the nature of the system. C-H bond breakage and expulsion of a proton in the last step complete the substitution process and provide stabilization by restoration of ring aromaticity [153]. It has been well established that the acylation reaction proceeds through an acylium intermediate RCO^+, generated from the adsorption of the acylating agent onto the Brønsted acidic sites of the zeolite catalyst, which then reacts with the aromatic substrate [65], [145], [156], [158-161]. **Figure 1.9.6.1** shows the catalytic cycle of a plausible mechanism for the acylation of anisole with acetic anhydride by the Brønsted acid sites of a zeolite.

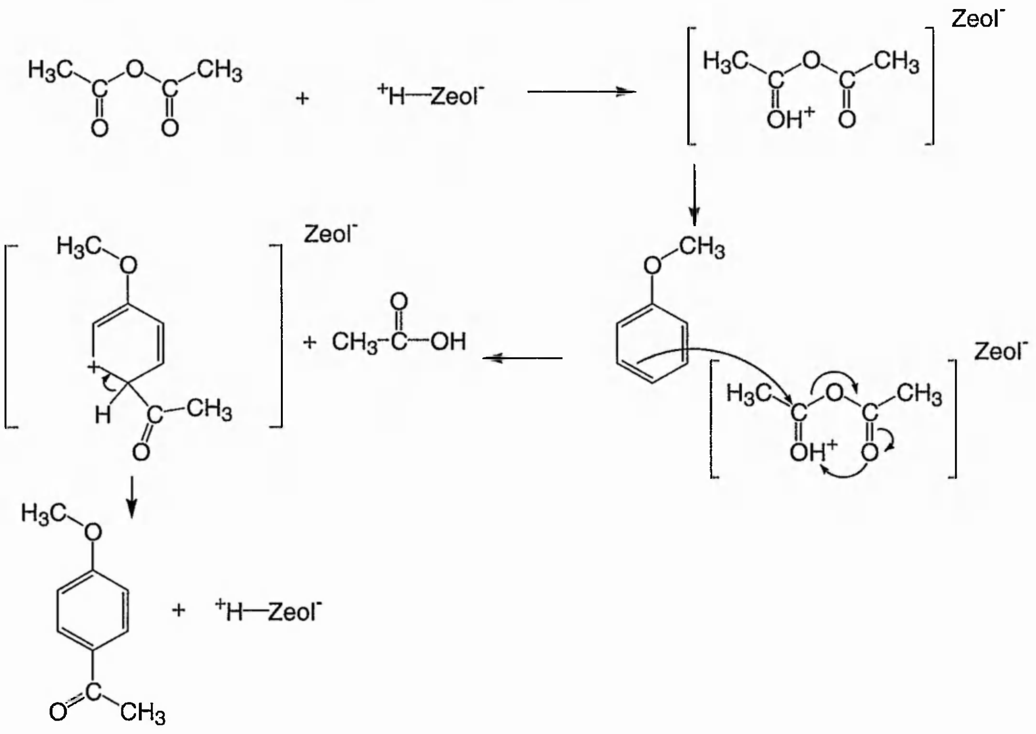

Figure 1.9.6.1 Plausible mechanism for the acylation of anisole with acetic anhydride by Brønsted acid sites [61].

The acylating agent can be adsorbed competitively on equivalent Brønsted acid sites of the surface, such a possibility is a characteristic of a Langmuir-Hinshelwood process, where the initial rate presents a maximum as a function of the initial concentration of each reactant. The reaction can also proceed through the attack of the acylium ion on the aromatic substrate in the liquid phase, which corresponds to a pure Eley-Rideal mechanism, where a first order is observed, whatever is the initial substrate concentration. Moreau *et al.*, [155] studied the acylation of dimethoxybenzenes with acetic anhydride and their results did not correspond to any of these two possibilities. They suggested that a modified Eley-Rideal type process, where a molecule of the adsorbed acetic anhydride reacts with veratrole in the liquid phase, but in which veratrole is also adsorbed on the active sites of the catalyst, acting in some way as a poison. Ma *et al.*, [142] studied the acylation of anisole over zeolite catalysts. These workers found that in faujasite, Lewis acid sites were more active and selective than Brønsted acid sites for the Friedel Crafts acylation of the aromatic ring with carboxylic acids. The electrophilic intermediate formed from anhydrides would be the acylium cation; while when carboxylic acid was used as acylating agent, the carboxylic acid protonated by the Brønsted acid sites or coordinated on the Lewis acid sites of the zeolite catalyst would react directly with the aromatic ring. The protonated carboxylic acid form was less reactive than the coordinated one for attack at the aromatic ring, but more reactive for the acylation at the oxygen atom of the anisole. Along similar lines, Kouwenhoven *et al.*, [162] studied the acylation of aromatics over zeolite catalysts. They found that Lewis acid catalysts were preferred when applying acid chlorides, and Brønsted acid catalysts when using acid anhydrides or carboxylic acids as acylating agents. The acylating agents form adducts with Lewis acid catalysts *via* the carbonyl oxygen atoms. As a result the carbonyl bond is strongly polarized, and the carbon atom becomes sufficiently electrophilic to interact with the aromatic π electron system, so that a reaction may occur. With Brønsted acid catalysts the carbonyl bond is protonated. The resulting complex is the acylating agent or an acylium ion, formed in a cleavage reaction with HX as by-product. Haouas *et al.*, [147] studied the effect of flexible lattice aluminium in zeolite Beta during the nitration of toluene with nitric acid and acetic anhydride. They concluded that surface bonded acetylnitrate was the active nitrating species, and that acetylnitrate coordinates to lattice aluminium forming an adsorption complex of distorted octahedral geometry. The formation of this adsorption complex was possible because of the flexible framework aluminium species, which are abundantly available in H-Beta zeolite. **Figure 1.9.6.2** shows the most likely structure of the active nitrating species.

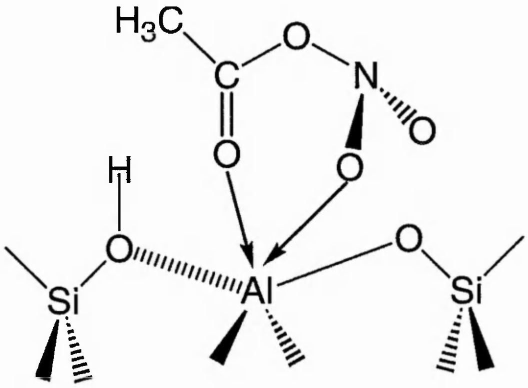

Figure 1.9.6.2 Most likely structure responsible for the active nitrating species [147].

References

(1) McMurry, J. *Organic Chemistry*; Fourth Edition ed.; Brook/Cole Publishing Company, 1996; pp 583.

(2) Szostak, R. *Molecular Sieves (Principles of Synthesis and Identification)*; Van Nostrand Reinhold, 1989.

(3) *Catalysis - An integrated approach to Homogeneous, Heterogeneous and Industrial Catalysis*; Moulijn, J. A., Van Leeuwen, P. W. N. M., van Santen, R. A., Eds.; Elsevier Science: Amsterdam, 1993; pp 318.

(4) Breck, D. W. *US patent 3 130 007* 1964.

(5) Argauer, R. J.; Landolt, G. R. *US patent 3 702 886* 1972.

(6) Csicsery, S. M. *Zeolites* 1984, ***4***, 202.

(7) Derouane, E. G. *Catalysis on the Energy Scene*; Kaliaguine, S., Mahay, Eds.; Elsevier: Amsterdam, 1984; pp 1.

(8) Chen, N. Y.; Gorring, R. L.; Ireland, H. R.; Stein, T. R. *Oil Gas J.* 1977, ***165***, 6.

(9) Thomas, J. M.; Thomas, W. J. *Principles and Practice of Heterogeneous Catalysis*; VCH, 1997.

(10) Derouane, E. G.; Dejaifve, P.; Gabelica, Z.; Vedrin, J. C. *Disc. Faraday Soc* 1981, ***72***, 331.

(11) Gates, B. C. *Catalytic Chemistry*; John Wiley and Sons, 1992; pp 270.

(12) Lombardo, E. A.; Sill, G. A.; Hall, W. K. *J. Catal.* 1989, ***119***, 426.

(13) Aronson, N. T.; Gorte, R. J.; Farneth, W. E. *J. Catal.* 1986, ***98***, 434.

(14) Uytterhoven, J. B.; Christ, L. G.; Hall, W. K. *J. Phys. Chem.* 1965, ***69***, 2117.

(15) Sohn, J. R.; DeCanio, S. J.; Fritz, P. O.; Lunsford, J. H. *J. Phys. Chem.* 1986, ***90***, 4847.

(16) Haag, W. O.; Lago, R. M.; Weisz, P. B. *Nature* 1984, ***309***, 589.

(17) Lunsford, J. H. *J. Phys. Chem.* 1968, ***72***, 4163.

(18) Miradatos, C.; Barthomeuf, D. *J. Chem. Soc. Chem. Commun.*. 1981, ***39***.

(19) McVicker, G. B.; Kramer, G. M.; Ziemiak, J. J. *J. Catal.* 1983, ***83***, 286.

(20) Dyer, A.; Singh, A. P. *Zeolites* 1988, ***8***, 242.

(21) Beyerlein, R. A.; McVicker, G. B.; Yacullo, L. N.; Ziemiak, J. J. *ACS Meet. Div. Pet. Chem.* 1986, ***31***, 190.

(22) Fritz, P. O.; Lunsford, J. H. *J. Catal.* 1989, ***115***, 85.

(23) Yin, F.; Blumenfeld, A. L.; Gruver, V.; Fripiat, J. J. *J. Phys. Chem B* 1997, ***101***, 1824.

(24) Hidalgo, C. V.; Itoh, H.; Hattori, T.; Niwa, M.; Murakami, Y. *J. Catal.* 1984, ***85***, 362.

(25) Pfeifer, H. *NMR Basic Principles and Progress*; Springer, Ed. Berlin, 1994; pp 31.

(26) Karge, H. G. *Stud. Surf. Sci. Catal.* 1991, ***65***, 133.

(27) Dwyer, J. *Stud. Surf. Sci. Catal.* 1987, ***37***, 33.

(28) Knozinger, H. *Elementary Reaction Steps in Heterogeneous Catalysis*; Joyner, R. W., van Santen, R. A., Eds.; Kluwer Academic Publishers: Dordrecht, 1993; pp 267.

(29) Brunner, E.; Pfeifer, H. *Molecular Sieves -- Science and Technology*; Karge, H. G., Weitkamp, J., Eds.; Springer; Vol. 6.

(30) Bellussi, G.; Pazzuconi, G.; Perego, C.; Girotti, G.; Terzoni, G. *J. Catal.* 1995, ***157***, 227.

(31) Hoefnagel, A. J.; van Bekkum, H. *Appl. Catal. : A* 1993, ***97***, 87.

(32) Rigutto, M. S.; Vries, H. J. A.; Magill, S. R.; Hoefnagel, A. J.; van Bekkum, H. *Stud. Surf. Sci. Catal.* 1993, ***78***, 661.

(33) Smith, K.; Musson, A.; DeBoos, G. A. *J. Chem. Soc. Chem. Commun.* 1996, 469.

(34) de Jong, K. P.; Mesters, C. M. A. M.; Peferoen, D. G. R.; van Brugge, P. T. M.; de Groot, C. *Chem. Eng. Sci* 1996, ***51***, 2053.

(35) Jansen, J. C.; Creyghton, E. J.; Njo, S. L.; van Koningsveld, H.; van Bekkum, H. *Catal. Today* 1997, ***38***, 205.

(36) van Koningsveld, H.; Jansen, J. C. *Microporous Mater.* 1996, ***6***, 156.

(37) Jacobs, P. A.; von Ballmoos, R. *J. Phys. Chem.* 1982, ***86***, 3050.

(38) Barthomeuf, D.; Beaumont, R. *J. Catal.* 1993, ***30***, 288.

(39) Rastelli, H.; Lok, B. M.; Duisman, J. A.; Earls, D. E.; Mullhaupt, J. T. *Can. J. Chem. Eng.* 1982, ***60***, 44.

(40) Cesteros, Y.; Haller, G. L. *Microporous Mater.* 2001, ***43***, 171.

(41) Kosslick, H.; Landmesser, H.; Fricke, R. *J. Chem. Soc., Faraday Trans.* 1997, ***93***, 1849.

(42) Sheldon, R. A.; Downing, R. S. *Appl. Catal. : A* 1999, ***189***, 163.

(43) Franck, H. G.; Stadelhofer, J. W. *Industrial Aromatic Chemistry*; Springer-Verlag, Ed. Berlin/Heidelberg, 1987.

(44) van Bekkum, H.; Hoefnagel, A. J.; van Koten, M. A.; Gunnewegh, E. A.; Vogt, A. H. G.; Kouwenhoven, H. W. *Stud. Surf. Sci. Catal.* 1994, ***83***, 379.

(45) Gore, P. H. *Friedel-Crafts and Related Relations*; Olah, G. A., Ed.; Wiley Interscience: New York, 1964; Vol. 3, part 1.

(46) Harvey, G.; Mader, G. *Collect. Czech. Chem. Commun.* 1992, ***57***, 862.

(47) Fazzini, F.; Fornasari, G.; Vaccari, A.; Valdiserri, L.; Carrozza, P. *Book of abstracts of 3rd International Symposium on Acid-Base Catalysis*; Rolduc, Ed. The Netherlands, April 1997.

(48) Richard, F.; Carreyre, H.; Pérot, G. *J. Catal.* 1996, ***159***, 427.

(49) *Encyclopedia of Chemical Technology*; Fourth Edition ed.; Kroschwitz, J. I., Howe-Gremt, M., Eds.; Wiley Interscience: New York; Vol. 11; pp 1055.

(50) Hino, M.; Arata, K. *Chem. Lett.* 1978, 325.

(51) Arata, K.; Hino, M. *Chem. Lett.* 1980, 1479.

(52) Effenberger, F.; Epple, G. *Angew Chem. Int. Ed. Engl.* 1972, ***11***, 300.

(53) Kaward, A.; Mitamurd, S.; Kobayashi, S. *J. Chem. Soc. Chem. Commun..* 1993, 1157.

(54) Hino, M.; Arata, K. *J. Chem. Soc. Chem. Commun.* 1985, 112.

(55) Arata, K.; Hino, M. Proc. 9th Int. Congr. on Catalysis, Chem. Soc. , Canada; Phillips, M. J., Ternan, M., Eds., 1998; pp 1727.

(56) Choudary, B. M.; Kantam, M. L.; Sateesh, M.; Rao, K. K.; Santhi, P. L. *Appl. Catal. : A* 1997, ***149***, 257.

(57) Choudary, B. M.; Sateesh, M.; Kantam, M. L.; Prasad, K. V. R. *Appl. Catal. : A* 1998, ***171***, 155.

(58) Breck, D. W. *Zeolite Molecular Sieves*; Wiley: New York, 1974.

(59) Dyer, A. *An introduction to Zeolite Molecular Sieves*; John Wiley and Sons: New York, 1988; pp 13.

(60) Spagnol, M.; Gilbert, L.; Alby, D. *The Roots of the Organic Development*; Desmurs, J. R., Ratton, S., Eds.; Elsevier: Amsterdam, 1996; Vol. 8.

(61) Pandey, A. K.; Singh, A. P. *Catal. Lett.* 1997, ***44***, 129.

(62) Neves, I.; Jayat, F.; Magnoux, P.; Perot, G.; Ribeiro, F. R.; Gubelmann, M.; Guisnet, M. *J. Mol. Catal. : A* 1994, ***93***, 164.

(63) Sreekumar, R.; Padmakumar, R. *Synthetic Commun.* 1997, ***27***, 777.

(64) Chiche, B.; Finiels, A.; Gauthier, C.; Geneste, P.; Graille, J.; Pioch, D. *J. Org. Chem.* 1986, ***51***, 2128.

(65) Corma, A.; Climent, M. J.; García, H.; Primo, J. *Appl. Catal.* 1989, ***49***, 109.

(66) Smith, K.; Zhenhua, Z.; Hodgson, P. K. G. *J. Mol. Catal. : A* 1998, ***134***, 121.

(67) Freese, U.; Heinrich, F.; Roessner, F. *Catal. Today* 1999, ***49***, 237.

(68) Botella, P.; Corma, A.; Sastre, G. *J. Catal.* 2001, ***197***, 81.

(69) Spagnol, M.; Gilbert, L.; Guillot, H.; Tirel, P. J. *Patent PCT, Int. Appl WO 97 48, 665* 1997.

(70) Gilbert, L.; Spagnol, M. *Patent PCT, Int. Appl WO 97 17,324* 1997.

(71) Harvey, G.; Binder, G.; Prins, R. *Stud. Surf. Sci. Catal.* 1995, ***94***, 397.

(72) Heinichen, H. K.; Holderich, W. F. *J. Catal.* 1999, ***185***, 408.

(73) Spagnol, M.; Gilbert, L.; Benazzi, E.; Marcilly, C. *Patent PCT, Int. Appl WO 96 35,655* 1996.

(74) Harvey, G.; Vogt, A. H. G.; Kouwenhoven, H. W.; Prins, R. *Proc. 9th Int. Zeol. Conf.* , Montreal, 1992; pp 363.

(75) Hölderich, W. F.; Lermer, H.; Schwarzmann, M. *DEOS 3 618 964* 1987.

(76) Rohan, D.; Canaff, C.; Fromentin, E.; Guisnet, M. *J. Catal.* 1998, ***177***, 296.

(77) Castro, C. D.; Primo, J.; Corma, A. *J. Mol. Catal. : A* 1998, ***134***, 215.

(78) Spagnol, M.; Gilbert, L.; Alby, D. *Ind. Chem. Lib* 1996, ***8***, 29.

(79) Richard, F.; Carreyre, H.; Pérot, G. *Catalysis of Organic Reactions*; Malz, R. E., Ed.; Marcel Dekker, Inc., 1996; pp 405.

(80) Gunnewegh, E. A.; Downing, R. S.; van Bekkum, H. *Zeolites A Refined Tool for Designing Catalytic Sites* 1995, 447.

(81) Spagnol, M.; Gilbert, L.; Jacquot, R.; Guillot, H.; Tirel, P. J.; Le Gouic, A. M. *Proc. 4th Int. Symp. Heterog. Catal. Fine Chem.*, Basel, Switzerland, September 8-12, 1996.

(82) Derouane, E. G. *J. Mol. Catal. : A* 1998, ***134***, 29.

(83) Corma, A.; Garcia, H. *Catal. Today* 1997, ***38***, 257.

(84) Rabo, J. A.; Gadja, G. J. *Guidelines for Mastering the properties of molecular sieves*; Barthomeuf, D., Derouane, E. G., Holderich, W. F., Eds.; NATO ASI Ser., 1990; Vol. 221; pp 273.

(85) Venuto, P. B.; Landis, P. S. *Advances in Catalysis*; New York, 1968; Vol. 18; pp 259.

(86) Venuto, P. B.; Hamilton, L. A.; Landis, P. S. *J. Catal.* 1966, ***5***, 484.

(87) Venuto, P. B.; Hamilton, L. A.; Landis, P. S.; Wise, J. J. *J. Catal.* 1966, ***5***, 81.

(88) Venuto, P. B.; Wu, E. L. *J. Catal.* 1969, ***15***, 205.

(89) Venuto, P. B.; Wu, E. L.; Cattanach, J. Molecular Sieves. In *J. Catal.*; Industry, S. O. C., Ed. London, 1968; pp 117.

(90) Venuto, P. B. *Chemtech* 1971, 215.

(91) Venuto, P. B. *J. Org. Chem.* 1967, ***32***, 1272.

(92) Haag, W. O.; Chen, N. Y. *Catalyst design -- Progress and Perspectives*; Hegedus, L. L., Ed.; John Wiley and Sons: New York, 1987; Vol. chapter 6.

(93) Ward, J. W. *ACS Monogr.* 1976, ***171***, 118.

(94) Barthomeuf, D. *Stud. Surf. Sci. Catal.* 1980, ***5***, 55.

(95) Chen, N. Y.; Garwood, W. E.; Dwyer, F. G. *Shape selective catalysis in Industrial Applications*; Dekker, M., Ed. New York, 1989; pp 1.

(96) Brunner, E. *Catal. Today* 1997, ***38***, 361.

(97) Brunner, E. *J. Mol. Struct.* 1995, ***355***, 61.

(98) Lercher, J. A.; Gründling, C.; Eder-Mirth, G. *Catal. Today* 1996, ***27***, 353.

(99) Hunger, M. *Solid State Nuclear Magnetic Resonance* 1996, ***6***, 1.

(100) Borade, R.; Sayari, A.; Adnot, A.; Kaliaguine, S. *J. Phys. Chem.* 1990, ***94***, 5989.

(101) Batamack, P.; Dorémieux-Morin, C.; Vincent, R.; Fraissard, J. *J. Phys. Chem.* 1993, ***97***, 9779.

(102) Apelian, M. R.; Degnan, T. F.; Fung, A. S.; Kennedy, G. J. *US patent 5,200,168* 1993.

(103) Beyer, H. R.; Belenykaja, I. *Catalysis by zeolites, Studies in Surface Science and Catalysis*; Imelik, B., Naccache, C., Ben Taarit, Y., Vedrine, J. C., Coudurier, G., Praliaud, H., Eds.; Elsevier: Amsterdam, 1980; Vol. 5; pp 203.

(104) Akporiaye, D.; Chapple, A. P.; Clark, D. M.; Dwyer, J.; Elliott, I. S.; Rawlence, D. J. *Stud. Surf. Sci. Catal.* 1986, ***28***, 351.

(105) Zukal, A.; Patzelova, V.; Lohse, U. *Zeolites* 1986, ***6***, 133.

(106) Fernandez, C.; Vedrin, J. C.; Grosmangin, J.; Szabo, G. *Zeolites* 1993, ***13***, 462.

(107) Sauer, J. *J. Mol. Catal. : A* 1989, ***54***, 312.

(108) Kiricsi, I.; Flego, C.; Pazzuconi, G.; Parker, W. O.; Millini, R.; Perego, C.; Bellussi, G. *J. Phys. Chem.* 1994, ***98***, 4627.

(109) Bourgeat-Lami, E.; Massiani, P.; Di Renzo, F.; Espiau, P.; Fajula, F.; Courieres, T. D. *Appl. Catal.* 1991, ***72***, 139.

(110) Zholobenko, V. L.; Kustov, L. M.; Kazansky, V. B.; Loefler, E.; Lohse, U.; Peuker, C.; Oehlmann, G. *Zeolites* 1990, ***10***, 266.

(111) Heinichen, H. K.; Hölderich, W. F. *12th International Zeolite Conference* 1999, 1085.

(112) Jia, C.; Massiani, P.; Barthomeuf, D. *J. Chem. Soc. Faraday Trans.* 1993, ***89***, 3659.

(113) Trombetta, M.; Busca, G.; Storaro, L.; Lenarda, M.; Casagrande, M.; Zambon, A. *Phys.Chem.Chem.Phys.* 2000, **2**, 3529.

(114) Kunkeler, P. J.; Zuurdeeg, B. J.; van der Waal, J. C.; van Bokhoven, J. A.; Koningsberger, D. C.; van Bekkum, H. *J. Catal.* 1998, ***180***, 234.

(115) Brunner, E.; Ernst, H.; Freude, D.; Frohlich, T.; Hunger, M.; Pfeifer, H. *J. Catal.* 1991, ***127***, 34.

(116) Ray, G. J.; Meyers, B. L.; Marshall, C. L. *Zeolites* 1987, ***7***, 307.

(117) Rocha, J.; Carr, S. W.; Klinowski, J. *Chem. Phys. Lett.* 1991, ***187***, 401.

(118) Freude, D.; Brunner, E.; Pfeifer, H.; Drager, D.; Jerschkewitz, H. G.; Lohse, U.; Oehlmann, G. *Chem. Phys. Lett.* 1987, ***139***, 325.

(119) Freude, D.; Klinowski, J.; Hamdan, H. *Chem. Phys. Lett.* 1988, ***149***, 355.

(120) Campbell, S. M.; Bibby, D. M.; Coddington, J. M.; Howe, R. F.; Meinhold, R. H. *J. Catal.* 1996, ***161***, 338.

(121) Klinowski, J.; Thomas, J. M.; Fyfe, C. A.; Gobbi, G. C. *Nature* 1982, ***296***, 533.

(122) Fyfe, C. A.; Gobbi, G. C.; Kennedy, G. J. *J. Phys. Chem.* 1984, ***88***, 3248.

(123) Klinowski, J.; Fyfe, C. A.; Gobbi, G. C. *J. Chem. Soc. Faraday Trans. I* 1985, ***81***, 3003.

(124) Bosacek, V.; Freude, D.; Frohlich, T.; Pfeifer, H.; Schniedel, H. *J. Coll. Interface Sci* 1982, ***85***, 502.

(125) Coster, D.; Fripiat, J. J. *J. Chem. Mater.* 1993, ***5***, 1204.

(126) Engelhardt, G.; Michel, D. *High Resolution Solid State NMR of Silicates and Zeolites*; Wiley, Ed. New York, 1987; pp 148.

(127) Kuehl, G. H.; Timken, H. K. C. *Microporous Mater.* 2000, ***35-36***, 521.

(128) Pérez-Pariente, J.; Sanz, J.; Fornés, V.; Corma, A. *J. Catal.* 1990, ***124***, 217.

(129) Müller, M.; Harvey, G.; Prins, R. *Microporous Mater.* 2000, ***34***, 135.

(130) Hunger, M. *Catal.Rev.-Sci.Eng.* 1997, ***39***, 345.

(131) Klug, H. P.; Alexander, L. E. *X-ray Diffraction Procedures for Polycrystalline and Amorphous Solids*; Wiley: New York, 1974; pp 618.

(132) Camblor, M. A.; Corma, A.; Valencia, S. *Microporous Mater.* 1998, ***25***, 59.

(133) Hegde, S. G.; Kumar, R.; Bhat, R. N.; Ratnasamy, P. *Zeolites* 1989, ***9***, 231.

(134) Camiloti, A. M.; Jahn, S. L.; Velasco, N. D.; Moura, L. F.; Cardoso, D. *Appl. Catal. : A* 1999, ***182***, 107.

(135) Borade, R. B.; Clearfield, A. *J. Phys. Chem.* 1992, ***96***, 6729.

(136) Jacobs, P.; Martens, J. A.; Weitkamp, J.; Beyer, H. K. *Disc. Faraday Soc* 1981, ***72***, 353.

(137) Kanazirev, V.; Borisova, N. *Zeolites* 1982, ***2***, 23.

(138) Mauvezin, M.; Delahay, G.; Coq, B.; Kieger, S.; Jumas, J. C.; Olivier-Fourcade, J. *J. Phys. Chem. B* 2001, ***105***, 928.

(139) Joyner, R.; Stockenhuber, M. *J. Phys. Chem. B* 1999, ***103***, 5963.

(140) Feng, X.; Hall, W. K. *Catal. Lett.* 1996, ***41***, 45.

(141) Gaare, K.; Akporiaye, D. *J. Mol. Catal. : A* 1996, ***109***, 177.

(142) Ma, Y.; Wang, Q. L.; Jiang, W.; Zuo, B. *Appl. Catal. : A* 1997, ***165***, 199.

(143) Bhattacharya, D.; Sharma, S.; Singh, A. P. *Appl. Catal. : A* 1997, ***150***, 53.

(144) Quaschning, V.; Deutsch, J.; Druska, P.; Niclas, H.-J.; Kemnitz, E. *J. Catal.* 1998, ***177***, 164.

(145) Singh, A. P.; Bhattacharya, D.; Sharma, S. *J. Mol. Catal. : A* 1995, ***102***, 139.

(146) Isaev, Y.; Fripiat, J. J. *J. Catal.* 1999, ***182***, 257.

(147) Haouas, M.; Kogelbauer, A.; Prins, R. *Catal. Lett.* 2000, ***70***, 61.

(148) Nagy, S. M.; Yarovoy, K. A.; Shubin, V. G.; Vostrikova, L. A. *J. Phys. Org. Chem* 1994, ***7***, 385.

(149) Weekman, V. W. *AIChE J* 1970, ***20***, 274.

(150) Karge, H. G.; Laniecki, M.; Ziolek, M.; Onyestyak, G.; Kiss, A.; Kleinschmit, P.; Siray, M. *Stud. Surf. Sci. Catal.* 1989, ***49***, 1327.

(151) Karge, H. G. *Stud. Surf. Sci. Catal.* 1991, ***58***, 531.

(152) Wolthuizen, J. P.; van den Berg, J. P.; van Hooff, J. H. C. *Stud. Surf. Sci. Catal.* 1980, ***5***, 85.

(153) Venuto, P. B. *Microporous Mater.* 1994, ***2***, 297.

(154) Derouane, E. G.; Dillon, C. J.; Bethell, D.; Derouane-Abd Hamid, S. B. *J. Catal.* 1999, ***187***, 209.

(155) Moreau, P.; Finiels, A.; Meric, P. *J. Mol. Catal. : A* 2000, ***154***, 185.

(156) Jacob, B.; Sugunan, S.; Singh, A. P. *J. Mol. Catal. : A* 1999, ***139***, 43.

(157) Derouane, E. G.; Crehan, G.; Dillon, C. J.; Bethell, D.; He, H.; Derouane-Abd Hamid, S. B. *J. Catal.* 2000, ***194***, 410.

(158) Hachiya, I.; Mariwaki, M.; Kobayashi, S. *Tetrahedron Lett.* 1995, ***36***, 409.

(159) Olah, G. A.; Kobayashi, S. *J. Am. Chem. Soc* 1971, ***93***, 6964.

(160) Izumi, Y.; Ogawa, M.; Nohara, W.; Urabe, K. *Chem. Lett.* 1992, 1987.

(161) Wang, Q. L.; Ma, Y.; Ji, X.; Yan, H.; Qiu, Q. *J. Chem. Soc. Chem. Commun.* 1995, 2307.

(162) Kouwenhoven, H. W.; van Bekkum, H. *Handbook of Heterogeneous Catalysis*; Ertl, G., Knozinger, H., Weitkamp, J., Eds.; VCH, 1997; Vol. 5; pp 2358.

Chapter 2. Experimental

2.1 Materials

The parent zeolites chosen for this investigation are shown in **Table 2.1.1**.

Zeolite	Cation form	Si/Al ratio	Code	Supplier
Beta	NH_4^+	12.5	CT 121	CATAL
Faujasite	NH_4^+	2.36	33,444-8	ALDRICH
ZSM-5	NH_4^+	25	CT 411	CATAL
Mordenite	NH_4^+	10	CT 406	CATAL
MCM-41	Various	Various	-	Dr. G. Grubert

Table 2.1.1 Information on the zeolites used in the investigation.

Supplier's addresses:

Catal:

CATAL International Ltd
Box 507
Sheffield
510 3YT
England, UK
Tel: +44 (0) 114 221 1800
Fax: +44 (0) 114 230 2458
E-Mail: CATAL@btinternet.com

Aldrich:

ALDRICH
The Old Brickyard
New Road
Gillingham
Dorset
SP8 4XT
Tel: +44 (0) 1747 822211
Fax: +44 (0) 1747 823779
E-Mail: ukcustsv@eurnotes.sial.com

2.2 Catalyst preparation

2.2.1 Preparation of MCM-41

Si-MCM-41 was prepared in a heterogeneous system following the procedure of Grün *et al.*, [1]. Cetyltrimethylammoniumbromide (CTAB, Aldrich, 99%, 2.4 g) was dissolved in water (120 ml) at 299 K, followed by the addition of ammonia solution (8 ml, 25%) and tetraethylorthosilicate (TEOS, Aldrich, 98%, 10 ml). After the solution was stirred for 1 h, the precipitated sample was dried overnight at 353 K and calcined at 823 K for 12 h. To introduce iron and/or aluminium atoms during the synthesis, $Fe(NO_3)_3.9H_2O$ (0.95 g) and/or $Al(NO_3)_3.9H_2O$ (1.12 g) were added to the CTAB-water solution.

2.2.2 Zeolite activation and modification

2.2.2.1 Calcination

Zeolites were prepared using various calcination procedures. In general, the maximum calcination temperature, the amount of time the catalyst remained at this temperature, and the atmosphere (air or vacuum) were altered in order to obtain materials with varying degrees of acidity. The heating rate was kept constant at 5 K min^{-1} throughout all the procedures. For practicality throughout this thesis, samples prepared by various treatments shall be designated using the following general procedure:

Regeneration number (where applicable) or **Spent number** (where applicable) or **Chemical treatment** (where applicable) – **Counter cation** – **Zeolite type** – **Si/Al ratio** – **Atmosphere** – **Temperature** – **Time**

Where:

Regeneration number = R1, R2, R3 (number of reactions the zeolite has been exposed to and subsequently regenerated in air as described in **2.2.2.5**)

Spent number = S1 (number of reactions the zeolite has been exposed to without regeneration)

Chemical treatment = H_4EDTA, ammonia gas, steamed

Counter cation = NH_4^+, H^+, Na^+, Fe, Cu

Zeolite type = β (Beta), Y (faujasite), ZSM-5, MOR (mordenite), MCM-41

Si/Al ratio = ratio of silicon to aluminium in the zeolite lattice

Atmosphere = A (Air), V (Vacuum)

Temperature = calcination temperature (K)

Time = time at maximum calcination temperature (h)

Examples:

NH_4^+-β-12.5-A-1023-18 (Corresponds to the ammonium form of zeolite Beta (Si/Al=12.5) which has been calcined in air at 1023 K for 18 hours.

R2-H^+-β-12.5-A-773-1 (Corresponds to the hydrogen form of zeolite Beta (Si/Al=12.5) which has been calcined in air at 773 K for 1 hour, after exposure to 2 previous reactions and subsequent regeneration).

As a quick reference, the notations for the whole range of zeolite materials used throughout the investigation are summarized **Table 2.1.2** and **Table 2.1.3**.

Sample notation	Sample Description
NH_4^+-β-12.5-V-773-1	Ammonium form zeolite Beta (Si/Al = 12.5) activated under vacuum to 773 K for 1 h
NH_4^+-β-12.5-A-773-1	Ammonium form zeolite Beta (Si/Al = 12.5) activated in air to 773 K for 1 h
NH_4^+-β-12.5-A-1023-18	Ammonium form zeolite Beta (Si/Al = 12.5) activated in air to 1023 K for 18 h
EDTA-β-12.5-A-773-1	Ammonium form zeolite Beta (Si/Al = 12.5) H_4EDTA treated and activated in air to 773 K for 1 h
Steamed2h-β-12.5-A-773-1	Ammonium form zeolite Beta (Si/Al = 12.5) steam treated for 2h and activated in air to 773 K for 1 h
Steamed6h-β-12.5-A-773-1	Ammonium form zeolite Beta (Si/Al = 12.5) steam treated for 6h and activated in air to 773 K for 1 h
Cu-β-12.5-A-773-1	Copper exchanged Beta (Si/Al = 12.5) activated in air to 773 K for 1 h
Fe-β-12.5-A-773-1	Iron exchanged Beta (Si/Al = 12.5) activated in air to 773 K for 1 h
Na-β-12.5-A-773-1	Na exchanged Beta (Si/Al = 12.5) activated in air to 773 K for 1 h
NH_3 treated-NH_4^+-β-12.5 -A-1023-18	Ammonium form zeolite Beta (Si/Al = 12.5) activated in air to 1023 K for 18 h followed by treatment with ammonia gas at 423 K for 2 h
Spent-NH_4^+-β-12.5-A-773-1	Ammonium form zeolite Beta (Si/Al = 12.5) activated in air to 773 K for 1 h followed by 1 reaction
R1-H^+-β-12.5-A-773-1	Ammonium form zeolite Beta (Si/Al = 12.5) activated in air to 773 K for 1 h after 1 reaction and subsequent regeneration
R2-H^+-β-12.5-A-773-1	Ammonium form zeolite Beta (Si/Al = 12.5) activated in air to 773 K for 1 h after 2 reactions and subsequent regeneration after each reaction
R3-H^+-β-12.5-A-773-1	Ammonium form zeolite Beta (Si/Al = 12.5) activated in air to 773 K for 1 h after 3 reactions and subsequent regeneration after each reaction

Table 2.1.2 Sample notations and their corresponding descriptions for zeolite Beta samples.

Sample notation	Sample Description
NH_4^+-ZSM-5-25-A-773-1	Ammonium form ZSM-5 (Si/Al = 25) activated in air to 773 K for 1 h
Fe-ZSM-5-25-A-773-1	Iron exchanged ZSM-5 (Si/Al = 25) activated in air to 773 K for 1 h
Cu-ZSM-5-25-A-773-1	Copper exchanged ZSM-5 (Si/Al = 25) activated in air to 773 K for 1 h
NH_4^+-MOR-10 -A-823-1	Ammonium form mordenite (Si/Al = 10) activated in air to 823 K for 1 h
Fe-MOR-10-A-823-1	Iron exchanged mordenite (Si/Al = 10) activated in air to 823 K for 1 h
Cu-MOR-10-A-823-1	Copper exchanged mordenite (Si/Al = 10) activated in air to 823 K for 1 h
NH_4^+-FAU-2.36-A-573-8	Ammonium form faujasite (Si/Al = 2.36) activated in air to 573 K for 1 h
Si-MCM-41-A-773-1	Purely siliceous MCM-41 activated in air to 773 K for 1 h
1Fe-MCM-41-A-773-1	Iron MCM-41 activated in air to 773 K for 1 h
30Al-MCM-41-A-773-1	Aluminium containing MCM-41 (Si/Al = 30) activated in air to 773 K for 1 h
30Al -MCM-41-Fe-5-A-773-1	Aluminium/Iron containing MCM-41 (Si/Al = 30) activated in air to 773 K for 1 h
15Al-MCM-41-A-773-1	Aluminium containing MCM-41 (Si/Al = 15) activated in air to 773 K for 1 h
5Al-MCM-41-A-773-1	Aluminium containing MCM-41 (Si/Al = 5) activated in air to 773 K for 1 h

Table 2.1.3 Sample notations and their corresponding descriptions for ZSM-5, faujasite, mordenite, and MCM-41 samples.

2.2.2.2 Steaming

Samples were prepared by steaming at 873 K for 2 h and 6 h. The ramp rate was 5 K min^{-1} to treatment temperature under a dry nitrogen flow of 100 ml min^{-1}. Steam treatment was carried out at the desired temperature and time under a water vapour pressure of approximately 20 mbar generated by diversion of the nitrogen gas stream through a water bubbler (saturator) at room temperature. From the water bubbler, the saturated gas was then directed into a Carbolite furnace via a silica glass tube, where the sample was subjected to steam for the chosen time and temperature. After the designated time, the nitrogen was diverted from the water bubbler, and the sample was allowed to cool to room temperature under flowing dry nitrogen.

2.2.2.3 H_4EDTA treatment

Aluminium can be extracted from zeolites by treating them with chelating agents such as H_4EDTA at moderate temperatures [2]. Parent zeolites (ammonium exchanged if necessary, as described in **2.2.3.1**) were dealuminated with H_4EDTA according to the method proposed by Datka *et al.*, [3]. Dealumination was carried out by 1 h treatment of a zeolite suspension (water: zeolite = 15:1) using various concentrations of H_4EDTA (Aldrich, 99%) at 373 K. Dealuminated samples were washed with hot distilled water and dried at 433 K. The amount of H_4EDTA used was adjusted according to the desired level of dealumination.

2.2.2.4 Treatment with gaseous ammonia

Adsorption of ammonia at 423 K for 2 h was carried out on selected zeolite samples. Bourgeat-Lami *et al.*, [4] reported that treatment of a dealuminated zeolite Beta sample with gaseous ammonia at 373 K allowed for all the aluminium atoms of the solid to recover a tetrahedral framework symmetry. Ammonia was adsorbed in a silica glass tube supported in a Carbolite furnace, connected at one end with the *in situ* vacuum FTIR apparatus depicted in **Figure 2.8.2.1**, and with a stopper at the other end.

2.2.2.5 Regeneration of spent catalysts

Spent catalysts were recycled and used in subsequent reactions. Following a reaction, the spent catalyst was filtered, dried in air at room temperature for 24 h, and then regenerated in air at 823 K for 24 h in a muffle furnace.

2.2.3 Preparation of ion exchanged materials

2.2.3.1 Preparation of iron, copper, and sodium exchanged zeolites by aqueous exchange

5 g of zeolite (ammonium form) was added to 250 ml of a 1 M solution of copper (II) nitrate, iron (III) nitrate, and sodium nitrate in distilled water to form the Cu, Fe, and Na forms of the zeolite respectively. In each case, the solution was stirred at room temperature overnight. The catalyst was then separated by filtration, washed with distilled water and then dried in air at 373 K for 24 h. This exchange procedure was then repeated a further 2 times, until the desired level of exchange was achieved.

2.3 Zeolite dissolution method

30 mg of ion-exchanged zeolite was added to a PTFE beaker, where 5 ml of HNO_3 (Aldrich, 70%), 1 ml of HCl (Aldrich, 37%), and 1 ml of HF (Aldrich, 48%) was introduced. The solution was heated to 353 K until dry. Then 1 ml of HNO_3 was added to the dry sample, along with a small amount of distilled water, until the solid was completely dissolved, this solution was then transferred to a 25 ml volumetric flask and made level to the mark with distilled water. These solutions, along with appropriate calibration solutions, were then analysed by atomic absorption spectroscopy. From these experiments, Fe-Beta was found to contain 1.2 wt% Fe and Cu-Beta contained 2.2 wt% Cu.

2.4 Atomic Absorption Spectroscopy

2.4.1 Theory [5]

Atomic absorption spectroscopy (AAS) is extremely useful when used in combination with the zeolite dissolution method described in **2.3**. It determines the presence of metals in liquid samples. Metals include Fe, Cu, Al, Pb, Ca, Zn, Cd, among others. It also measures the concentration of metals in the samples. Typical detection limits in Flame Atomic Absorption Spectroscopy (FAAS) are in the low ng/mL range. The first step in FAAS is to deliver the analyte to the flame; this requires the analyte to be dissolved in a solution in order to undergo nebulisation. The wet chemistry necessary to dissolve the sample in a matrix suitable for flame atomisation is often an important component of the analytical process. The device that introduces the sample into the flame plays a major role in determining the accuracy of analysis. The most popular sampling method is nebulisation of a liquid sample to provide a steady flow of aerosol into a flame. An introduction system for liquid samples consists of three components: (1) a nebuliser that breaks up the liquid into smaller droplets, (2) an aerosol modifier that removes large droplets from the stream, and (3) the flame or atomiser that converts the analyte into free atoms. The atomisation step must convert the analyte within the aerosol into free analyte atoms in the ground state for AAS analysis. The flame remains the most generally useful atomiser for atomic spectroscopy. A satisfactory flame source must provide the temperature and fuel/oxidant ratio required for a given analysis. The maximum operating temperature of the flame is determined by the identities of the fuel and oxidant, whereas the exact flame temperature is fixed by the fuel/oxidant ratio. The most commonly employed mixtures include Acetylene/Air and Acetylene/Nitrous oxide. The absorption of radiation by free atoms (those analyte atoms removed from their chemical environment but not ionised) in the flame involves a transition of these atoms from the highly populated ground state to an excited electronic state. Although other electronic states are possible, the atomic absorption spectrum of an element consists of a series of resonance lines, all originating with the ground electronic state and terminating in various excited states. Usually the transition between the ground state and the first excited state, known as the first resonance line, is the line with the strongest absorptivity. A hollow-cathode lamp, where the cathode is made of (or lined on the interior with) the element to be determined, has become the light source most often used in AAS. The flame gases are considered as a sample cell that contains free, unexcited analyte atoms capable of absorbing radiation at the wavelength of the resonance line emitted by the external source. Unabsorbed radiation passes through a monochromator that isolates the resonance line and then into a photodetector that measures the power of the transmitted radiation. Absorption is determined by the difference in radiant power of the resonance line in the presence and absence of analyte atom in the flame. **Figure 2.4.1.1** shows a schematic diagram of an atomic absorption experiment.

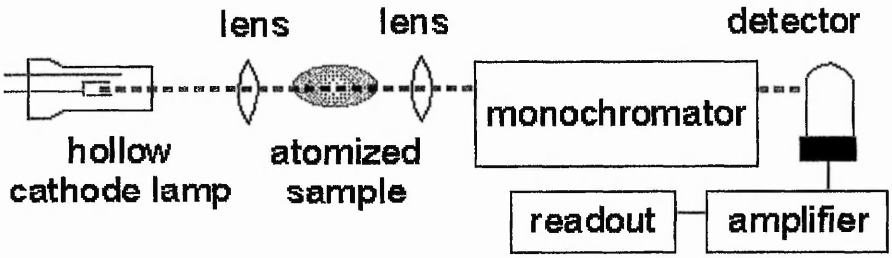

Figure 2.4.1.1 Schematic diagram of an atomic absorption experiment.

2.4.2 Analysis of AAS results

An analytical (working curve) technique was used to determine concentrations. A series of standard solutions containing known concentrations of analyte were prepared covering the concentration range of interest. Standard solutions were prepared using distilled water as the sample matrix. Standard solutions, and a blank solution containing only the sample matrix were analysed, and the net readings (standard solution minus blank) were plotted against the concentrations of the standard solutions to obtain the working calibration curve.

2.5 Temperature Programmed Reduction

2.5.1 Theory

Reduction is an inevitable step in the preparation of metallic catalysts. It is often a critical step, because if it is not done correctly, the catalyst may sinter or may not reach its optimum state of reduction. The reduction of a metal oxide MO_n by H_2 is described by the equation:

Equation 2.5.1.1 $$MO_n + nH_2 \rightarrow M + nH_2O$$

Thermodynamics predicts under which conditions a catalyst can be reduced. As with every reaction, the reduction will proceed when the change in Gibbs free energy, ΔG, has a negative value. The expression below shows how ΔG depends on pressure and temperature:

Equation 2.5.1.2 $$\Delta G = \Delta G^\circ + nRT\ln\left(\frac{P_{H_2O}}{P_{H_2}}\right)$$

Where : ΔG = the change in Gibbs free energy for the reduction

ΔG° = the same under standard conditions

n = the stoichiometric coefficient of reaction

R = gas constant

T = temperature

P = partial pressure

If the catalyst is reduced under flowing hydrogen, the reaction product water is removed efficiently and the second term in **Equation 2.5.1.2** is therefore always negative. For many oxides, such as those of cobalt, nickel, and the noble metals, ΔG° is already negative and reduction is thermodynamically feasible. In these cases, it is only necessary to find the temperature where the kinetics is rapid enough to achieve complete reduction. Oxides such as Fe_2O_3 and SnO_2, however, have a positive ΔG°. Now the second term in equation 2 determines whether ΔG is negative or not. To determine whether reduction is thermodynamically permitted, **Equation 2.5.1.2** is written in the form:

Equation 2.5.1.3 $$\Delta G = \Delta G^\circ + nRT\ln\left[\left(\frac{P_{H_2O}}{P_{H_2}}\right) / \left(\frac{P_{H_2O}}{P_{H_2}}\right)_{eq}\right]$$

with the symbols as defined above and the subscript 'eq' for the equilibrium ratio. Thus, ΔG is negative when the ratio $p(H_2O)/p(H_2)$ is smaller than the equilibrium value and the efficiency with which water is removed from the reactor becomes the decisive factor. In order to reduce bulk iron oxide to metallic iron at 600 K, the water content of the hydrogen gas above the sample must be below a few percent, which is easily achieved. However, in order to reduce Cr_2O_3, the water content should be as low as a few parts per billion, which is more difficult to realize. In many cases only partial reduction to a lower oxide may be expected, the reduction of Mn_2O_3 to MnO is thermodynamically allowed at relatively high water contents, but further reduction to manganese is unlikely. Reduction reactions of metal oxides by hydrogen start with the dissociative adsorption of H_2, which is a much more difficult process on oxides than on metals. Atomic hydrogen is responsible for the actual reduction. Depending on how fast or how slow the dissociative adsorption is with respect to subsequent reduction reactions, comprising diffusion of atomic hydrogen into the lattice, reactions with oxygen and removal of the hydroxyl species formed, two limiting cases are distinguished. If the initial step, the activation of H_2, is fast, as may be the case on noble metal oxides or highly defect oxide surfaces, the shrinking core or contracting sphere model applies. The essence of this model is that nuclei of reduced metal atoms form rapidly over the entire surface of the particle and grow into a shell of reduced metal. Further reduction is limited by the transport of lattice oxygen out of the particle. The extent of reduction increases rapidly initially, but slows down as the metal shell grows. The nucleation model represents the other extreme. In this, dissociation of hydrogen is the slow step. Once a nucleus of reduced metal exists, it acts as a catalyst for further reduction, as it provides a site where H_2 is dissociated. Atomic hydrogen diffuses to adjacent sites on the surface or into the lattice and reduces the oxide. As a result the nuclei grow in three dimensions until the whole surface is reduced, after which further reduction takes place as in the shrinking core model [6]. Temperature programmed reduction techniques can yield direct information on the reducibility of catalysts and catalyst precursors and is an excellent technique for characterizing a variety of catalysts. The technique consists of exposing the sample to a flowing mixture of a reducing agent, such as hydrogen, in an inert gas while linearly ramping the temperature. The rate of consumption of the reducing agent is monitored and related to the rate of reduction of the sample. The reduction profile gives information concerning the ease of reducibility (temperature at maximum) as well as the extent of reducibility (signal area) of the material being studied.

2.5.2 Experimental

Temperature programmed reduction was performed using an in house designed computerized system, equipped with a thermal conductivity detector. Approximately 80 mg of catalyst was packed into a silica glass tube held centrally in the heated zone of a tube furnace. The catalyst was preheated to 773 K in flowing air for 1 h, cooled to room temperature, then heated in a 12 ml min^{-1} flow of 2% hydrogen in argon with a ramp rate of 5 K min^{-1} from room temperature to 1273 K. The reduction profile was automatically logged to a computer and the hydrogen consumption was calculated using copper (II) oxide (Aldrich, 99+%), under the conditions outlined above.

2.6 Catalyst Testing: Reaction procedure

2.6.1 Reaction over zeolite materials

The acylation reaction was carried out in the liquid phase in a batch reactor consisting of a three-necked flask allowing attachment of a reflux condenser, thermometer, and a stopper. Into this vessel, 0.2 mol of acetic anhydride (Aldrich, 99+%) and 0.4 mol of anisole (Aldrich, 99%) were added to the flask and mixed for 5 minutes using a combination stirrer/heater. After which, a sample was extracted and analysed by gas chromatography (GC). Then 300 mg of powdered activated catalyst was added to the reaction mixture and the system was heated to 333 K. The mixture was stirred for 24 h, with samples taken at 30-minute intervals for the initial 5 h. n-decane (Aldrich, 99%) was used as internal standard in the analysis and its validity crosschecked in a repeat experiment with nitrobenzene. The reaction was monitored with a Shimadzu GC-8A gas chromatograph equipped with a packed column containing an OV101 liquid phase (10% loading) on a chromosorb WHP support. At reaction completion, the spent catalyst was filtered and retained for either exposure to a fresh reaction mixture or future regeneration. The performance of the catalyst was determined from the output from the gas chromatograph. Although the standard procedure outlined above was carried out for all reactions, certain parameters were altered in order to determine their effect on catalytic activity. These parameters are listed below:

1) Substrate (toluene, anisole)
2) Acylating agent (acetic anhydride, acetic acid)
3) Reaction temperature (303 → 398 K)
4) Amount of catalyst (100 → 1500 mg)

5) Concentration of reactants
6) Particle size (powdered and sieved (0.6 - 1.0 mm))

To investigate the possible inhibition by the product, 0.03 mol and 0.05 mol of p-methoxyacetophenone was also added to the reaction mixture in some cases.

2.6.2 Reaction over $AlCl_3$

The reaction procedure and analysis was identical to that of the zeolite catalysed reaction. However, in this case, the stopper on the three-necked flask was replaced by a separatory funnel. 0.4 mol of anhydrous, finely powdered aluminium chloride (Aldrich, 99%) was added to 0.4 mol of anisole (Aldrich, 99%). 0.2 mol of acetic anhydride (Aldrich, 99+%) was added slowly via the separatory funnel over a 30-minute period. After all the acetic anhydride was introduced, the solution was heated to 323 K for 1 h in order to complete the reaction.

2.7 Gas Chromatographic Analysis

2.7.1 Theory

The feature that distinguishes chromatography from most other physical and chemical methods of separation is that two mutually immiscible phases are brought into contact; one phase is stationary and the other is mobile. A sample introduced into a mobile phase is carried along through a column (manifold) containing a distributed stationary phase. Species in the sample undergo repeated interactions (partitions) between the mobile phase and the stationary phase. When both phases are properly chosen, the sample components are gradually separated into bands in the mobile phase. At the end of the process, separated components emerge in order of increasing interaction with the stationary phase. The least retarded component emerges first; the most strongly retained component elutes last. Partition between the phases exploits differences in the physical and/or chemical properties of the components in the sample. Adjacent components (peaks) are separated when the later-emerging peak is retarded sufficiently to prevent overlap with the peak that emerges ahead of it [5]. Gas chromatography is the technique of choice for the separation of thermally stable and volatile organic and inorganic compounds. The underlying principle of gas chromatography is the separation of mixtures in microgram quantities by passage of the vaporized sample in a gas stream through a stationary liquid or solid phase, the components migrate at different rates due to differences in boiling point, solubility, or adsorption [7], [8]. Gas chromatography, so called because the mobile phase is a gas, comprises gas-liquid chromatography (glc) and gas-solid chromatography (gsc). For glc the stationary phase is a high boiling point liquid and the sorption process is predominantly one of partition. For gsc the stationary phase is a solid and adsorption plays the major role. Samples, which must be volatile and thermally stable at the operating temperature, are introduced into the gas flow *via* an injection port located at the top of the column. A continuous flow of gas elutes the components from the column in order of increasing distribution ratio from where they pass through a detector connected to a recording system. A schematic diagram of a gas chromatograph is shown in **Figure 2.7.1.1**.

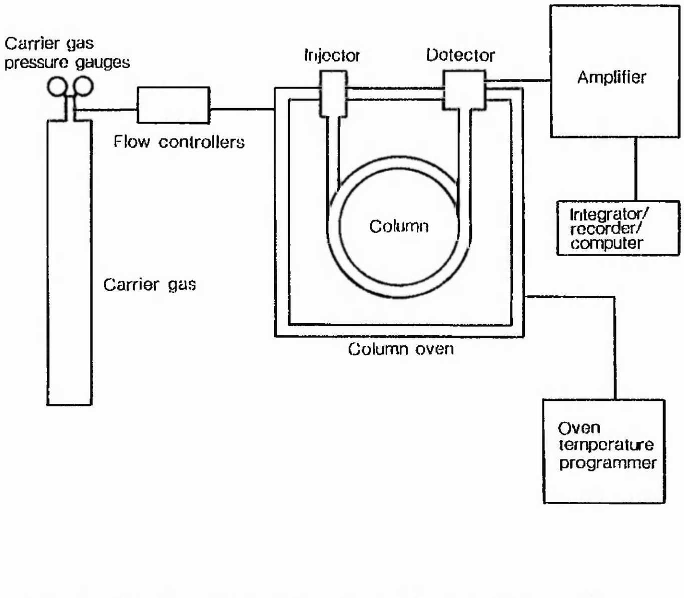

Figure 2.7.1.1 Schematic diagram of a gas chromatograph.

The detector, located at the exit of the separation column, senses the presence of the individual components as they leave the column. The two types of detector most commonly used in gas chromatography are the thermal conductivity detector (TCD) and the flame ionization detector (FID). The TCD is based on the principle that a hot body loses heat at a rate that is dependent on the thermal conductivity, and therefore the composition, of the surrounding gas [7]. The TCD consists of two heated filaments of a metal which has a high coefficient of resistance, and which forms two arms of a Wheatstone bridge-circuit. The two separate filaments are situated in separate channels on a heated metal block. Pure carrier gas flows through one channel (reference channel) and the effluent from the column through the other. A change in thermal conductivity of the gas flowing through the sample channel, arising from elution of a sample component, alters the temperature and hence the resistance of the filament in the channel. This produces an out of balance signal in the bridge circuit that manifests itself as a peak on the integrator trace. The FID adds hydrogen to the column effluent. Subsequently, the mixture is passed through a jet where it is mixed with external air and burned. In a general FID configuration, a flame jet and a cylinder positioned 0.5 - 1 cm above the tip of the flame constitute the twin electrodes. A potential of about 400 V is applied across the two electrodes, which lowers the resistance between the electrodes and causes a current (~10^{-12} A) to flow. The current arises from the ions and free electrons generated in a pure hydrogen/air flame. When ionisable material from the column effluent enters the flame and is burned, the current markedly increases. The current flows through an external resistor, is sensed as a voltage drop, amplified, and finally sent to an output device, a recorder or computer. The FID responds to virtually all organic compounds except formic acid, air, and other inorganic gases. Its response to water is low. It has a very high sensitivity and the widest linear range (10^7) of any detector in common use. A schematic diagram of an FID is shown in **Figure 2.7.1.2.**

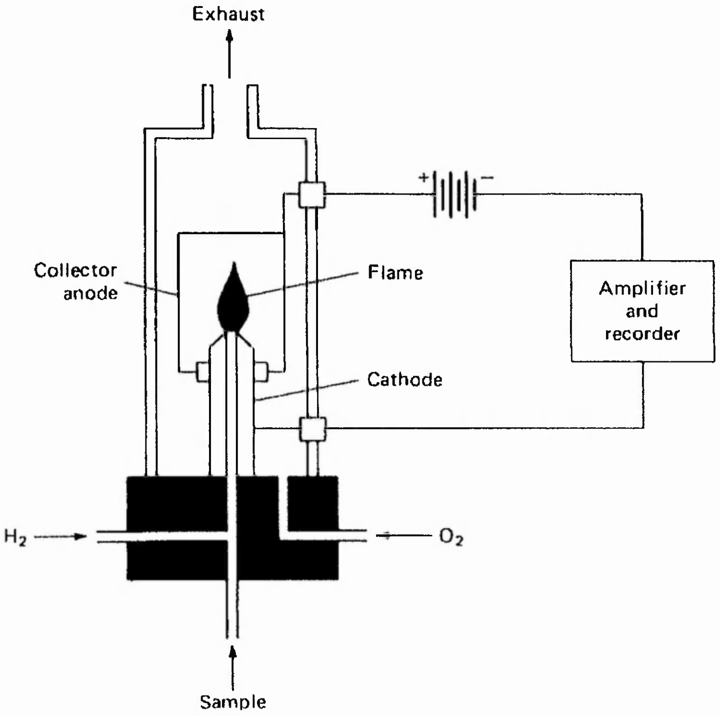

Figure 2.7.1.2 Schematic diagram of an FID.

2.7.2 Experimental

The apparatus used was a Shimadzu GC-8A equipped with a packed column containing an OV101 liquid phase (10% loading) on a chromosorb WHP support, and fitted with an FID. The gas chromatograph operating conditions employed were a column oven temperature programme from 353 K to 473 K, with a temperature ramp of 8 K min^{-1}, and a detector temperature of 623 K. In order to analyze for products, samples were taken from the reaction mixture at 30 minute intervals for a period of 5 h, and in addition a 24 h sample was also extracted to determine the loss of activity of the catalyst with time. Sample extraction was achieved by taking a small amount of liquid from the reaction mixture with a teat pipette and transferring it into a sample bottle. Then a 0.2 μl sample was taken up in a 5 μl syringe and injected into the column through a self sealing silicone-rubber septum. **Figure 2.7.2.1** shows a typical gas chromatograph trace from the standard reaction involving the acylation of anisole with acetic anhydride over zeolite Beta using N-Decane as internal standard.

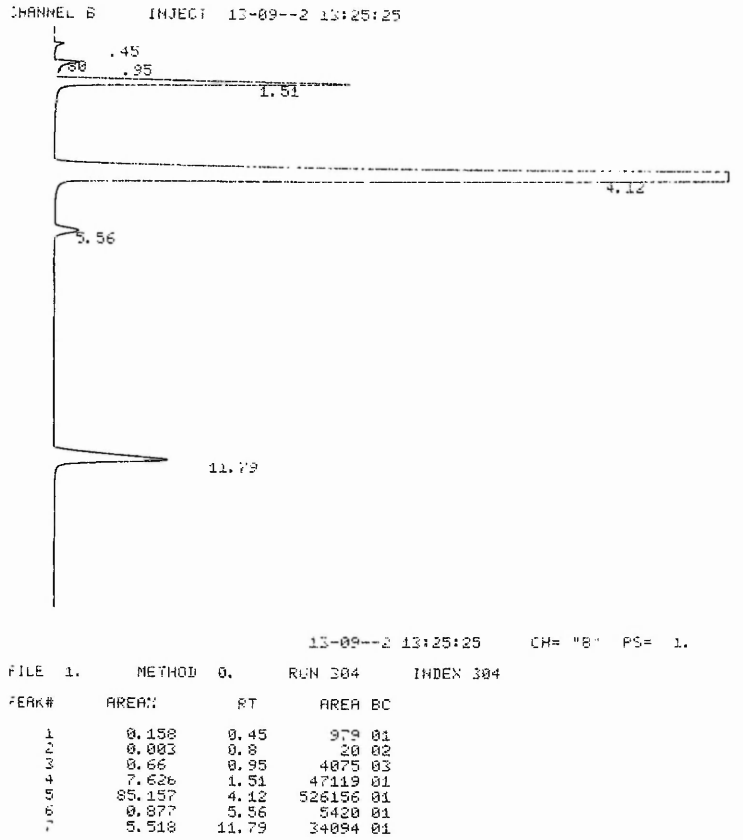

```
CHANNEL B      INJECT  13-09--2 13:25:25

                                  13-09--2 13:25:25     CH= "B"  PS=  1.

FILE  1.      METHOD  0.     RUN 304      INDEX 304

PEAK#      AREA%         RT        AREA BC

   1        0.158      0.45        979 01
   2        0.003      0.8          20 02
   3        0.66       0.95       4075 03
   4        7.626      1.51      47119 01
   5       85.157      4.12     526156 01
   6        0.877      5.56       5420 01
   7        5.518     11.79      34094 01
```

Figure 2.7.2.1 A typical GC trace for product analysis.

Table 2.7.2.1 shows the retention time and the corresponding identification of each of the reaction components in the above trace.

Retention time (minutes)	Reaction component
0.95	acetic acid
1.51	acetic anhydride
4.12	anisole
5.56	decane
11.79	methoxyacetophenone

Table 2.7.2.1 Retention times of major reaction components.

2.7.3 Analysis of GC results

Data from chromatograms may be used to obtain the relative concentrations of components in a mixture, providing good resolution is achieved. Peak area, from integration of the detector signal during elution of a component, is proportional to the amount of that component in the sample. However, the response of a detector varies from one compound to another. Thus a set of detector response factors needs to be determined for a particular analysis. The internal standard method is recommended for accurate quantification and was chosen for this investigation. It eliminates the need for accurate injections since a reference standard is included in each sample analysed. An internal standard is selected which elutes in a suitable 'gap' in the chromatogram. The procedure involves analyzing a test sample containing known amounts of each component plus a predetermined amount of internal standard. Since peak area is proportional to the amount of an eluted component and the detector response factor (D_{RF}):

Equation 2.7.3.1 For an individual component x: $A_X = D_{RFX} \times C_X$

Equation 2.7.3.2 And for the internal standard: $A_{IS} = D_{RFIS} \times C_{IS}$

Where C is the amount of component x or internal standard, IS. The relative response of a component ($D_{RF'X}$) to the internal standard is therefore:

Equation 2.7.3.3 $D_{RF'X} = (D_{RFX}/ D_{RFIS}) = (A_X/ C_X)/(A_{IS}/ C_{IS})$

$= (A_X/ A_{IS}) \times(C_{IS}/ C_X)$

Response factors for all components are calculated in the same way. Analysis of an unknown mixture is achieved by adding an accurately known amount of internal standard and then carrying out the chromatography. The concentration of each component calculated using the equation above rearranged to give:

Equation 2.7.3.4 $C_X = (A_X/ A_{IS}) \times (C_{IS}/ D_{RFX})$

2.8 Fourier Transform Infrared Spectroscopy (FTIR)

2.8.1 Theory

The infrared region of the electromagnetic spectrum extends from the red end of the visible spectrum to the microwave region. The region includes radiation at wavelengths between 0.7 and 500 μm or, in wavenumbers (the reciprocal of the wavelength), between 14,000 to 200 cm^{-1}. The spectral range used most is the mid-infrared region, which covers frequencies from 4000 to 200 cm^{-1} (2.5 to 50 μm). The energy of most molecular vibrations corresponds to that of the infrared region of the electromagnetic spectrum. Molecular vibrations may be detected and measured either in an infrared spectrum or indirectly in a raman spectrum. Upon interaction with infrared radiation, portions of the incident radiation are absorbed at specific wavelengths. The multiplicity of vibrations occurring simultaneously produces a highly complex absorption spectrum that is uniquely characteristic of the functional groups that make up the molecule. Infrared light is absorbed when the oscillating dipole moment (due to a molecular vibration) interacts with the oscillating electric vector of the infrared beam. A simple rule for deciding if this interaction (and hence the adsorption of light) occurs is that the dipole moment at one extreme must be different from the dipole moment at the other extreme of the vibration. The most important consequence of this selection rule is that in a molecule with a centre of symmetry, those vibrations symmetrical about the centre of symmetry are active in the raman and inactive in the infrared; those vibrations that are not centrosymmetric are inactive in the raman and usually active in the infrared. Organic chemists find that infrared studies are more informative than raman studies since most functional groups are not centrosymmetric. A complex molecule has a large number of vibrational modes that involve the whole molecule. To a good approximation, however, some of these molecular vibrations are associated with the vibrations of individual bonds or functional groups (localized vibrations) while others must be considered as vibrations of the whole molecule. The localized vibrations are either stretching, bending, rocking, twisting, or wagging. Many localized vibrations are very useful for the identification of functional groups. The soggy vibrations of the molecule as a whole give rise to a series of absorption bands at low energy, below 1500 cm^{-1}, the positions of which are characteristic of that molecule. Frequently bands are observed which do not correspond to any of the fundamental vibrations of the molecule and are due to overtone bands and combination bands, the latter as a result of interaction between two or more vibrations. The net result, when a spectrum has been taken, a region above 1500 cm^{-1} showing absorption bands assignable to a number of functional groups and a region, characteristic of the compound in question and no other compound, containing many bands below 1500 cm^{-1}. For many years infrared spectroscopy was performed using dispersive spectrometers. In a dispersive instrument radiation of only a single wavelength is incident on the sample at any time and the spectrum is obtained by measuring the absorption as the wavelength is scanned. The technique of infrared spectroscopy has been revolutionized by application of Fourier transform methods. In this method, infrared radiation is analyzed by means of a scanning Michelson interferometer. This consists of an infrared source, a moving mirror, a fixed mirror, a beamsplitter, and a detector, as shown schematically in **Figure 2.8.1.1**. Radiation from the infrared source is collimated by a mirror, and the resulting beam is divided at the beamsplitter; half the beam passes to a fixed mirror and half is reflected to the moving mirror. After reflection, the two beams recombine at the beamsplitter and, for any particular wavelength, constructively or destructively interfere, depending on the difference in optical paths between the two arms of the interferometer. With a constant mirror velocity, the intensity of the emerging radiation at any particular wavelength modulates in a regular sinusoidal manner. In the case of a broadband source the emerging beam is a complex mixture of modulation frequencies that, after passing through the sample compartment, is focused onto the detector.

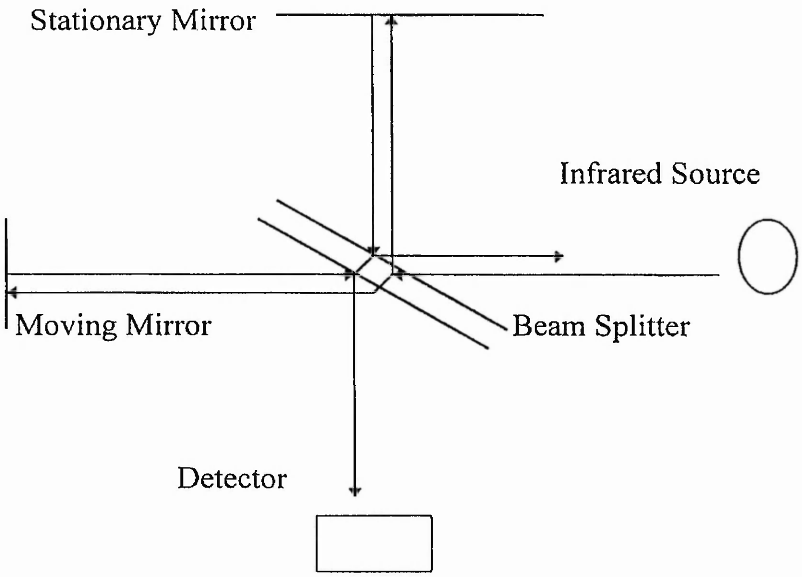

Figure 2.8.1.1 Interferometer optical system.

The detector signal is sampled at precise intervals during the mirror scan. Both the sampling rate and the mirror velocity are controlled by a reference signal incident upon a second detector, which is produced by modulation of the beam from a helium-neon laser. The interferogram produced is converted to a spectrum using a Fourier transform mathematical function that is built into the machine. There are several ways in which the quality of the IR spectrum is improved by Fourier transform methods over traditional dispersive instruments, and these are referred to as advantages.

1) Fellgets advantage is the ability to sample all wavelengths of interest simultaneously, leading to an increased speed of analysis and also leads to a significant improvement in the signal to noise ratio compared to dispersive instruments.
2) Jacquinots advantage results from the fact that in a Fourier transform instrument there are no slits and fewer optical elements, and so the energy used and the sample size may both be bigger than in dispersive instruments leading to improved sensitivity.

3) Connes advantage relates to the accuracy with which the frequency can be defined in the spectrometer. FTIR spectrometers use a laser of accurately known, constant frequency, to calibrate the interferogram. As a result, frequencies are very accurately defined.

2.8.2 Experimental

For IR study wafers weighing approximately 25 mg were prepared by pressing the zeolite powder between stainless steel surfaces. Measurements were performed using an ATI RS1 Fourier transform spectrometer equipped with an in situ stainless steel cell with calcium fluoride windows, allowing the recording of transmission IR spectra between 303 → 973 K, and capable of a base pressure of $< 10^{-7}$ mbar. **Figure 2.8.2.1** and **Figure 2.8.2.2** show the in situ vacuum FTIR apparatus and the in situ IR cell respectively.

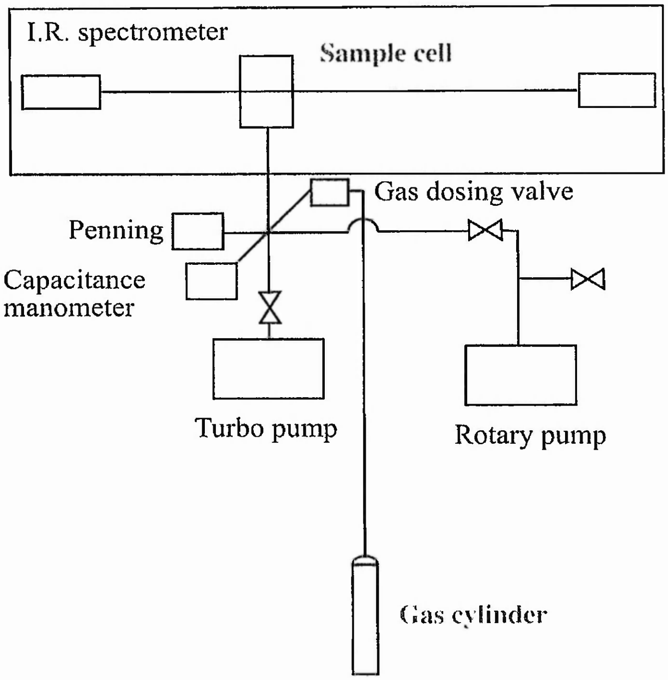

Figure 2.8.2.1 In situ vacuum FTIR apparatus.

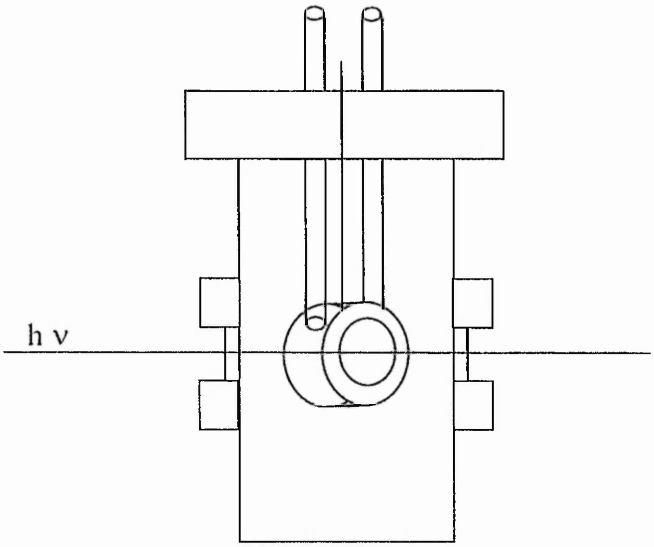

Figure 2.8.2.2 In situ IR cell.

In order to probe the acidic properties of a zeolite, the respective wafer was activated under vacuum (10^{-7} mbar) from 303 to 773 K, with a constant heating rate of 5 K min^{-1}. The sample was kept at 773 K for 1 h in order to ensure that all the ammonia had been evacuated, with the concomitant formation of the proton form of the zeolite. After cooling the cell to 423 K, ammonia (Argo, 99.96%) was admitted into the cell at a starting pressure of 10^{-4} mbar, and the pressure was continually increased at regular time intervals up to a maximum of 2 mbar. After adsorption of ammonia at 423 K, the wafer was outgassed at the same temperature to eliminate any physisorbed ammonia. Finally, ammonia was desorbed in the TPD (Temperature Programmed Desorption) experiment, following the same procedure as the activation.

To identify the types of iron species present in iron-exchanged zeolite Beta, NO (Argo, 99.0%) was absorbed between 10^{-3} and 10 mbar at room temperature, followed by evacuation and desorption.

Deuterium oxide (Aldrich, 99%) was adsorbed at a pressure of 10 mbar and a temperature of 473 K for 5 h, in order to convert H-Beta to D-Beta. The D-Beta was activated using the routine procedure in order to remove excess D_2O from the sample. Acetic anhydride was adsorbed from 10^{-3} to 10^{-1} mbar at 333 K, followed by evacuation and desorption.

In order to determine the adsorption and retention properties of reactants and products, adsorption of acetic anhydride, acetic acid, anisole, and p-methoxyacetophenone was carried out at the standard reaction temperature, 333 K, using the procedure outlined above.

2.8.3 Analysis of FTIR results

The measurement of the numbers of Brønsted and Lewis acid sites has been performed quantitatively using NH_3 as a probe molecule [9]. NH_3 is a hard Lewis base and it is small in size. The various forms of expected chemisorbed NH_3 species, namely coordinated and protonated NH_3, can be detected and discriminated by their characteristic normal vibrations. The protonated form, NH_4^+, is assigned to bands near 1450 and 3130 cm^{-1} [9], while NH_3 coordinated to aprotonic sites is assigned to bands near 1250, 1630, and 3330 cm^{-1} [9]. Using a GRAMS/32 software package, it is possible to integrate the peaks responsible for the Brønsted (NH_4^+) band and Lewis (NH_3) band, and to determine the relative amounts of Brønsted and Lewis acid sites present in different samples. To allow quantitative comparisons, the intensity of the Brønsted (NH_4^+) band (1371-1542 cm^{-1}) and Lewis (NH_3) band (1582-1645 cm^{-1}), were normalized for varying wafer thickness using the intensity of the zeolite lattice overtone bands (1753-2095 cm^{-1}). Similarly, the intensity of the bridged OH band (3572-3641 cm^{-1}), the extralattice OH band (3643-3679 cm^{-1}), and the very high frequency band (3769-3794 cm^{-1}) were normalized for varying wafer thickness. The major peaks indicative of anisole (1414-1536 cm^{-1}), acetic anhydride (1713-1794 cm^{-1}), acetic acid (1526-1818 cm^{-1}), and p-MAP (1475-1721 cm^{-1}) were also normalized in a similar manner.

The intensity of the bands responsible for NH_4^+, anisole, acetic anhydride, acetic acid, and p-methoxyacetophenone were differentiated with respect to temperature by Savitsky-Golay differentiation [10], in order to obtain conventional TPD curves.

Selected FTIR spectra and TPD traces where overlapping of peaks was significant were subject to peak fitting using a mixed Gaussian and Lorentzian peak function, corresponding to a 30% Gaussian, 70% Lorentzian line shape.

2.9 Nuclear Magnetic Resonance Spectroscopy

2.9.1 Theory

The phenomenon of Nuclear Magnetic Resonance (NMR) was first developed in 1946, and it has been routinely applied in organic chemistry since about 1960. NMR is considered to be the most valuable spectroscopic technique available to organic chemists. It provides a map of the carbon-hydrogen framework. Many kinds of nuclei behave as though they were spinning about an axis. Since they are positively charged, these spinning nuclei act like tiny magnets and therefore interact with an external magnetic field. Not all nuclei behave this way, but fortunately, both the proton (^{1}H) and the ^{13}C nucleus do have spins. In the absence of an external magnetic field, the nuclei are orientated randomly. When a sample containing these nuclei is placed between the poles of a strong magnet, however, the nuclei adopt specific orientations. A spinning ^{1}H or ^{13}C nucleus can orientate so that its own tiny magnetic field is aligned with (parallel to) or against (anti-parallel) to the external field. The parallel orientation is slightly lower in energy making this spin state slightly favoured over the anti-parallel orientation [11]. If the orientated nuclei are now irradiated with electromagnetic radiation of the right frequency, energy absorption occurs and the lower energy state spin flips to the higher energy state. When this spin flip occurs, the nuclei are in resonance with the applied radiation. The exact frequency necessary for resonance depends both on the strength of the external magnetic field and on the identity of the nuclei. If a very strong magnetic field is applied, the energy difference between the two spin states is large, and higher frequency (higher energy) radiation is required for a spin flip. If a weaker magnetic field is applied, less energy is required to effect the transition between nuclear spin states. ^{1}H and ^{13}C are not unique in their ability to exhibit the NMR resonance phenomenon. All nuclei with an odd number of protons, and all nuclei with an odd number of neutrons show magnetic properties. Only nuclei with even numbers of both protons and neutrons do not give rise to magnetic phenomenon. All nuclei in molecules are surrounded by electrons. When an external magnetic field is applied to a molecule, the electrons set up tiny local magnetic fields of their own. These local magnetic fields act in opposition to the applied field so that the effective field actually felt by the nucleus is smaller than the applied field. The nuclei are shielded from the full effect of the applied field by the circulating electrons that surround them. Since each specific nucleus in a molecule is in a slightly different electronic environment, each nucleus is shielded to a slightly different extent, and the effective magnetic field is not the same for each nucleus. If the NMR instrument is sensitive enough, the tiny differences in the effective magnetic field experienced by different nuclei can be detected, and a distinct NMR signal can be seen for each chemically distinct carbon or hydrogen nucleus in a molecule. NMR spectra are displayed on charts that show the applied field strength increasing from left to right. The left part of the chart is the low field, or downfield, side, and the right side is the high field, or upfield, side. To define the position of an absorption, the NMR chart is calibrated and a reference point is used. Tetramethylsilane (TMS) is used as a reference for both ^{1}H and ^{13}C measurements because it produces in both kinds of spectrum a single peak that occurs upfield of other absorptions normally found in organic compounds. The position of the chart at which a nucleus absorbs is called its chemical shift. By convention, the chemical shift of TMS is set as the zero point, and the other absorptions normally occur downfield. NMR charts are calibrated using an arbitrary scale called the delta scale. One delta unit (δ) is equal to 1 part per million (ppm) of the spectrometer operating frequency. By using this method, the chemical shift of an NMR absorption given in δ units is constant, regardless of the operating frequency of the spectrometer, thus comparisons of spectra obtained on different instruments are possible. Nuclei that are more strongly shielded by electrons require a higher applied field to bring them into resonance and therefore absorb on the right side of the NMR chart. Nuclei that are less strongly shielded need a lower applied field for resonance to occur and therefore absorb on the left of the NMR chart. Nuclei can interact with each other to cause mutual splitting of otherwise sharp resonance lines into multiplets, called spin-spin coupling. This phenomenon is characteristic of ^{1}H NMR spectra. These multiplets arise because magnetic moments of nuclei interact with each other through the strongly magnetic electrons in the intervening bonds. The strength of the coupling, denoted by J, is given by the spacing of the multiplets, and expressed in hertz. No such splitting occurs in ^{13}C NMR spectroscopy for two reasons. Firstly, the low natural abundance of ^{13}C makes it unlikely that two such nuclei will be adjacent. Secondly, no coupling of a ^{13}C nucleus with nearby hydrogens is seen because ^{13}C spectra are normally recorded using double resonance (or spin decoupling). At the same time that the sample is irradiated with a pulse of rf energy to cover the carbon resonance frequencies, it is also irradiated by a second broad band of rf energy covering all the hydrogen resonance frequencies. This second irradiation makes the hydrogens flip spin so rapidly that their local magnetic fields average to zero and no coupling with carbon spins occurs. In a conventional NMR spectrometer either the rf frequency is held constant while the strength of the field is varied or the strength of the magnetic field is held constant while the rf frequency is varied. In either case, each signal in the spectrum is recorded sequentially. In the Fourier Transform NMR (FT-NMR) techniques used by modern spectrometers, a sample is placed in a magnetic field of constant strength and is irradiated with a short burst, or 'pulse' of rf frequency that covers the entire range of useful frequencies at once. All nuclei in the sample resonate at once, giving a complex, composite signal. In essence, this pulse distorts the equilibrium population of the nuclear energy levels; afterwards the system reverts towards the equilibrium population by emitting its excess energy in the relaxation process. The spin system strives to re-establish its equilibrium via two relaxation processes, spin-spin and spin-lattice relaxation. In spin-lattice relaxation (T_1) the magnetic energy is transferred to the surrounding medium, appearing largely as translational and rotational energy. Spin-spin relaxation (T_2), on the other hand, involves mutual exchange of spins with neighbouring nuclei. Large values of T_1 lead to broadened lines in the NMR spectrum, and this is one of the reasons why solids containing spin ½ nuclei, which generally have large values of T_1, yield broad peaks. Nuclei with spin > ½ (i.e., those that are quadrupolar) relax more efficiently than spin ½ nuclei; in some cases the relaxation is so rapid that quadrupolar nuclei also exhibit line broadening. The emission observed as the spin system reverts to equilibrium takes the form of radiation at all the allowed transition frequencies, thereby yielding an oscillating decaying signal known as the free induction decay (FID), the oscillation resulting from the beats between all the contributing frequencies. The FID contains all the NMR spectral information associated with the sample; this information is retrieved mathematically by Fourier transformation using a computer [12]. Since all resonance signals are collected at once, it only takes a few seconds rather than a few minutes to record an entire spectrum. Furthermore, no longer are chemists restricted to examining NMR spectra from liquid solutions. For nuclei, such as ^{13}C, line broadening for a polycrystalline material arises from the fact that the molecules are orientated in all possible directions. The shielding any particular nucleus receives from its electronic environment is thus a function of the orientation of the molecules that contains it. This type of line broadening due to chemical shift anisotropy can largely be removed by rotating the sample very rapidly (faster than 2 kHz) about an axis orientated at an angle of approximately 54.7° (the magic angle) with respect to the external magnetic field. Magic-angle-spinning NMR (MAS-NMR) is now a standard method of obtaining high resolution spectra of solids. MAS-NMR is often employed alongside two other additional means of improving the quality of solid state NMR signals; decoupling and cross polarization. The process of decoupling is carried out by a double-resonance technique (as described earlier) where two radio frequencies are needed. One is used to observe signals due to the nuclei under investigation; the other irradiates strongly the resonance of the nucleus to be decoupled. This procedure is extremely valuable in eliminating broadening influences arising from heteronuclear interactions (e.g. ^{29}Si and ^{1}H in silica gels and silicates). Cross polarization (CP) is designed to overcome the problems associated with low sensitivity of rare spins and their long relaxation times (e.g. in improving ^{13}C signals). CP is based on the fact that the relatively strong spin polarization of abundant spins (e.g. ^{1}H) can be transferred to enhance the weak polarization of rare spins (e.g. ^{13}C). It results in higher signal intensity for ^{13}C, and the effective relaxation time of rare spins is greatly reduced as a consequence of opening up for them a new relaxation path. This means that more FIDs can be accumulated in a given time, thereby accelerating the rate at which spectra can be recorded. The procedure consists of four basic timed sequences of rf pulses. The four part procedure is (1) polarizing the ^{1}H spin system by applying a 90° rf pulse at the ^{1}H resonance frequency, (2) spin locking in the rotating frame by applying a 90° phase shift to the foregoing field, (3) establishing ^{13}C - ^{1}H contact by applying a rf field at the ^{13}C resonance frequency, and (4) observing the ^{13}C free induction decay while the ^{1}H field is maintained for decoupling [5]. Solid state MAS-NMR techniques have greatly extended the ability to characterize zeolites and clay catalysts. The formation of these solids in their embryonic state of crystallization and the details of the short range Si-Al ordering and other relevant properties can be monitored. Other ways in which ^{29}Si and ^{27}Al MAS-NMR have elucidated the structure of zeolite catalysts include; (1) distinguishing all five possible Si(nAl) building units, (2) providing a non-destructive means of determining framework Si/Al ratios from the intensities of the Si(nAl) peaks, (3) determining the number of crystallographically non-equivalent tetrahedral (Si) sites in the unit cell, and (4) distinguishing unambiguously and quantitatively between tetrahedrally and octahedrally coordinated Al, even in non-crystalline material [12].

2.9.2 Experimental

2.9.2.1 ^{27}Al MAS NMR instrument settings

^{27}Al MAS NMR spectra were obtained on a Varian UNITY plus with a 7.05T Oxford instruments magnet at 78.2 MHz with a spectral width of 400.0 KHz, and a spin rate of 10000 Hz. The acquisition time was 5.0 ms with a relaxation delay of 0.2 seconds. Approximately 7800 repetitions were recorded. The pulse angle was 22.2°. Chemical shifts were referenced externally to aqueous $AlCl_3$.

2.9.2.2 ^{29}Si MAS NMR instrument settings

^{29}Si MAS NMR spectra were obtained on the Varian UNITY plus at 59.582 MHz with a spectral width of 30.0 KHz, and a spin rate of 4100 Hz. The acquisition time was 15.0 ms with a relaxation delay of either 1.0, 30.0, or 60.0 seconds. Approximately 1184 repetitions were recorded. The pulse angle was 90.0°. For CP-MAS (cross-polarization) experiments the contact was 3.00 ms. Chemical shifts of silicon were referenced to tetramethylsilane (TMS).

2.9.2.3 Sample preparation

Zeolite samples for NMR analysis were activated in a silica glass tube supported in a horizontal furnace, sealed at one end with an air tight stopper, and connected to the *in situ* vacuum FTIR apparatus depicted in **Figure 2.8.2.1** at the opposite end, capable of a base pressure of 10^{-7} mbar. Samples were activated to 773 K under vacuum for 1 h, with a heating rate of 5 K min^{-1}, to obtain the proton form of the zeolite. After cooling to either 333 K or 398 K (comparable to the standard reaction temperature and reflux temperature), acetic anhydride, anisole, or p-methoxyacetophenone (p-MAP) was adsorbed at 1 mbar for 2 h. In the case of the solid p-MAP, heating to 323 K was required in order to convert to the liquid form. Desorption was carried out at 773 K for 6 h. Activated and desorbed samples were rehydrated in a desiccator over a saturated ammonium sulphate solution at room temperature for 24 h prior to NMR analysis, in order to fully rehydroxylate the sample. In addition, the same activated and desorbed samples were also analysed with acetylacetone adsorbed in order to determine if any invisible aluminium species were present [4]. In order to allow quantitative comparison, samples were accurately weighed before NMR analysis.

2.9.3 Analysis of NMR results

All NMR MAS spectra were subject to Gaussian peak fitting in order to observe overlapping peaks. Using peak area measurement with correction for sample mass, the relative amount of aluminium in framework tetrahedral, distorted tetrahedral, and octahedral coordination was quantified.

2.10 X-ray Diffraction

2.10.1 Theory

X-rays have wavelengths in the Ångstrøm range, and are sufficiently energetic to penetrate solids and are well suited to probe their internal surface [6]. XRD is used to identify bulk phases, to monitor the kinetics of bulk transformations, and to estimate particle size. Every atom in a crystal scatters an X-ray beam incident upon it in all directions. Because even a small crystal contains a very large number of atoms, the chance that these scattered waves would constructively interfere would be almost zero except for the fact that the atoms in crystals are arranged in a regular, repetitive manner. XRD is based on the principle that when a beam of X-rays is incident on a crystalline solid, diffraction occurs when the angle of incidence on planes of atoms in the structure satisfies the Bragg equation:

Equation 2.10.1.1 $n\lambda = 2d.\sin\theta$

Where n is a small integer, λ is the wavelength of the monochromatic X-ray beam (1.542 Å for a copper target), d is the separation between planes in the crystal, and θ is the angle of incidence of the X-rays. For a single crystal the Bragg condition will not be satisfied at any arbitrary angle of incidence, only at specific orientations of the crystal with respect to the source and detector are X-rays reflected from planes. If the sample is a finely ground crystalline powder containing many randomly orientated crystallites some will always satisfy the Bragg equation and diffraction will occur. Atoms located exactly on the crystal planes contribute maximally to the intensity of the diffracted beam, atoms exactly halfway between the planes exert maximum destructive interference, and those at some intermediate location interfere constructively or destructively depending on their exact location but with less than their maximum effect. Furthermore, the scattering power of an atom for X-rays depends on the number of electrons it possesses. Thus the position of the diffraction beams from the crystal depend only on the size and shape of the repetitive unit of a crystal and the wavelength of the incident X-ray beam, whereas the intensities of the diffracted beams depend on the type of atoms in the crystal and the location of the atoms in the fundamental repetitive unit, the unit cell. No two substances, therefore, have absolutely identical diffraction patterns when the direction and intensity of all the diffracted beams are considered. By using the Bragg equation, it is also possible to derive lattice spacings. By measuring the angles, 2θ, under which constructively interfering X-rays leave the crystal; the Bragg relation gives the corresponding lattice spacings, which are characteristic for a certain compound. A conventional X-ray source consists of a target that is bombarded with high energy electrons. The emitted X-rays arise from two processes; Electrons slowed down by the target emit a continuous spectrum of Bremsstrahlung, superimposed on this are characteristic narrow lines. The CuKα line, with an energy of 8.04 keV and a wavelength of 0.154 nm, arises because a primary electron creates a core hole in the K shell, which is filled by an electron from the L shell under emission of an X-ray quantum. Kβ radiation is emitted when the K-hole is filled from the M shell, and so on. The process is called X-ray fluorescence, and is the basis for X-ray sources [13]. The XRD pattern of a powdered sample is measured with a stationary X-ray source (usually CuKα) and a movable detector, which scans the intensity of the diffracted radiation as a function of the angle 2θ between the incoming and the diffracted beams. **Figure 2.10.1.1** shows the basic features of an XRD experiment.

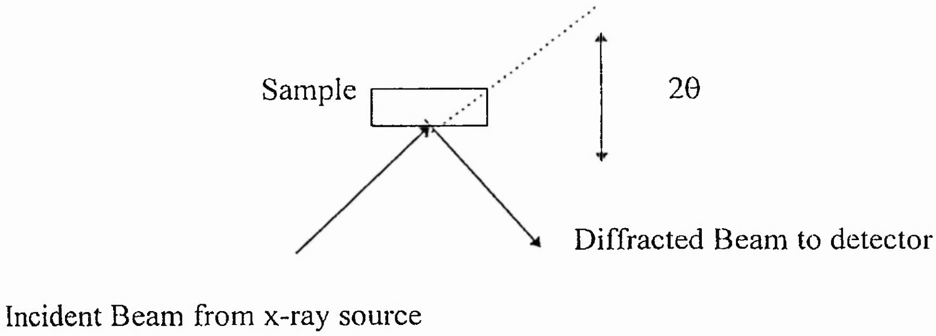

Figure 2.10.1.1 Basic features of an XRD experiment.

In catalyst characterization, diffraction patterns are mainly used to identify the crystallographic phases that are present in the catalyst. XRD has an important limitation: Clear diffraction peaks are only observed when the sample possesses sufficient long range order. The advantage of this limitation is that the width (or rather the shape) of diffraction peaks carries information on the dimensions of the reflecting planes. Diffraction lines from perfect crystals are very narrow, for crystallite sizes below 100 nm, line broadening occurs due to incomplete destructive interference in scattering directions where the X-rays are out of phase. Amorphous phases and small particles give either broad and weak diffraction lines or no diffraction at all, with the consequence that if catalysts contain particles with a size distribution, XRD may only detect larger ones. Hence, it is not possible to determine whether there are any other phases present other than those detected in the XRD. In particular, the surface, where catalytic activity resides, is invisible in standard XRD. The Scherrer formula relates crystal size to line width:

Equation 2.10.1.2 $$\langle L\rangle = \frac{K\lambda}{\beta\cos\theta}$$

Where $\langle L\rangle$ = a measure for the dimension of the particle in the direction perpendicular to the reflecting plane

λ = X-ray wavelength

β = peak width

θ = angle between the beam and the normal on the reflecting plane

K = constant (often taken as 1)

X-ray line broadening provides a quick but not always reliable estimate of the particle size. Better procedures are based on line-profile analysis with Fourier transform methods. The X-ray powder diffraction pattern of zeolites is generally taken between the values 5° 2θ and 40° 2θ. It is within this range that the most intense peaks characteristic of the zeolite structure occurs. The peaks at values higher than 40° 2θ are of significantly low intensity, and, depending on the level of crystallinity, may not be observable. Therefore, for most routine X-ray identification of zeolite phases, the range between 5 and 40° 2θ is examined.

2.10.2 Experimental

Diffraction experiments were carried out on a Hiltonbrooks modified Philips 1050 powder diffractometer, using CuKα radiation, operating the generator at 42.5 kV and 18 mA. The scan range used was 5-60° 2θ with a step size of 0.02° and a step time of 6 seconds.

2.11 Soxhlet extraction [14]

2.11.1 Theory

In soxhlet extraction, the solid to be extracted is packed into a special thimble made of thick filter paper. The thimble is placed in the apparatus shown in **Figure 2.11.1.1** and the whole soxhlet extractor is placed on top of a well-supported round-bottomed flask containing the organic solvent.

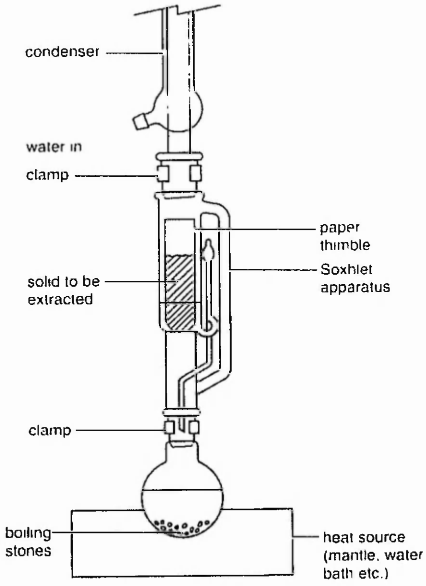

Figure 2.11.1.1 Soxhlet apparatus.

A reflux condenser is placed on top of the soxhlet extractor. The flask is heated using a water or steam bath (for flammable solvents) or some form of electrical heating, so that the solvent boils. Solvent vapour passes up the large diameter outer tube of the apparatus, and the condensed solvent then drips down through the thimble containing the solid. Material is extracted out of the solid into the hot solvent. When the solution reaches the top of the siphon tube, the solution siphons automatically through the narrow tube, and returns to the flask, where the extracted material accumulates. The process is efficient, since the same batch of solvent is repeatedly recycled through the solid. If the extraction is run for prolonged periods it is possible to extract materials that are only very slightly soluble in organic solvents.

2.11.2 Experimental

1 g of deactivated catalyst was treated in a soxhlet apparatus for 24 h with methylene chloride. A small amount of liquid was extracted from the round-bottomed flask after soxhlet treatment and analysed by GC.

2.12 Experimental error

Errors occur naturally in the process of making measurements and can arise from a number of factors. Typical causes of error include those arising from the skill of the experimenter, instrumental limitations, and those associated with analysis of raw data. Bearing such factors in mind, wherever possible, experiments were carried out in triplicate in order to minimise experimental error and increase accuracy. Throughout the thesis, tables state the coefficient of variation for the corresponding set of data. The coefficient of variation is used to give an indication of the amount of variability present in the data. It is calculated by expressing the standard deviation as a percentage of the mean.

Equation 2.12.1

$$\sigma = \sqrt{\frac{\Sigma\left(x-\bar{x}\right)^2}{n-1}}$$

Equation 2.12.2

$$CV = \frac{\sigma}{\bar{x}} \times 100$$

Where σ = Standard deviation

CV = Coefficient of variation

x = One specific value in the set of data

$\bar{x}$ = Mean

n = The number of values of x in the set of data

References

(1) Grün, M.; Unger, K. K.; Matsumoto, A.; Tsutsumi, K. *Microporous Mater.* 1999, ***27***, 207.

(2) Féjes, P.; Hannus, I.; Kiricsi, I. *Zeolites* 1984, ***4***, 73.

(3) Datka, J.; Kolidziejski, W.; Klinowski, J.; Sulikowski, B. *Catal. Lett.* 1993, ***19***, 159.

(4) Bourgeat-Lami, E.; Massiani, P.; Di Renzo, F.; Espiau, P.; Fajula, F.; Courieres, T. D. *Appl. Catal. : A* 1991, ***72***, 139.

(5) Willard, H. H.; Merrit, J. L. L.; Dean, J. A.; Settle, J. F. A. *Instrumental Methods of Analysis*, 7th ed.; Wadsworth Publishing Company, 1988.

(6) Niemantsverdriet, J. W. *Spectroscopy in Catalysis*; VCH, 1993; pp 138.

(7) Fifield, F.; Kealy, D. *Principles and Practice of Analytical Chemistry*; 4th ed.; Blackie Academic and Professional Press, 1995.

(8) Braithwaite, A.; Smith, F. J. *Chromatographic Methods*; 5th ed.; Chapman and Hall, 1996.

(9) Knozinger, H. *Elementary Reaction Steps in Heterogeneous Catalysis*; Joyner, R. W., van Santen, R. A., Eds.; Kluwer Academic Publishers: Dordrecht, 1993; pp 267.

(10) Azambre, B.; Heintz, O.; Schneider, M.; Krzton, A.; Weber, J. V. *Talanta* 1999, ***50***, 359.

(11) McMurry, J. *Organic Chemistry*; Fourth Edition ed.; Brook/Cole Publishing Company, 1996; pp 583.

(12) Thomas, J. M.; Thomas, W. J. *Principles and Practice of Heterogeneous Catalysis*; VCH, 1997.

(13) *Catalysis - An integrated approach to Homogeneous, Heterogeneous and Industrial Catalysis*; Moulijn, J. A., Van Leeuwen, P. W. N. M., van Santen, R. A., Eds.; Elsevier Science: Amsterdam, 1993; pp 318.

(14) Harwood, L. M.; Moody, C. J.; Percy, J. M. *Experimental Organic Chemistry*, 2 ed.; Blackwell Science (UK), 1998.

Chapter 3. Results

3.1 The influence of calcination procedure, ion exchange and regeneration on the acidic properties of zeolite Beta

3.1.1 Abstract

In this section, the acidity results as determined by FTIR, XRD, and MAS NMR studies are presented for zeolite Beta. To a lesser extent, XRD and FTIR studies for zeolite ZSM-5, faujasite, mordenite, and mesoporous MCM-41 are also presented. The following experiments highlight the effect of calcination procedure, ion exchange, and regeneration of spent catalysts on the aluminium content and acidic properties of zeolite Beta. The calcination of ZSM-5, faujasite, mordenite, and MCM-41 were carried out using the recommended calcination procedures as provided in related literature, and their acidic properties probed by FTIR and XRD. The inclusion of zeolites other than zeolite Beta is useful since it allows one to compare different zeolite structure types, with different acidic properties, and relate these properties to their catalytic activity.

3.1.2 Background

Acidity is one of the important characteristics of zeolites which make it catalytically effective [1]. Zeolites are widely used to catalyse various reactions at the solid-liquid interface. In order to understand the mechanism of their catalytic action and to predict their catalytic activity and selectivity, quantitative information on the number, type, and strength of the acid centres on their surface is required. In the 1950's the indicator method of determining the strength of acid centres and the indicator titration method of determining their number were proposed: both of these methods were based on a study of the interaction of indicator molecules (probes) with the surface. Moreover, most of the classical techniques including titration methods, determination of the adsorption isotherms and isobars, and calorimetric measurements do not permit discrimination between acid sites of different quality, i.e. protonic (Brønsted) and non-protonic (Lewis) acid sites. More recently, infrared and nuclear magnetic resonance spectroscopies are the most popular methods for determining the number, type, and strength of acid sites in zeolites. Both of these methods rely on a judicious choice of a chemisorbed molecular probe. The modification of the molecular probe and the extent of its interaction with the acid sites yield the desired information.

3.1.3 Acidity of zeolite Beta

FTIR RESULTS: ***effect of various hydrothermal, thermal, and chemical modifications on the acidic properties of zeolite H-Beta.***

Figure 3.1.3.1 shows a typical FTIR spectrum of the ammonium form of zeolite Beta before and after activation.

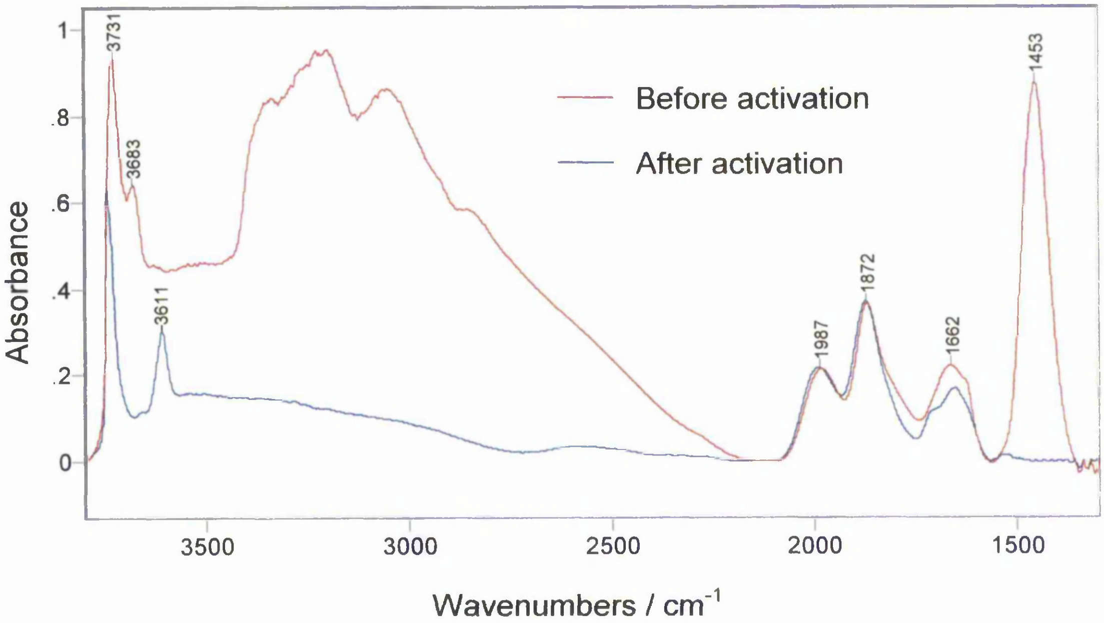

Figure 3.1.3.1 FTIR spectrum of the ammonium form of zeolite Beta before and after activation.

Essentially activation utilising thermal treatment is the final step in producing the zeolite acid catalyst from the ammonium form. Heating decomposes the ammonium cation, releasing ammonia gas and leaving protons as the counter-cations [2]. **Figure 3.1.3.2** and **Figure 3.1.3.3** show the effect of various hydrothermal, thermal, and chemical modifications on the acidic properties of zeolite H-Beta.

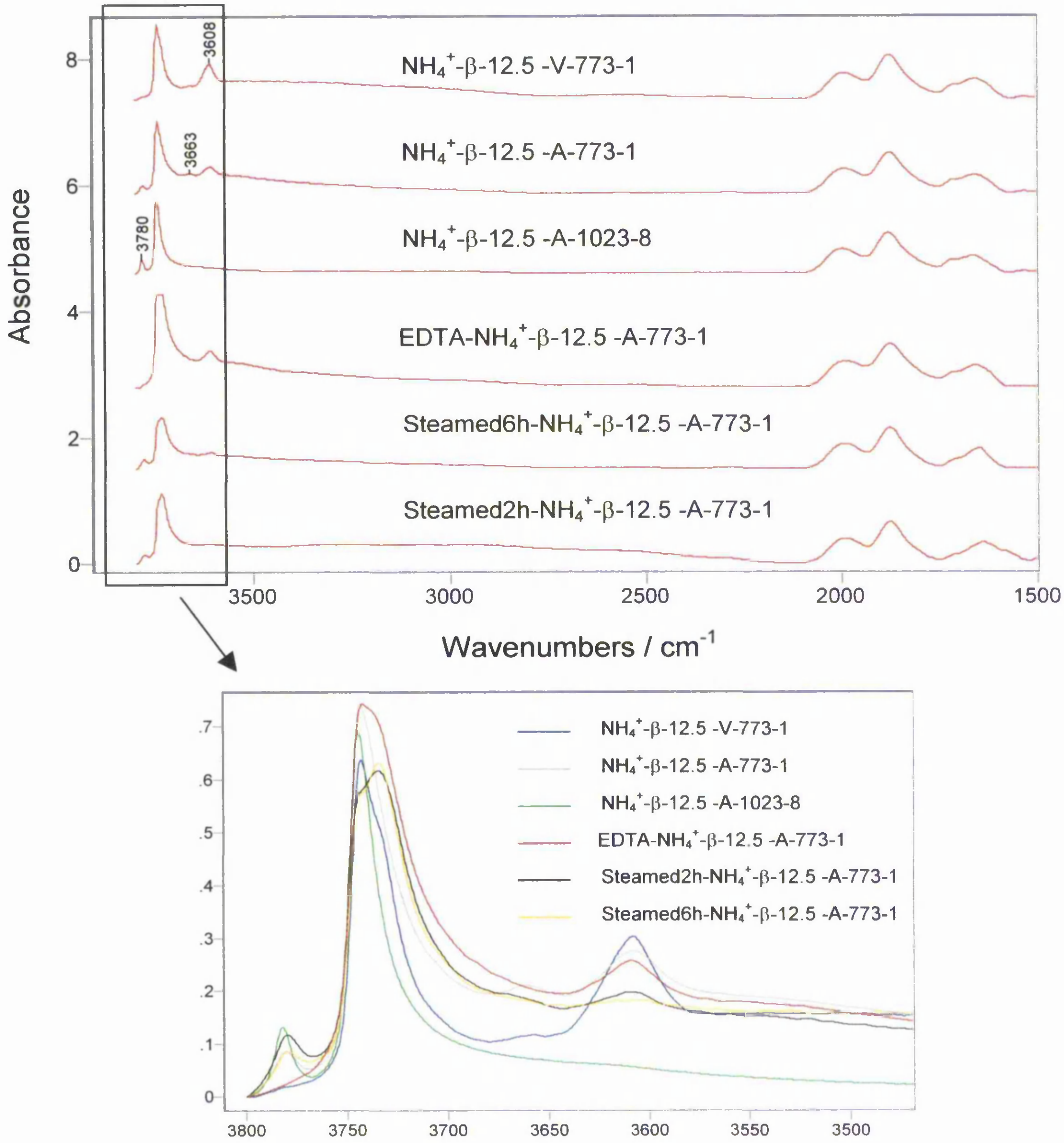

Figure 3.1.3.2 FTIR spectra in the hydroxyl region of zeolite H-Beta after various hydrothermal, thermal, and chemical modifications. Spectra taken at 423 K and normalised to the zeolite lattice overtones at 1987 and 1872 cm^{-1}.

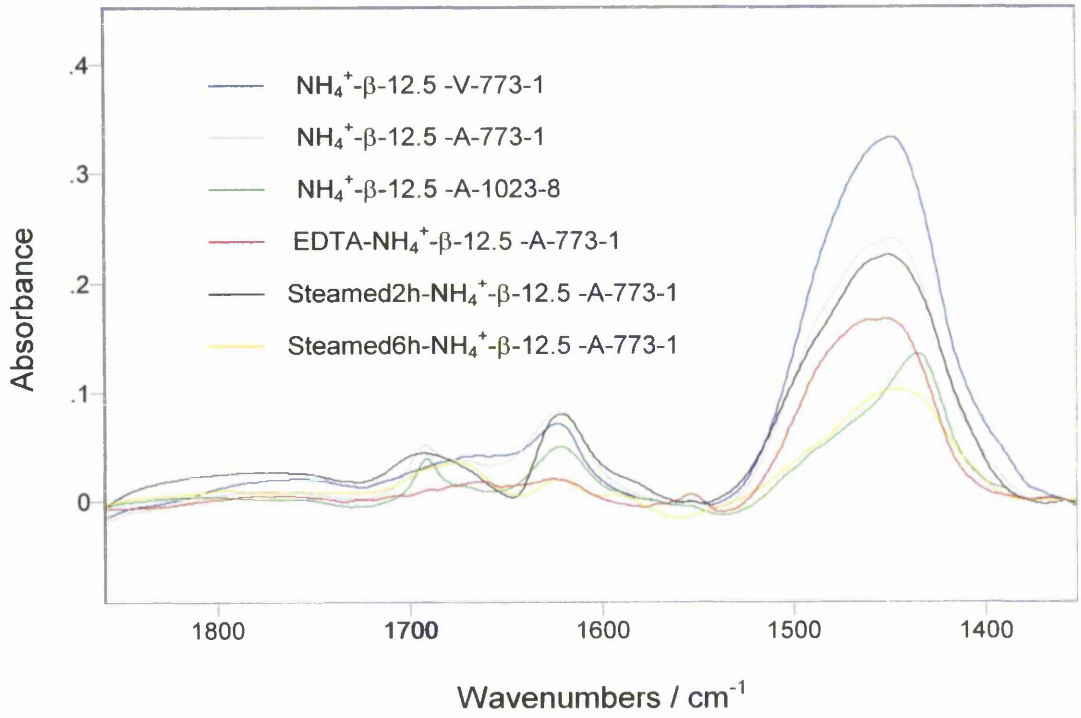

Figure 3.1.3.3 FTIR spectra in the NH deformation region of zeolite H-Beta after various hydrothermal, thermal, and chemical modifications showing the change in bands at 1450 cm^{-1} (NH_4^+) and 1623 cm^{-1} (NH_3). Spectra taken at 423 K and normalised to the zeolite lattice overtones at 1987 and 1872 cm^{-1}.

The integration of the respective absorption bands shown in **Figure 3.1.3.2** and normalisation to the lattice overtone absorption bands gives the relative concentration of bridged OH (3608 cm^{-1}), extralattice OH (3663 cm^{-1}) and very high frequency OH (3780 cm^{-1}) groups for each sample, as presented in **Table 3.1.3.1** and **Figure 3.1.3.4**. The relative concentration of Brønsted and Lewis acid sites depicted in **Figure 3.1.3.3** were calculated in the same way and are presented in **Table 3.1.3.2** and **Figure 3.1.3.5**. Since this method involves dividing the absorbance of the band of interest by the absorbance of the lattice overtones, the value obtained is a ratio and has no units, but serves as a useful means of quantitatively comparing similar bands in various samples. It is important to note that quantitative comparison of different bands in the same sample is complicated by differences in extinction coefficients.

Table 3.1.3.1 Relative concentration of VHF, bridged, and extralattice OH groups.

Sample	**Integral area of absorption band**				**Relative concentration* ± 2%****		
	VHF OH (3769-3794 cm^{-1})	**Bridged OH** (3572-3641 cm^{-1})	**Extralattice OH** (3643-3679 cm^{-1})	**Lattice Overtones** (1753-2095 cm^{-1})	**VHF OH**	**Bridged OH**	**Extralattice OH**
NH_4^+-β-12.5-V-773-1	0	2.87	0	31.89	**0**	**0.09**	**0**
NH_4^+-β-12.5-A-773-1	0.604	2.53	0.312	54.86	**0.011**	**0.046**	**0.005**
NH_4^+-β-12.5-A-1023-18	1.062	0	0	47.69	**0.022**	**0**	**0**
EDTA-β-12.5-A-773-1	0	1.946	0	40.05	**0**	**0.049**	**0**
Steamed 2h-β-12.5-A-773-1	0.484	0.701	0.033	43.46	**0.011**	**0.016**	**0.0008**
Steamed 6h-β-12.5-A-773-1	0.233	0.447	0.026	43.54	**0.005**	**0.010**	**0.0006**

* Relative concentrations are calculated by normalising the integral area of the band of interest to the integral area of the lattice overtone bands.

** Approximate experimental error expressed as the coefficient of variation.

Table 3.1.3.2 Relative concentration of Brønsted and Lewis acid sites.

Sample	Integral area of absorption band			Relative concentration* ± 2%**	
	Brønsted (NH_4^+) band (1371-1542 cm^{-1})	Lewis (NH_3) band (1582-1645 cm^{-1})	Lattice Overtones (1753-2095 cm^{-1})	Brønsted	Lewis
NH_4^+-β-12.5-V-773-1	23.53	1.21	31.89	**0.740**	**0.038**
NH_4^+-β-12.5-A-773-1	29.588	1.481	54.86	**0.539**	**0.027**
NH_4^+-β-12.5-A-1023-18	8.710	1.162	47.69	**0.183**	**0.024**
EDTA-β-12.5-A-773-1	10.87	0.302	40.05	**0.271**	**0.008**
Steamed 2h-β-12.5-A-773-1	9.78	2.07	43.46	**0.225**	**0.048**
Steamed 6h-β-12.5-A-773-1	8.49	0.650	43.54	**0.195**	**0.015**

* Relative concentrations are calculated by normalising the integral area of the band of interest to the integral area of the lattice overtone bands.

** Approximate experimental error expressed as the coefficient of variation.

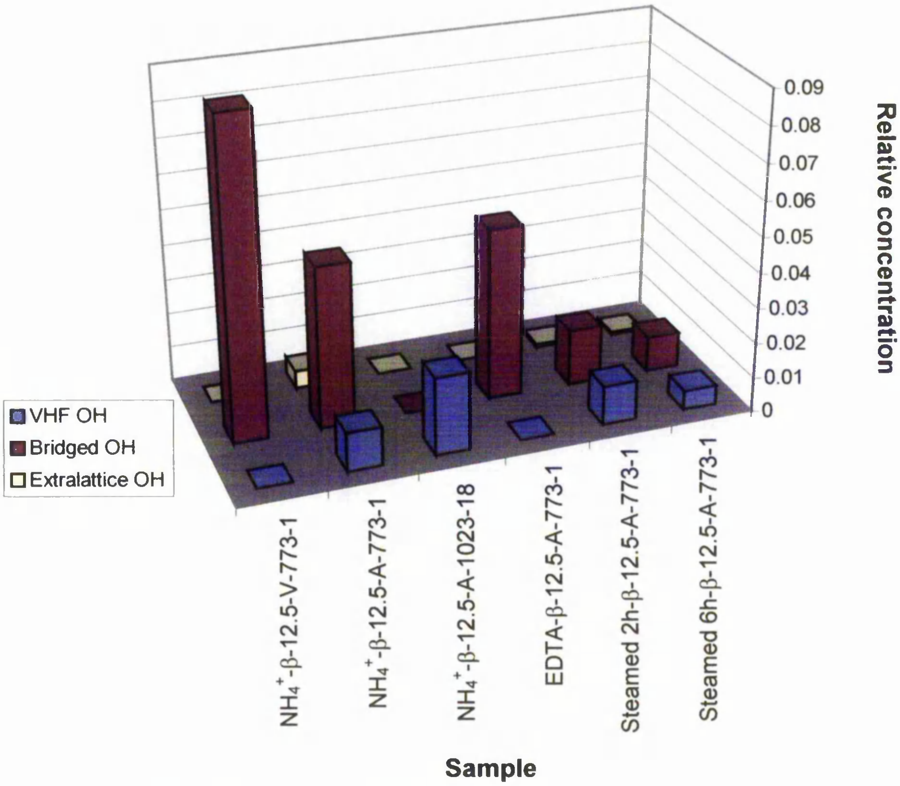

Figure 3.1.3.4 Relative concentration of different hydroxyl groups.

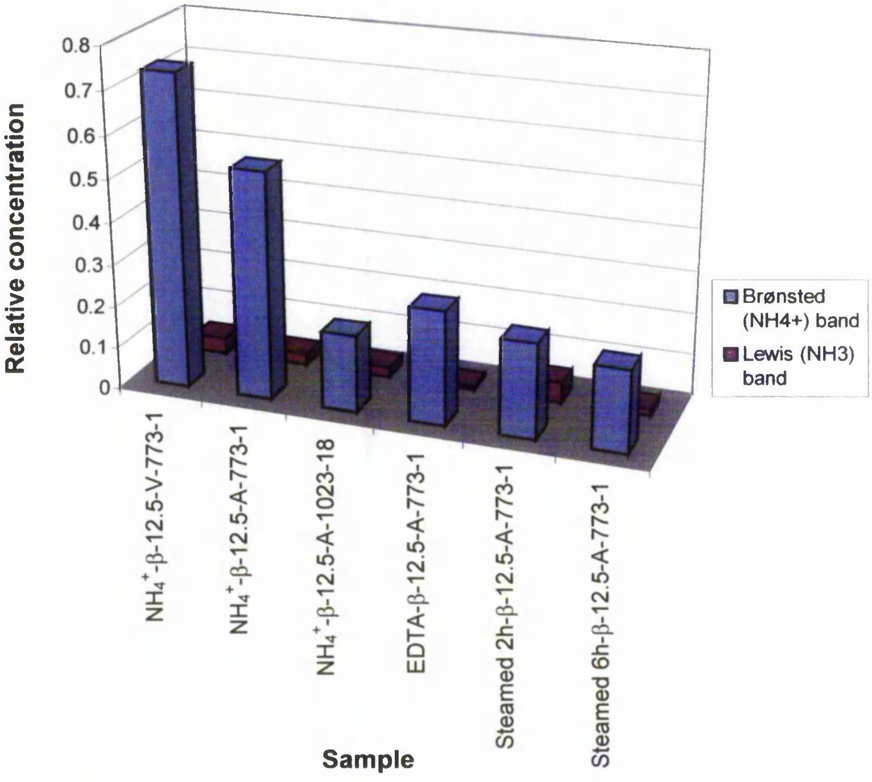

Figure 3.1.3.5 Relative concentration of Brønsted and Lewis acid sites.

Figure 3.1.3.6 shows the relative concentration of NH_4^+ versus the relative concentration of Brønsted acidic OH groups for samples treated by various thermal, hydrothermal, and chemical modifications as described in the key. Values used in the plot were obtained from **Table 3.1.3.1** and **Table 3.1.3.2**. The concentration of Brønsted acidic OH groups was taken as the sum of bridged OH and very high frequency OH groups since these species disappeared upon ammonia adsorption. Extralattice OH groups did not disappear upon ammonia adsorption and thus were considered as non-acidic.

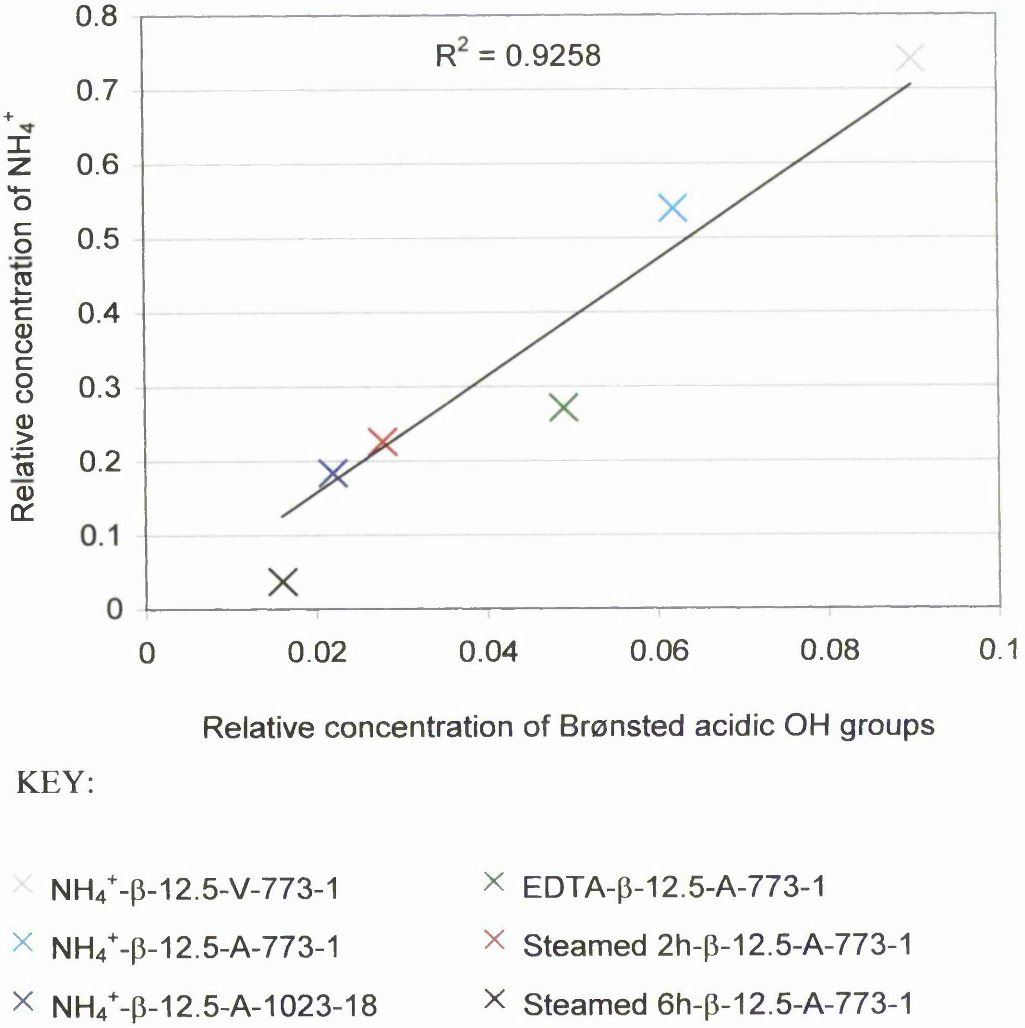

Figure 3.1.3.6 Concentration of NH_4^+ versus concentration of Brønsted acidic OH groups.

A reasonably good correlation exists between the relative concentration of NH_4^+ and the relative concentration of OH groups, indicating that bridged OH and very high frequency OH groups are acting as Brønsted acid sites.

In order to determine the effect of sample treatment on silanol groups in zeolite Beta, the FTIR spectra in the region of 3680 cm^{-1} to 3760 cm^{-1} were subject to peak fitting. Internal SiOH groups (3730 cm^{-1}) and terminal SiOH groups (3745 cm^{-1}) can be difficult to interpret in the FTIR spectra of zeolites since overlapping of the peaks can occur, peak fitting in the appropriate region can allow for more accurate qualitative and quantitative information to be obtained. **Figure 3.1.3.7** to **Figure 3.1.3.12** show the results of peak fitting using a mixed Gaussian and Lorentzian peak function, corresponding to a 30% Gaussian, 70% Lorentzian line shape, in the silanol region of zeolite Beta samples prepared by various thermal, hydrothermal, and chemical modifications, and **Table 3.1.3.3** summarises the findings.

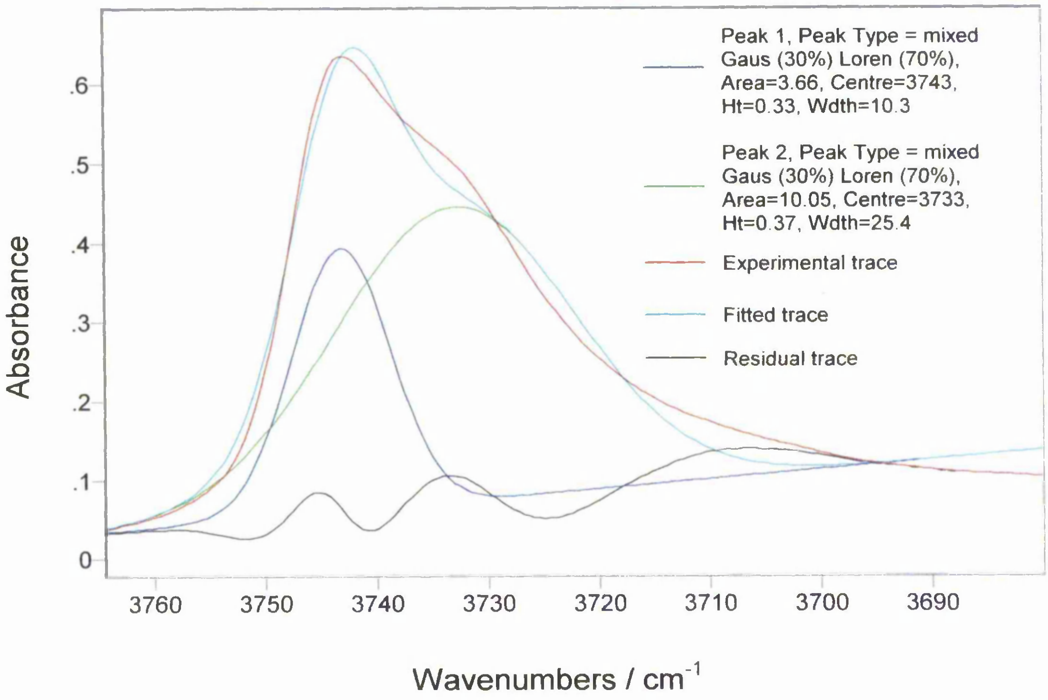

Figure 3.1.3.7 Silanol region of NH_4^+-β-12.5-V-773-1 after peak fitting.

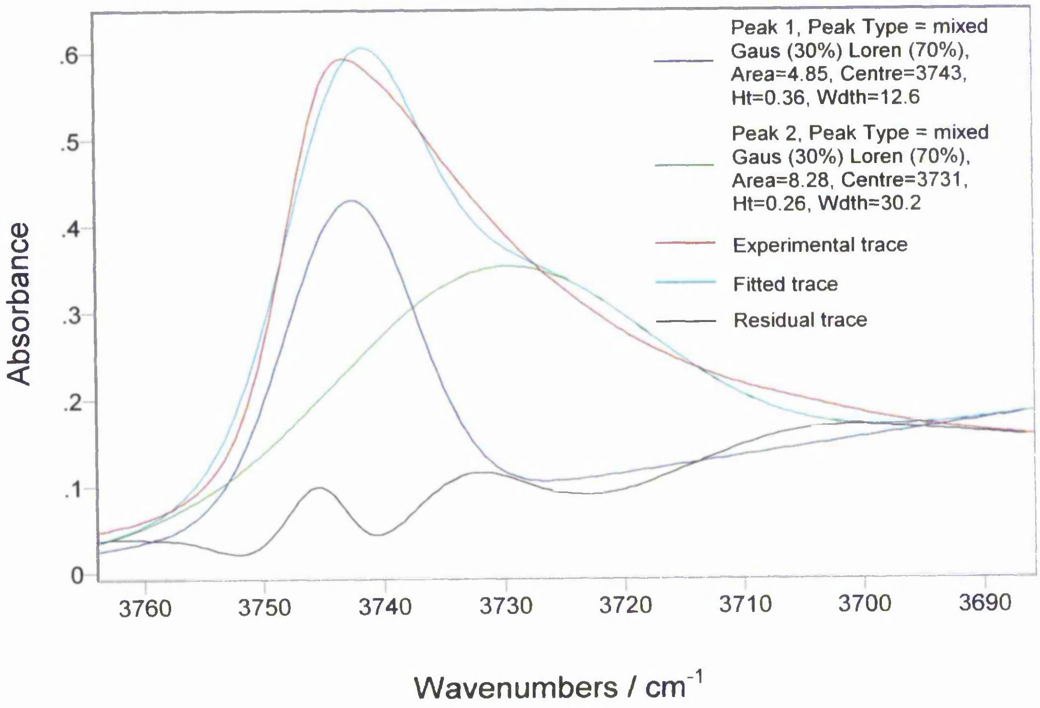

Figure 3.1.3.8 Silanol region of NH_4^+-β-12.5-A-773-1 after peak fitting.

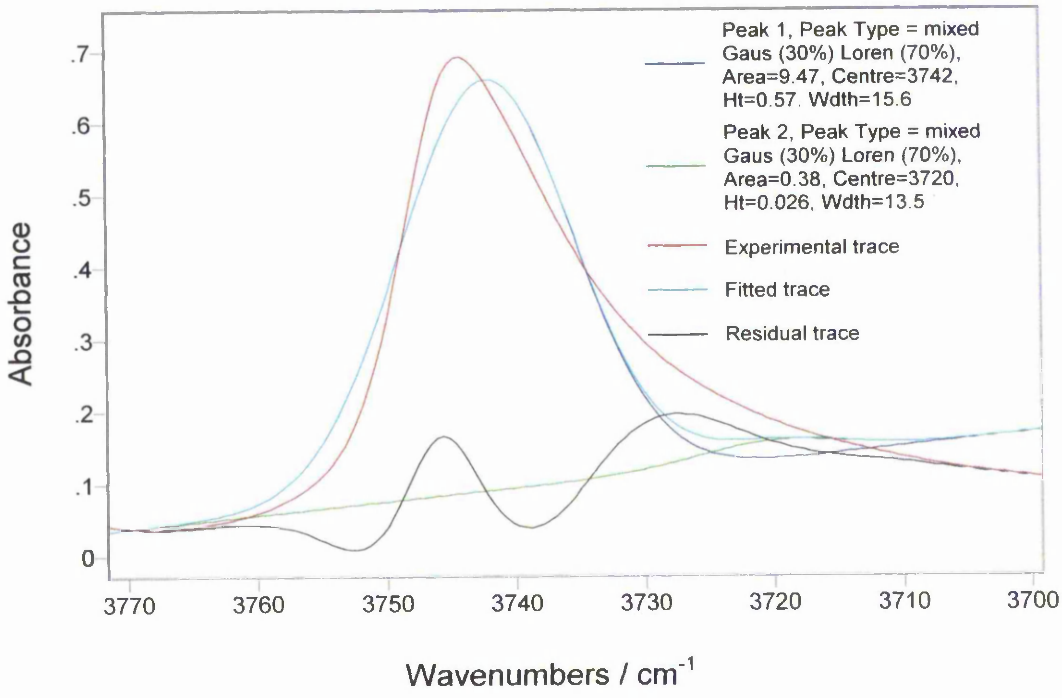

Figure 3.1.3.9 Silanol region of NH_4^+-β-12.5-A-1023-18 after peak fitting.

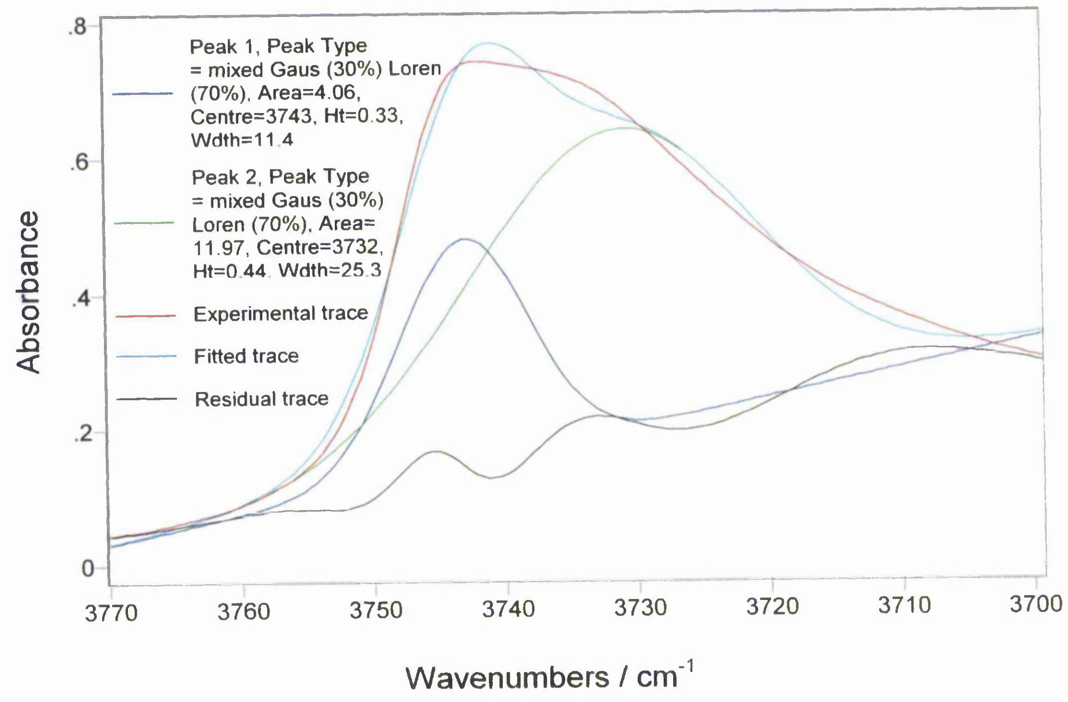

Figure 3.1.3.10 Silanol region of EDTA-β-12.5-A-773-1 after peak fitting.

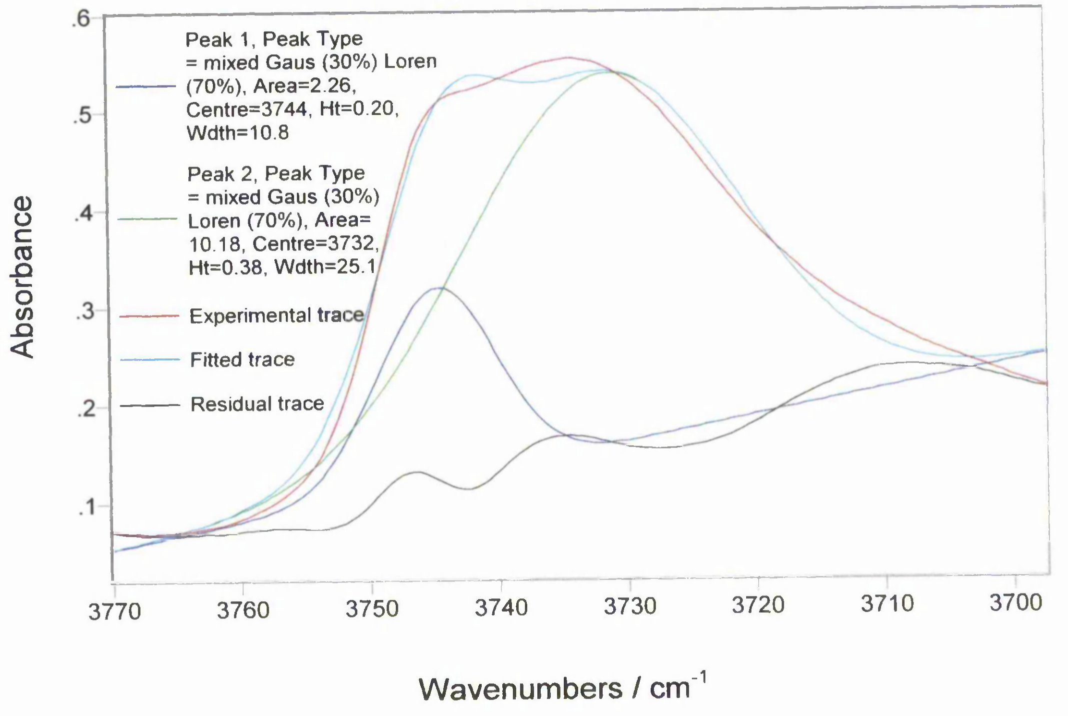

Figure 3.1.3.11 Silanol region of Steamed 2h-β-12.5-A-773-1 after peak fitting.

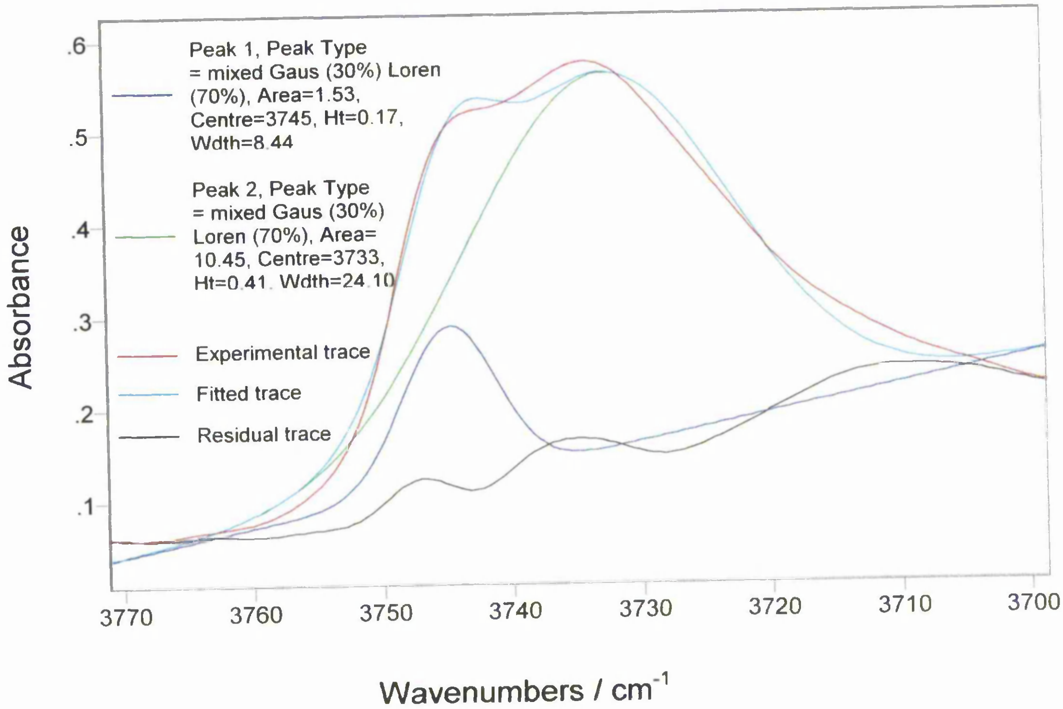

Figure 3.1.3.12 Silanol region of Steamed 6h-β-12.5-A-773-1 after peak fitting.

Table 3.1.3.3 Peak fitting data in the silanol region of treated samples.

Sample	**Integral areas in the silanol region after mixed Gaus (30%) Loren (70%) peak fitting ± 2%***			
	Internal SiOH (3730 cm^{-1})		**External (terminal) SiOH (3745 cm^{-1})**	
	Centre / cm^{-1}	**Area %**	**Centre / cm^{-1}**	**Area %**
NH_4^+-β-12.5-V-773-1	3733	73	3743	27
NH_4^+-β-12.5-A-773-1	3731	63	3743	37
NH_4^+-β-12.5-A-1023-18	-	-	3742	100
EDTA-β-12.5-A-773-1	3732	75	3743	25
Steamed 2h-β-12.5-A-773-1	3732	82	3744	18
Steamed 6h-β-12.5-A-773-1	3733	87	3745	13

* Approximate experimental error expressed as the coefficient of variation.

In order to probe the acidic strength of the identified OH groups present **in** various samples, the intensity of bands responsible for NH_4^+ (1450 cm^{-1}) were differentiated with respect to temperature by Savitsky-Golay differentiation, in order to obtain conventional TPD (Temperature Programmed Desorption) curves. **Figure 3.1.3.13** to **Figure 3.1.3.18** show the TPD curves obtained for samples prepared by different heat treatments and chemical modifications, and **Table 3.1.3.4** summarises the findings. TPD curves were subject to peak fitting using a mixed Gaussian and Lorentzian peak function, corresponding to a 30% Gaussian, 70% Lorentzian line shape in order to observe overlapping peaks.

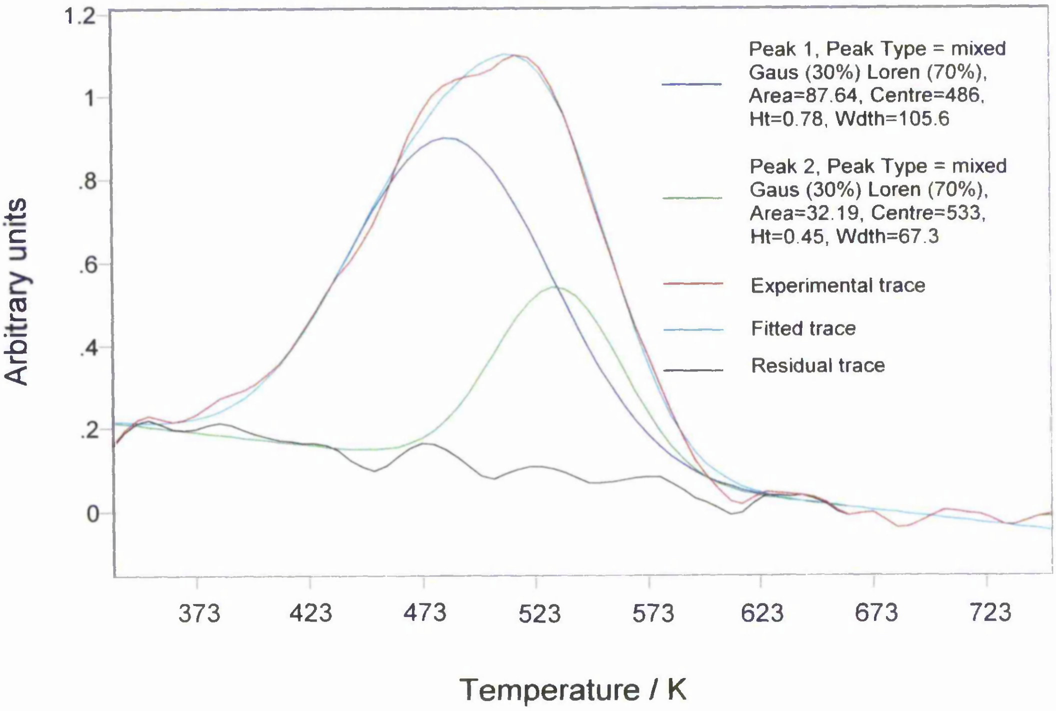

Figure 3.1.3.13 TPD trace of the NH_4^+ band (1371-1542 cm^{-1}) for NH_4^+-β-12.5-V-773-1.

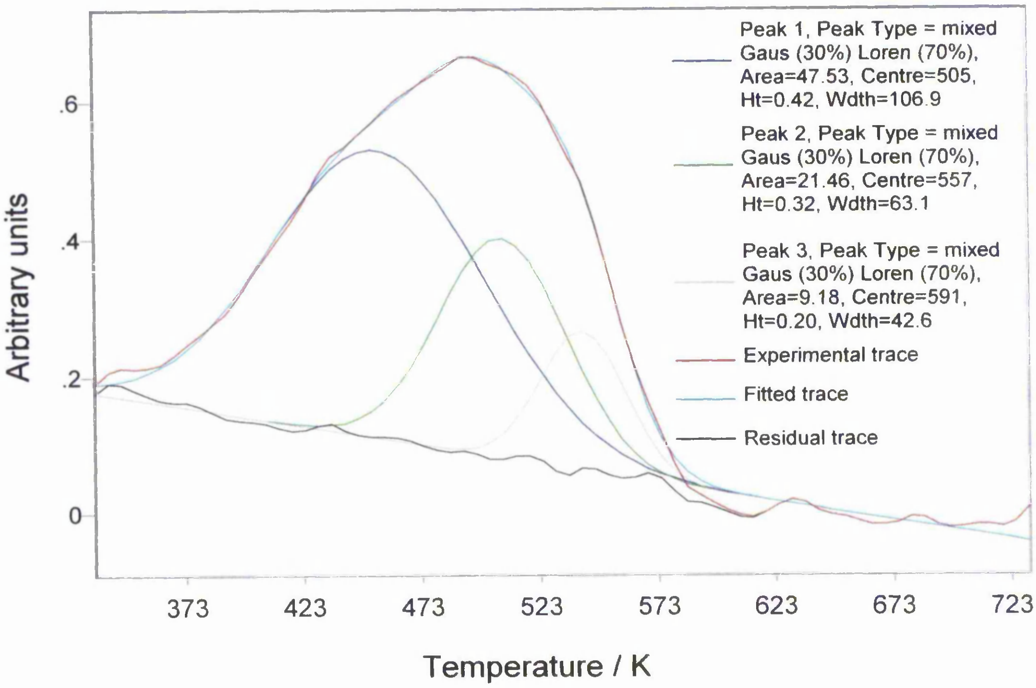

Figure 3.1.3.14 TPD trace of the NH_4^+ band (1371-1542 cm^{-1}) for NH_4^+-β-12.5-A-773-1.

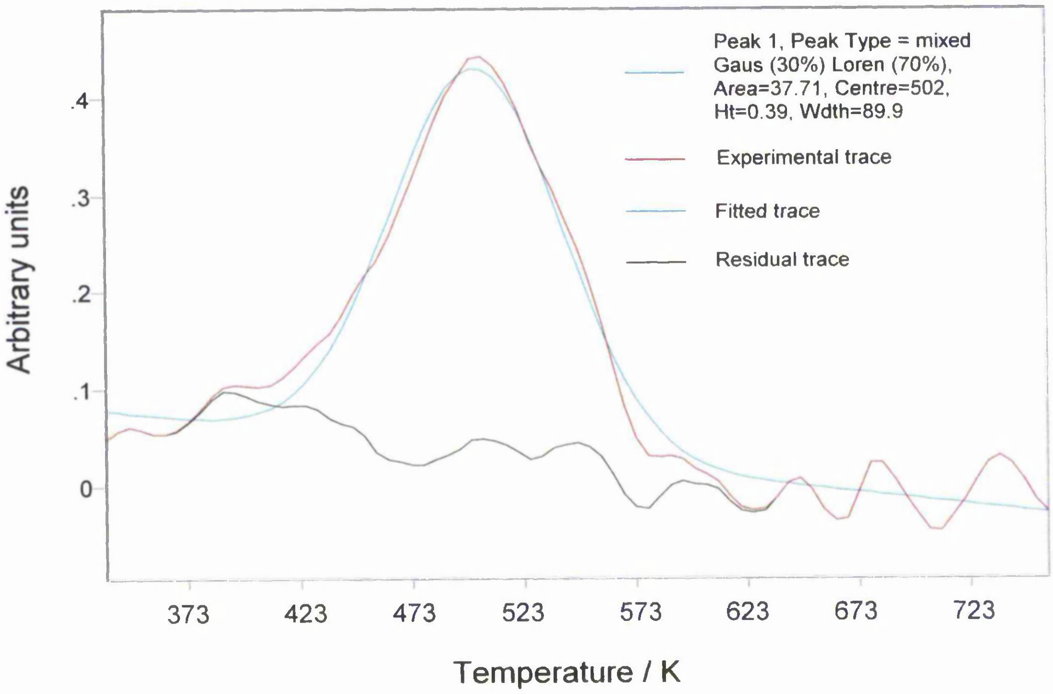

Figure 3.1.3.15 TPD trace of the NH_4^+ band (1371-1542 cm^{-1}) for NH_4^+-β-12.5-A-1023-18.

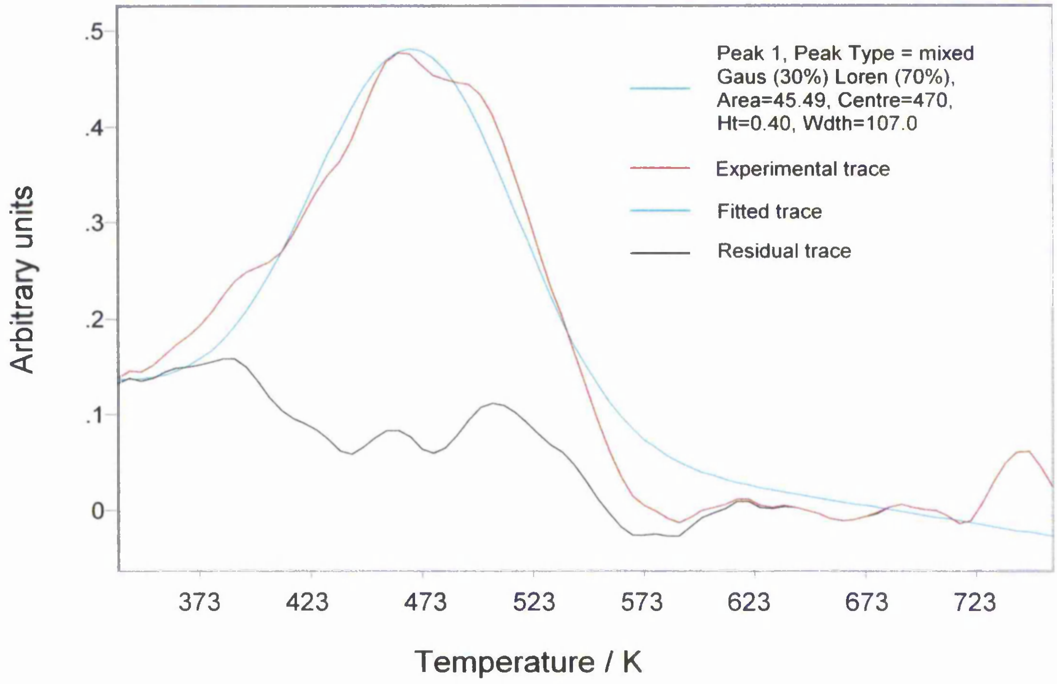

Figure 3.1.3.16 TPD trace of the NH_4^+ band (1371-1542 cm^{-1}) for EDTA-β-12.5-A-773-1.

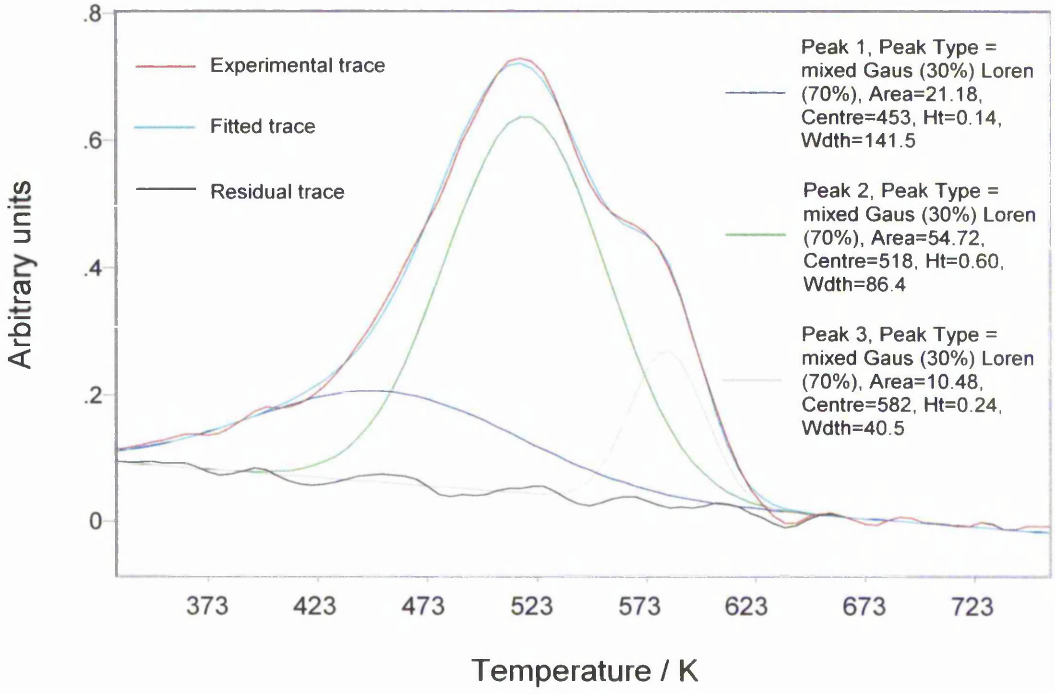

Figure 3.1.3.17 TPD trace of the NH_4^+ band (1371-1542 cm^{-1}) for Steamed 2h-β-12.5-A-773-1.

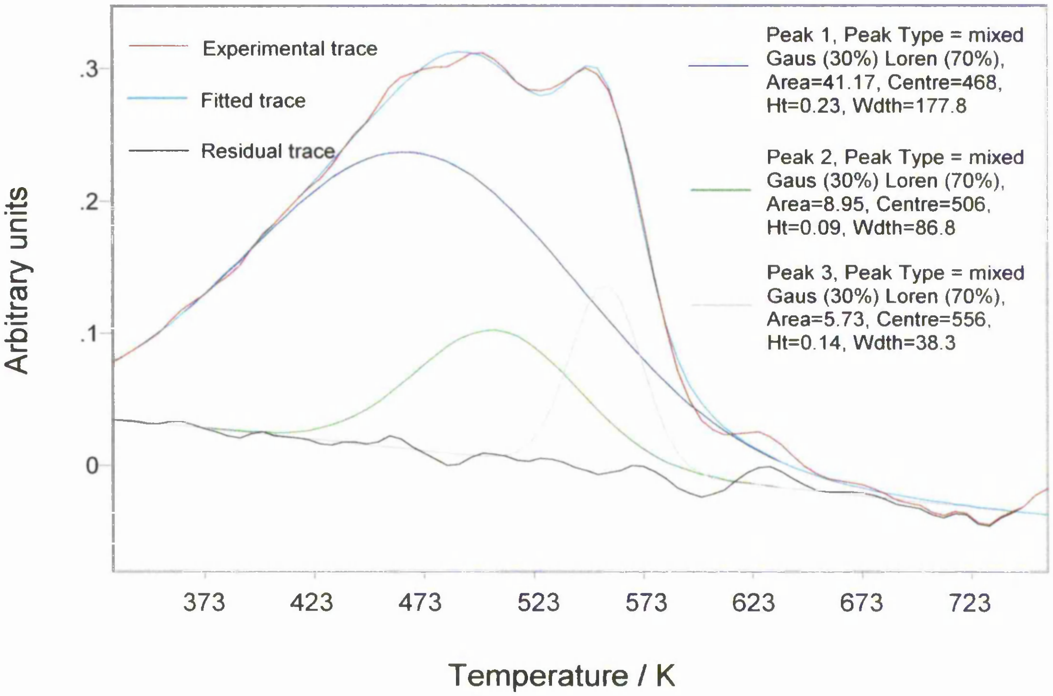

Figure 3.1.3.18 TPD trace of the NH_4^+ band (1371-1542 cm^{-1}) for Steamed 6h-β-12.5-A-773-1.

Table 3.1.3.4 Peak fitting data regarding the TPD of ammonia from Brønsted acid sites.

Sample	**TPD data corresponding to the NH_4^+ band (1371-1542 cm^{-1}) ± 3%***					
	Peak 1		**Peak 2**		**Peak 3**	
	Centre / K	**Area %**	**Centre / K**	**Area %**	**Centre / K**	**Area %**
NH_4^+-β-12.5-V-773-1	486	73	533	27	-	-
NH_4^+-β-12.5-A-773-1	505	61	557	27	591	12
NH_4^+-β-12.5-A-1023-18	502	100	-	-	-	-
EDTA-β-12.5-A-773-1	470	100	-	-	-	-
Steamed 2h-β-12.5-A-773-1	453	25	518	63	582	12
Steamed 6h-β-12.5-A-773-1	468	74	506	16	556	10

* Approximate experimental error expressed as the coefficient of variation.

DISCUSSION

It is evident from **Figure 3.1.3.1** and **Table 3.1.3.1** that the method of sample preparation has a dramatic effect on the type of OH groups present and their concentration. In addition to internal SiOH groups (3730 cm^{-1}) and terminal SiOH groups (3745 cm^{-1}) which are normally present in zeolite Beta [3] (the effect of sample treatment on the relative amounts of these silanol groups will be discussed later), NH_4^+-β-12.5-V-773-1 showed only bridged OH groups (3608 cm^{-1}). Samples treated under high vacuum (10^{-6} mbar) during thermo-treatment such as NH_4^+-β-12.5-V-773-1 favoured the production of samples which showed little or no dealumination. The explanation for this behaviour is the rapid elimination of water that is inevitably present in zeolite samples prior to calcination; this limits the process of auto-steaming [4]. Similarly, a shallow-bed calcination was preferable in cases where auto-steaming was to be kept to a minimum. In a deep bed, the water present in the sample will spend more time in the zeolite than would be the case in a shallow bed and thus increases the possibility of auto-steaming [4]. Steaming can also occur in a moisture-free environment if dehydroxylation is occurring because the latter reaction produces water [5]. Dehydroxylation involves the elimination of water from two active sites (hydroxyl groups) to form different types of sites [6]. Dehydroxylation is thought to occur in zeolite ZSM-5 above 773 K [7]. Samples prepared under such conditions where dealumination is negligible normally contain a maximum number of bridged OH groups and thus Brønsted acid sites, as is the case with NH_4^+-β-12.5-V-773-1. The thermal decomposition of ammonium cations is widely and efficiently used for the preparation of protonic (acidic) zeolites, and Bourgeat-Lami *et al.*, [8] designed experiments to test whether a true H-form of zeolite Beta, i.e. not containing extra-framework species, could be obtained in this way. These workers calcined a sample of NH_4^+-Beta for two hours at increasing temperatures using dry air or nitrogen as gas purge, and characterised the solid at each step. They monitored the decomposition of the ammonium cation by IR spectroscopy and found that the decomposition of the ammonium cations began at 250°C and was completed at 450°C, which is considered as a relatively low temperature for the deammoniation of a zeolite. Despite the low temperature calcination, Al^{27} NMR gave evidence for the presence of octahedral aluminium and thus removal of aluminium from tetrahedral framework positions. In addition they found that the NMR signal present at 0 ppm was already present at 250°C, and increased with deammoniation. The experiments they performed under nitrogen led to similar behaviour. These workers demonstrated a low thermal stability of tetrahedral sites occupied by aluminium atoms in zeolite Beta. A similar phenomenon was found in the present study, and it proved extremely difficult to produce an H-form of zeolite Beta with negligible amounts of octahedral aluminium species, although, as discussed previously, employing a shallow bed and high vacuum proved to be the most effective calcination procedure for limiting the formation of extralattice aluminium species. NH_4^+-β-12.5-A-773-1 contains three types of OH groups, bridging hydroxyls (3608 cm^{-1}), OH groups bonded to extralattice aluminium (3663 cm^{-1}) and very high frequency OH groups (3780 cm^{-1}). Because the calcination was carried out in air rather than vacuum, there is a significant amount of dealumination. This was observed as a decrease in the concentration of bridged OH groups and the concomitant increase in extralattice and very high frequency OH groups, as shown in **Table 3.1.3.1**. Additionally, there is a large decrease in the concentration of Brønsted acid sites in NH_4^+-β-12.5-A-773-1 when compared with NH_4^+-β-12.5-V-773-1 (reduced by 27% when compared with NH_4^+-β-12.5-V-773-1) which is expected due to dealumination and removal of aluminium from the zeolite framework [9], [10]. The exact nature of the very high frequency band is still unknown, but attempts have been made by numerous workers to resolve the structure of this species. The very high frequency OH group is referred to as a transient species according to Kiricsi *et al.*, [3], as an aluminium species still connected to the framework by Jia *et al.*, [11], and Beck *et al.*, [12] refer to it as an unusual aluminium site associated with the framework. Loeffler *et al.*, [13] suggested that such a high frequency OH stretching vibration, in zeolites, would correspond to isolated AlOOH species. In addition, more recently, Trombetta *et al.*, [14] concluded that the band at 3780 cm^{-1} is due to OH groups on extraframework small alumina clusters, which they referred to as "alumina nanoparticles", formed mainly upon dealumination during calcination. The infrared absorption observed at 3663 cm^{-1} in the infrared spectra of NH_4^+-β-12.5-A-773-1 is attributed to hydroxyl groups associated with extralattice aluminium species [8]. It has been well established that calcination and hydrothermal treatment of the ammonium form of zeolite Beta can remove significant amounts of aluminium from the zeolite lattice. The so-called 'extralattice' or 'extraframework' aluminium formed after calcination remains in the zeolite sample after detachment from the framework, however certain post-calcination treatments, in particular acid-washing [15] or treatment with an aqueous solution of hexafluorosilicate [16] can be used to extract extralattice aluminium from a sample. According to Kiricsi *et al.*, [3] the removal of aluminium from framework positions possessing the highest instability can be accounted for by the appearance of this band, and it occurs at approximately 700 K. The true nature of extralattice aluminium is unknown although studies employing different physical methods have been made [17], [18]. Loeffler *et al.*, [13] proposed that the band at 3660 cm^{-1} corresponds to protons compensating negative charges of AlO_4 tetrahedra where the aluminium atom is connected with the zeolite framework only by one or two remaining chemical bonds. NH_4^+-β-12.5-A-1023-18 contains only very high frequency OH groups at 3780 cm^{-1} and also shows a drastic reduction in the number of Brønsted acid sites as shown in **Table 3.1.3.2**. The number of Brønsted acid sites has reduced by 75% when compared with NH_4^+-β-12.5-V-773-1. This is the expected result since activation to 1023 K would lead to increased dealumination and a concomitant decrease in Brønsted acid sites. In addition, the broad background signal in the region of 3600-3200 cm^{-1}, present in both NH_4^+-β-12.5-V-773-1 and NH_4^+-β-12.5-A-773-1, has been significantly reduced. This feature has already been observed by other workers [19], and is thought to arise due to the presence of hydroxyl nests ($(SiOH)_4$) created by imperfections of the lattice [10], or to Si(OH)Al groups interacting via H-bonds with neighbouring oxygen [20]. According to Anderson *et al.*, [21] the OH nests in defect sites consist mainly of $Si(OH)(OSi)_3$ and $Si(OH)_2(OSi)_2$, and Féjes *et al.*, [22] suggested that complete OH nests ($(SiOH)_4$) exist only near 298 K and are rapidly consumed at higher temperatures. More recently, Pazè *et al.*, [23] assigned this broad feature to a second family of Brønsted acid sites consisting of bridged hydroxyls which are perturbed by H-bond interactions with the zeolite framework. The sample treated with H_4EDTA, EDTA-β-12.5-A-773-1, contains only bridged OH groups, and shows a significant decrease in the number of Brønsted acid sites and bridged OH groups (approximately 60% decrease when compared with NH_4^+-β-12.5-V-773-1). It has been shown by Datka *et al.*, [24] that the treatment of zeolite Y by H_4EDTA dealuminates the zeolite framework. They also concluded that since no extraframework aluminium was found after H_4EDTA treatment, all the Al removed from the framework is subsequently washed out of the crystallites in the form of an H_4EDTA complex. The same phenomenon was found in this investigation, where dealumination was observed but no extraframework species were present, indicating that H_4EDTA treatment is a useful means of dealuminating a zeolite sample and removing any extraframework species formed at the same time. The steamed zeolite Beta samples, Steamed 2h-β-12.5-A-773-1 and Steamed 6h-β-12.5-A-773-1 both show signs of dealumination and reduced concentrations of Brønsted acid sites, a 70% decrease in the former case and a 74% decrease in the latter case when compared with NH_4^+-β-12.5-V-773-1. Both samples result in a reduction in the number of bridged hydroxyl groups and a concomitant increase in the number of extraframework and very high frequency OH groups. An interesting observation, which is most evident from **Figure 3.1.3.5**, is that although there is a very significant variation in the number of Brønsted acid sites after various thermal, hydro-thermal and chemical modifications, the number of Lewis acid sites as probed by NH_3 adsorption show very little variation. The most notable exception is in the case of Steamed 2h-β-12.5-A-773-1 where a slight increase in Lewis acidity is observed. It is widely accepted that zeolite Beta has a high number of defect sites, these are generated when a tertiary building unit is rotated 90° around the c-direction with respect to

TBU's in the same layer. The rotated TBU cannot connect properly with adjacent layers, resulting in partially coordinated T atoms which can create potential Lewis acid sites [25]. The theory proposed by Jansen *et al.*, [25] would explain the presence of Lewis acid sites in all the zeolite Beta samples. Additionally, Campbell *et al.*, [16] found that a small number of Lewis acid sites were present on carefully calcined HZSM-5 and attributed this to the presence of residual sodium cations in the zeolite, which may also account for the presence of some Lewis acidity in all the samples. A common observation during the dealumination of HY is an increase in the relative concentration of Lewis acid sites at the expense of Brønsted acid sites [26]. In USY (ultrastable zeolite Y), the Lewis acidity formed during severe calcination is believed to be solely generated by extraframework aluminium species [27]. Dumesic *et al.*, [28] also observed an increase in the number of Lewis sites by increasing the severity of the steam dealumination for USY samples. In contrast, Zhang *et al.*, [29] showed that the dealumination of ZSM-12 results in the complete disappearance of Lewis sites. Robb *et al.*, [30] observed that in zeolite Beta both the Lewis and Brønsted acid site concentration decreases with dealumination. Similarly, Trombetta *et al.*, [14] found that the calcination of zeolite H-Beta results in a decrease in the absolute amount of Lewis acid sites, despite an increase in the ratio of Lewis to Brønsted acid sites. However, Kuehl *et al.*, [9] demonstrated the formation of Lewis acid sites during the calcination of zeolite Beta. They observed octahedral aluminium species connected to the framework structure of zeolite Beta, and that these aluminium sites exhibit characteristics of Lewis acid sites. They suggested that such aluminium species are created by partial hydrolysis of framework Si-O-Al bonds. They also found that when zeolite Beta is severely steamed, a substantial portion of the framework aluminium is completely hydrolysed, and non-framework aluminium species are generated. Similarly, Jia *et al.*, [11] and Beck *et al.*, [12] mention that framework aluminium atoms in a non-tetrahedral coordination may exhibit Lewis acidic properties. Clearly the results in **Table 3.1.3.2** indicate that Lewis acid sites are present in all zeolite Beta samples. The absence of Lewis acidic metal ions as the charge compensating cations indicates that coordinatively unsaturated aluminium atoms are the most likely candidates, and these are present due to the high number of defect sites in zeolite Beta.

Peak fitting using a mixed Gaussian and Lorentzian peak function, corresponding to a 30% Gaussian, 70% Lorentzian line shape in the silanol region of the FTIR spectra of prepared samples are presented in **Figure 3.1.3.7** to **Figure 3.1.3.12** and the results summarised in **Table 3.1.3.3**. This data yields some interesting information on the relative amounts of internal SiOH (3730 cm^{-1}) and external SiOH (3745 cm^{-1}) [4]. It can be seen that sample NH_4^+-β-12.5-V-773-1 contains a significant amount of internal SiOH groups, accounting for 70% of the total amount of silanols, the other 30% being due to the presence of external SiOH. This result would suggest that even during careful calcination a significant amount of defect sites containing SiOH groups are formed, or it may be possible that the majority of these defects sites are present prior to calcination and are an inherent part of the zeolite Beta structure, this seems to be quite plausible since zeolite Beta is known to contain a large number of stacking faults [25]. In sample NH_4^+-β-12.5-A-773-1 there is a slight decrease in the number of internal SiOH groups and a concomitant increase in the number of external SiOH groups. Kunkeler *et al.*, [4] proposed that the decrease in the amount of bridging hydroxyls can be explained by breaking of the Si-OH-Al bond into a SiOH group, leading to an increase in intensity of the band at 3745 cm^{-1} indicative of terminal silanol groups. The two steamed samples, Steamed 2h-β-12.5-A-773-1 and Steamed 6h-β-12.5-A-773-1, both resulted in an increase in the number of internal SiOH groups, which was most pronounced in the case of the samples steamed for a longer time period. Müller *et al.*, [31] proposed that the more severe the calcination conditions, the more defect sites were formed. It would seem likely that the presence of steam would promote the formation of internal SiOH groups since steaming leads to hydrolysis of Si-O-Al bonds [9]. Interestingly, the sample, NH_4^+-β-12.5-A-1023-18, was found to contain no internal SiOH groups, contradicting the finding of Müller *et al.*, [31], and the general hypothesis that the dealumination process should produce new defects. However, few workers have subjected zeolite Beta to temperatures as high as

1023 K for 18 hours, and in addition a study by Trombetta *et al.*, [14] found that the amount of internal SiOH groups decreases on calcination at increasing temperature. They concluded that calcination can result in some 'reconstruction' of internal defects so that the amount of defective silanols is decreased. This result is also in full agreement with the fact that the broad signal between 3600-3200 cm^{-1} indicative of SiOH groups in 'nests' is missing in the FTIR spectrum of the sample NH_4^+-β-12.5-A-1023-18. Trombetta *et al.*, [14] also evidenced a decrease in the broad absorption in the 3600-3200 cm^{-1} region, of the shoulder at 3735 cm^{-1} and the band at 3610 cm^{-1}, while the band at 3745 cm^{-1} and the band at 3785 cm^{-1} increase in intensity at higher calcination temperatures. They suggested that the band at 3735 cm^{-1} and the broad absorption in the 3600-3200 cm^{-1} region are associated with those species that disappear on calcination at high temperatures.

There are few publications dealing with the acidic strength of acid sites in zeolite Beta [32], [33]. Borade *et al.*, [33] determined the acidity of zeolite Beta using the temperature programmed desorption of pyridine, and Hegde *et al.*, [32] established the strength of acid sites in zeolite Beta using the temperature programmed desorption of ammonia. Temperature programmed desorption of ammonia has also been reported on various kinds of zeolite [34], [35], [36]. It is considered to be a potential method to determine the strength of acid sites in zeolites. Peak fitting of TPD traces corresponding to the NH_4^+ band (1371-1542 cm^{-1}) using a mixed Gaussian and Lorentzian peak function, corresponding to a 30% Gaussian, 70% Lorentzian line shape, for various samples are presented in **Figure 3.1.3.13** to **Figure 3.1.3.18** and the results summarised in **Table 3.1.3.4**. It can be seen from **Table 3.1.3.4** that sample NH_4^+-β-12.5-V-773-1 contains two different strengths of Brønsted acid sites, one of lower acidic strength with a maximum desorption temperature of 486 K which accounts for 73% of the total amount of Brønsted acid sites, and one of higher acidic strength with a maximum desorption temperature at 533 K which accounts for the remaining Brønsted acid sites. Guisnet *et al.*, [37], [38] observed two different kinds of Brønsted site with different acidity in protonated Beta samples. Sample NH_4^+-β-12.5-A-773-1 contains three different strengths of Brønsted acid site, the first, of lower acidic strength with a maximum desorption temperature of 505 K could be considered to be comparable with the site of lower strength in NH_4^+-β-12.5-V-773-1, and similarly, the second peak, with a maximum desorption temperature at 557 K could be considered to be comparable with the site of higher acidic strength in NH_4^+-β-12.5-V-773-1, however both sites have slightly higher maximum desorption temperatures in the case of NH_4^+-β-12.5-A-773-1. The most interesting observation in NH_4^+-β-12.5-A-773-1 is the appearance of a site of significantly higher acidic strength with a maximum desorption temperature at 591 K and accounting for 12% of the total number of Brønsted acid sites. A similar pattern is found in the case of the two steamed samples, Steamed 2h-β-12.5-A-773-1 and Steamed 6h-β-12.5-A-773-1, where the appearance of a Brønsted acid site of higher acidic strength than those found in NH_4^+-β-12.5-V-773-1 is observed. Guisnet *et al.*, [37], [38] found that the number of sites with lower acidity decreased with increasing dealumination, as is observed in the present study. It was also proposed that dealumination increases the strength of the remaining Brønsted acid sites [39]. This is because Si is more electronegative than Al and therefore a more siliceous zeolite will contain more polarised (acidic) hydroxyl groups. Interestingly, the sample treated at higher temperatures, NH_4^+-β-12.5-A-1023-18, exhibited one large desorption peak with a maximum desorption temperature at 502 K, indicating that firstly no higher acidic strength Brønsted acid sites have been formed in this case, and secondly that the higher acidic strength Brønsted acid sites observed in NH_4^+-β-12.5-V-773-1 are absent. A study carried out by Zhang *et al.*, [40] on mordenite and ZSM-12 concluded that an increase in the extent of dealumination results in a decrease in the strength of Brønsted acid sites, and this was due to the strong Brønsted acid sites been preferentially lost with an increase in the dealumination severity. It could be possible that the higher temperatures used in the calcination of NH_4^+-β-12.5-A-1023-18 led to a similar effect where instead of observing an increase in the strength of acid sites, the stronger Brønsted acid sites were preferentially lost.

These findings coincide well with the fact that the Brønsted acid sites associated with bridged OH groups are considered to be higher in acidic strength than those associated with extraframework or VHF OH groups [3]. NH_4^+-β-12.5-A-1023-18 contains no bridged OH groups, this may explain the loss of the higher acidic strength Brønsted acid sites which are present in NH_4^+-β-12.5-V-773-1, and the presence of the one large desorption peak at 502 K indicative of lower Brønsted acidic strength could well be associated with the VHF OH groups, of which this sample consists of entirely. It seems likely that a similar phenomenon is occurring in the sample treated with H_4EDTA, EDTA-β-12.5-A-773-1, where strong Brønsted acid sites are preferentially extracted leaving a preponderance of the weaker Brønsted acid sites. A study by Robb *et al.*, [30] found that all the zeolite Beta samples they studied possessed Brønsted acid sites with three different levels of strength, and the weakest Brønsted acid sites were the most numerous. The same general trend was found in the present study, with the weakest Brønsted acid sites being the most numerous in all cases. The same study also found that all ammonia desorbing above 523 K could be assigned to Brønsted acid sites, and in the present study, no desorption peaks were observed below 453 K which eliminates the possibility of any physisorbed ammonia being present on the samples, the likely explanation for this is that all physisorbed ammonia was removed during the evacuation process prior to desorption.

XRD RESULTS: ***effect of various hydrothermal, thermal, and chemical modifications on the acidic properties of zeolite H-Beta.***

The framework structure of zeolite Beta is made up of an intergrowth of tetragonal polymorph A and monoclinic polymorph B, with fault probabilities of about 40% and 60% respectively [41]. As a consequence, the X-ray diffraction (XRD) profile is a combination of sharp and broad reflections. Line broadening in X-ray powder diffraction is related to both the crystal size (or, more properly, the size of coherent crystalline domains) and lattice imperfections or strains [42]. In the case of zeolite Beta, for relatively large crystals in the micro-scale range the width of the peaks is also much dependent on their h, k, l indices as a consequence of its complex inter-grown structure [41]. Thus, the highly disordered structure of zeolite Beta produces sharp (h = 3n, k = 3n) and broad peaks in the XRD pattern, consistent with faulting by a/3 and b/3 displacements on (001) planes [43]. Thus, as a first approximation, the width of sharp (3n, 3n, l) reflections will mainly be determined by the crystallite size, while that of the broad reflections is related to faulting. **Figure 3.1.3.19** shows the comparison of the X-ray powder diffraction pattern of zeolite Beta (CuK_{alpha}) with the calculated pattern for the ordered tetragonal A polytype. Six sharp reflections on the zeolite Beta pattern are indexed on the tetragonal unit cell [43].

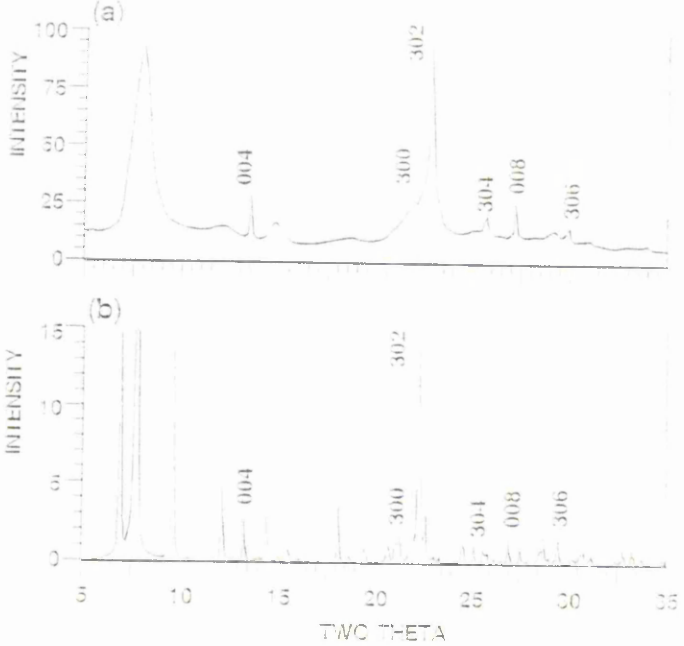

Figure 3.1.3.19 Comparison of (a) the X-ray powder diffraction of zeolite Beta (CuK_{alpha}) with (b) the calculated pattern for the ordered tetragonal A polytype.

DISCUSSION

Figure 3.1.3.20 shows the XRD profiles of zeolite Beta after different treatments. It can be seen that all zeolite Beta samples have a well-defined zeolite Beta structure. **Figure 3.1.3.20** also zooms in on a small section of the XRD profile in the region of 22.2 → 22.8° 2θ. By observing this region, it becomes evident that the peak associated with the sample treated to higher calcination temperature, NH_4^+-β-12.5-A-1023-18, shifts to higher 2θ values (22.55° 2θ) when compared with the peak associated with the sample treated to intermediate temperature, NH_4^+-β-12.5-A-773-1 (22.50° 2θ).

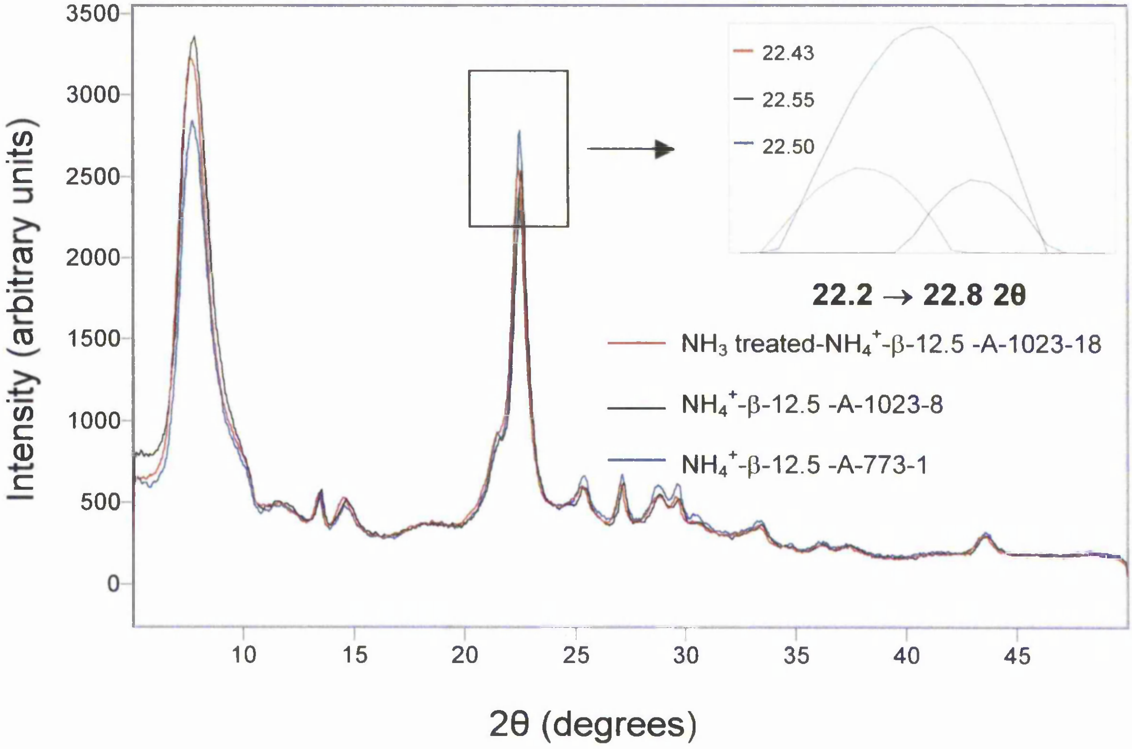

Figure 3.1.3.20 XRD profiles of zeolite Beta after different treatments.

Interestingly, if NH_4^+-β-12.5-A-1023-18 is treated with gaseous ammonia at 423 K for 2 h, the position of the peak shifts to a lower 2θ value (22.43° 2θ), even lower than in the case of NH_4^+-β-12.5-A-773-1. Camblor *et al.*, [44] reported an increased peak broadening and a shift to lower 2θ values as the Al content of their nanocrystalline zeolite Beta increased. Thus, it can be said that the position of the peak shifts towards higher 2θ values as the amount of aluminium in the framework decreases. Using this theory, it becomes clear that sample NH_4^+-β-12.5-A-1023-18 has lost aluminium from framework positions as evidenced by the shift to higher 2θ values. What is also clear from **Figure 3.1.3.20** is that the sample treated with gaseous ammonia, NH_3 treated-NH_4^+-β-12.5-A-1023-18, has undergone a 'realumination' of the zeolite surface, indicating that the ammonia treatment has re-inserted aluminium back into the framework. It is also interesting to note that the peak in the region of 22.2 → 22.8° 2θ associated with NH_3 treated-NH_4^+-β-12.5-A-1023-18 has shifted to a lower 2θ value than NH_4^+-β-12.5-A-773-1, indicating that the latter sample has also undergone some degree of dealumination during calcination. This result is in agreement with the FTIR results for the sample, NH_4^+-β-12.5-A-773-1, which was discussed earlier, where it was found to have undergone dealumination. This result may suggest that a large proportion, if not all (with the possible exception of aluminium which has been subject to complete hydrolysis) of the aluminium removed from the framework of zeolite Beta during calcination can be re-inserted into the framework following treatment with gaseous ammonia. Trombetta *et al.*, [14] reported similar findings; they observed that the peak moves from 22.43 to 22.48° 2θ values when the treatment temperature increases from 773 K to 923 K, confirming that thermal treatment causes progressive dealumination. Additionally, they found that when the thermal treatment was followed by an acid washing, the 2θ value increased further up to 22.62. Bourgeat-Lami *et al.*, [10] reported that treatment of a dealuminated zeolite Beta sample with a solution of pyridine in ethanol at room temperature or with gaseous ammonia at 373 K allowed for all the aluminium atoms of the solid to recover a tetrahedral framework symmetry, they also reported that ion exchange with cations such as Na^+ and K^+ had a similar effect. In an earlier study, Bourgeat-Lami *et al.*, [8] also concluded that tetrahedral sites disappearing upon calcination could be readily restored by treatment in ammonium nitrate solution. In this study, they observed dealumination of the framework, as evidenced by the appearance of a ^{27}Al NMR signal of non-framework octahedral aluminium at 0 ppm. When this material was treated with ammonium nitrate solution, the signal of octahedral aluminium was no longer detected while that of tetrahedral aluminium (50 ppm) narrowed and increased to 95% of its original value. The unit cell parameters and the crystallinity increased and the IR lattice frequencies decreased, all these changes are consistent with a re-insertion of aluminium into the framework. Similarly, Kuehl *et al.*, [9] also reported that the octahedral aluminium species connected to the framework structure of zeolite Beta created by partial hydrolysis of framework Si-O-Al bonds could convert reversibly to tetrahedral aluminium sites upon aqueous NH_4^+ exchange or reaction with NH_3 gas. The same workers also concluded that framework aluminium adopts a tetrahedral symmetry when protons are not the charge compensating cations. Similarly, Bourgeat-Lami *et al.*, [10] concluded that the presence of protons contributes to the appearance of non-tetrahedral NMR signals. These workers demonstrated that the state of aluminium in zeolite Beta depends on the nature of the cation balancing the lattice negative charges. In the ammonium, sodium, and potassium forms, all aluminium atoms occupy tetrahedral framework positions whereas octahedral aluminium species are formed when the above cations are exchanged for protons. An extensive report by van Bekkum *et al.*, [45] describes the role of protons on the coordination environment of aluminium in zeolite Beta. From this study, and other recent literature, the general conclusion is that octahedral aluminium can be present in the framework of many zeolites. The starting material in most cases is the NH_4^+ exchanged material. A heat treatment removes gaseous ammonia, yielding the acidic zeolite. According to the literature [46-48], only the presence of water can induce the creation of framework octahedral aluminium. It is thought that the Brønsted acidic zeolite attracts water molecules to stabilize the strong electric field induced by the proton and the cationic charge is delocalised. Throughout the framework, the zeolite is not able to accommodate too many of these strong electric field centres, and thus water molecules are attracted and part of the framework tetrahedral aluminium may convert to octahedral aluminium, reducing the strong electric fields in the framework. This could well be accompanied by hydrolysis of part of the Al-O-Si linkages. No other cations can induce such an effect, which can be understood since protons are catalysts for hydrolysis reactions. Once the proton is re-exchanged for other cations, the framework octahedral aluminium is no longer detected [10]. Likewise, an ammonium treatment at 373 K can revert the octahedral aluminium back to tetrahedral. An ammonium treatment at 373 K has an effect very similar to ion exchange and it introduces NH_4^+ as the charge compensating cation, thereby removing the water molecules, and returning the coordination of aluminium back to tetrahedral. van Bekkum *et al.*, [45] suggested that the original structure of zeolite Beta after mild calcination can be completely restored by ammonia treatment, however upon severe steaming, the high temperature and water partial pressure causes complete hydrolysis of the framework tetrahedral aluminium, which is then extracted from the framework. In order to determine the crystallinity of the samples, the area under the peak in the 19.33 → 23.87° 2θ range was measured, and the sample which had undergone the most careful calcination procedure, NH_4^+-β-12.5-A-773-1, was taken as 100% crystallinity, and the other samples were measured relative to this. As expected, the sample treated to higher temperature, NH_4^+-β-12.5-A-1023-18, shows some loss of crystallinity, with a value of 93% relative to NH_4^+-β-12.5-A-773-1, which could be linked to the formation of extralattice aluminium and framework octahedral aluminium since XRD signal intensity and line width are effected by distortions due to TO_4 tetrahedra not connected to 4T atoms (where T= Si, Al). The sample treated with ammonia gas, NH_3 treated-NH_4^+-β-12.5-A-1023-18, results in a slight increase in crystallinity with a value of 96% relative to NH_4^+-β-12.5-A-773-1, this could certainly be due to the transformation of framework octahedral aluminium back to framework tetrahedral aluminium.

MAS NMR RESULTS: ***effect of various hydrothermal, thermal, and chemical modifications on the acidic properties of zeolite H-Beta.***

^{27}Al MAS NMR

^{27}Al MAS NMR spectroscopy is a well-established tool to determine the aluminium co-ordinations in zeolites [49-51]. Based on ^{27}Al MAS NMR studies on zeolite H-Y and the steamed H-USY [27], various aluminium configurations have been proposed. Interpretation of ^{27}Al NMR data, however, is complicated by the quadrupole moment of the aluminium nucleus ($I = 5/2$) causing quadrupole broadening. Also not all the aluminium present in the sample might be detected by NMR techniques [10], [52]. Besides tetrahedral framework aluminium and octahedral extraframework aluminium, several other species (neutral or cationic) have been proposed, including penta-coordinated aluminium [53], and distorted tetrahedral aluminium [27]. When aluminium atoms are present which are connected to the framework and are in tetrahedral coordination ($Al(OSi)_4$), then a peak at a chemical shift of ~60 ppm is visible in the spectrum. Extraframework aluminium species are usually octahedrally coordinated, and the corresponding signal has a chemical shift of ~0 ppm. In the ^{27}Al spectra of strongly dealuminated samples, a further peak or shoulder is often visible between 30 and 50 ppm, which has been assigned to penta-coordinated aluminium atoms [27], [54], as well as to distorted tetrahedrally coordinated aluminium atoms in extraframework species [55]. Although ^{27}Al MAS NMR has been used to determine the presence of four, five, and six-coordinated aluminium in zeolites, the half integer quadrupolar spin of aluminium complicates the interpretation of ^{27}Al MAS NMR spectra. The recently developed multiple quantum MQ MAS NMR technique [56], [57] allows detection of pure isotropic spectra, yielding a very significant increase in resolution. This technique permits an unambiguous assignment of the aluminium coordination's in the spectra [45]. In addition, the use of high spinning speeds and high external magnetic field strength minimizes the chance that aluminium escapes detection [58]. van

Bokhoven *et al.*, [45] in their quantitative analysis of the ^{27}Al MQ MAS NMR spectra of dealuminated zeolite Beta showed that aluminium atoms in positions T1 and T2 resist dealumination and do not adopt an octahedral coordination. They also showed that a heat treatment at 723 K of NH_4^+-Beta gives a single type of fairly symmetrical framework octahedral aluminium, which can be reconverted to framework tetrahedral aluminium by ammonia treatment. A more severe treatment (823 K under steam) causes some of the tetrahedral framework aluminium atoms on positions T3-T9 to convert to at least two different types of octahedral aluminium that are connected to the framework.

In order to determine the effect of calcination procedure on the coordination environment of aluminium in zeolite H-Beta, the carefully calcined sample, NH_4^+-β-12.5-V-773-1, and the sample treated to high temperature, NH_4^+-β-12.5-A-1023-18 were subject to ^{27}Al MAS NMR spectroscopy.

Figure 3.1.3.21 shows the fitted ^{27}Al MAS NMR spectrum of NH_4^+-β-12.5-V-773-1 and the results are summarized in **Table 3.1.3.5**.

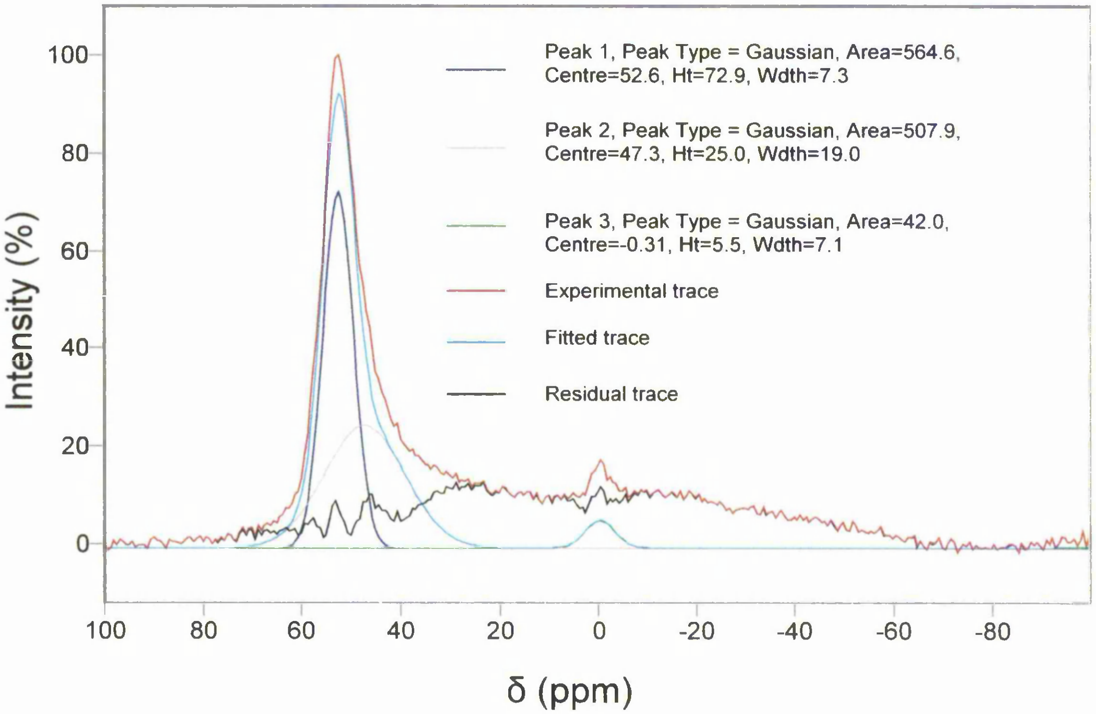

Figure 3.1.3.21 Fitted ^{27}Al MAS NMR spectrum of NH_4^+-β-12.5-V-773-1.

Sample	Fitted ^{27}Al MAS NMR results					
	Peak 1		Peak 2		Peak 3	
	Position	Area %	Position	Area %	Position	Area %
NH_4^+-β-12.5-V-773-1	52.6	50	47.3	46	-0.31	4

Table 3.1.3.5 Fitted ^{27}Al MAS NMR data for NH_4^+-β-12.5-V-773-1.

Figure 3.1.3.22 shows the fitted ^{27}Al MAS NMR spectrum of NH_4^+-β-12.5-A-1023-18 and the results are summarized in **Table 3.1.3.6**.

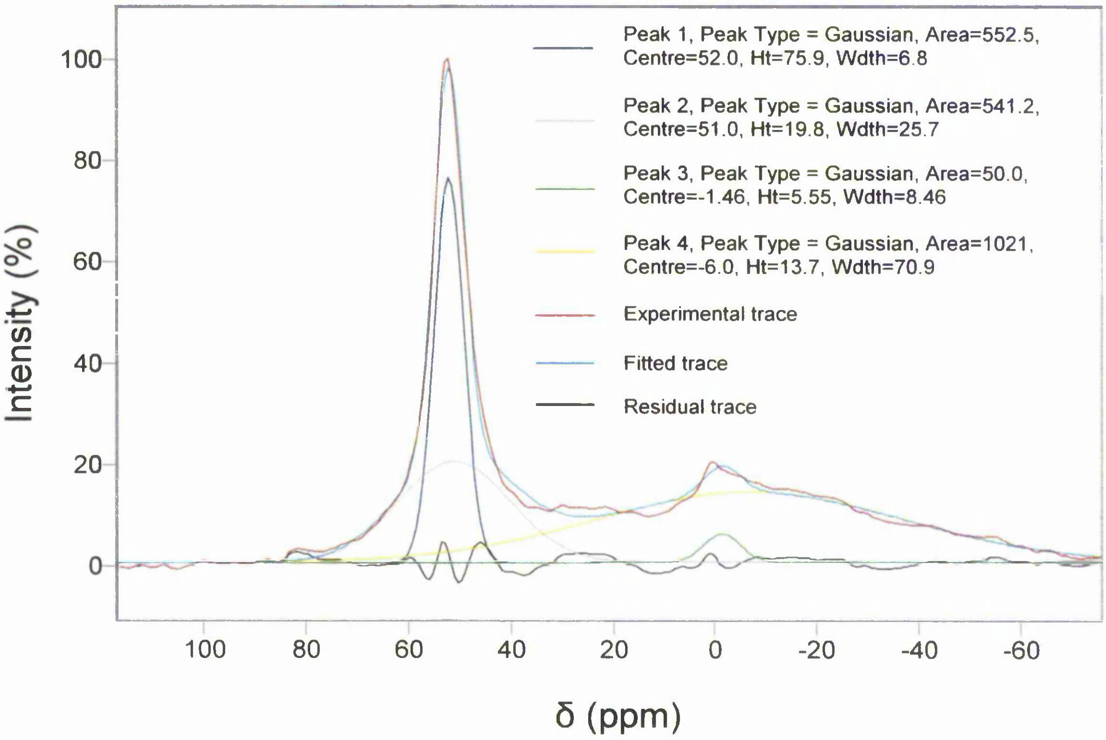

Figure 3.1.3.22 Fitted ^{27}Al MAS NMR spectrum of NH_4^+-β-12.5-A-1023-18.

Sample	Fitted ^{27}Al MAS NMR results							
	Peak 1		Peak 2		Peak 3		Peak 4	
	Position	Area %	Position	Area %	Position	Area %	Position	Area %
NH_4^+-β-12.5-A-1023-18	52.0	26	51.0	25	-1.46	2	-6.0	47

Table 3.1.3.6 Fitted ^{27}Al MAS NMR data for NH_4^+-β-12.5-A-1023-18.

DISCUSSION

It can be seen from both **Figure 3.1.3.21** and **Table 3.1.3.5** that the sample, NH_4^+-β-12.5-V-773-1, has a peak centred at 52.6 ppm, which accounts for 50% of the total amount of aluminium present in the sample (providing there is no undetectable or 'invisible' aluminium present, however, results regarding the adsorption of acetylacetone yielded the same total amount of aluminium as in H-Beta samples hydrated over a saturated ammonium sulphate solution which is a good indication that no 'invisible' aluminium is present [10]). As was discussed previously, the peak centred at 52.6 ppm is representative of tetrahedral aluminium in framework positions. Additionally, a small peak is observed at -0.31 ppm, accounting for 4% of the total amount of aluminium present. This peak is indicative of octahedral aluminium, and is usually associated with dealumination. From the FTIR results discussed earlier, the sample, NH_4^+-β-12.5-V-773-1, was shown to undergo only slight dealumination, this finding is also evidenced by this NMR result. The most interesting finding is the presence of a peak at 47.3 ppm, accounting for 46% of all aluminium present. As was discussed previously, a peak is often visible in the ^{27}Al MAS NMR of zeolites in the region between 30 and 50 ppm and has been associated with penta-coordinated aluminium [54] as well as to distorted tetrahedrally coordinated aluminium atoms [55]. Others workers [59], [14] have also associated peaks in the region of 28 ppm to either penta-coordinated aluminium or to an Al atom in highly distorted tetrahedral coordination. Campbell *et al.*, [16] also observed a broad NMR signal, centred around 30-40 ppm and also associated it with aluminium in a distorted tetrahedral environment or 5-coordinate aluminium. Clearly, different workers observe NMR peaks between 28-50 ppm in the ^{27}Al MAS NMR spectra of zeolites. This region, which lies between the chemical shift positions of tetrahedral and octahedral aluminium probably accounts for both penta-coordinated aluminium and distorted tetrahedral aluminium. Workers observing NMR peaks at higher ppm values, towards the region of tetrahedral aluminium are most likely observing a slightly distorted tetrahedral aluminium species, and as this peak shifts towards lower ppm values, the tetrahedral aluminium becomes more distorted, and at some point the peak is probably more indicative of a 5-coordinate aluminium species, although no workers have proposed such a theory. The presence of a peak at 47.3 ppm would suggest that its presence is not due to either penta or highly distorted aluminium, but rather to tetrahedral aluminium in a slightly distorted environment (its almost tetrahedral, explaining its rather high ppm value, but it is still within the range of distorted tetrahedral aluminium as given by Müller *et al.*, [31]). This slight distortion of tetrahedral aluminium in NH_4^+-β-12.5-V-773-1 is most likely due to the presence of nearby defects, which are an inherent characteristic of the structure of zeolite Beta. The high number of defect sites in zeolite Beta would also explain the high proportion of 'slightly' distorted tetrahedral aluminium atoms, which account for almost half of the total amount of aluminium present in NH_4^+-β-12.5-V-773-1. It can be observed from **Figure 3.1.3.22** and **Table 3.1.3.6** that the sample, NH_4^+-β-12.5-A-1023-18, shows significant differences to the carefully calcined sample, NH_4^+-β-12.5-V-773-1. The most obvious difference is the presence of two types of octahedral aluminium, one at –1.46 ppm, and accounting for 2% of the total amount of aluminium, and another at –6 ppm accounting for 47% of the total amount of aluminium. The former peak is narrow and more indicative of a highly symmetrical octahedral aluminium species, and the latter peak is extremely broad which would indicate a more distorted octahedral aluminium species. van Bokhoven *et al.*, [45] in a study of the stepwise dealumination of zeolite Beta with ^{27}Al MAS and ^{27}Al MQ MAS NMR found that mild heat treatment of the ammonium form of zeolite Beta resulted in the appearance of a single type of fairly symmetrical framework octahedral aluminium. A more severe heat treatment caused some of the tetrahedral aluminium to convert to at least two different types of octahedral aluminium that are connected to the framework. The different octahedral aluminium species observed by these workers were proposed to represent different steps in the process of hydrolysis of tetrahedral aluminium during dealumination. An increased hydrolysis of tetrahedral aluminium is represented in the ^{27}Al MAS NMR spectra by a more distorted octahedral coordination, much like what is observed in the present study. Similarly, Kuehl *et al.*, [9] also reported that dealumination of zeolite Beta results in broadening of the octahedral aluminium signal. The peaks at 52 and 51 ppm in **Figure 3.1.3.22** are indicative of undistorted and slightly distorted framework tetrahedral aluminium respectively. These species account for 51% of the total amount of aluminium present, thus the total amount of framework tetrahedral aluminium (undistorted and distorted) is significantly reduced in NH_4^+-β-12.5-A-1023-18 when compared with NH_4^+-β-12.5-V-773-1. Interestingly, in NH_4^+-β-12.5-A-1023-18, the position of the peak indicative of slightly distorted aluminium is shifted towards higher ppm values, indicating a less distorted species. For NH_4^+-β-12.5-V-773-18, the slightly distorted aluminium was thought to arise due to the presence of a significant amount of internal SiOH groups (observed by FTIR), which would be indicative of defect sites, causing some distortion of nearby tetrahedral aluminium sites. In NH_4^+-β-12.5-A-1023-18, FTIR showed that few internal SiOH groups were present, due to reconstruction of such sites at high temperature, this may explain the shift of slightly distorted framework aluminium to higher ppm values in NH_4^+-β-12.5-A-1023-18. It is also interesting to note that the FTIR spectrum of NH_4^+-β-12.5-A-1023-18 showed no bridged OH groups, only VHF OH groups, bridged OH groups are normally associated with tetrahedral aluminium. The ^{27}Al MAS NMR spectrum of NH_4^+-β-12.5-A-1023-18 clearly shows that tetrahedral aluminium is present, and since no bridged OH groups were observed in the FTIR spectrum, this result may suggest that very high frequency groups are also associated with tetrahedral aluminium. This would contradict the findings of Trombetta *et al.*, [14] who concluded that the VHF band is due to OH groups on extraframework small alumina clusters, but would be more in agreement with Beck *et al.*, [12] who refer to it as an unusual aluminium site associated with the framework.

^{29}Si MAS NMR

^{29}Si MAS NMR studies can be used to determine the composition and Si/Al ordering of zeolite frameworks. Using this technique it is possible to distinguish all five possible Si(nAl) building units, where Si(nAl) represents a SiO_4 tetrahedron linked to $nAlO_4$ tetrahedra and to (4-n) other SiO_4 tetrahedra. Kunkeler *et al.*, [4] and other workers have assigned these five possible building units to the following chemical shift positions, -98 ppm $Si(OSi)_2(OAl)_2$, -105 ppm $Si(OSi)_3(OAl)_1$ or $Si(OSi)_3(OH)_1$, -111 and -115 ppm both attributed to $Si(OSi)_4$ [4], [11], [60]. The ratio of tetrahedral silicon and aluminium atoms in the zeolite framework can be directly calculated from the Si(nAl) peak intensities in a ^{29}Si MAS NMR spectrum according to the formula :[61], [62]

Equation 3.1.3.1

$$Si/Al_{NMR} = \frac{I_4 + I_3 + I_2 + I_1 + I_0}{I_4 + 0.75I_3 + 0.5I_2 + 0.25I_1}$$

where I_n denotes the intensity (peak area) of the NMR signal corresponding to the Si(nAl) building unit. The resulting Si/Al_{SiNMR} ratio, however, does not correspond to the actual Si/Al_{fw} when defect sites (SiOH groups) are present in the framework because peaks due to Si(nAl) and Si(nOH) overlap in the ^{29}Si MAS NMR spectrum, Therefore, Si/Al_{SiNMR} always give lower values than the actual Si/Al_{fw} ratio. **Figure 3.1.3.23** shows the fitted ^{29}Si MAS NMR spectrum of NH_4^+-β-12.5-V-773-1 and the results are summarized in **Table 3.1.3.7**.

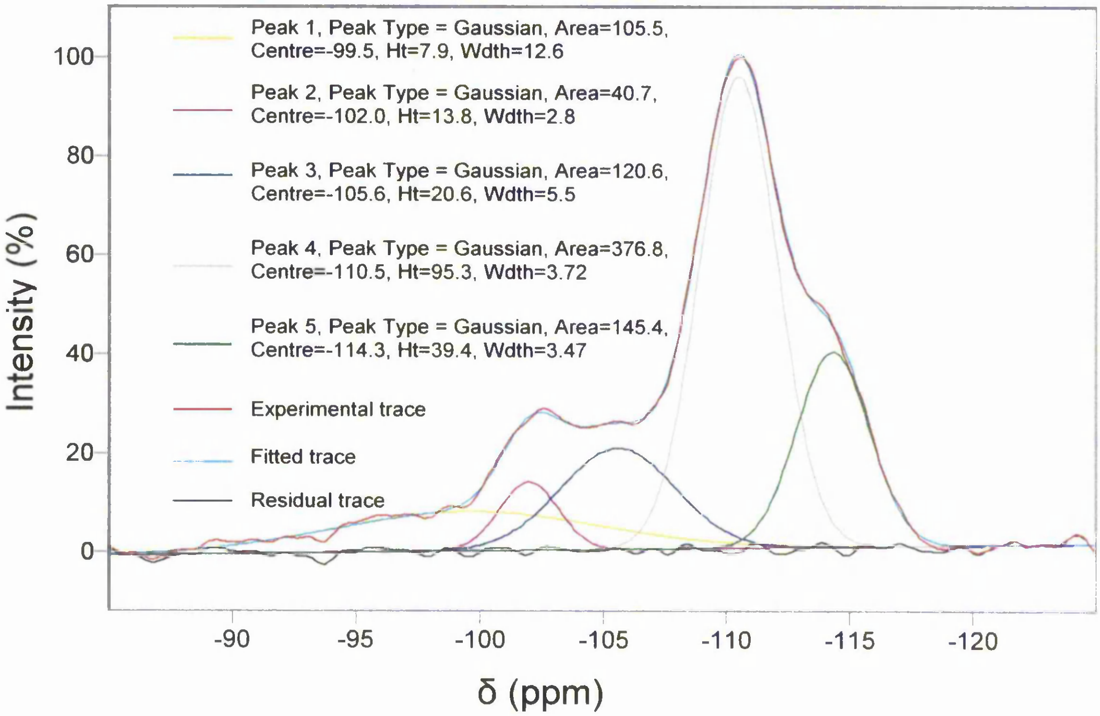

Figure 3.1.3.23 Fitted ^{29}Si MAS NMR spectrum of NH_4^+-β-12.5-V-773-1.

Sample	Fitted ^{29}Si MAS NMR results									
	Peak 1		Peak 2		Peak 3		Peak 4		Peak 5	
	Position	Area %	Position	Area %	Position	Area %	Position	Area %	Position	Area %
NH_4^+-β-12.5-V-773-1	-99.5	13	-102	5	-105	16	-110	48	-114	18

Table 3.1.3.7 Fitted ^{29}Si MAS NMR data for NH_4^+-β-12.5-V-773-1.

Figure 3.1.3.24 shows the fitted ^{29}Si MAS NMR spectrum of NH_4^+-β-12.5-A-1023-18 and the results are summarized in **Table 3.1.3.8**.

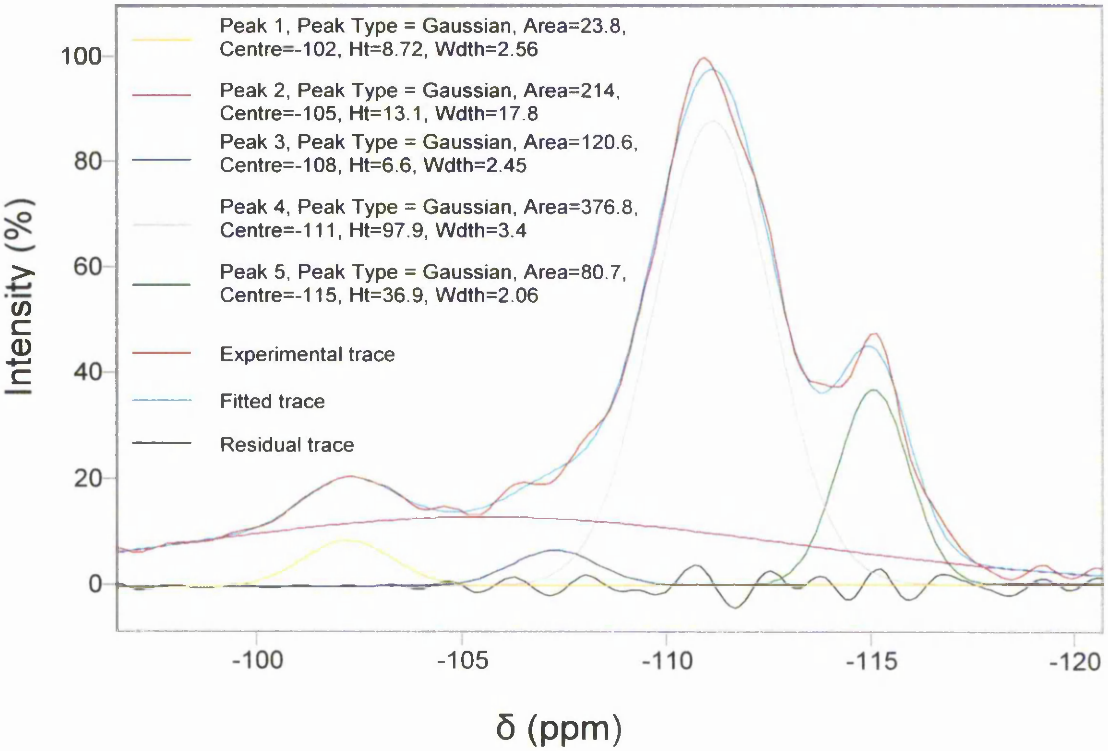

Figure 3.1.3.24 Fitted ^{29}Si MAS NMR spectrum of NH_4^+-β-12.5-A-1023-18.

Sample	Fitted ^{29}Si MAS NMR results									
	Peak 1		Peak 2		Peak 3		Peak 4		Peak 5	
	Position	Area %	Position	Area %	Position	Area %	Position	Area %	Position	Area %
NH_4^+-β-12.5-A-1023-18	-102	3	-105	26	-108	15	-111	46	-115	10

Table 3.1.3.7 Fitted ^{29}Si MAS NMR data for NH_4^+-β-12.5-A-1023-18.

DISCUSSION

Using the peak areas shown in **Figure 3.1.3.23** and substituting them into **Equation 3.1.3.1** gives the Si/Al$_{SiNMR}$ ratio for NH_4^+-β-12.5-V-773-1.

$$\text{Si/Al}_{\text{NMR}} = \frac{106+121+377+145}{0.5\times106+0.25\times121}$$

$$\text{Si/Al}_{\text{NMR}} = \frac{749}{83}$$

$$\text{Si/Al}_{\text{NMR}} = 9$$

As expected, the Si/Al$_{SiNMR}$ ratio of 9 for NH_4^+-β-12.5-V-773-1 is lower than the Si/Al ratio of the parent material which has a value of 12.5 (assuming the accuracy of the Si/Al ratio provided with the as-received zeolite Beta is high). The presence of a high number of SiOH groups in NH_4^+-β-12.5-V-773-1 would account for the lower Si/Al ratio calculated from the fitted ^{29}Si MAS NMR spectrum. The spectra of NH_4^+-β-12.5-V-773-1 shows two peaks centred at -110 and -114 ppm, both assigned to $Si(OSi)_4$, which account for 76% of the total amount of silicon in the framework. Another peak centred at -105 ppm can be assigned to either $Si(OSi)_3(OAl)_1$ or $Si(OSi)_3(OH)_1$, and this peak accounts for 16% of the total amount of silicon present in the framework. The peak in the ^{29}Si MAS NMR spectrum of NH_4^+-β-12.5-V-773-1 centred at -102 ppm can be assigned to $Si(OSi)_3(OH)_1$ according to Camblor *et al.*, [44], and this accounts for 5% of the total amount of silicon present in the framework. The final peak in the ^{29}Si MAS NMR spectrum of NH_4^+-β-12.5-V-773-1 is centred at -99.5 ppm and could be to due $Si(OSi)_3(OH)_1$ [44] or $Si(OSi)_2(OAl)_2$ [4] and accounts for 13% of the total amount of silicon in the framework. Substituting the values from **Figure 3.1.3.24** into **Equation 3.1.3.1** gives the Si/Al$_{SiNMR}$ ratio for NH_4^+-β-12.5-A-1023-18.

$$\mathrm{Si/Al_{NMR}} = \frac{214+121+377+81}{0.25\times 214}$$

$$\mathrm{Si/Al_{NMR}} = \frac{793}{53.5}$$

$$\mathrm{Si/Al_{NMR}} = 15$$

The higher $\mathrm{Si/Al_{SiNMR}}$ ratio of 15 for NH_4^+-β-12.5-A-1023-18 would suggest that dealumination has taken place, and is in line with XRD results where a shift to higher 2θ values was observed, which is also indicative of loss of aluminium from framework positions. The assignment of bands is identical to that described for NH_4^+-β-12.5-V-773-1.

It is important to note that the ^{29}Si MAS NMR spectrum only allows for the interpretation of framework aluminium species in zeolites, comparison of Si/Al ratios measured by other techniques, such as A.A.S, allows for the quantitative determination of extraframework aluminium.

CONCLUSION

It is clear that thermal, hydrothermal, and chemical modification have a dramatic effect on the acidic properties of zeolite Beta. Dealumination seems to be a progressive phenomenon, the more severe the conditions applied; the more aluminium is removed from the zeolite framework. It is also evident that much of the aluminium removed from tetrahedral framework positions during the dealumination process can be reinserted by treatment with ammonia gas. The presence of protons as the charge compensating cation seems to be linked to the formation of aluminium coordination's other than tetrahedral, and the attraction of water molecules in the H-form of zeolite Beta and the formation of framework octahedral aluminium occur to compensate for the strong electric field conferred by the presence of protons. In all cases, a reduction in the total number of Brønsted acid sites was observed after treatment, although the number of Lewis acid sites remained unchanged. Additionally, in all cases, except the most carefully treated sample, NH_4^+-β-12.5-V-773-1, the formation of different types of hydroxyl groups was observed, but the formation of these species occurred at the expense of bridged OH groups. The formation of extralattice OH and VHF OH groups seem to be associated with changes in the acidic strength of zeolite Beta. What is also evident is that the number of internal and external silanol groups can be affected by different treatments. Hydrothermal modification increases the number of internal SiOH groups, the more prolonged the steam treatment, the more internal SiOH groups were formed. In contrast, calcination in air to high temperature resulted in a complete disappearance of internal SiOH groups, suggesting that 'healing' or 'reconstitution' of internal SiOH groups occurs under such conditions. What is most apparent from the observations made in this section is that zeolite Beta is very susceptible to dealumination, and as a consequence of this, the number, type, and strength of acid sites can be altered in a number of ways depending on the treatment applied.

3.1.4 Acidity of zeolite Beta

FTIR RESULTS: ***effect of ion exchange on the acidic properties of zeolite Beta.***

A growing area of research over the past few years has been in metal-exchanged zeolites. Zeolites are known to be excellent catalysts due to their cage-like framework, which provides high selectivity towards penetrating molecules based on size and shape. When metal cations are exchanged into the zeolite, the framework acts as a ligand and alters the catalytic properties of the cation. Zeolites containing basic cations, such as Ca^+ or Mg^{2+}, are highly effective in the petroleum industry as catalysts for the alkylation of aromatics, dehydrocyclization of n-alkanes, hydrogenation and dehydrogenation of hydrocarbons and oxygenated compounds, and a variety of condensation reactions [63]. Additionally, the loosely bound nature of the extraframework metal ions (such as in zeolite NaA) means that they are often readily exchanged for other types of metal when in aqueous solution. This is exploited in a major way in water softening, where alkali metals such as sodium or potassium prefer to exchange out of the zeolite, being replaced by the 'hard' calcium and magnesium ions from the water. Many commercial washing powders contain substantial amounts of zeolite. Commercial wastewater containing heavy metals, and nuclear effluent containing radioactive isotopes can also be cleaned up using such zeolites. Metal-exchanged zeolites containing transition metal-exchanged cations, such as Cu^{2+}, Fe^{3+}, or Zn^{2+}, on the other hand, have shown great potential in catalysing the decomposition of gaseous NO_X pollutants produced by automobiles and factories [64-66].

Figure 3.1.4.1 shows the effect of ion exchange on the acidic properties of zeolite Beta.

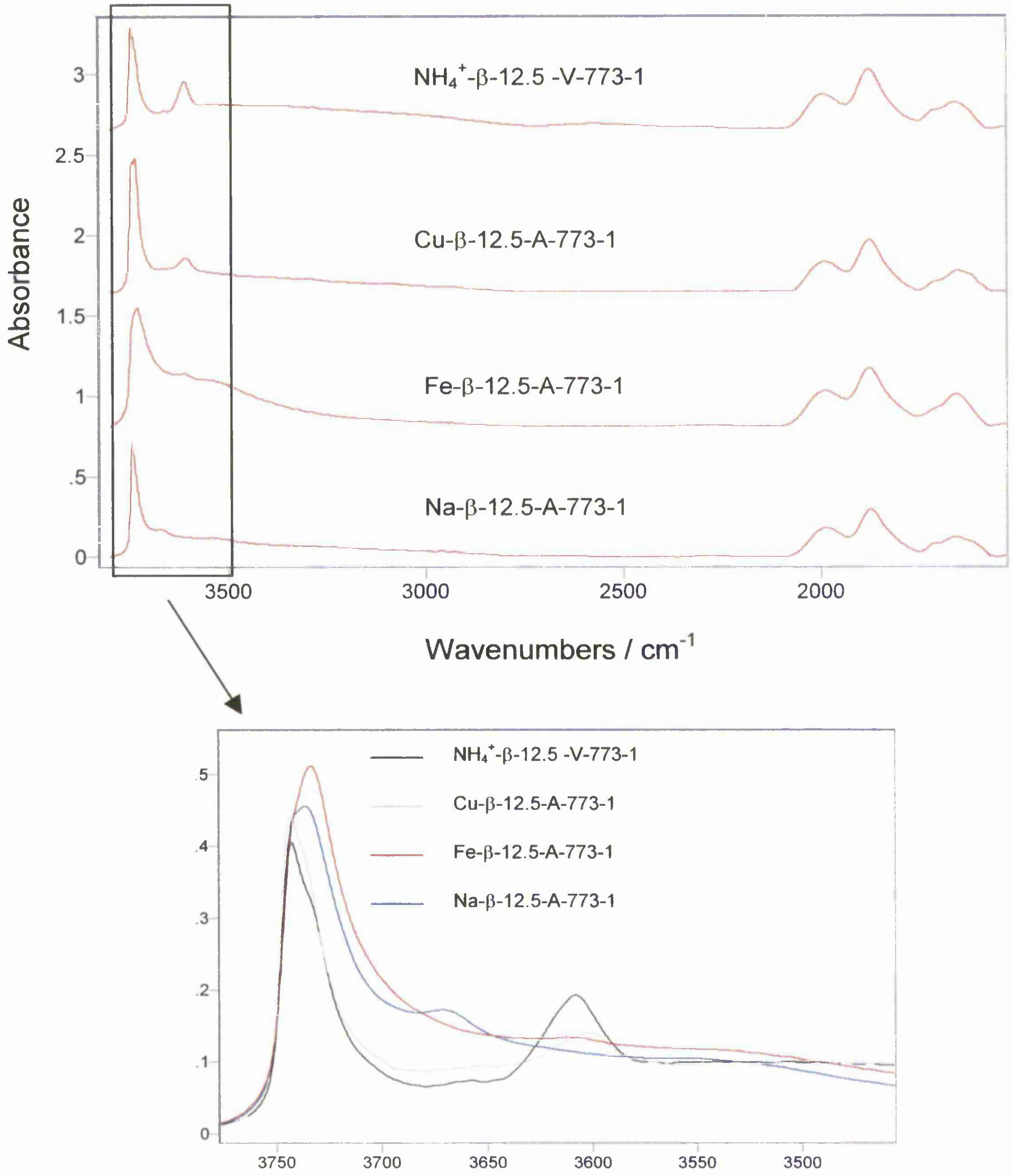

Figure 3.1.4.1 FTIR spectra in the hydroxyl region of ion-exchanged zeolite Beta samples. Spectra taken at 423 K and normalised to the zeolite lattice overtones at 1987 and 1872 cm^{-1}.

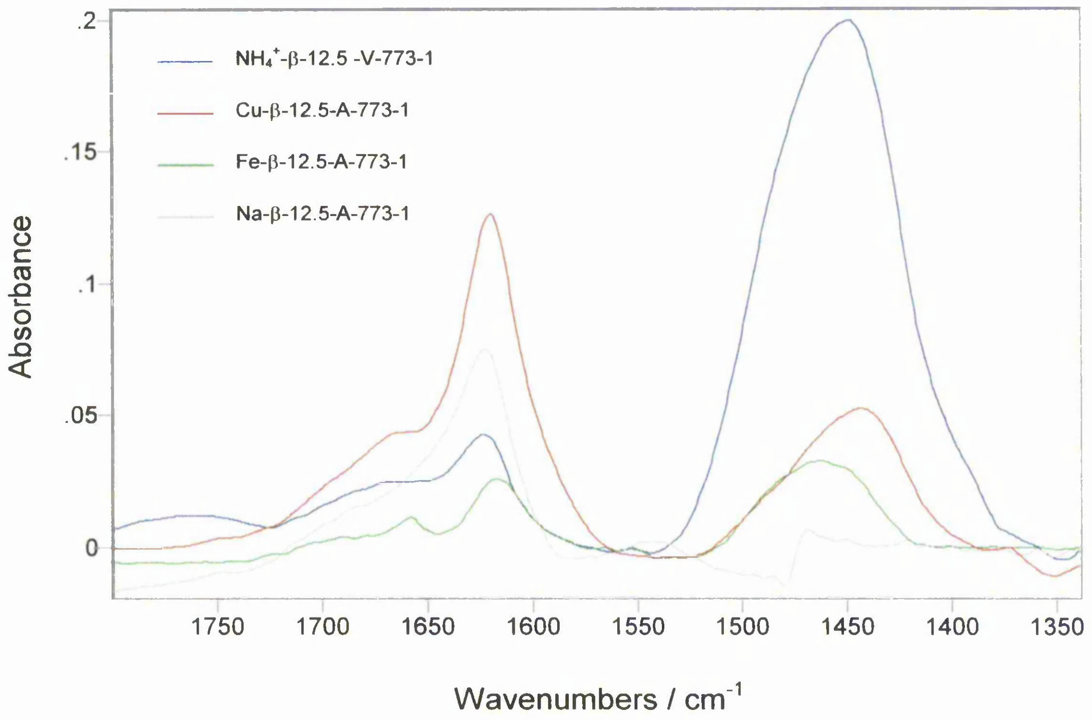

Figure 3.1.4.2 FTIR spectra in the NH deformation region of ion-exchanged zeolite Beta samples showing the changes in bands at 1450 cm^{-1} (NH_4^+) and 1623 cm^{-1} (NH_3). Spectra taken at 423 K and normalised to the zeolite lattice overtones at 1987 and 1872 cm^{-1}.

The integration of the respective bands shown in **Figure 3.1.4.1** and normalisation to the lattice overtones gives the relative amount of bridged OH (3608 cm^{-1}), extralattice OH (3663 cm^{-1}) and very high frequency OH (3780 cm^{-1}) as presented in **Table 3.1.4.1** and **Figure 3.1.4.3**. The relative concentration of Brønsted and Lewis acid sites depicted in **Figure 3.1.4.2** were calculated in the same way and are presented in **Table 3.1.4.2** and **Figure 3.1.4.4**.

Table 3.1.4.1 Relative concentration of VHF, bridged, and extralattice OH groups.

Sample	**Integral area of absorption band**				**Relative concentration* ± 2%****		
	VHF OH (3769-3794 cm^{-1})	**Bridged OH** (3572-3641 cm^{-1})	**Extralattice OH** (3643-3679 cm^{-1})	**Lattice Overtones** (1753-2095 cm^{-1})	**VHF OH**	**Bridged OH**	**Extralattice OH**
NH_4^+-β-12.5-V-773-1	0	2.87	0	31.89	**0**	**0.09**	**0**
Cu-β-12.5-A-773-1	0	0.72	0	24.22	**0**	**0.030**	**0**
Fe-β-12.5-A-773-1	0	0.18	0	48.4	**0**	**0.0037**	**0**
Na-β-12.5-A-773-1	0	0	0.55	75.3	**0**	**0**	**0.007**

* Relative concentrations are calculated by normalising the integral area of the band of interest to the integral area of the lattice overtone bands.

** Approximate experimental error expressed as the coefficient of variation.

Table 3.1.4.2 Relative concentration of Brønsted and Lewis acid sites.

Sample	**Integral area of absorption band**			**Relative concentration* ± 2%****	
	Brønsted (NH_4^+) band (1371-1542 cm^{-1})	**Lewis (NH_3) band (1582-1645 cm^{-1})**	**Lattice Overtones (1753-2095 cm^{-1})**	**Brønsted**	**Lewis**
NH_4^+-β-12.5-V-773-1	23.53	1.21	31.89	**0.740**	**0.038**
Cu-β-12.5-A-773-1	4.92	2.49	24.22	**0.203**	**0.103**
Fe-β-12.5-A-773-1	4.67	1.36	48.4	**0.096**	**0.028**
Na-β-12.5-A-773-1	0.73	1.33	75.3	**0.009**	**0.018**

* Relative concentrations are calculated by normalising the integral area of the band of interest to the integral area of the lattice overtone bands.

** Approximate experimental error expressed as the coefficient of variation.

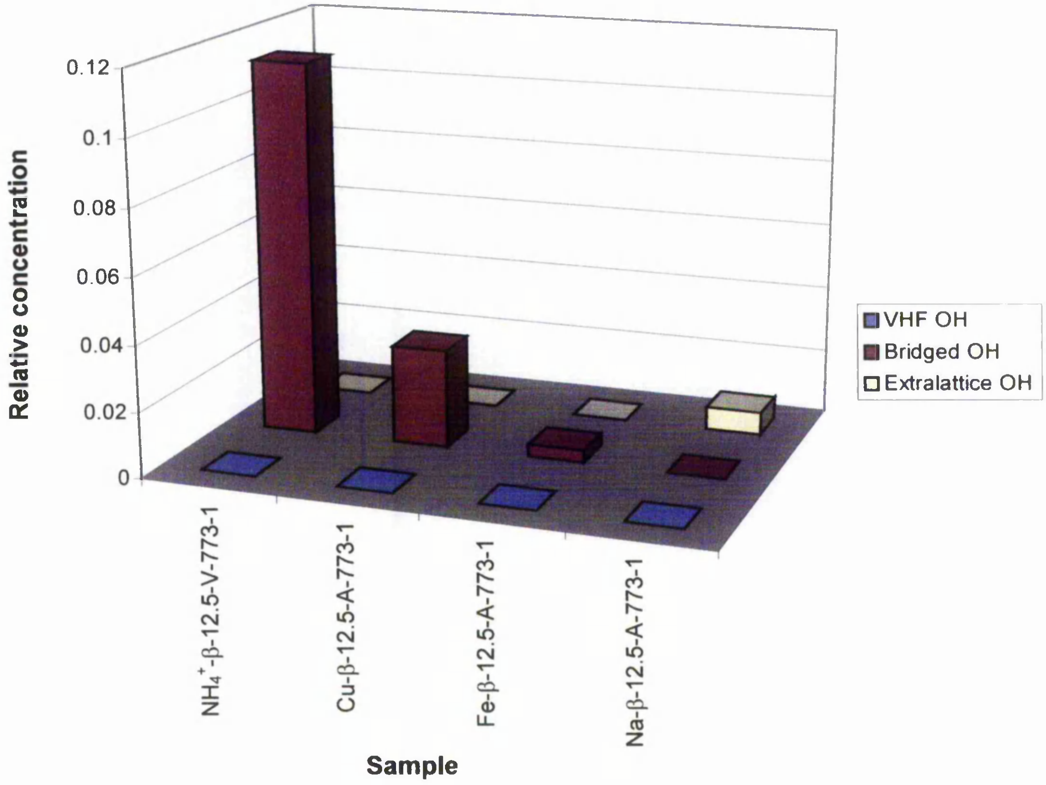

Figure 3.1.4.3 Relative concentration of different hydroxyl groups.

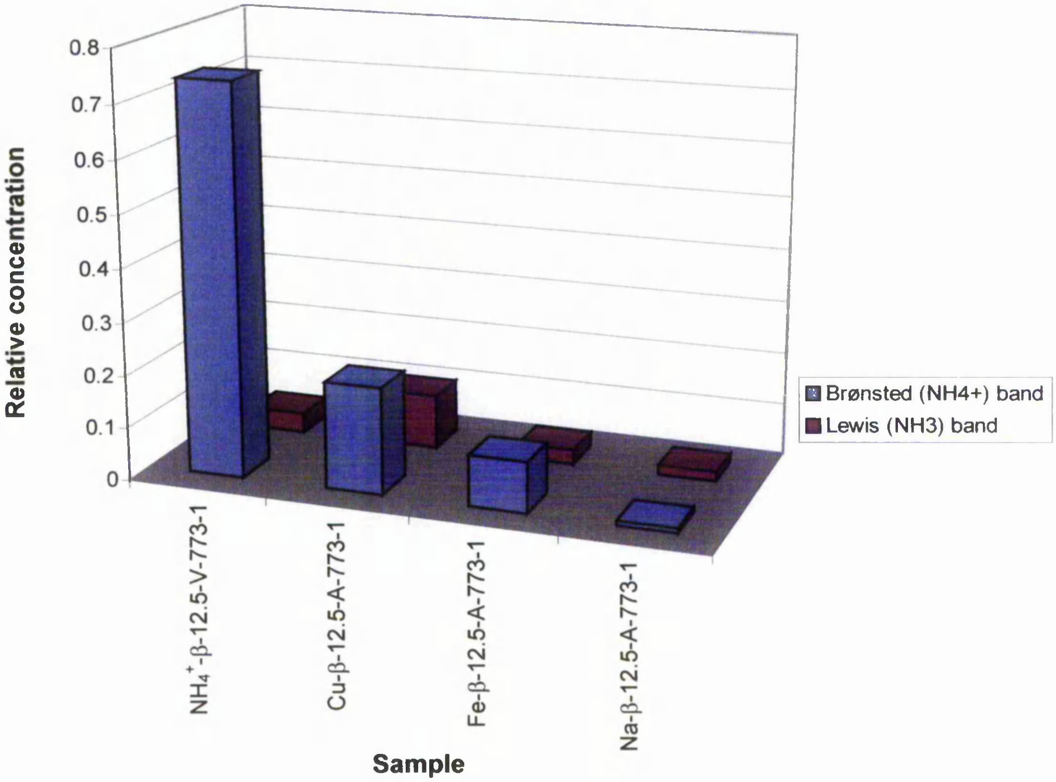

Figure 3.1.4.4 Relative concentration of Brønsted and Lewis acid sites.

Figure 3.1.4.5 shows the relative concentration of NH_4^+ versus the relative concentration of Brønsted acidic OH groups for ion-exchanged zeolite Beta as described in the key. Values used in the plot were obtained from **Table 3.1.4.1** and **Table 3.1.4.2**. The concentration of Brønsted acidic OH groups was taken as the sum of bridged OH groups.

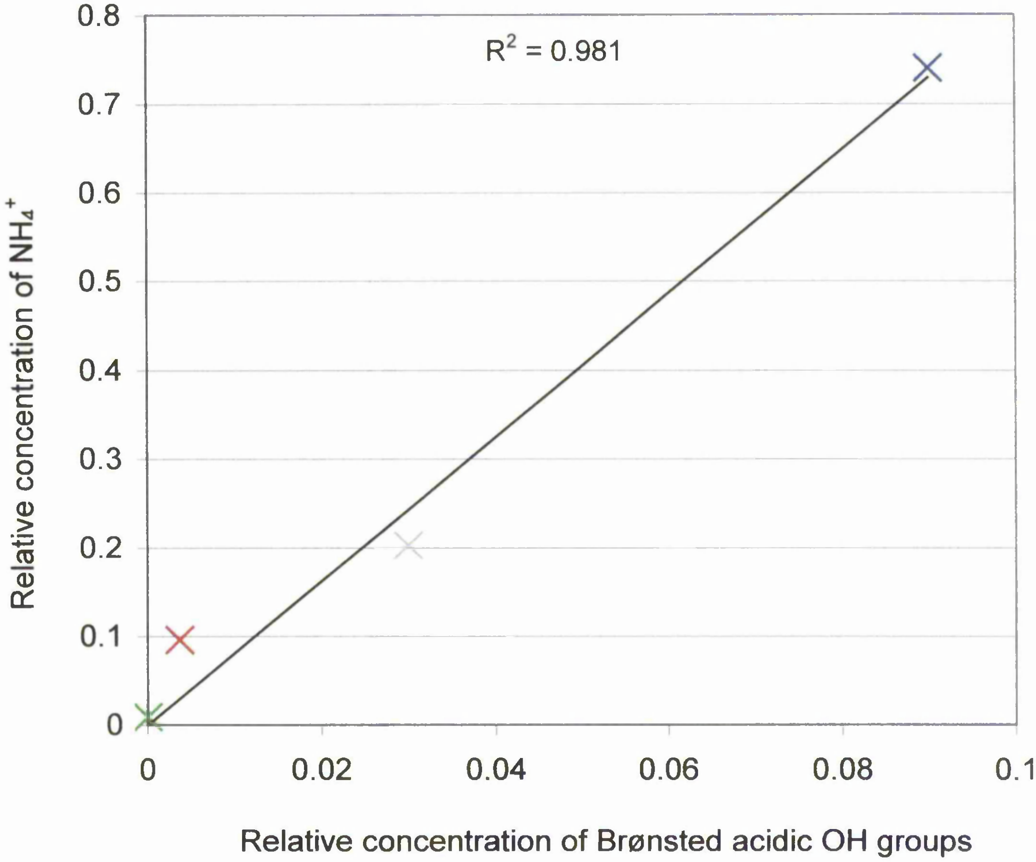

KEY:

× NH_4^+-β-12.5-V-773-1

× Cu-β-12.5-A-773-1

× Fe-β-12.5-A-773-1

× Na-β-12.5-A-773-1

Figure 3.1.4.5 Concentration of NH_4^+ versus concentration of Brønsted acidic OH groups.

A reasonably good correlation exists between the relative concentration of NH_4^+ and the relative concentration of Brønsted acidic OH groups, indicating that bridged OH groups are acting as Brønsted acid sites.

In order to determine the effect of sample treatment on silanol groups in zeolite Beta, the FTIR spectra in the region of 3680 cm^{-1} to 3760 cm^{-1} were subject to a peak-fitting program. **Figure 3.1.4.6** to **Figure 3.1.4.9** show the results of peak fitting using a mixed Gaussian and Lorentzian peak function, corresponding to a 30% Gaussian, 70% Lorentzian line shape, in the silanol region of ion exchanged zeolite Beta samples, and **Table 3.1.4.3** summarises the findings.

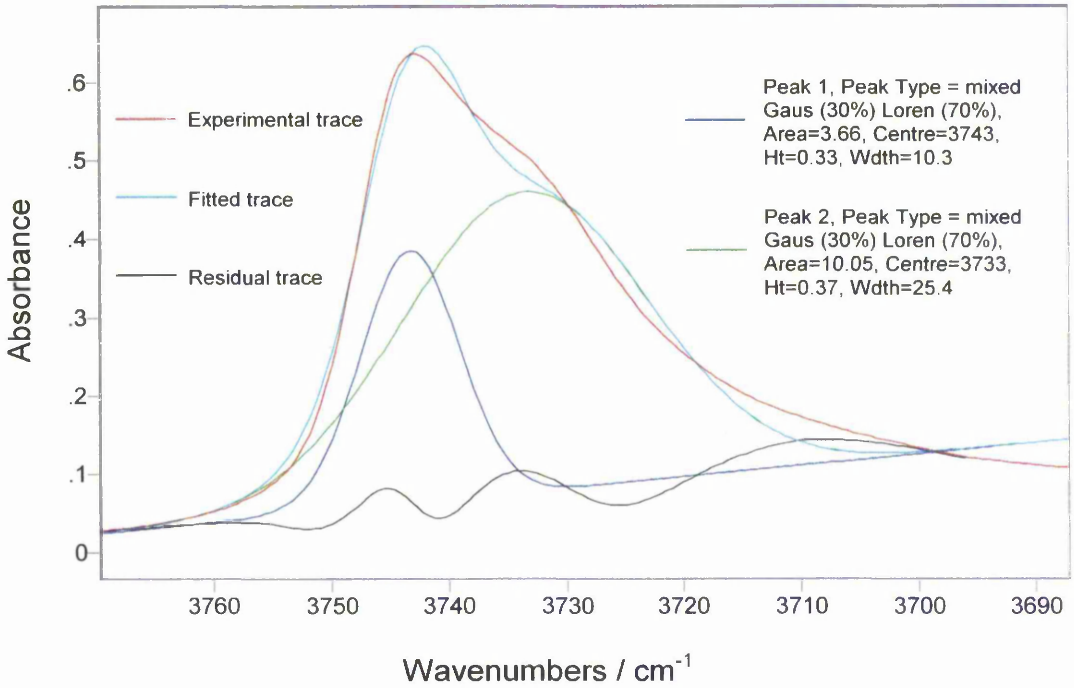

Figure 3.1.4.6 Silanol region of NH_4^+-β-12.5-V-773-1 after peak fitting.

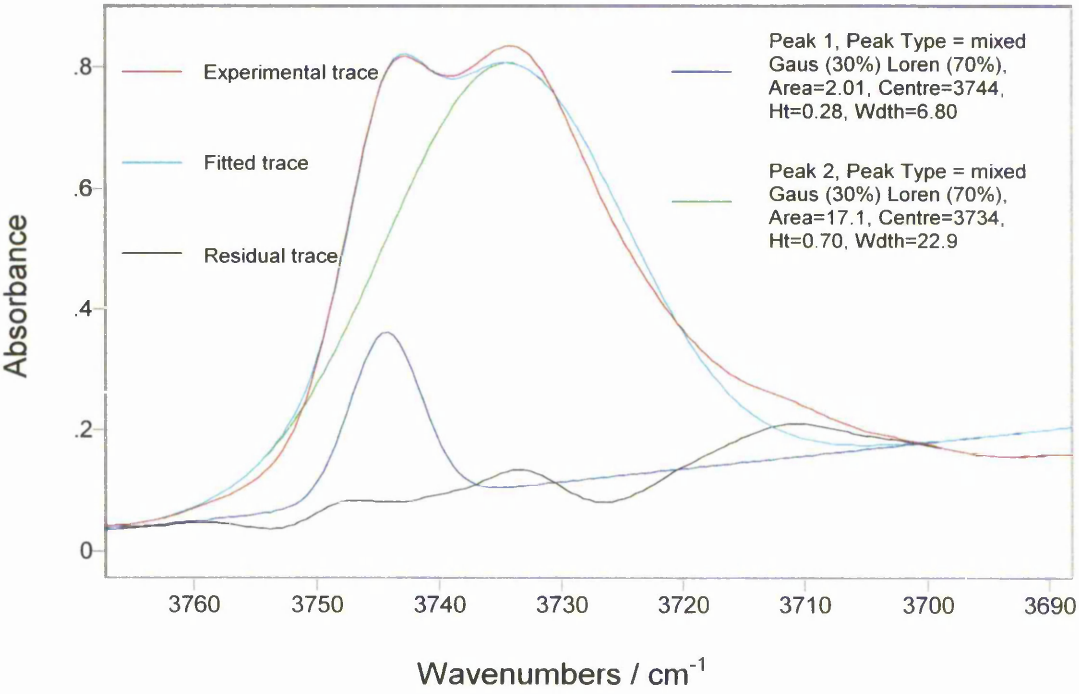

Figure 3.1.4.7 Silanol region of Cu-β-12.5-A-773-1 after peak fitting.

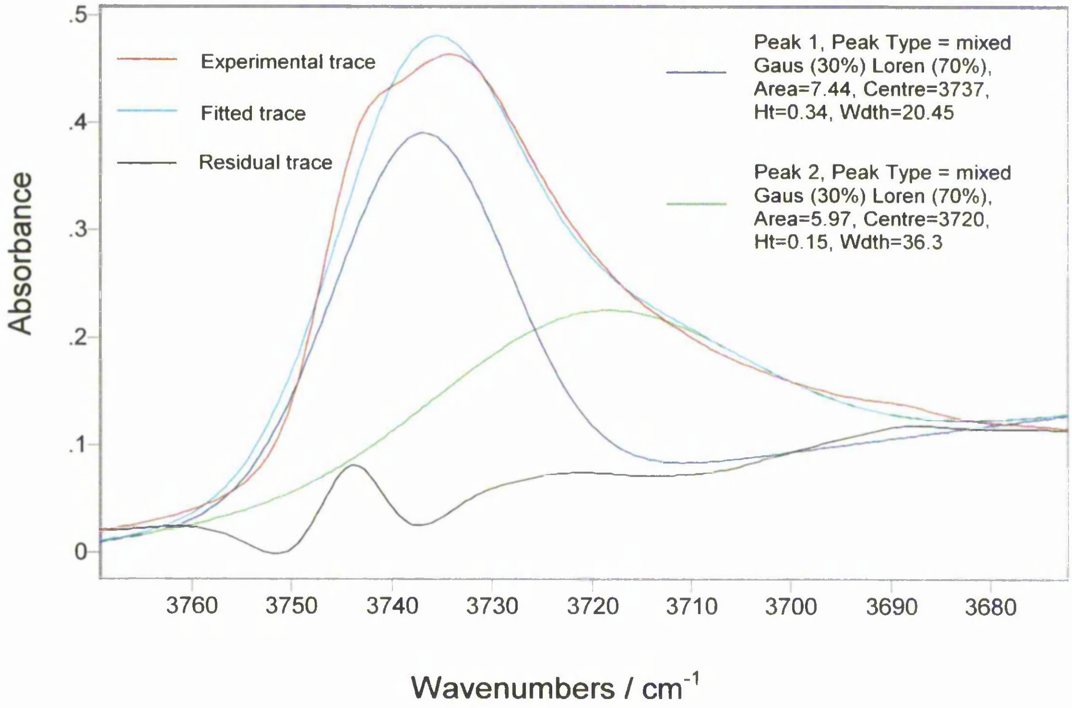

Figure 3.1.4.8 Silanol region of Fe-β-12.5-A-773-1 after peak fitting.

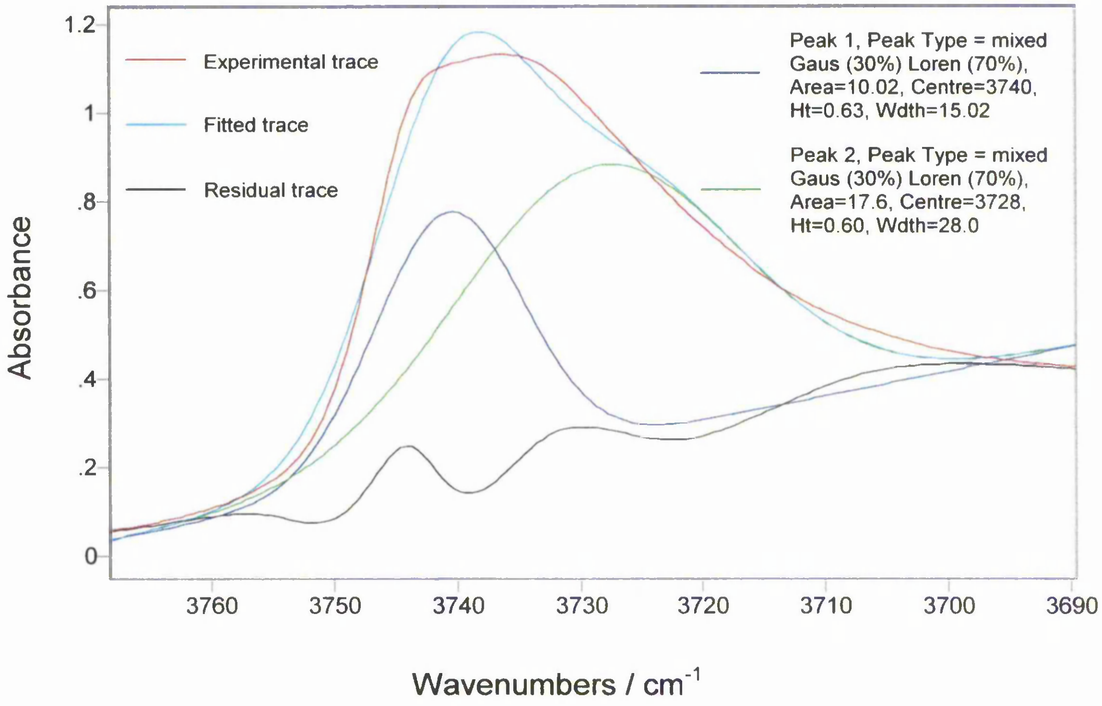

Figure 3.1.4.8 Silanol region of Na-β-12.5-A-773-1 after peak fitting.

Table 3.1.4.3 Peak fitting data in the silanol region of ion-exchanged zeolite Beta samples.

Sample	**Integral areas in the silanol region after mixed Gaus (30%) Loren (70%) peak fitting ± 2%***			
	Internal SiOH (3730 cm^{-1})		**External SiOH (3745 cm^{-1})**	
	Centre / cm^{-1}	**Area %**	**Centre / cm^{-1}**	**Area %**
NH_4^+-β-12.5-V-773-1	3733	73	3743	27
Cu-β-12.5-A-773-1	3734	89	3744	11
Fe-β-12.5-A-773-1	3720	45	3737	55
Na-β-12.5-A-773-1	3728	64	3740	36

* Approximate experimental error expressed as the coefficient of variation.

In order to probe the acidic strength of the identified OH groups present in various ion-exchanged samples, the intensity of bands responsible for NH_4^+ (1450 cm^{-1}) were differentiated with respect to temperature by Savitsky-Golay differentiation, in order to obtain conventional TPD (Temperature Programmed Desorption) curves. **Figure 3.1.4.9** to **Figure 3.1.4.11** show the TPD curves obtained for ion-exchanged zeolite Beta samples, and **Table 3.1.4.4** summarises the findings. TPD curves were subject to peak fitting using a mixed Gaussian and Lorentzian peak function, corresponding to a 30% Gaussian, 70% Lorentzian line shape in order to observe overlapping peaks.

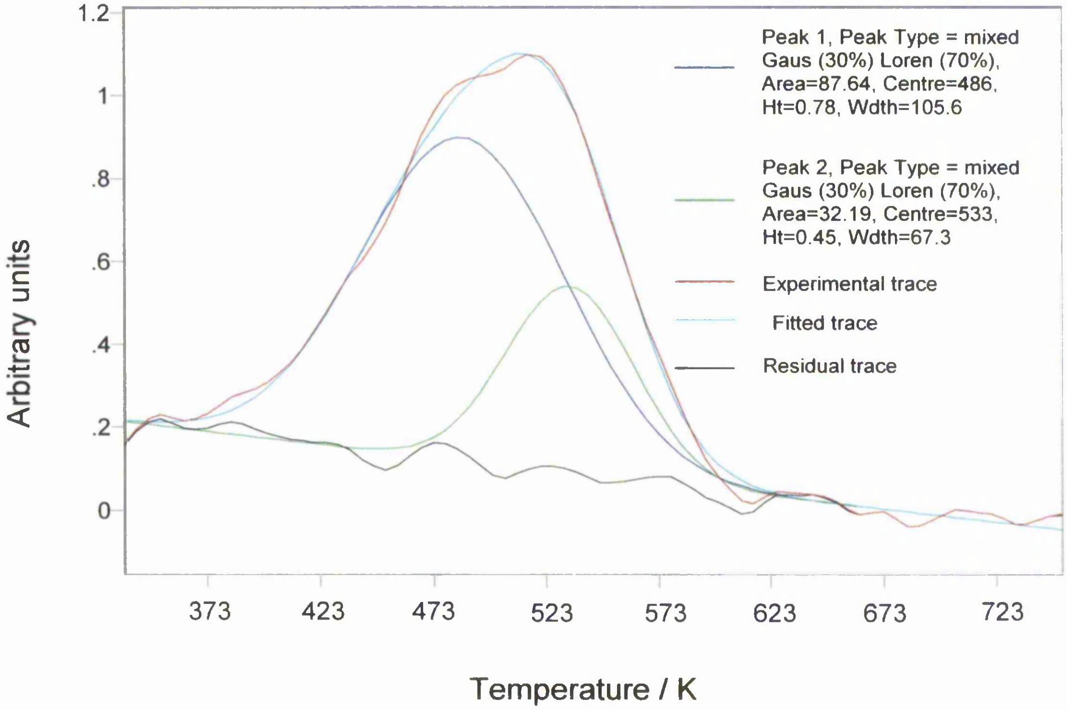

Figure 3.1.4.9 TPD trace of the NH_4^+ band (1371-1542 cm^{-1}) for NH_4^+-β-12.5-V-773-1.

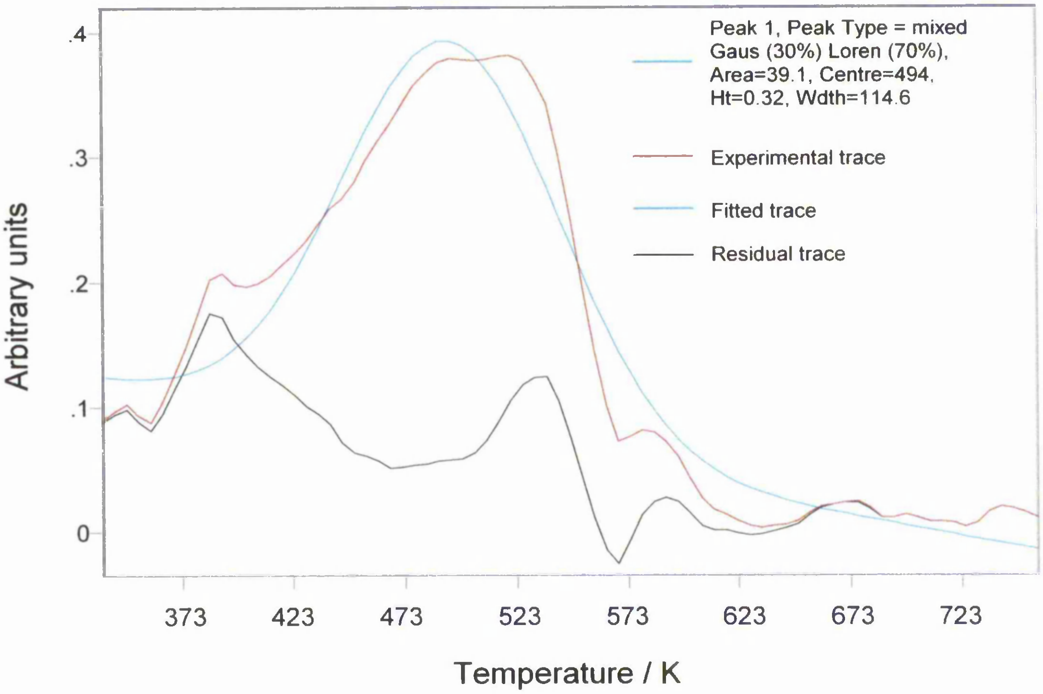

Figure 3.1.4.10 TPD trace of the NH_4^+ band (1371-1542 cm^{-1}) for Cu-β-12.5-A-773-1.

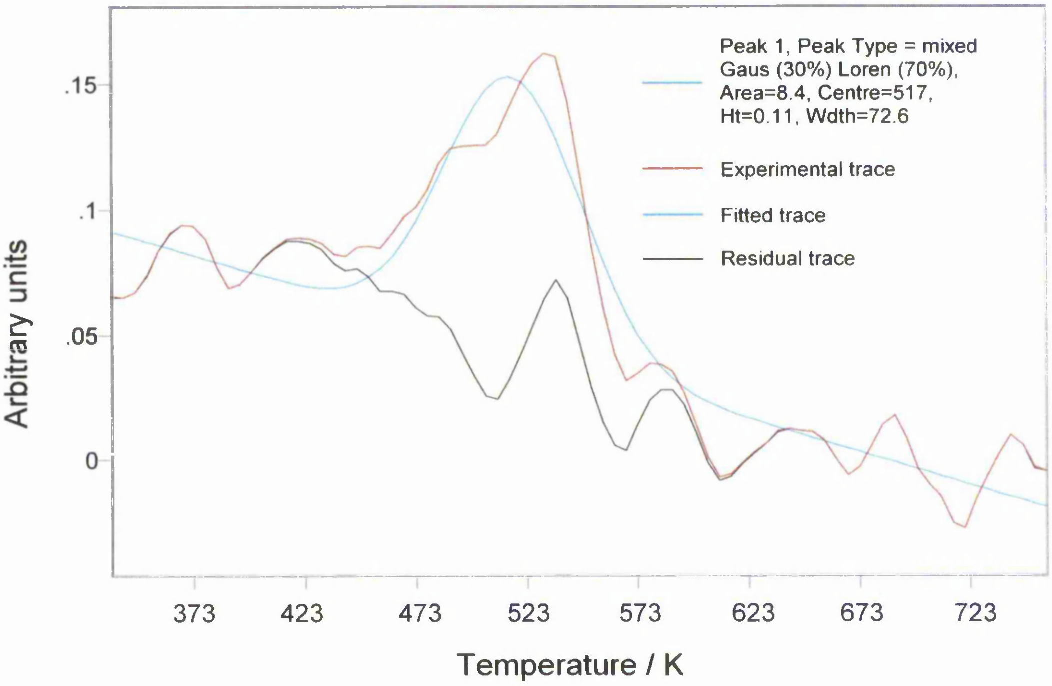

Figure 3.1.4.11 TPD trace of the NH_4^+ band (1371-1542 cm^{-1}) for Fe-β-12.5-A-773-1.

Table 3.1.4.4 Peak fitting data regarding the TPD of ammonia from Brønsted acid sites.

Sample	TPD data corresponding to the NH_4^+ band (1371-1542 cm^{-1}) ± 3%*					
	Peak 1		Peak 2		Peak 3	
	Centre / K	Area %	Centre / K	Area %	Centre / K	Area %
NH_4^+-β-12.5-V-773-1	486	73	533	27	-	-
Cu-β-12.5-A-773-1	494	100	-	-	-	-
Fe-β-12.5-A-773-1	517	100	-	-	-	-

* Approximate experimental error expressed as the coefficient of variation.

DISCUSSION

It is evident from **Figure 3.1.4.1** and **Table 3.1.4.1** that ion exchange has a dramatic impact on the concentration of bridged OH groups. In Cu-β-12.5-A-773-1 the concentration of bridged OH groups has decreased by 74% when compared with NH_4^+-β-12.5-V-773-1. The effect is much more pronounced in Fe-β-12.5-A-773-1 where the relative concentration of bridged OH groups has been reduced by 97% when compared with NH_4^+-β-12.5-V-773-1. In Na-β-12.5-A-773-1, there is no evidence of any protons in the FTIR spectrum. As observed in **Figure 3.1.4.2** and **Table 3.1.4.2**, the concentration of Brønsted acid sites are also decreasing, a 73% reduction in the case of Cu-β-12.5-A-773-1, an 87% decrease in the case of Fe-β-12.5-A-773-1, and a 99% reduction in Brønsted acid sites in the case of Na-β-12.5-A-773-1 when compared with NH_4^+-β-12.5-V-773-1. In both Cu-β-12.5-A-773-1 and Na-β-12.5-A-773-1, the reduction in bridged OH groups seems to be consistent with the decrease in Brønsted acid sites, which is expected since bridged OH groups are known to be the main contributor of Brønsted acid sites. In Fe-β-12.5-A-773-1 however, the relative concentration of Brønsted acid sites seems to be higher than would be expected from the small amount of bridged OH groups remaining on the sample. This could be due to a small amount of iron in the sample which has acidic OH groups attached to it and contributing to the band at 1450 cm^{-1}. Another possibility is that a small amount of SiOH groups in Fe-β-12.5-A-773-1 are sufficiently acidic to protonate ammonia and give rise to an increased absorption at 1450 cm^{-1}. What is also apparent from **Table 3.1.4.1** is the absence of extralattice and VHF OH groups in both Fe-β-12.5-A-773-1 and Cu-β-12.5-A-773-1. This would certainly suggest the possibility of reduced dealumination and thus an increased thermostability in these transition metal exchanged samples. And as mentioned earlier, the presence of protons has been associated with the appearance of non-tetrahedral aluminium and dealumination [10], and the same authors also suggested that the presence of charge compensating cations other than protons prevent the formation of non-tetrahedral aluminium species, indeed they found that the presence of cations other than protons results in a sample where all aluminium atoms occupy tetrahedral framework positions. In both Fe-β-12.5-A-773-1 and Cu-β-12.5-A-773-1, a large proportion of Fe or Cu respectively has been exchanged for protons in zeolite Beta, so it would seem likely that this would prevent the formation of octahedral aluminium species formed as a result of dealumination. There is some evidence of a very small amount of extralattice aluminium in Na-β-12.5-A-773-1, these species are most likely formed as a result of the ion exchange process. Cu-β-12.5-A-773-1 shows a significant increase in the number of Lewis acid sites when compared with NH_4^+-β-12.5-V-773-1. Cu in zeolites is known to act as a Lewis acid [67], and a recent publication by Dědeček *et al.*, [68] studied the catalytic activity of Cu-Beta in NO decomposition. These workers observed three types of Cu species in Cu-Beta zeolites depending on the loading. Cu ions incorporated at low Cu loading were found to be balanced by two framework Al atoms and were inactive in NO decomposition. At high Cu loading, another type of inactive, non-cationic Cu species was formed. Species responsible for NO decomposition were formed at medium Cu loading and were representative of Cu ions balanced by single framework Al atoms. Na-β-12.5-A-773-1 exhibits a rather large reduction in the relative concentration of Lewis acid sites when compared with NH_4^+-β-12.5-V-773-1, as was also observed by Dědeček *et al.*, [68]. These authors attributed this reduction to the fact that all the aluminium atoms in Na-Beta were located in framework positions, and no extraframework aluminium was present. Additionally, the concentration of Lewis acid sites in Fe-β-12.5-A-773-1 was reduced to a small extent when compared with NH_4^+-β-12.5-V-773-1. The results of the mixed Gaussian and Lorentzian peak fitting in the silanol region of ion exchanged zeolite Beta samples are presented in **Table 3.1.4.3**. It is apparent that Fe-β-12.5-A-773-1 and Na-β-12.5-A-773-1 show reduced concentrations of internal SiOH groups when compared with NH_4^+-β-12.5-V-773-1, and this reduction is accompanied by a concomitant increase in the number of external SiOH groups. The reduction in the number of internal SiOH groups would suggest that some reconstruction of internal defects has occurred as a result of altering the charge compensating cation. Reconstruction or 'healing' of internal defects has been reported by Trombetta *et al.*, [14]. There seems to be some link between the decrease in internal SiOH groups in Fe-β-12.5-A-773-1 and Na-β-12.5-A-773-1 and the decrease in Lewis acidity. It is widely accepted that zeolite Beta contains a large number of defect sites, and these have been linked to Lewis acidity [25]. It could be that reconstruction of internal defects results in a reduction in the number of Lewis acid sites in these two samples. The opposite is true in Cu-β-12.5-A-773-1, which shows an increased concentration of internal SiOH groups when compared with NH_4^+-β-12.5-V-773-1. Although in this case the likelihood is that the Cu acting as the charge compensating cation is responsible for the majority of the Lewis acid sites in the sample, although an increase in the number of internal SiOH groups and thus defect sites could certainly contribute to some of its Lewis acidity.

The results regarding the TPD of ammonia are presented in **Table 3.1.3.4**. It can be seen that in both Cu-β-12.5-A-773-1 and Fe-β-12.5-A-773-1 there is only one desorption peak as opposed to the two observed in NH_4^+-β-12.5-V-773-1. In the transition metal exchanged samples, the stronger Brønsted acid sites present in NH_4^+-β-12.5-V-773-1 are missing, and only the Brønsted sites of lower acidic strength remain. It would seem that the protons associated with the Brønsted sites of higher acidic strength are preferentially exchanged for the transition metal cation.

XRD RESULTS: ***effect of ion exchange on the acidic properties of zeolite Beta.***

Figure 3.1.4.12 shows the XRD profiles of ion-exchanged zeolite Beta samples. It can be seen that all zeolite Beta samples have a well-defined zeolite Beta structure. **Figure 3.1.4.12** also zooms in on a small section of the XRD profile in the region of 22.2 → 22.8° 2θ.

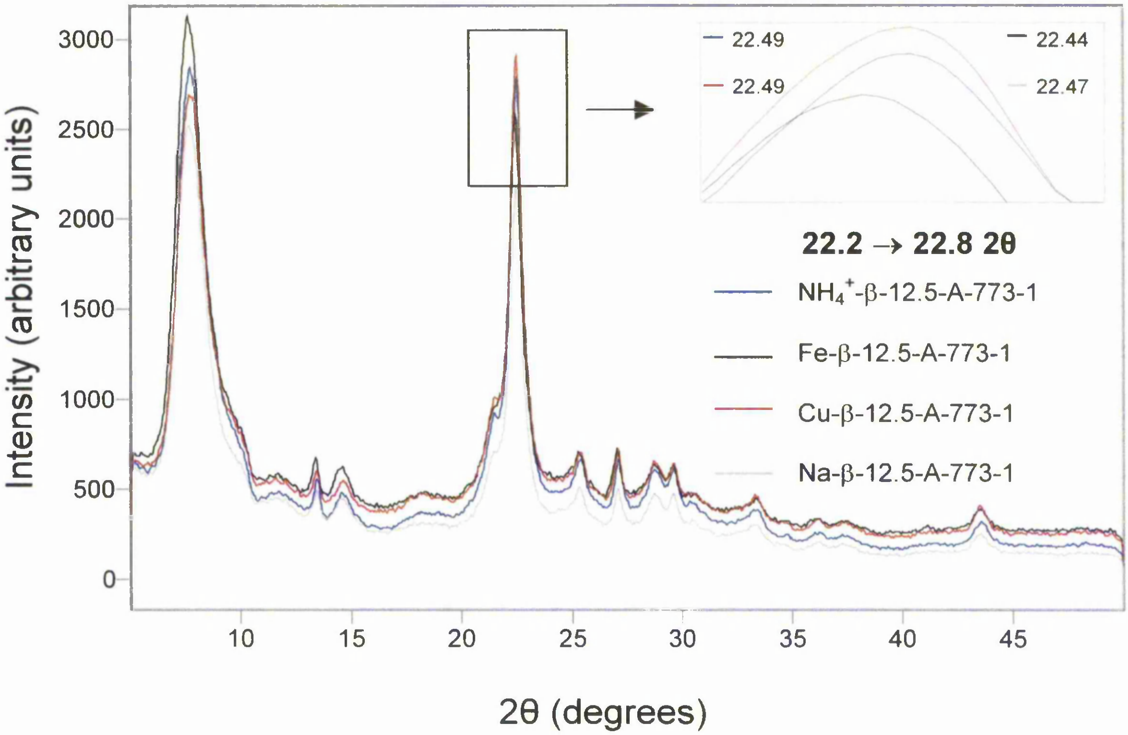

Figure 3.1.4.12 XRD profiles of ion-exchanged zeolite Beta samples.

DISCUSSION

Figure 3.1.4.12 shows the XRD profiles of ion-exchanged zeolite Beta samples. It can be seen that all the samples show a well-defined zeolite Beta structure. By observing the region between 22.2 and 22.8° 2θ it can be seen that all samples exhibit similar peak positions with the exception of Fe-β-12.5-A-773-1, which is shifted towards lower 2θ values. This suggests that ion-exchanged samples contain the same amount of framework tetrahedral aluminium species as NH_4^+-β-12.5-A-773-1, thus dealumination has not taken place in ion-exchanged samples since no shift towards higher 2θ values is observed when compared with NH_4^+-β-12.5-A-773-1. This would suggest, in line with FTIR results, that replacement of protons in the zeolite lattice for alternative charge compensating cations is accompanied by a resistance to dealumination. It has been shown by Müller *et al.*, [31] that the extent of dealumination in zeolite Beta increases with the number of Brønsted acid sites interacting with the zeolite framework. Although there are no signs of dealumination in the ion-exchanged samples, some loss of crystallinity is observed in Fe-β-12.5-A-773-1 (92%) and Na-β-12.5-A-773-1 (89%) when compared with NH_4^+-β-12.5-A-773-1 (100%). This would indicate that some loss of structural integrity has occurred as a result of the ion-exchange process.

CONCLUSION

It is evident that ion exchange has a dramatic effect on the number of bridged OH groups, especially in Fe-β-12.5-A-773-1 and Na-β-12.5-A-773-1 where only very few protons and no protons are remaining respectively. Additionally, both FTIR and XRD results suggest that no dealumination is occurring in ion-exchanged samples, which is almost certainly due to the reduction in the number of protons interacting with the zeolite framework. There is quite a significant increase in the number of Lewis acid sites in Cu-β-12.5-A-773-1, which has been attributed to the Cu in the zeolite acting as a Lewis acid site. In Fe-β-12.5-A-773-1 and Na-β-12.5-A-773-1, a reduction in the number of Lewis acid sites is observed, this could possibly be linked to the reduction in internal SiOH groups in these two sample, the reconstruction of defect sites could lead to a reduction in the number of Lewis acid sites.

3.1.5 Acidity of zeolite Beta

***FTIR RESULTS:** effect of regeneration on the acidic properties of zeolite H-Beta.*

In order to probe the effect of catalyst aging/deactivation and subsequent regeneration on the acidic properties of zeolite H-Beta, FTIR, XRD, and MAS NMR studies were employed. Deactivation, or the time-dependent decay of catalyst activity and/or selectivity can be caused by a change in the number, nature, or accessibility of the catalytic sites. The major contributor of catalyst deactivation in zeolites is 'coke' which generally consists of higher molecular weight materials formed within zeolite pores or on the external surface [69-71]. Coke may range in nature from simple olefin oligomers or other species with low diffusivities that are strongly chemisorbed at acid sites through to highly aromatic, hydrogen-deficient carbonaceous material that may be the end result of hydrogen-transfer processes and high temperature reactions, which can only be removed by oxidative regeneration or other severe processes. In the present study, oxidative regeneration to 823 K overnight was necessary to remove all the coke from the zeolite (deactivation of zeolite H-Beta is described in section **3.7**). Unfortunately, prolonged or multiple-cycle exposure of a zeolite to steam (e.g. in oxidative regeneration), particularly at higher temperature, can result in loss of tetrahedral aluminium sites or other structural damage. This section highlights the effects of multiple-cycle oxidative regeneration on the acidic properties and structural integrity of zeolite H-Beta.

Figure 3.1.5.1 shows the effect of regeneration on the acidic properties of zeolite H-Beta.

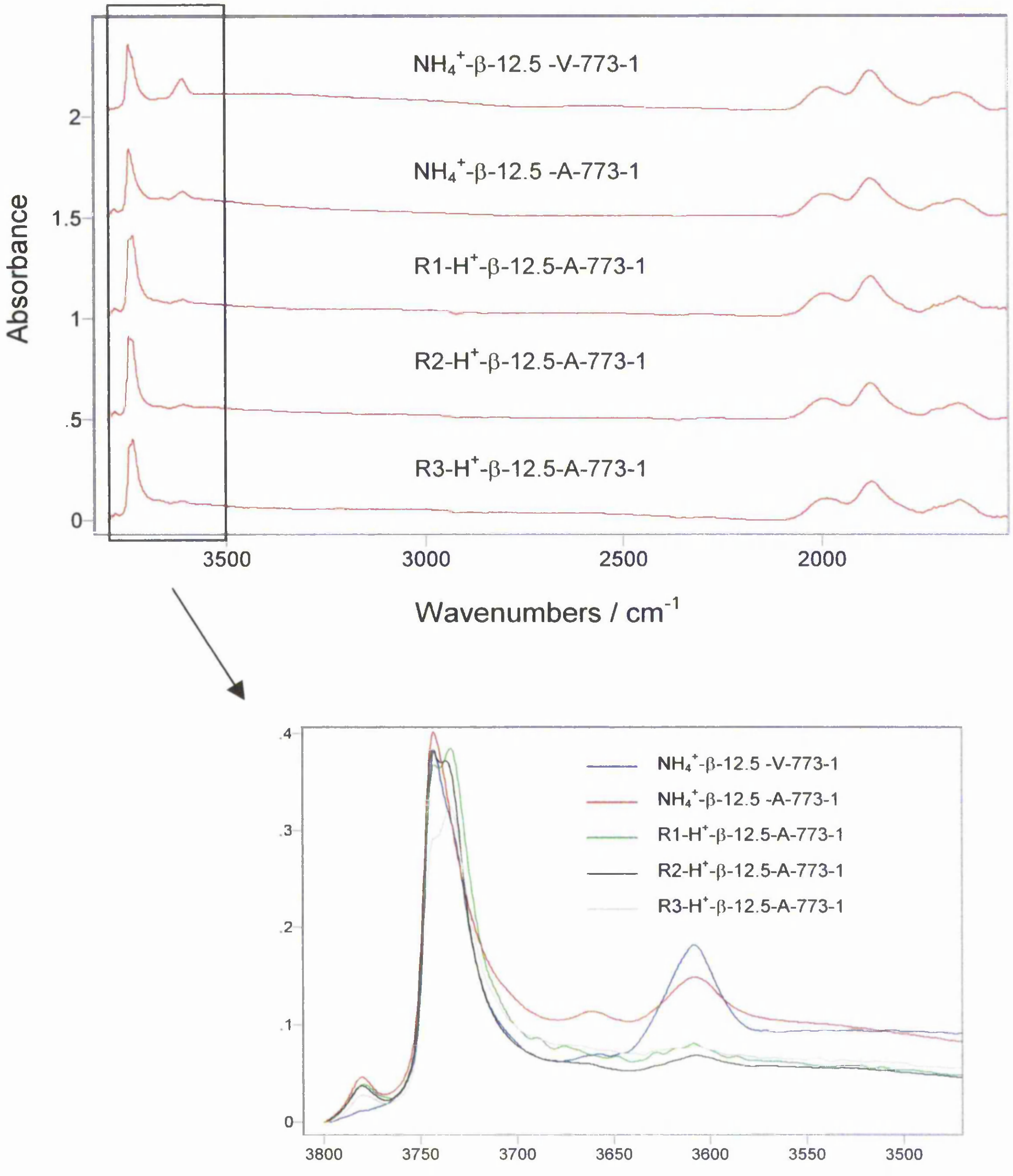

Figure 3.1.5.1 FTIR spectra in the hydroxyl region of regenerated zeolite H-Beta samples. Spectra taken at 423 K and normalised to the zeolite lattice overtones at 1987 and 1872 cm^{-1}.

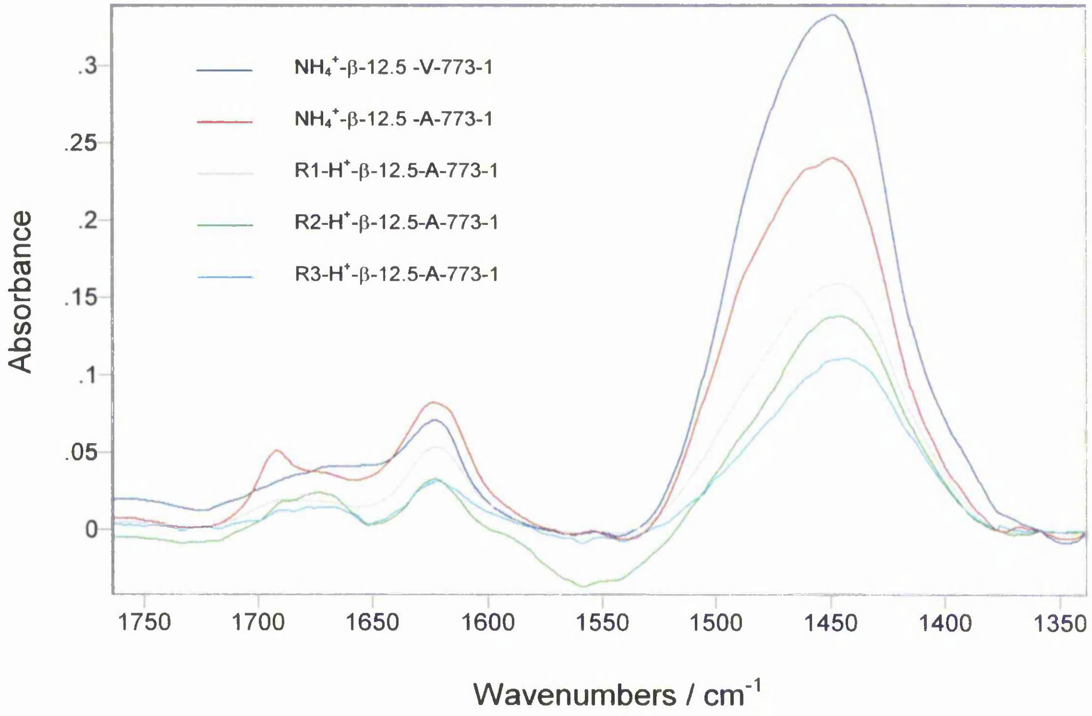

Figure 3.1.5.2 FTIR spectra in the NH deformation region of regenerated zeolite H-Beta samples showing the changes in bands at 1450 cm^{-1} (NH_4^+) and 1623 cm^{-1} (NH_3). Spectra taken at 423 K and normalised to the zeolite lattice overtones at 1987 and 1872 cm^{-1}.

The integration of the respective bands shown in **Figure 3.1.5.1** and normalisation to the lattice overtones gives the relative amount of bridged OH (3608 cm^{-1}), extralattice OH (3663 cm^{-1}) and very high frequency OH (3780 cm^{-1}) as presented in **Table 3.1.5.1** and **Figure 3.1.5.3**. The relative concentration of Brønsted and Lewis acid sites depicted in **Figure 3.1.5.2** were calculated in the same way and are presented in **Table 3.1.5.2** and **Figure 3.1.5.4**.

Table 3.1.5.1 Relative concentration of VHF, bridged, and extralattice OH groups.

Sample	**Integral area of absorption band**				**Relative concentration* ± 2%****		
	VHF OH (3769-3794 cm^{-1})	**Bridged OH** (3572-3641 cm^{-1})	**Extralattice OH** (3643-3679 cm^{-1})	**Lattice Overtones** (1753-2095 cm^{-1})	**VHF OH**	**Bridged OH**	**Extralattice OH**
NH_4^+-β-12.5-V-773-1	0	2.87	0	31.89	**0**	**0.09**	**0**
NH_4^+-β-12.5-A-773-1	0.604	2.53	0.312	54.86	**0.011**	**0.046**	**0.005**
R1-H^+-β-12.5-A-773-1	0.274	0.515	0.051	24.37	**0.011**	**0.021**	**0.002**
R2-H^+-β-12.5-A-773-1	0.367	0.546	0.034	29.86	**0.012**	**0.018**	**0.001**
R3-H^+-β-12.5-A-773-1	0.229	0.364	0.055	24.28	**0.009**	**0.015**	**0.002**

* Relative concentrations are calculated by normalising the integral area of the band of interest to the integral area of the lattice overtone bands.

** Approximate experimental error expressed as the coefficient of variation.

Table 3.1.5.2 Relative concentration of Brønsted and Lewis acid sites.

Sample	Integral area of absorption band			Relative concentration* ± 2%**	
	Brønsted (NH_4^+) band ($1371-1542\ cm^{-1}$)	Lewis (NH_3) band ($1582-1645\ cm^{-1}$)	Lattice Overtones ($1753-2095\ cm^{-1}$)	Brønsted	Lewis
NH_4^+-β-12.5-V-773-1	23.53	1.21	31.89	**0.740**	**0.038**
NH_4^+-β-12.5-A-773-1	29.59	1.48	54.86	**0.539**	**0.027**
R1-H^+-β-12.5-A-773-1	9.99	0.96	24.37	**0.410**	**0.039**
R2-H^+-β-12.5-A-773-1	10.45	1.16	29.86	**0.350**	**0.039**
R3-H^+-β-12.5-A-773-1	7.79	0.79	24.28	**0.321**	**0.032**

* Relative concentrations are calculated by normalising the integral area of the band of interest to the integral area of the lattice overtone bands.

** Approximate experimental error expressed as the coefficient of variation.

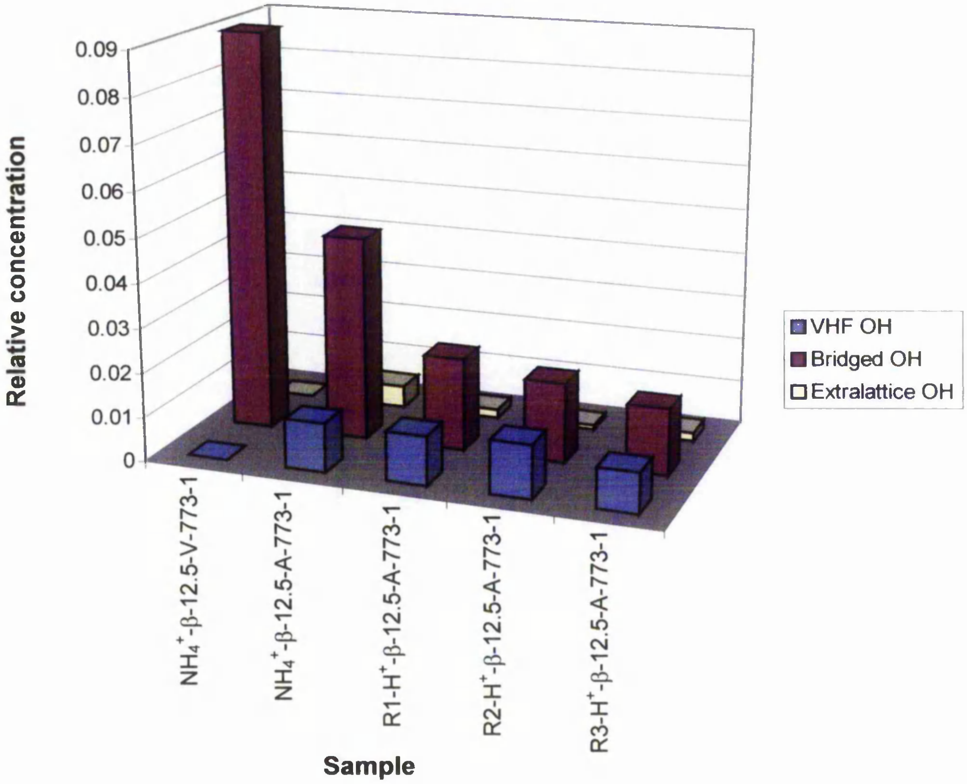

Figure 3.1.5.3 Relative concentration of different hydroxyl groups.

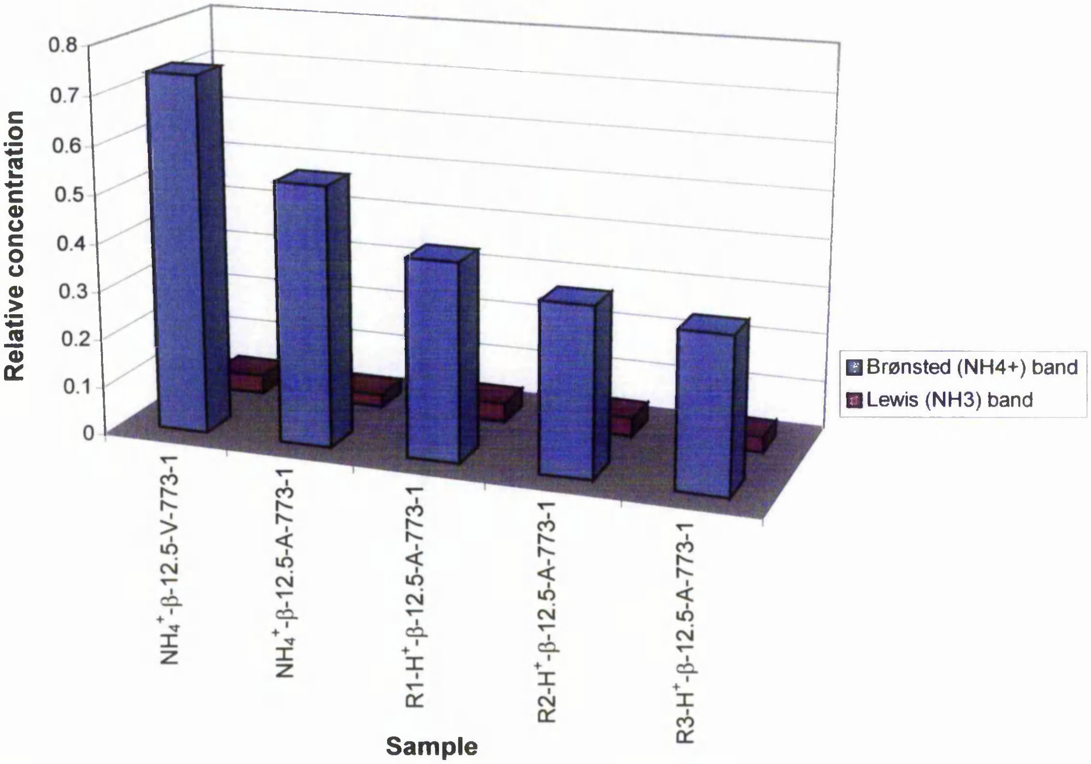

Figure 3.1.5.4 Relative concentration of Brønsted and Lewis acid sites.

Figure 3.1.5.5 shows the relative concentration of NH_4^+ versus the relative concentration of Brønsted acidic OH groups for regenerated zeolite H-Beta samples as described in the key. Values used in the plot were obtained from **Table 3.1.5.1** and **Table 3.1.5.2**. The concentration of Brønsted acidic OH groups was taken as the sum of bridged OH and very high frequency OH groups.

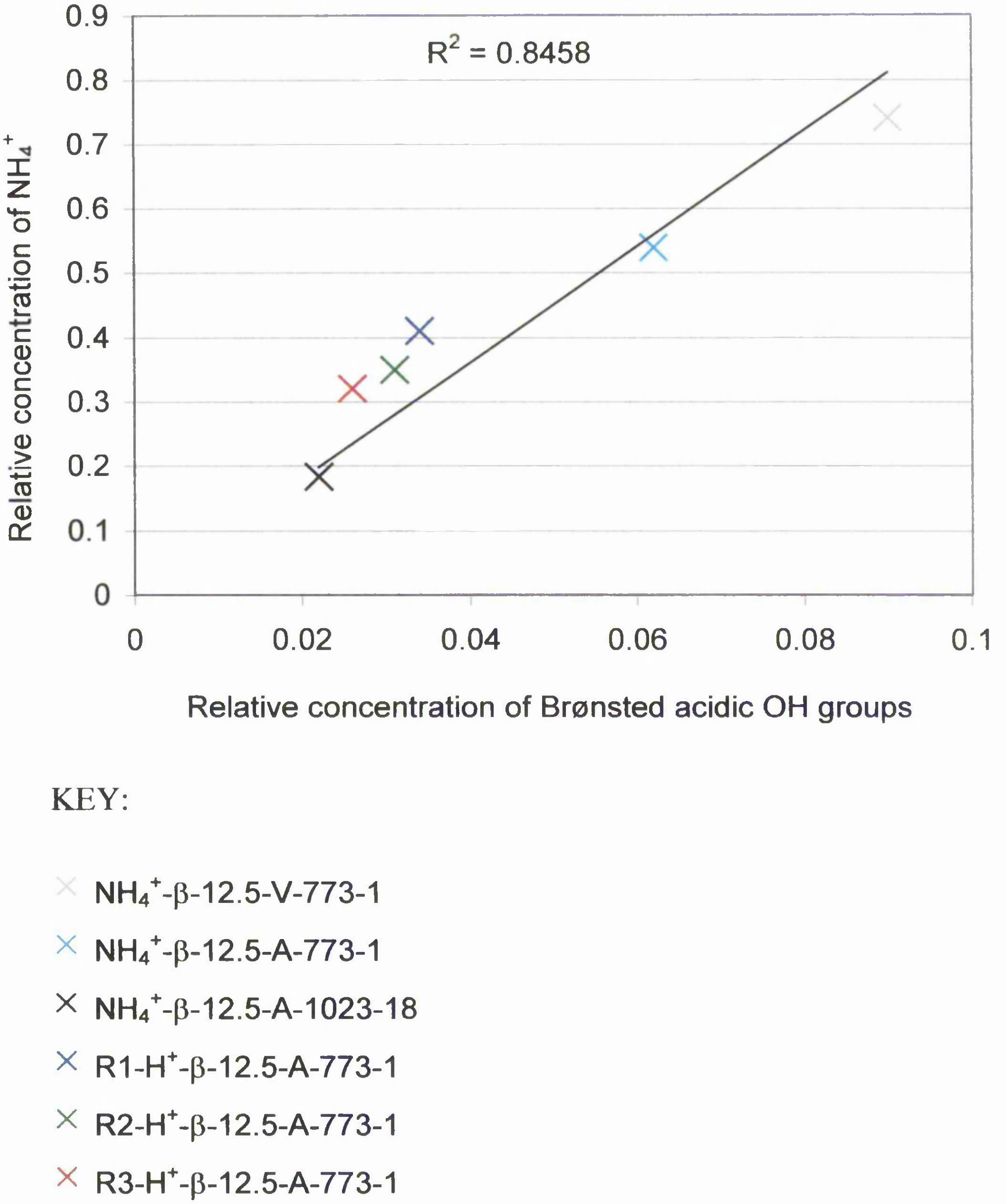

Figure 3.1.5.5 Concentration of NH_4^+ versus concentration of Brønsted acidic OH groups.

A reasonably good correlation exists between the relative concentration of NH_4^+ and the relative concentration of Brønsted acidic OH groups, indicating that bridged OH and very high frequency OH groups are acting as Brønsted acid sites.

In order to determine the effect of regeneration on the silanol groups in zeolite H-Beta samples, the FTIR spectra in the region of 3680 cm^{-1} to 3760 cm^{-1} were subject to a peak-fitting program. **Figure 3.1.5.6** to **Figure 3.1.5.9** show the results of peak fitting using a mixed Gaussian and Lorentzian peak function, corresponding to a 30% Gaussian, 70% Lorentzian line shape, in the silanol region of regenerated zeolite Beta samples, and **Table 3.1.5.3** summarises the findings.

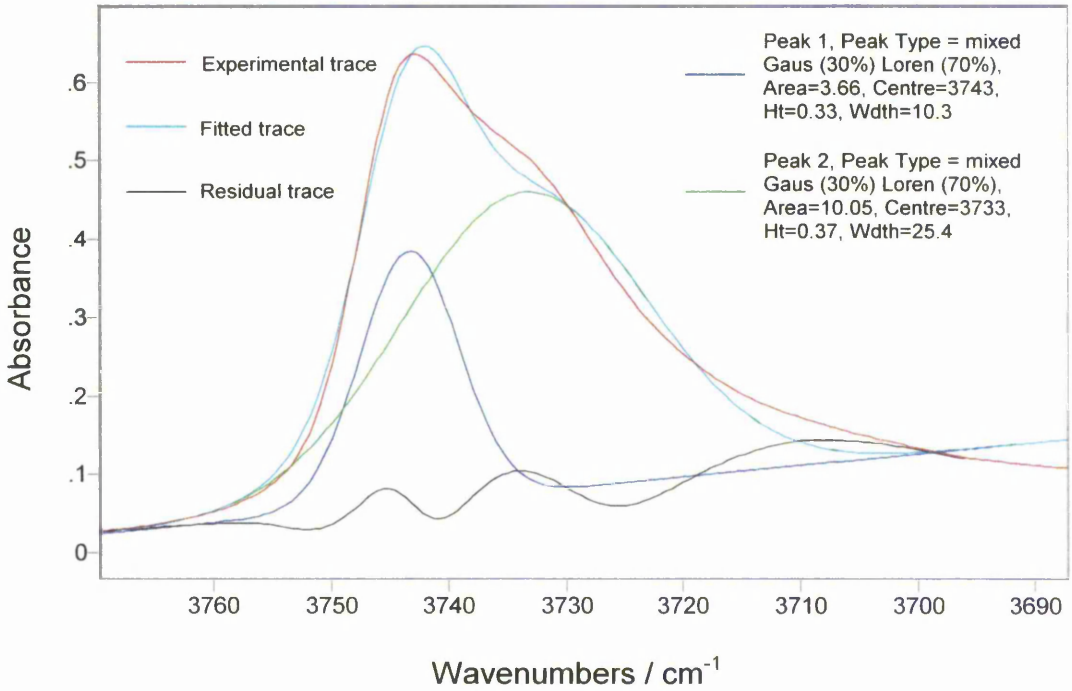

Figure 3.1.5.6 Silanol region of NH_4^+-β-12.5-V-773-1 after peak fitting.

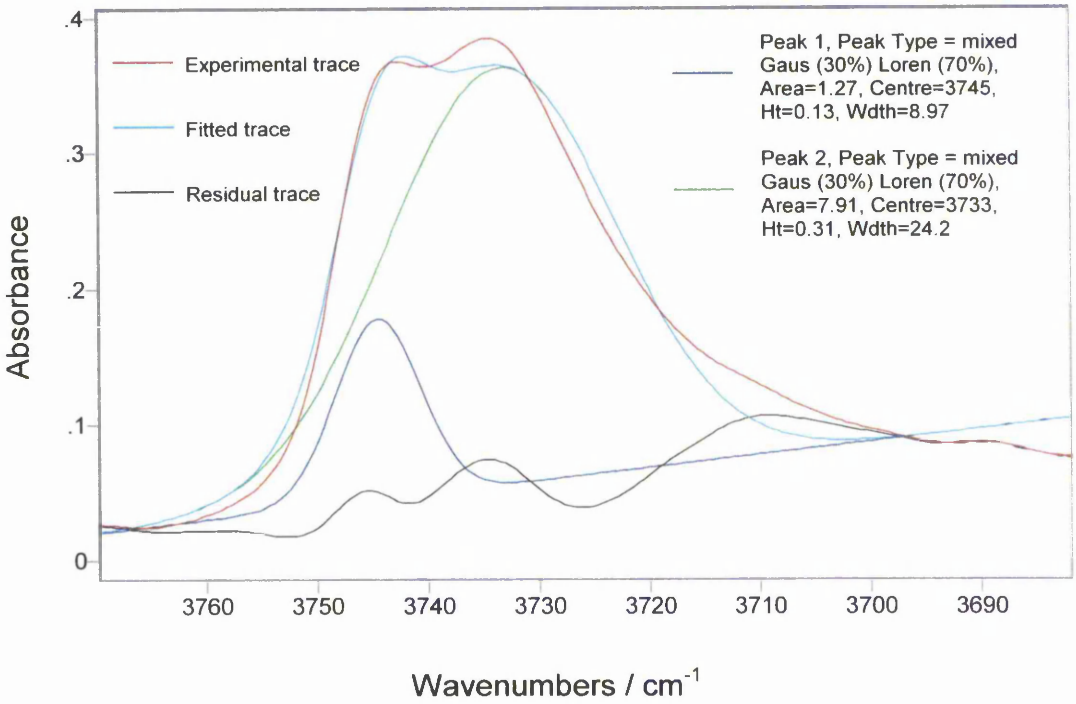

Figure 3.1.5.7 Silanol region of R1-H$^+$-β-12.5-A-773-1 after peak fitting.

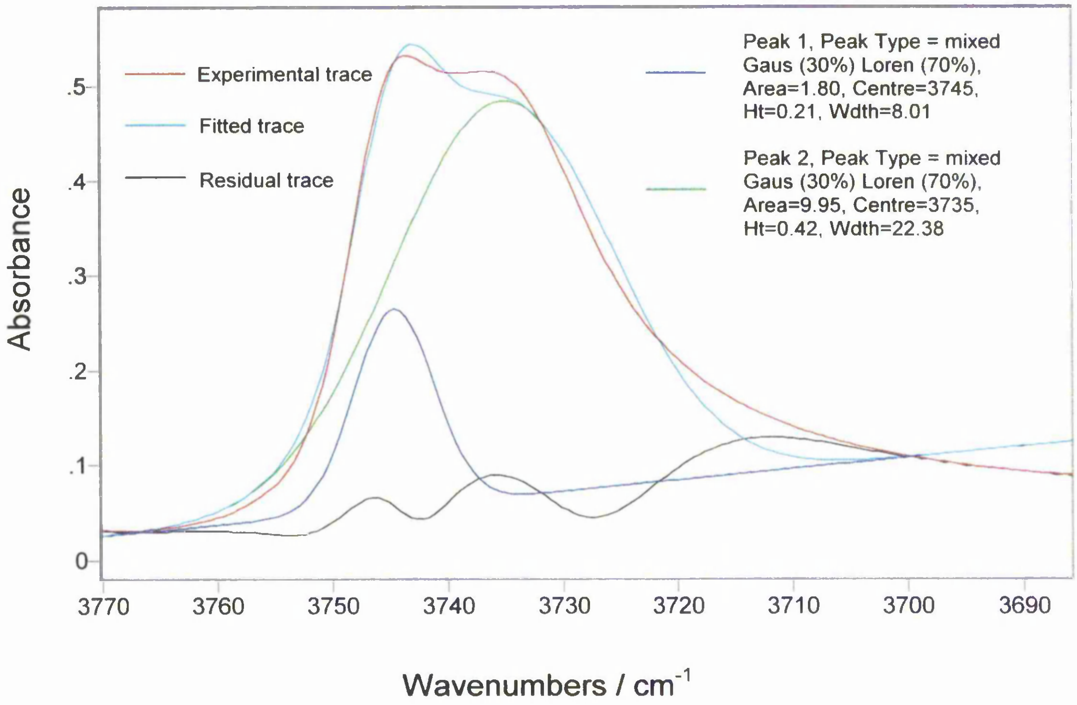

Figure 3.1.5.8 Silanol region of R2-H$^+$-β-12.5-A-773-1 after peak fitting.

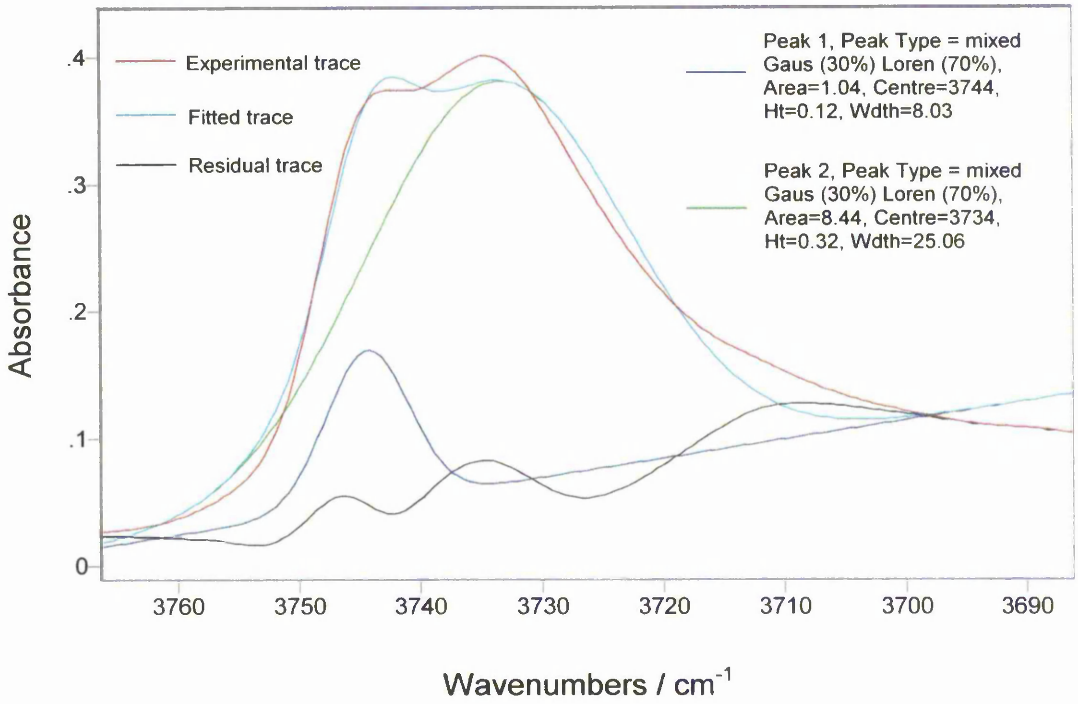

Figure 3.1.5.9 Silanol region of R3-H$^+$-β-12.5-A-773-1 after peak fitting.

Table 3.1.5.3 Peak fitting data in the silanol region of regenerated zeolite H-Beta samples.

Sample	**Integral areas in the silanol region after mixed Gaus (30%) Loren (70%) peak fitting ± 2%***			
	Internal SiOH (3730 cm^{-1})		**External SiOH (3745 cm^{-1})**	
	Centre / cm^{-1}	**Area %**	**Centre / cm^{-1}**	**Area %**
NH_4^+-β-12.5-V-773-1	3733	73	3743	27
R1-H^+-β-12.5-A-773-1	3733	86	3745	14
R2-H^+-β-12.5-A-773-1	3735	85	3745	15
R3-H^+-β-12.5-A-773-1	3734	89	3744	11

* Approximate experimental error expressed as the coefficient of variation.

In order to probe the acidic strength of the identified OH groups present in various regenerated samples, the intensity of bands responsible for NH_4^+ (1450 cm^{-1}) were differentiated with respect to temperature by Savitsky-Golay differentiation, in order to obtain conventional TPD (Temperature Programmed Desorption) curves. **Figure 3.1.5.9** to **Figure 3.1.5.11** show the TPD curves obtained for regenerated zeolite H-Beta samples, and **Table 3.1.5.4** summarises the findings. TPD curves were subject to peak fitting using a mixed Gaussian and Lorentzian peak function, corresponding to a 30% Gaussian, 70% Lorentzian line shape in order to observe overlapping peaks.

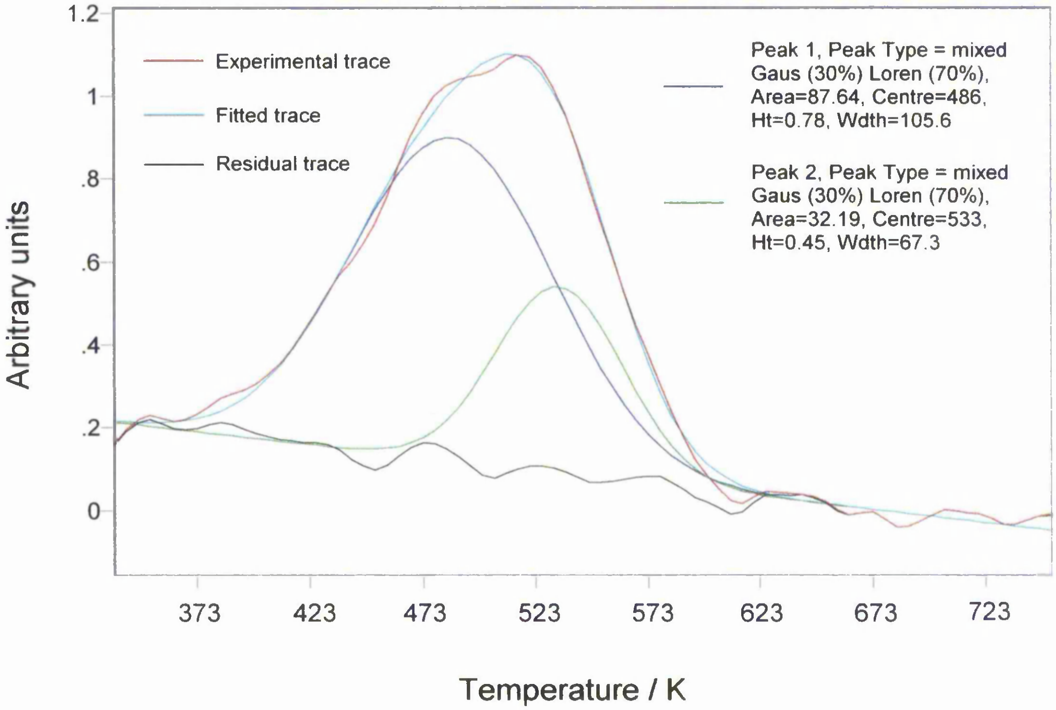

Figure 3.1.5.9 TPD trace of the NH_4^+ band (1371-1542 cm^{-1}) for NH_4^+-β-12.5-V-773-1.

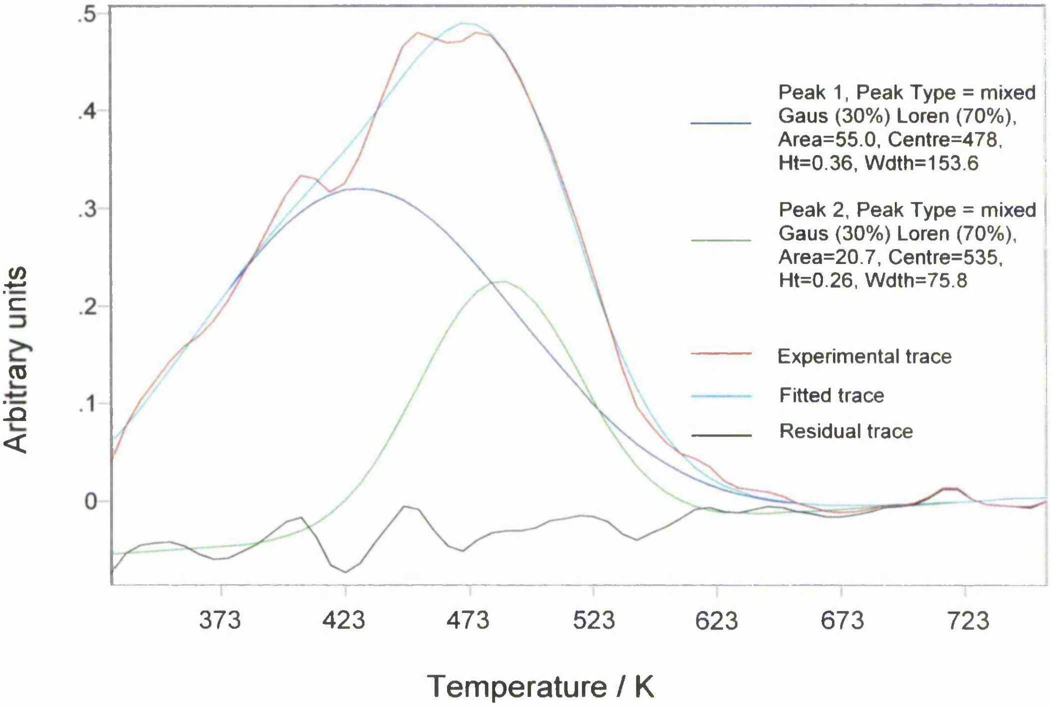

Figure 3.1.5.10 TPD trace of the NH_4^+ band (1371-1542 cm^{-1}) for R1-H$^+$-β-12.5-A-773-1.

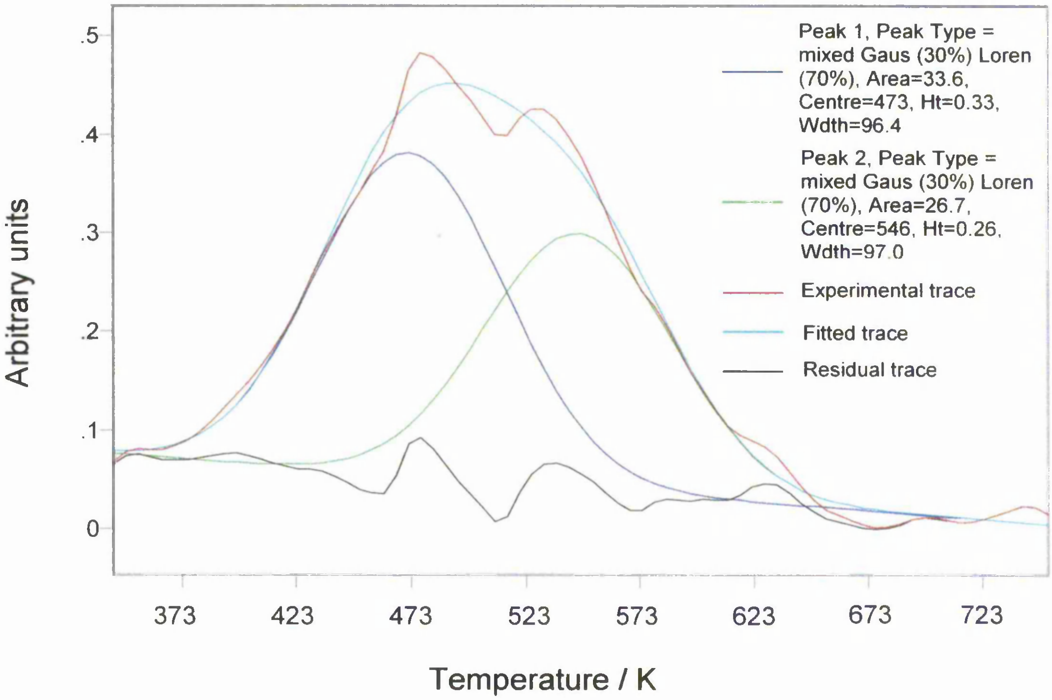

Figure 3.1.5.11 TPD trace of the NH_4^+ band (1371-1542 cm^{-1}) for R2-H$^+$-β-12.5-A-773-1.

Table 3.1.5.4 Peak fitting data regarding the TPD of ammonia from Brønsted acid sites.

Sample	**TPD data corresponding to the NH_4^+ band (1371-1542 cm^{-1}) ± 3%***					
	Peak 1		**Peak 2**		**Peak 3**	
	Centre / K	**Area %**	**Centre / K**	**Area %**	**Centre / K**	**Area %**
NH_4^+-β-12.5-V-773-1	486	73	533	27	-	-
R1-H^+-β-12.5-A-773-1	478	73	535	27	-	-
R2-H^+-β-12.5-A-773-1	473	56	546	34	-	-

* Approximate experimental error expressed as the coefficient of variation.

DISCUSSION

It is evident from **Figure 3.1.5.1** and **Table 3.1.5.1** that multiple-cycle regenerations have a dramatic effect on the relative concentration of OH groups in zeolite H-Beta. All the regenerated samples contain the same three types of OH groups present in the sample, NH_4^+-β-12.5-A-773-1, namely bridged OH, extralattice OH, and VHF OH groups, the origin of these species was described in detail earlier. The three regenerated samples contain a comparable amount of VHF OH groups as was present in NH_4^+-β-12.5-A-773-1, and there is also evidence of extralattice OH groups, but these species are only present in very small amounts. The most striking observation when comparing the regenerated samples to NH_4^+-β-12.5-A-773-1 is the large reduction in the number of bridged OH groups, 55% in the case of R1-H^+-β-12.5-A-773-1, and this reduction is more pronounced with subsequent regenerations, so that in R3-H^+-β-12.5-A-773-1 the number of bridged OH groups is further reduced to 68%. When comparing the regenerated samples to the carefully calcined sample, NH_4^+-β-12.5-V-773-1, the reduction becomes even more evident, 77% in the case of R1-H^+-β-12.5-A-773-1, and 84% in the case of R3-H^+-β-12.5-A-773-1. What is also interesting from these results is that the relative concentration of extralattice OH and VHF OH groups remain relatively constant with multiple-cycle regenerations, it is the bridged OH groups that are effected to the greatest extent. By observing **Figure 3.1.5.2** and **Table 3.1.5.2**, it becomes clear that the relative concentration of Brønsted acid sites reduces with multiple-cycle regenerations, which would be expected since the numbers of bridged OH groups are also decreasing, and bridged OH groups are known to be responsible for Brønsted acidity in zeolites. Interestingly, the relative concentration of Lewis acid sites remains fairly constant in the regenerated samples, and the concentration is comparable with that of NH_4^+-β-12.5-V-773-1. Clearly, multiple-cycle regeneration results in dealumination, not dissimilar to that observed in section **3.1.3**. Derouane *et al.*, [72] found that reuse of zeolite H-Beta after regeneration in air at 823 K overnight showed a substantial decrease in activity for the acetylation of anisole with acetic anhydride, and these workers were able to relate this decrease in catalytic activity with increasing dealumination of the zeolite lattice as evidenced by ^{27}Al MAS NMR spectroscopy. Similarly, Jacob *et al.*, [73] studied catalyst-recycling experiments on zeolite H-Beta used in the benzoylation of o-xylene. After reaction completion, the catalyst was removed by filtration, washed with acetone, and calcined at 773 K for 16 h in the presence of air. They observed that the activity of the catalyst decreases progressively on recycling, and they attributed this to the HCl liberated during the reaction, which promotes the extraction of aluminium from framework positions of the zeolite H-Beta. A study by Bhattacharya *et al.*, [74] on the selective benzoylation of naphthalene to 2-benzoylnaphthalene using zeolite H-Beta also found that when the catalyst was recycled four times a marginal decline in conversion was observed after each recycle. These workers attributed this decline in catalytic activity to the minor dealumination of the zeolite catalyst due to hydrogen chloride liberated during the reaction.

Results from Gaussian peak fitting in the silanol region of the FTIR spectra of regenerated samples are presented in **Table 3.1.5.3**. When compared with the sample, NH_4^+-β-12.5-V-773-1, regenerated samples show an increased number of internal SiOH groups and a concomitant decrease in the number of external SiOH groups. As a general trend, the number of internal SiOH groups increases with increasing numbers of recycles. As already discussed earlier, more severe calcination conditions result in an increase in the number of internal SiOH groups, as observed by Müller *et al.*, [31]. Oxidative regeneration would certainly result in an increase in the number of defects in the zeolite lattice, and hence an increase in the number of internal SiOH groups would be expected.

The TPD results regarding regenerated samples are shown in **Table 3.1.5.4**. It can be seen that both R1-H^+-β-12.5-A-773-1 and R2-H^+-β-12.5-A-773-1 exhibit two desorption peaks, one of lower acidic strength, accounting for the larger proportion of Brønsted acid sites in the sample, and one of higher acidic strength, which accounts for the remaining Brønsted acid sites. R1-H^+-β-12.5-A-773-1 exhibits similar acidic strength properties as NH_4^+-β-12.5-V-773-1, apart from a slight increase in acidic strength of the sites responsible for the higher temperature desorption peak. On the other hand, R2-H^+-β-12.5-A-773-1 shows a more significant increase in the number of higher acidic strength sites at the expense of lower acidic strength sites, which is to be expected since dealumination is known to create sites of higher acidic strength. Guisnet *et al.*, [37] found that the number of sites with lower acidity decreased with increasing dealumination, and additionally Hanke *et al.*, [39] proposed that dealumination increases the strength of remaining Brønsted acid sites.

XRD RESULTS: *effect of regeneration on the acidic properties of zeolite H-Beta.*

Figure 3.1.5.12 shows the XRD profiles of regenerated zeolite H-Beta samples. It can be seen that all zeolite Beta samples have a well-defined zeolite Beta structure. **Figure 3.1.5.12** also zooms in on a small section of the XRD profile in the region of 22.2 → 22.8° 2θ.

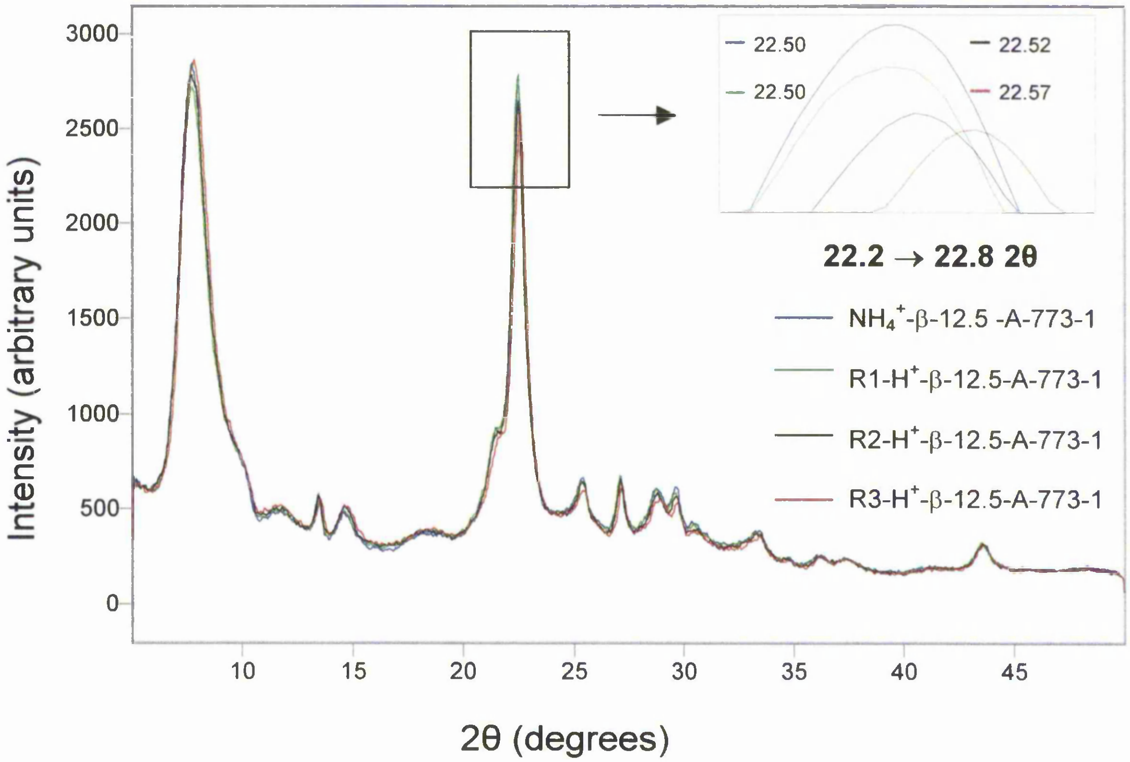

Figure 3.1.5.12 XRD profiles of regenerated zeolite H-Beta samples.

DISCUSSION

Figure 3.1.5.12 shows XRD profiles of regenerated zeolite H-Beta samples. It can be seen that all samples exhibit a well-defined zeolite Beta structure. By observing the region between 22.2 and 22.8° 2θ, it can be seen that the peak maximum shifts towards higher 2θ values after successive regenerations, indicating that dealumination, and hence removal of aluminium from framework positions is occurring [44]. In R1-H^+-β-12.5-A-773-1, no shift is observed when compared with NH_4^+-β-12.5-A-773-1, however the peak shifts from 22.50 to 22.52° 2θ in R2-H^+-β-12.5-A-773-1, and further to 22.57° 2θ in R3-H^+-β-12.5-A-773-1. In reinforcement of the FTIR results, XRD also suggests that dealumination is occurring as a result of multiple-cycle regeneration in zeolite H-Beta. Using the same procedure as described earlier in the section, the crystallinity of the samples was measured. R1-H^+-β-12.5-A-773-1 showed 100% crystallinity compared with NH_4^+-β-12.5-A-773-1. However, both R2-H^+-β-12.5-A-773-1 and R3-H^+-β-12.5-A-773-1 showed a progressive reduction in crystallinity with values of 96% and 93% respectively, indicating that in addition to dealumination, the structural integrity of zeolite H-Beta was damaged to a small extent due to multiple-cycle oxidative regeneration.

MAS NMR RESULTS: ***effect of regeneration on the acidic properties of zeolite H-Beta.***

^{27}Al MAS NMR

Figure 3.1.5.13 shows the fitted ^{27}Al MAS NMR spectrum of R3-H^{+}-β-12.5-A-773-1 and the results are summarized in **Table 3.1.5.5**.

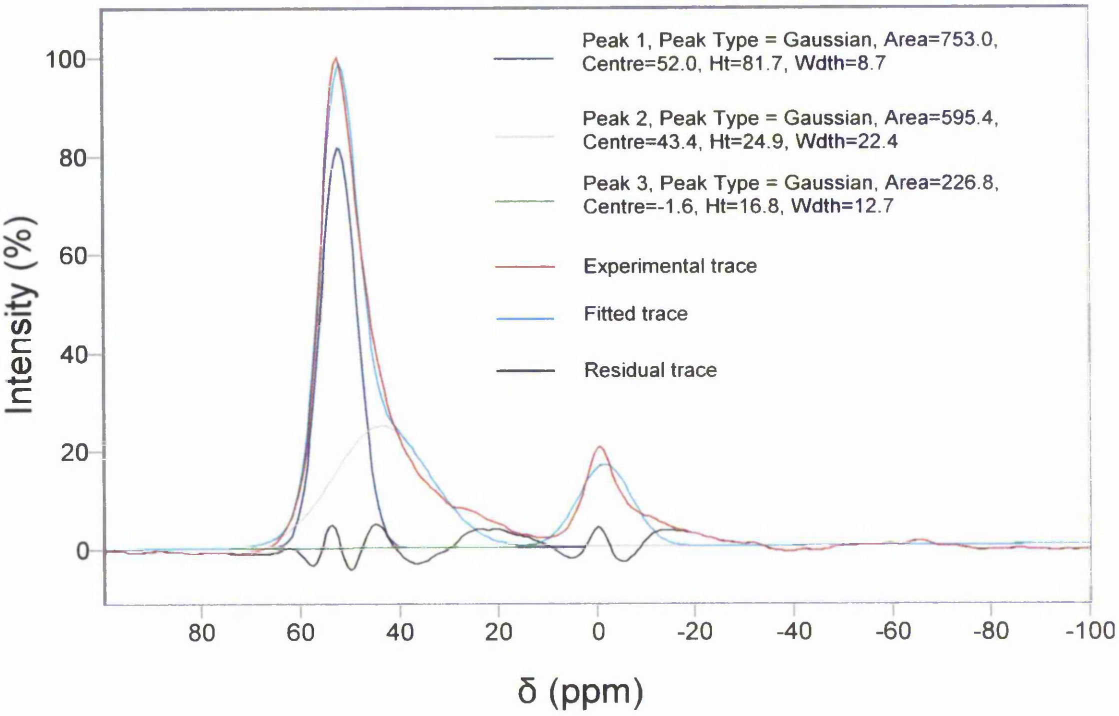

Figure 3.1.5.13 Fitted ^{27}Al MAS NMR spectrum of R3-H^{+}-β-12.5-A-773-1.

Sample	Fitted ^{27}Al MAS NMR results					
	Peak 1		Peak 2		Peak 3	
	Position	Area %	Position	Area %	Position	Area %
NH$_4^{+}$-β-12.5-V-773-1	52.6	50	47.3	46	-0.31	4
R3-H^{+}-β-12.5-A-773-1	52.0	48	43.4	38	-1.6	14

Table 3.1.5.5 Fitted ^{27}Al MAS NMR data.

DISCUSSION

By observing the data presented in **Table 3.1.5.5** it becomes clear that multiple-cycle regeneration results in a 10% increase in the band at 0 ppm when compared with NH_4^+-β-12.5-V-773-1, this band is indicative of octahedral aluminium [9], and the formation of octahedral aluminium species is generally associated with dealumination of the zeolite framework [3]. What is also apparent is that the band at 52 ppm indicative of tetrahedral aluminium is not affected by multiple-cycle regeneration, and in both NH_4^+-β-12.5-V-773-1 and R3-H^+-β-12.5-A-773-1, this species accounts for 50% of all the aluminium present. What is very interesting is the fact that the band at 47.3 ppm in NH_4^+-β-12.5-V-773-1 accounting for 46% of the total amount of aluminium present is shifted to 43.4 ppm and reduced to 38% in R3-H^+-β-12.5-A-773-1. As explained earlier, the band at 47.3 ppm was assigned to 'slightly distorted' tetrahedral aluminium because of its rather high ppm value making it almost fully tetrahedral, however, in R3-H^+-β-12.5-A-773-1, the peak position is shifted towards lower ppm values, indicating the formation of a more highly distorted tetrahedral aluminium species. Bearing in mind that there is an increase in internal SiOH groups (defect sites) in R3-H^+-β-12.5-A-773-1, it may be expected that this would be accompanied by an increased distortion of tetrahedral aluminium, since the formation of internal defect sites would certainly cause some strain and distortion of nearby tetrahedral aluminium sites. Additionally, another interesting observation from these results is that tetrahedral aluminium in a 'slightly distorted' environment is preferentially converted to octahedral aluminium with successive recycling, whereas the undistorted tetrahedral aluminium remains unaffected. Thus, as concluded by van Bokhoven *et al.*, [45], it would seem that there are tetrahedral aluminium sites in zeolite Beta that are resistant to dealumination, and other tetrahedral aluminium sites ('slightly distorted' tetrahedral aluminium) that are preferentially converted to octahedral aluminium upon dealumination.

^{29}Si MAS NMR

Figure 3.1.5.14 shows the fitted DP ^{29}Si MAS NMR spectrum of R3-H$^+$-β-12.5-A-773-1 and the results are summarized in **Table 3.1.5.6**.

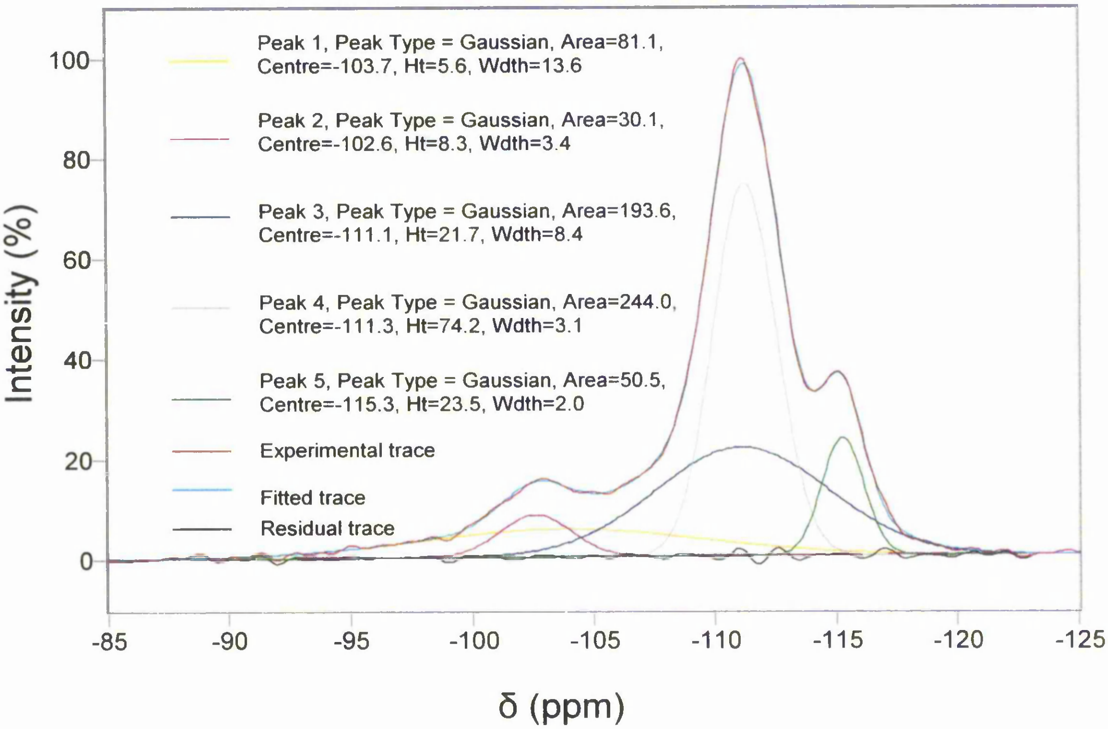

Figure 3.1.5.14 Fitted DP ^{29}Si MAS NMR spectrum of R3-H$^+$-β-12.5-A-773-1.

Sample	Fitted DP ^{29}Si MAS NMR results									
	Peak 1		Peak 2		Peak 3		Peak 4		Peak 5	
	Position	Area %	Position	Area %	Position	Area %	Position	Area %	Position	Area %
NH$_4$$^+$-β-12.5-V-773-1	-99.5	13	-102	5	-105	16	-110	48	-114	18
R3-H$^+$-β-12.5-A-773-1	-103	5	-104	14	-111	32	-111	41	-115	8

Table 3.1.5.6 Fitted DP ^{29}Si MAS NMR data.

Figure 3.1.5.15 shows the fitted CP ^{29}Si MAS NMR spectrum of R3-H^{+}-β-12.5-A-773-1 and the results are summarized in **Table 3.1.5.7**.

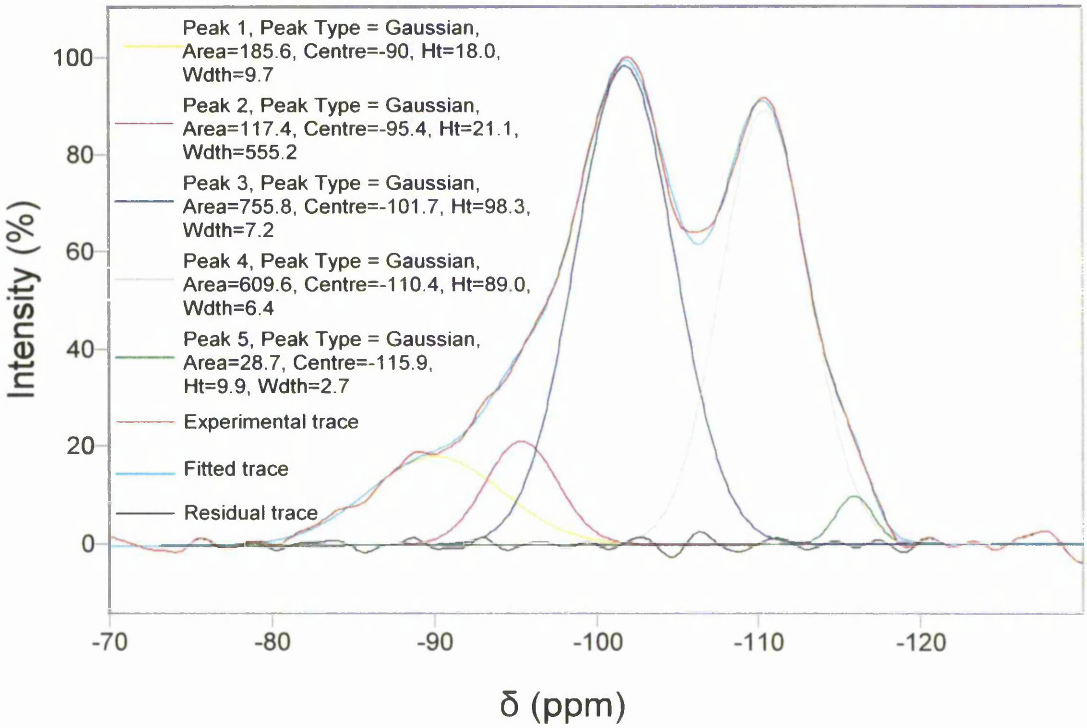

Figure 3.1.5.15 Fitted CP ^{29}Si MAS NMR spectrum of R3-H^{+}-β-12.5-A-773-1.

Sample	Fitted CP ^{29}Si MAS NMR results									
	Peak 1		Peak 2		Peak 3		Peak 4		Peak 5	
	Position	Area %	Position	Area %	Position	Area %	Position	Area %	Position	Area %
R3-H^{+}-β-12.5-A-773-1	-90	11	-95	6	-102	45	-110	36	-116	2

Table 3.1.5.7 Fitted CP ^{29}Si MAS NMR data.

DISCUSSION

By substituting the data in **Table 3.1.5.6** into **Equation 3.1.3.1** gives:

$$\mathrm{Si/Al}_{\mathrm{NMR}} = \frac{81+30+194+244+51}{0.25\times 81}$$

$$\mathrm{Si/Al}_{\mathrm{NMR}} = \frac{600}{20}$$

$$\mathrm{Si/Al}_{\mathrm{NMR}} = 30$$

The $\mathrm{Si/Al}_{\mathrm{SiNMR}}$ ratio calculated for R3-H^+-β-12.5-A-773-1 shows a significant increase when compared with the value obtained for NH_4^+-β-12.5-V-773-1 earlier in the section. This indicates that dealumination has taken place during multiple-cycle regeneration. The ^{29}Si MAS NMR spectrum of R3-H^+-β-12.5-A-773-1 shows two peaks centred at –111 and –115 ppm both assigned to $Si(OSi)_4$ and accounting for 81% of the total amount of silicon in the framework. Another peak centred at –104 ppm can be assigned to $Si(OSi)_3(OAl)_1$ or $Si(OSi)_3(OH)_1$, and this peak accounts for 14% of the total amount of silicon in the framework. The final peak centred at –103 ppm can be assigned to $Si(OSi)_3(OH)_1$ according to Kuehl *et al.*, [9]. By observing the data in **Table 3.1.5.7**, it can be seen that in the CP ^{29}Si MAS NMR experiment there is a clear enhancement in the peak at 102 ppm when compared with the DP ^{29}Si MAS NMR data in **Table 3.1.5.6**, although CP MAS NMR only yields qualitative information, this would suggest that there are a significant amount of SiOH groups present in the sample. Datka *et al.*, [24] in a study of the dealumination of zeolite Y found an enhancement in the respective bands in the CP ^{29}Si MAS NMR spectra and attributed this to the formation of hydroxyl nests in the zeolite framework. The enhancement in intensity of the peak at –102 ppm observed in the CP ^{29}Si MAS NMR spectrum of R3-H^{+}-β-12.5-A-773-1 would certainly suggest the formation of a significant amount of SiOH groups, and since the FTIR data discussed earlier suggested an increase in the number of internal SiOH groups in regenerated samples, it would seem sensible to conclude that the SiOH groups formed during multiple-cycle regeneration are present in hydroxyl nests.

CONCLUSION

It is clear that multiple-cycle regeneration has a significant impact on the acidic properties of zeolite H-Beta. The dealumination observed in regenerated samples seems to be progressive, becoming more evident with each subsequent recycle. With each recycle, a marked reduction in the number of bridged OH groups is observed, and a concomitant decrease in the number of Brønsted acid sites is evident, however, the number of Lewis acid sites remains fairly constant. Additionally, after only 1 generation, there is evidence of a small amount of extralattice and VHF OH groups, which are neither increased nor decreased to any great extent in subsequent recycles. The number of internal SiOH groups is also increased with multiple-cycle regeneration, and the FTIR results coupled with CP ^{29}Si MAS NMR would suggest the formation of a significant amount of hydroxyl nests in regenerated samples. The most interesting observation from these results suggests that there are two types of tetrahedral aluminium in zeolite H-Beta, one that is resistant to dealumination, and another, which is prone to dealumination and readily converts to octahedral aluminium. The two tetrahedral aluminium species can be readily resolved by ^{27}Al MAS NMR, as undistorted tetrahedral aluminium at 52 ppm, and 'slightly distorted' tetrahedral aluminium at 47 ppm, the latter species being the one that dealuminates quite readily. The 'slightly distorted' tetrahedral aluminium species at 47 ppm in NH_4^+-β-12.5-V-773-1 shifts to lower ppm values (43 ppm) in R3-H^+-β-12.5-A-773-1, indicating that as internal defects are introduced the 'slightly distorted' tetrahedral aluminium becomes more heavily distorted as evidenced by its shift to lower ppm values. The explanation for this could be that the formation of internal defect sites causes further strain to those tetrahedral sites which are prone to dealumination, causing then to adopt a more distorted tetrahedral symmetry, whereas the tetrahedral sites which are resistant to dealumination are unaffected. Such a shift is not observed for the sample treated to high temperature, NH_4^+-β-12.5-A-1023-18, since no internal SiOH are present due to reconstruction at high temperature.

3.1.6 A brief account of the acidic and structural properties of ZSM-5, mordenite, faujasite, and MCM-41.

In addition to zeolite Beta, other zeolites including ZSM-5, Mordenite, Faujasite, and the mesoporous MCM-41 were used throughout this investigation. What follows is a very brief overview of the acidic properties and structural integrity of these samples. The main objective of this overview is to prove that the samples are of good quality. Although zeolite Beta is the sample chosen for intensive investigation throughout this report, the use of a variety of zeolite type materials in the catalyst-testing phase is extremely useful for comparative investigation.

Figure 3.1.6.1 shows the FTIR spectra of ZSM-5 samples.

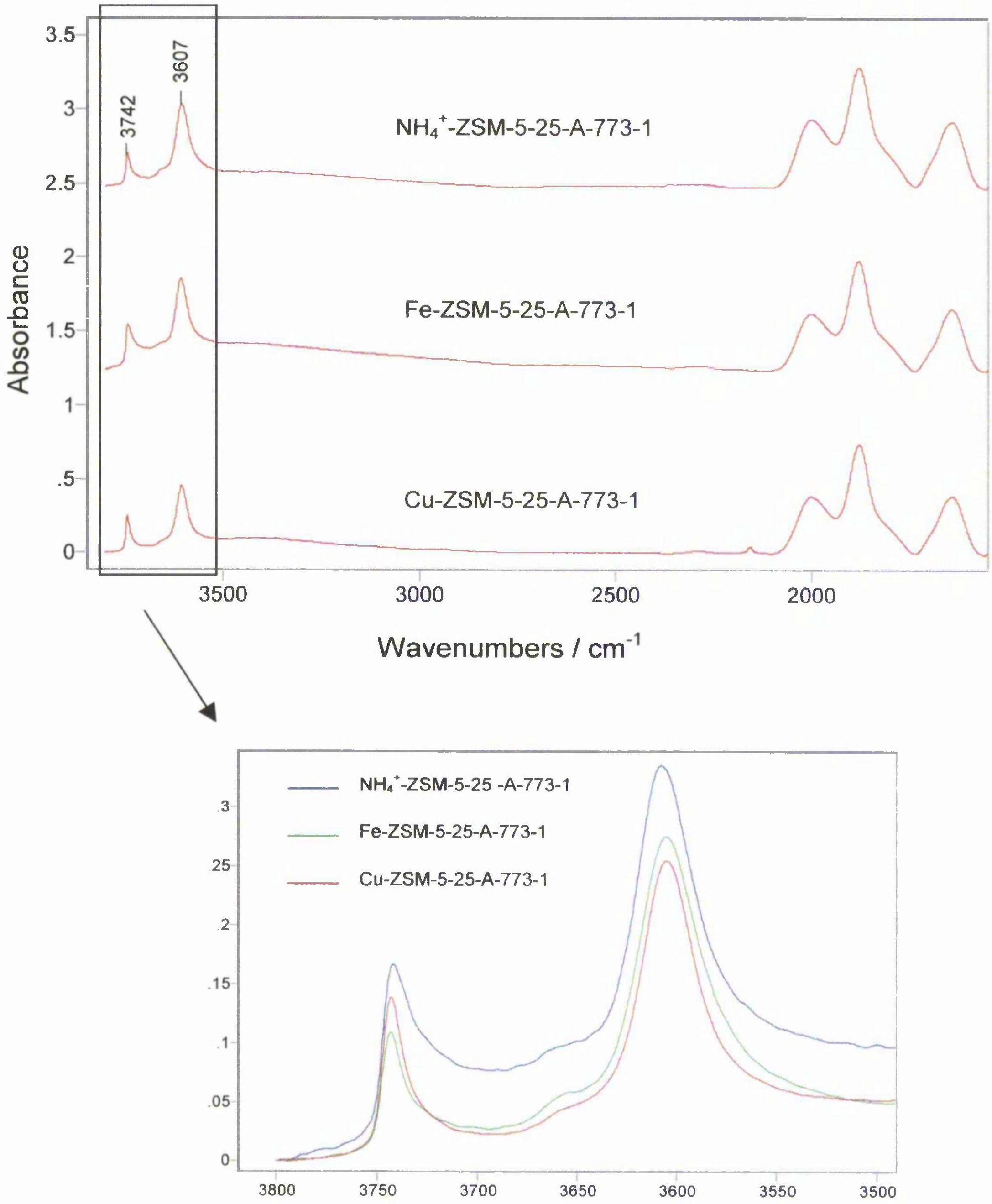

Figure 3.1.6.1 FTIR spectra in the hydroxyl region of ZSM-5 samples. Spectra taken at 423 K and normalised to the zeolite lattice overtones at 1987 and 1872 cm^{-1}.

Figure 3.1.6.2 shows the XRD profiles of ZSM-5 samples.

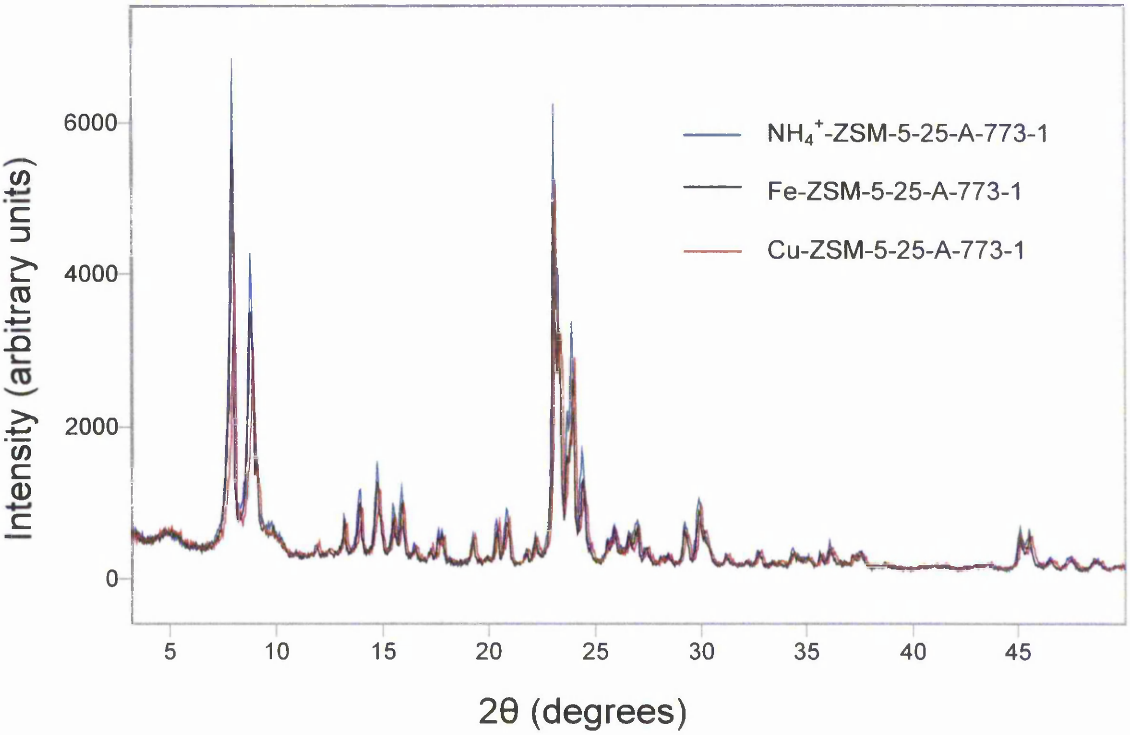

Figure 3.1.6.2 XRD profiles of ZSM-5 samples.

DISCUSSION

From **Figure 3.1.6.1** it can be seen that all ZSM-5 samples contain two bands in the FTIR spectrum, one at 3609 cm^{-1} and another at 3743 cm^{-1}, these have been assigned to bridged Si(OH)Al hydroxyls and external silanol groups respectively [75]. It can be also observed that there is a decreased number of bridging hydroxyl groups in the case of Fe-ZSM-5-25-A-773-1 and Cu-ZSM-5-25-A-773-1, whereas the external SiOH concentration remains relatively constant. The observed decrease in the concentration of bridged OH groups would suggest the exchange of protons for Fe and Cu cations during the ion exchange process. The XRD profiles presented in **Figure 3.1.6.2** shows that all ZSM-5 samples exhibit a well-defined ZSM-5 structure when compared with published XRD data [76].

Figure 3.1.6.3 shows the FTIR spectra of mordenite samples.

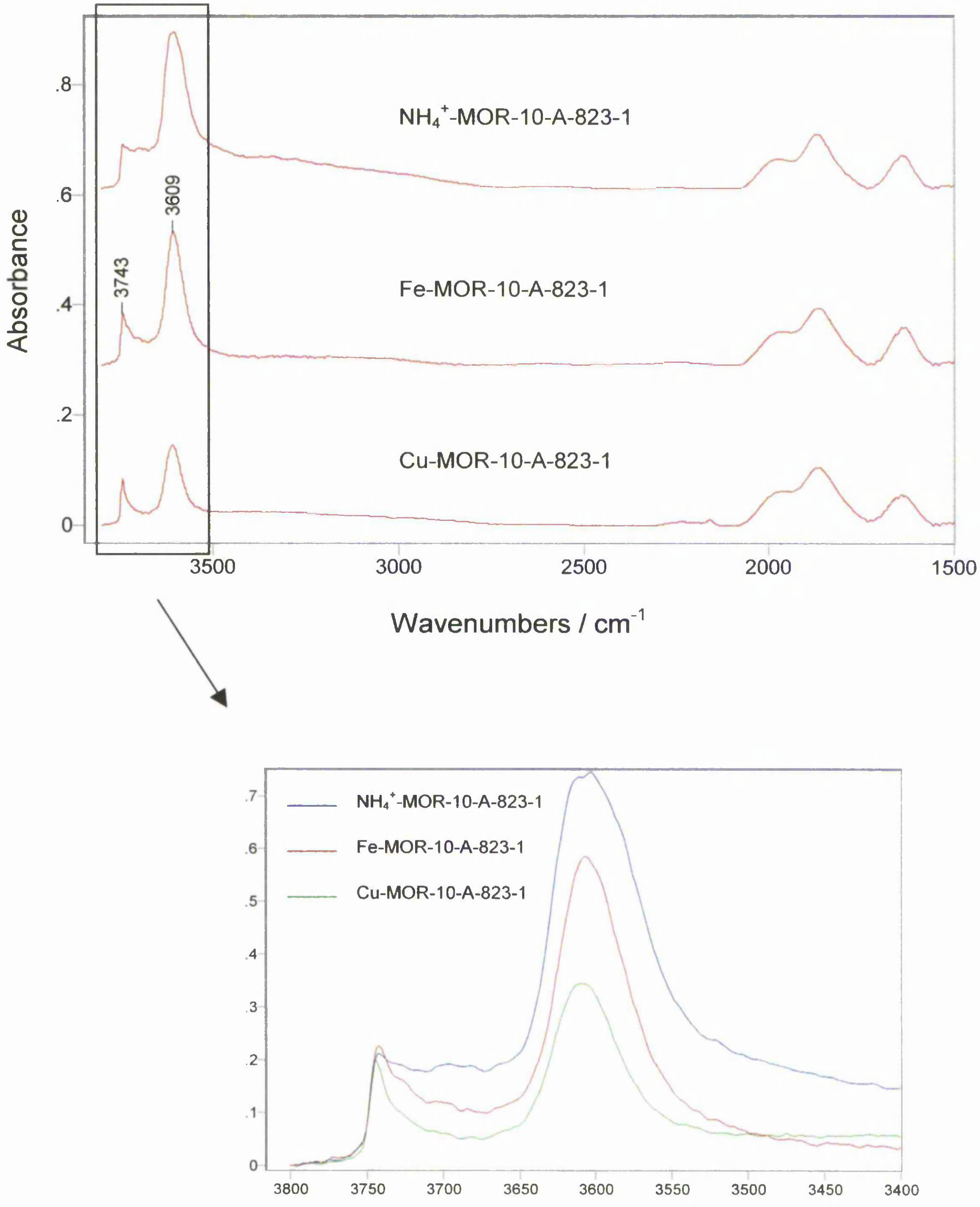

Figure 3.1.6.3 FTIR spectra in the hydroxyl region of Mordenite samples. Spectra taken at 423 K and normalised to the zeolite lattice overtones at 1987 and 1872 cm^{-1}.

Figure 3.1.6.4 shows the XRD profiles of mordenite samples.

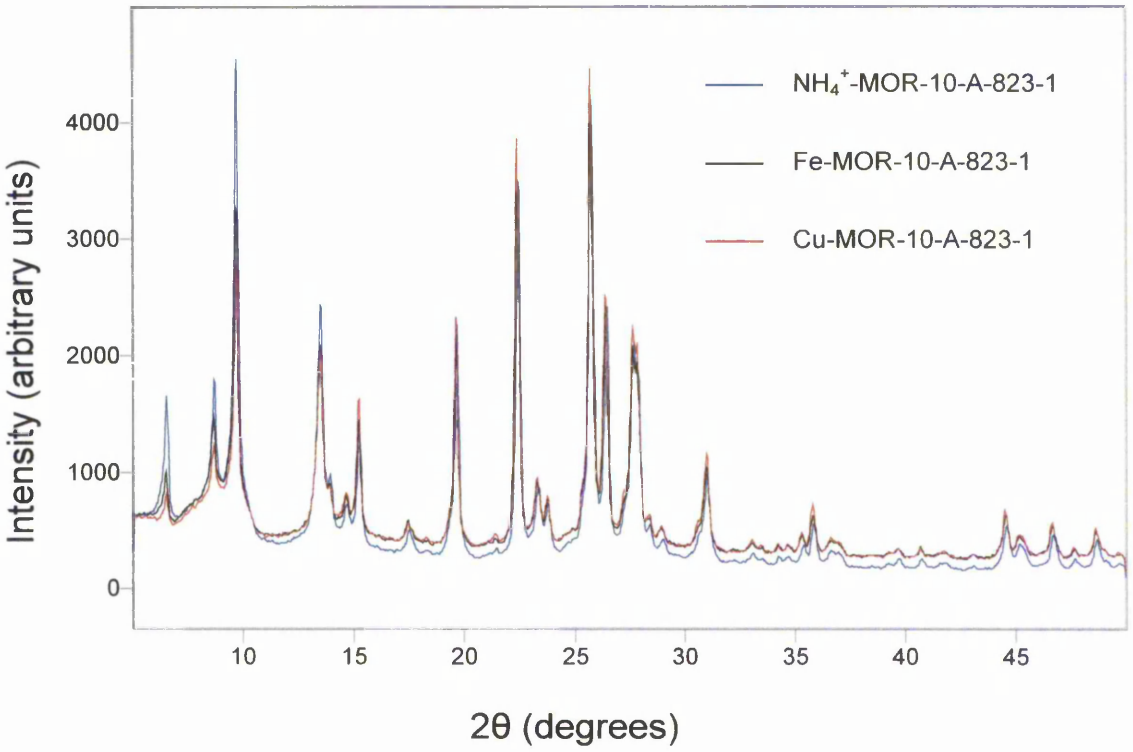

Figure 3.1.6.4 XRD profiles of mordenite samples.

DISCUSSION

From **Figure 3.1.6.3** it can be seen that all mordenite samples exhibit two bands in the FTIR spectrum, one at 3609 cm^{-1} and another at 3743 cm^{-1}, which have been assigned to structural hydroxyl groups (bridging hydroxyls) and silanol groups respectively [77]. As was observed with ZSM-5, there is clearly a reduction in the number of bridged OH groups in transition-exchanged materials, this effect is most pronounced in the case of Cu-MOR-10-A-823-1. Once again, this can be attributed to the exchange of protons for either Fe or Cu cations during the ion exchange process. The XRD profiles presented in **Figure 3.1.6.4** show that all mordenite sample possess a well-defined mordenite structure when compared with published XRD data [76].

Figure 3.1.6.5 shows the FTIR spectrum of NH_4^+-FAU-2.36-A-573-8.

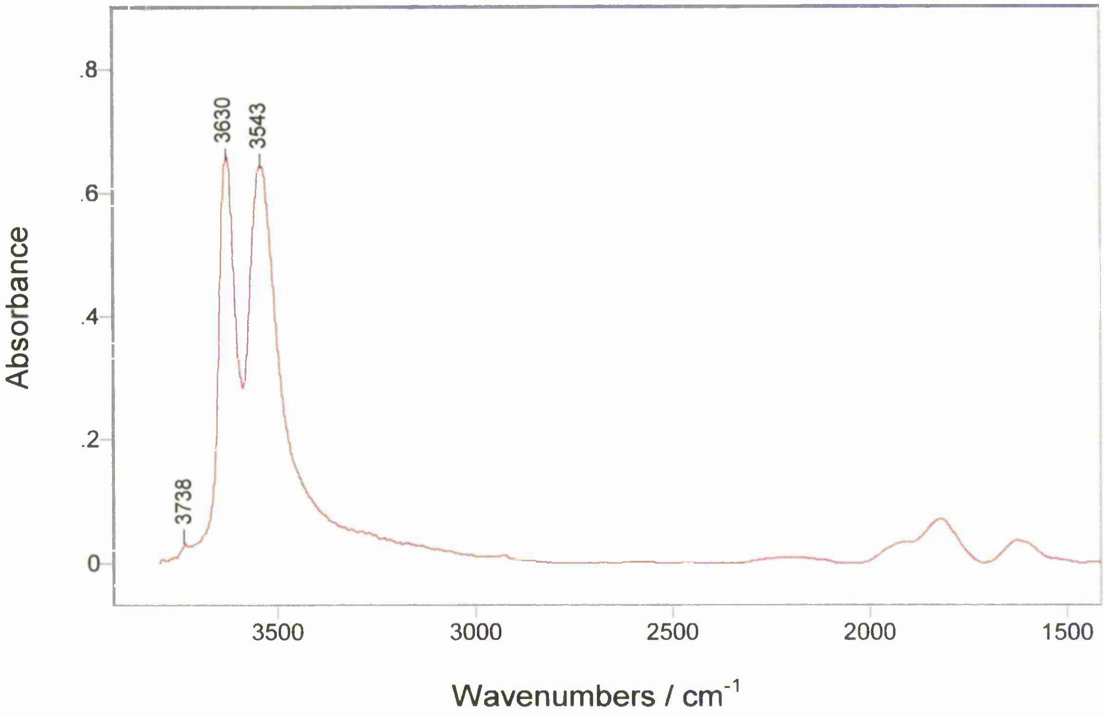

Figure 3.1.6.5 FTIR spectrum in the hydroxyl region of NH_4^+-FAU-2.36-A-573-8. Spectra taken at 423 K and normalised to the zeolite lattice overtones at 1987 and 1872 cm^{-1}.

Figure 3.1.6.6 shows the XRD profile of NH_4^+-FAU-2.36-A-573-8.

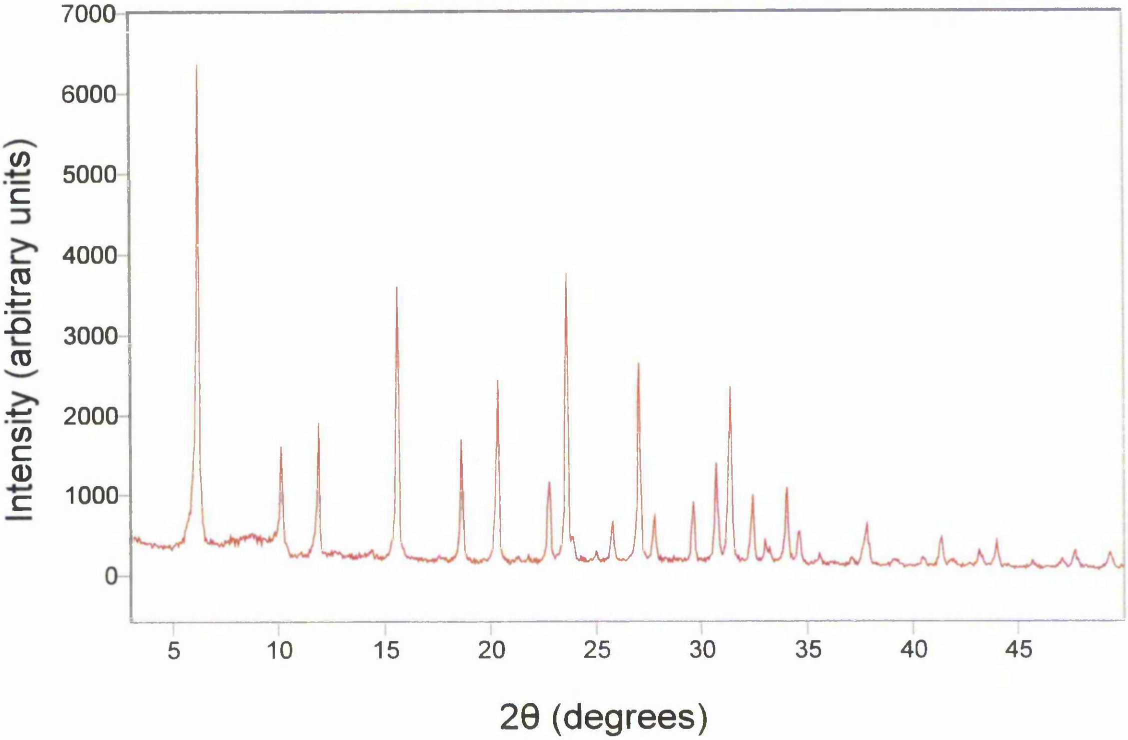

Figure 3.1.6.6 XRD profiles of NH_4^+-FAU-2.36-A-573-8.

DISCUSSION

Figure 3.1.6.5 shows that the FTIR spectrum of NH_4^+-FAU-2.36-A-573-8 exhibits three bands, one at 3543 cm^{-1}, another at 3630 cm^{-1}, and the final peak is centred at 3738 cm^{-1}, these have been assigned to (LF)OH, (HF)OH, and terminal silanols respectively [78]. The (LF)OH and (HF)OH are attributed to low frequency and high frequency hydroxyl groups vibrating in the supercages or in the sodalite cages [79]. The XRD profile presented in **Figure 3.1.6.6** shows that NH_4^+-FAU-2.36-A-573-8 exhibits a well-defined faujasite structure which compares well with previous findings [76].

Figure 3.1.6.7 shows the FTIR spectrum of Si-MCM-41-A-773-1.

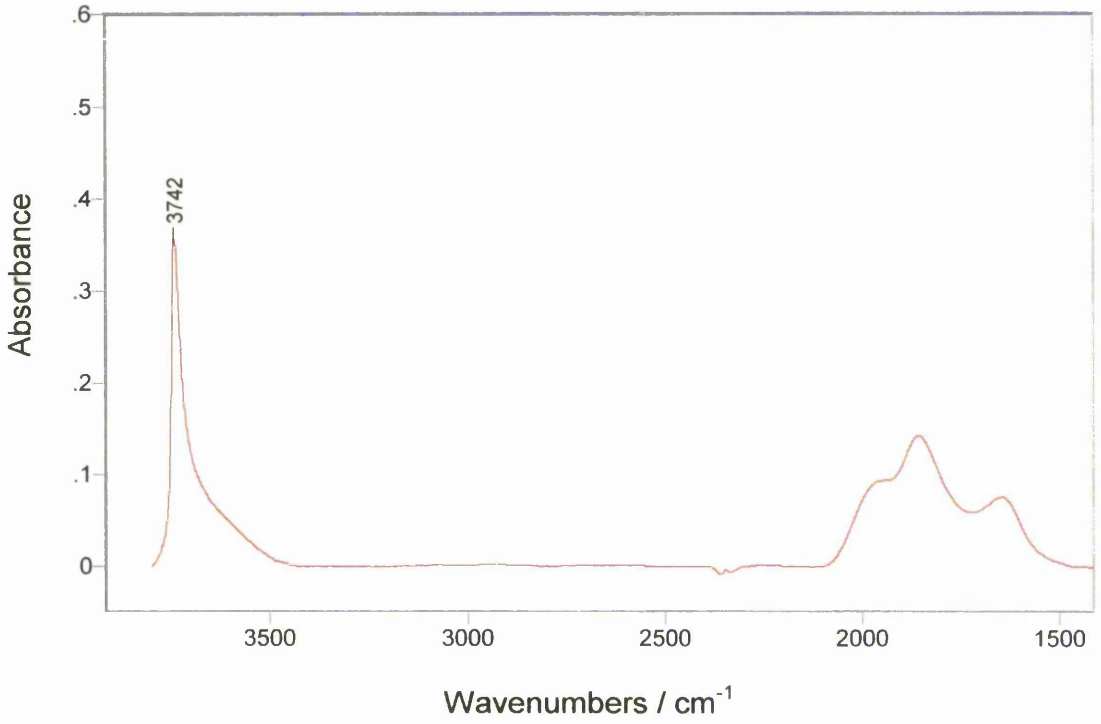

Figure 3.1.6.7 FTIR spectrum in the hydroxyl region of Si-MCM-41-A-773-1. Spectra taken at 423 K and normalised to the zeolite lattice overtones at 1987 and 1872 cm^{-1}.

Figure 3.1.6.8 shows the XRD profiles of MCM-41 samples.

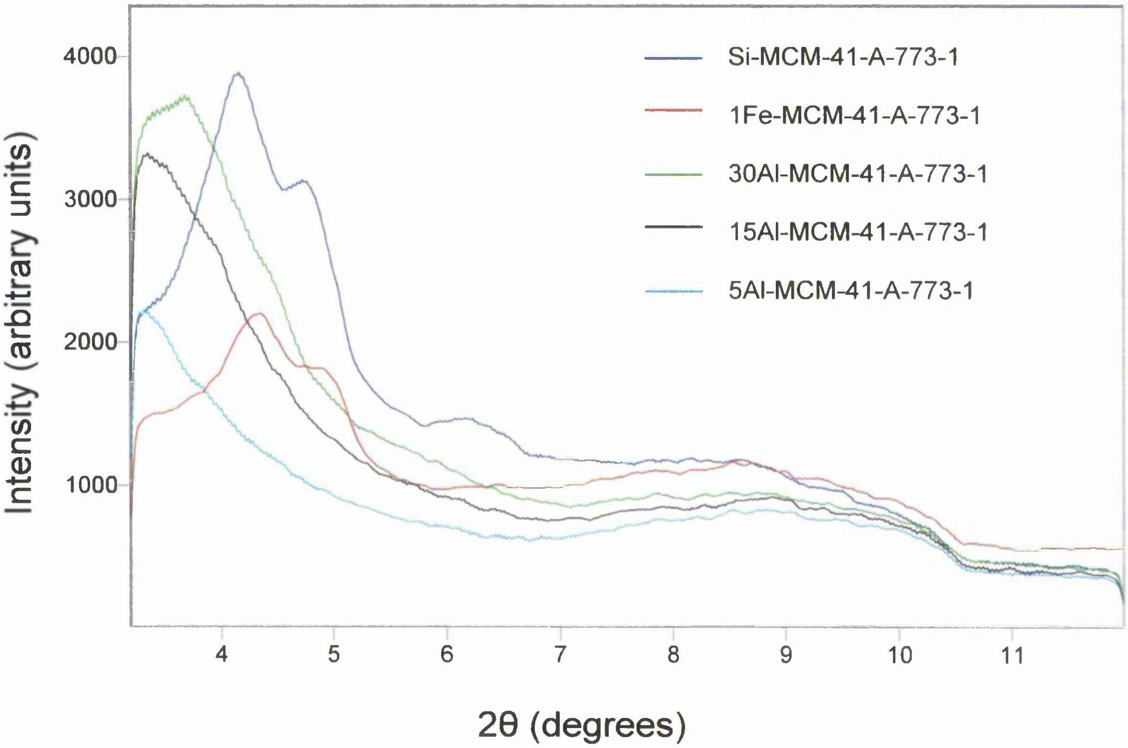

Figure 3.1.6.8 XRD profiles of MCM-41 samples.

DISCUSSION

From **Figure 3.1.6.7** it can be seen that the FTIR spectrum of Si-MCM-41-A-773-1 exhibits only one band at 3744 cm^{-1}, which has been assigned to the vibrations of isolated terminal silanol groups [80]. The same authors suggested that the rather high intensity of the band at 3744 cm^{-1} would imply that the silanols responsible for it must be located mainly at the internal surface. The XRD profiles of a range of MCM-41 samples are shown in **Figure 3.1.6.8**. Unfortunately, the limitation of the diffractometer used in the investigation hinders the observation of the most interesting region of the XRD profile of MCM-41. Despite this, the region that can be observed coincides well with the findings of other workers [81], [82].

CONCLUSION

It is clear from the FTIR and XRD results presented that the ZSM-5, mordenite, faujasite, and MCM-41 samples exhibit well-defined structures when compared with reference material, and their acidic characteristics coincide well with related literature.

REFERENCES

(1) Barthomeuf, D. In *Catalysis by Zeolites*; Imelik, B., Ed.; Elsevier, Amsterdam, 1980; pp 55.

(2) Szostak, R. *Molecular Sieves (Principles of Synthesis and Identification)*; Van Nostrand Reinhold, 1989; pp 28.

(3) Kiricsi, I.; Flego, C.; Pazzuconi, G.; Parker, W. O.; Millini, R.; Perego, C.; Bellussi, G. *J. Phys. Chem.* 1994, ***98***, 4627.

(4) Kunkeler, P. J.; Zuurdeeg, B. J.; van der Waal, J. C.; van Bokhoven, J. A.; Koningsberger, D. C.; van Bekkum, H. *J. Catal.* 1998, ***180***, 234.

(5) Kerr, G. T. *J. Catal.* 1969, ***15***, 200.

(6) Bolton, A. P.; Lanewala, M. A. *J. Catal.* 1970, ***18***, 154.

(7) Nayak, V. S.; Choudhary, V. R. *Appl. Catal.* 1982, ***4***, 333.

(8) Bourgeat-Lami, E.; Massiani, P.; Di Renzo, F.; Fajula, F.; Courieres, T. D. *Catal. Lett.* 1990, ***5***, 265.

(9) Kuehl, G. H.; Timken, H. K. C. *Microporous Mater.* 2000, ***35-36***, 521.

(10) Bourgeat-Lami, E.; Massiani, P.; Di Renzo, F.; Espiau, P.; Fajula, F.; Courieres, T. D. *Appl. Catal.* 1991, ***72***, 139.

(11) Jia, C.; Massiani, P.; Barthomeuf, D. *J. Chem. Soc. Faraday Trans.* 1993, ***89***, 3659.

(12) Beck, L.; Haw, J. F. *J. Phys. Chem.* 1995, ***99***, 1076.

(13) Zholobenko, V. L.; Kustov, L. M.; Kazansky, V. B.; Loefler, E.; Lohse, U.; Peuker, C.; Oehlmann, G. *Zeolites* 1990, ***10***, 266.

(14) Trombetta, M.; Busca, G.; Storaro, L.; Lenarda, M.; Casagrande, M.; Zambon, A. *Phys.Chem.Chem.Phys.* 2000, ***2***, 3529.

(15) Corma, A.; Grande, M.; Fornés, V. *Appl. Catal. : A* 1990, ***66***, 45.

(16) Campbell, S. M.; Bibby, D. M.; Coddington, J. M.; Howe, R. F.; Meinhold, R. H. *J. Catal.* 1996, ***161***, 338.

(17) Anderson, M. W.; Klinowski, J. *J. Chem. Soc. Faraday Trans. I* 1986, ***82***, 3569.

(18) Wang, Q. L.; Giannetto, G.; Torrealba, M.; Perot, G.; Kappenstein, C.; Guisnet, M. *J. Catal.* 1991, ***130***, 459.

(19) Zholobenko, V. L.; Kustov, L. M.; Borovkov, V. Y.; Kazansky, V. B. *Zeolites* 1988, ***8***, 175.

(20) Chen, F. R.; Davis, J. G.; Fripiat, J. J. *J. Catal.* 1992, ***133***, 263.

(21) Anderson, M. W.; Klinowski, J. *Zeolites* 1986, ***6***, 455.

(22) Féjes, P.; Kiricsi, I.; Hannus, I.; Oehme, W.; Freude, D.; Pfeifer, H. *Zeolites* 1985, ***5***, 45.

(23) Pazè, C.; Zecchina, A.; Spera, S.; Cosma, A.; Merlo, E.; Spanò, G.; Girotti, G. *Phys.Chem.Chem.Phys.* 1999, ***1***, 2627.

(24) Datka, J.; Kolidziejski, W.; Klinowski, J.; Sulikowski, B. *Catal. Lett.* 1993, ***19***, 159.

(25) Jansen, J. C.; Creyghton, E. J.; Njo, S. L.; van Koningsveld, H.; van Bekkum, H. *Catal. Today* 1997, ***38***, 205.

(26) Ward, J. W. *J. Catal.* 1967, ***9***, 225.

(27) Sanz, J.; Fornés, V.; Corma, A. *J. Chem. Soc. Faraday Trans.* 1988, ***84***, 3113.

(28) Chen, D.; Sharma, S.; Cardona-Martinez, N.; Dumesic, J. A.; Bell, V. A.; Hodge, G. D.; Madon, R. J. *J. Catal.* 1992, ***136***, 392.

(29) Zhang, W.; Smirniotis, P. G.; Gangoda, M.; Bose, N. *J. Phys. Chem. B* 2000, ***104***, 4122.

(30) Robb, G. M.; Zhang, W.; Smirniotis, P. G. *Microporous Mater.* 1998, ***20***, 307.

(31) Müller, M.; Harvey, G.; Prins, R. *Microporous Mater.* 2000, ***34***, 281.

(32) Hegde, S. G.; Kumar, R.; Bhat, R. N.; Ratnasamy, P. *Zeolites* 1989, ***9***, 231.

(33) Borade, R. B.; Clearfield, A. *J. Phys. Chem.* 1992, ***96***, 6729.

(34) Anderson, J. R.; Foger, K.; Mole, T.; Rajadhyakska, R. A.; Sanders, J. V. *J. Catal.* 1979, ***58***, 114.

(35) Jacobs, P.; Martens, J. A.; Weitkamp, J.; Beyer, H. K. *Disc. Faraday Soc* 1981, ***72***, 353.

(36) Kanazirev, V.; Borisova, N. *Zeolites* 1982, ***2***, 23.

(37) Guisnet, M.; Ayrault, P.; Coutanceau, C.; Alvarez, M. F.; Datka, J. *J. Chem. Soc. Faraday Trans.* 1997, ***93 (8)***, 1661.

(38) Coutanceau, C.; Silva, J. M. D.; Alvarez, M. F.; Ribeiro, F. R.; Guisnet, M. *J. Chem. Phys.* 1997, ***94***, 765.

(39) Hanke, W.; Moller, K. *Zeolites* 1984, ***4***, 244.

(40) Zhang, W.; Burckle, E. C.; Smirniotis, P. G. *Microporous Mater.* 1999, ***33***, 173.

(41) Newsam, J. M.; Treacy, M. M. J.; Koetsier, W. T.; de Gruyter, C. B. *Proc. R. Soc. London* 1988, ***A420***, 375.

(42) Klug, H. P.; Alexander, L. E. *X-ray Diffraction Procedures for Polycrystalline and Amorphous Solids*; Wiley: New York, 1974; pp 618.

(43) Higgins, J. B.; Lapierre, R. B.; Schlenker, J. L.; Rohrman, A. C.; Wood, J. D.; Kerr, G. T.; Rohrbaugh, W. J. 1988, ***8***, 446.

(44) Camblor, M. A.; Corma, A.; Valencia, S. *Microporous Mater.* 1998, ***25***, 59.

(45) van Bokhoven, J. A.; Koningsberger, D. C.; Kunkeler, P. J.; van Bekkum, H.; Kentgens, A. P. M. *J. Am. Chem. Soc.* 2000, ***122***, 12842.

(46) de Ménorval, L. C.; Buckermann, W.; Figueras, F.; Fajula, F. *J. Phys. Chem.* 1996, ***100***, 465.

(47) Wouters, B. H.; Chen, T.-H.; Grobet, P. J. *J. Am. Chem. Soc* 1998, ***120***, 11419.

(48) van der Eerden, A. M. J.; van Bokhoven, J. A.; Smith, A.; Koningsberger, D. C. *Rev. Sci. Instrum.* 2000, ***71***, 3260.

(49) Alemany, L. B. *Appl. Magn. Reson.* 1993, ***4***, 179.

(50) Smith, M. E. *Appl. Magn. Reson.* 1993, ***4***, 1.

(51) Kentgens, A. P. M. *Geoderma* 1997, ***80***, 271.

(52) Pellet, R. J.; Blackwell, C. S.; Rabo, J. A. *J. Catal.* 1988, ***114***, 71.

(53) Rocha, J.; Klinowski, J. *J. Chem. Soc. Chem. Commun..* 1991, 1121.

(54) Gilson, J. P.; Edwards, G. C.; Peters, A. W.; Rajagopalan, K.; Wormsbecher, R. F.; Roberie, T. G.; Shatlock, M. P. *J. Chem. Soc. Chem. Commun.* 1987, ***91***.

(55) Samoson, A.; Lippmaa, E.; Engelhardt, G.; Lohse, U.; Jerschkewitz, H. G. *Chem. Phys. Lett.* 1987, ***134***, 589.

(56) Frydman, L.; Harwood, J. S. *J. Am. Chem. Soc.* 1995, ***117***, 5367.

(57) Medek, A.; Harwood, J. S.; Frydman, L. *J. Am. Chem. Soc.* 1995, ***117***, 12779.

(58) Kraus, H.; Prins, R.; Kentgens, A. P. M. *J. Phys. Chem.* 1996, ***100***, 16336.

(59) Haouas, M.; Kogelbauer, A.; Prins, R. *Catal. Lett.* 2000, ***70***, 61.

(60) Pérez-Pariente, J.; Sanz, J.; Fornés, V.; Corma, A. *J. Catal.* 1990, ***124***, 217.

(61) Klinowski, J.; Ramdas, S.; Hartmann, J. S.; Gobbi, G. C.; Fyfe, C. A.; Thomas, J. M. *J. Chem. Soc. Faraday Trans II* 1982, ***78***, 1025.

(62) Engelhardt, G.; Michel, D. *High Resolution Solid State NMR of Silicates and Zeolites*; Wiley, Ed. New York, 1987; pp 148.

(63) Venuto, P. B. *Microporous Mater.* 1994, ***2***, 297.

(64) Chen, H. Y.; Voskoboinikov, T.; Sachtler, W. M. H. *J. Catal.* 1998, ***180***, 171.

(65) Aylor, A. W.; Larsen, S. C.; Reimer, J. A.; Bell, A. T. *J. Catal.* 1995, ***157***, 592.

(66) Dandekar, A.; Vannice, M. A. *Appl. Catal. : B* 1999, ***22***, 179.

(67) Connerton, J.; Joyner, R. W.; Padley, M. B. *J. Chem. Soc. Faraday Trans* 1995, ***91 (12)***, 1841.

(68) Dedecek, J.; Bortnovsky, O.; Vondrová, A.; Witcherlová, B. *J. Catal.* 2001, ***200***, 160.

(69) Venuto, P. B.; Landis, P. S. *Advances in Catalysis*; New York, 1968; Vol. 18; pp 259.

(70) Karge, H. G.; Laniecki, M.; Ziolek, M.; Onyestyak, G.; Kiss, A.; Kleinschmit, P.; Siray, M. *Stud. Surf. Sci. Catal.* 1989, ***49***, 1327.

(71) Karge, H. G. *Stud. Surf. Sci. Catal.* 1991, ***58***, 531.

(72) Derouane, E. G.; Dillon, C. J.; Bethell, D.; Derouane-Abd Hamid, S. B. *J. Catal.* 1999, ***187***, 209.

(73) Jacob, B.; Sugunan, S.; Singh, A. P. *J. Mol. Catal. : A* 1999, ***139***, 43.

(74) Bhattacharya, D.; Sharma, S.; Singh, A. P. *Appl. Catal. : A:* 1997, ***150***, 53.

(75) Marturano, P.; Drozdová, L.; Kogelbauer, A.; Prins, R. *J. Catal.* 2000, ***192***, 236.

(76) Szostak, R. *Handbook of Molecular Sieves*; Van Nostrand Reinhold: New York, 1992.

(77) Maache, M.; Janin, A.; Lavalley, J. C.; Benazzi, E. *Zeolites* 1995, ***15***, 507.

(78) Cairon, O.; Chevreau, T. *J.Chem.Soc., Faraday Trans.* 1998, ***94***, 323.

(79) Jacobs, P.; Uytterhoven, J. B. *J. Catal.* 1972, ***26***, 175.

(80) Kosslick, H.; Landmesser, H.; Fricke, R. *J. Chem. Soc., Faraday Trans.* 1997, ***93***, 1849.

(81) Selvam, P.; Bhatia, S. K.; Sonwane, C. G. *Ind. Eng. Chem. Res.* 2001, ***40***, 3237.

(82) Siahkali, A. G.; Philippou, A.; Garforth, A.; Cundy, C. S.; Anderson, M. W.; Dwyer, J. *J. Mater. Chem.* 2001, ***11***, 569.

Chapter 3. Results

3.2 Identification of iron species in zeolite Beta

3.2.1 Abstract

In this section, temperature programmed reduction and FTIR spectroscopy are used to determine the types of iron species present in Fe-Beta prepared by exchanging parent NH_4^+-Beta with Fe $(NO_3)_3$. The adsorption of nitric oxide is expected to provide evidence on the nature of the iron species present, particularly by comparison with the NO/Fe-ZSM-5 interactions reported by Joyner *et al.*, [1], where the assignment of bands is discussed in some detail. It was found in **3.1.4** that ion exchange of zeolite Beta with Fe $(NO_3)_3$ resulted in a 97% reduction in the number of protons associated with the zeolite framework, suggesting the incorporation of a significant amount of iron into the zeolite. This section aims to deal with the determination of the nature of these iron species.

3.2.2 Background

Iron-exchanged zeolites were first prepared and characterised in the late 1960's [2] [3]. Extensive research on ion-exchanged Fe-ZSM-5 has been carried out, particularly for its ability to decompose nitrous oxide [4], as a redox catalyst for the oxidation of benzene to phenol [5] [6], and the selective oxidation of methane [7]. Unlike other transition metal exchanged zeolites, in particular copper, there is only a small proportion of the literature regarding information on over exchanged or highly exchanged iron-containing ZSM-5 samples. The main reason for this is the difficulty in incorporating iron into porous materials due to its complex solution chemistry, however, reports by Feng *et al.*, [8], and Karge *et al.*, [9], indicate that over-exchange is possible under certain conditions. More recently, attempts have been made to incorporate iron into zeolite Beta. Zeolite Beta is attractive because of its widely open structure, comprising a three dimensional channel system with 12-membered ring apertures, with full accessibility to aluminium atoms and charge compensating cations in the structure, such properties make Fe-Beta catalysts attractive candidates for the catalytic reduction of NO and/or N_2O. The most recent article regarding the identification of iron species in Fe-Beta was by Mauvezin *et al.*, [10]. These workers used temperature programmed reduction, Mössbauer, and Drift spectroscopy to identify the iron species present in Fe-Beta.

3.2.3 Nature of iron species in Fe-β-12.5-A-773-1

FTIR RESULTS: ***NO adsorption on Fe-β-12.5-A-773-1.***

Figure 3.2.3.1 shows the FTIR spectra of NO adsorbed on Fe-β-12.5-A-773-1 between 10^{-3} and 10 mbar at 303 K, and **Figure 3.2.3.2** to **Figure 3.2.3.7** show the results of peak fitting at each pressure, the results of which are summarised in **Table 3.2.3.1**.

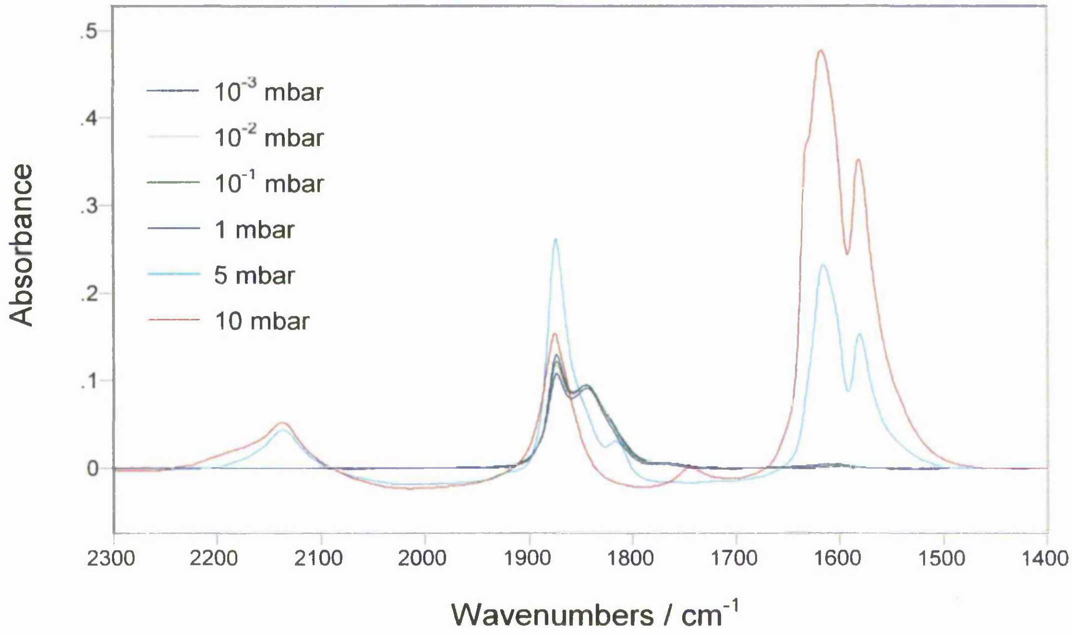

Figure 3.2.3.1 FTIR spectra of NO adsorbed on Fe-β-12.5-A-773-1 between 10^{-3} and 10 mbar at 303 K.

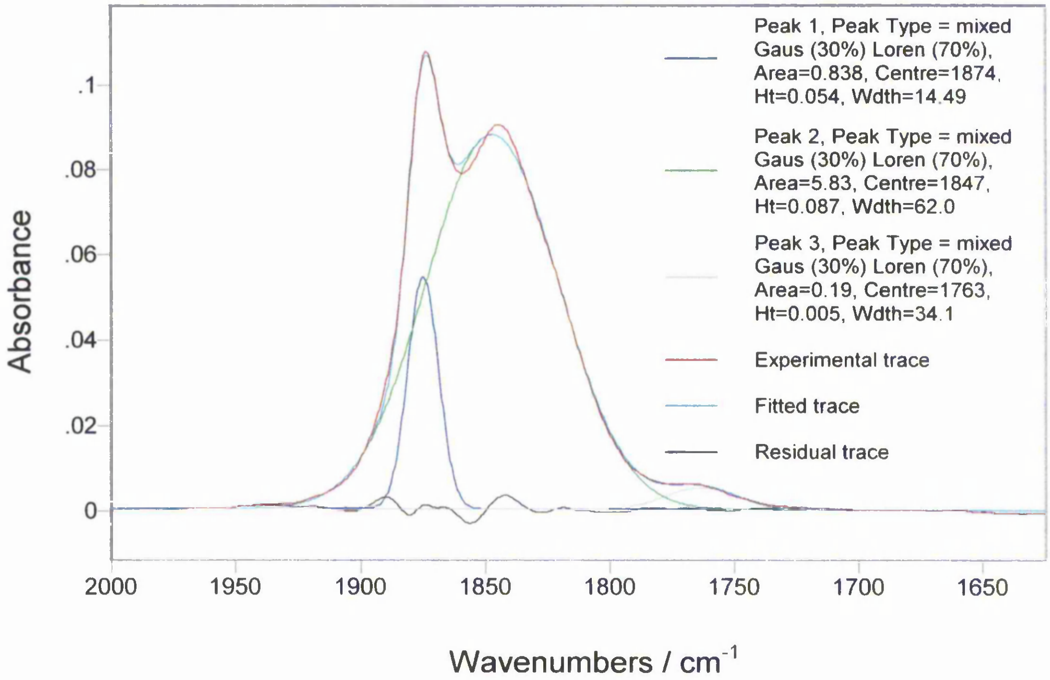

Figure 3.2.3.2 NO adsorption at 10^{-3} mbar.

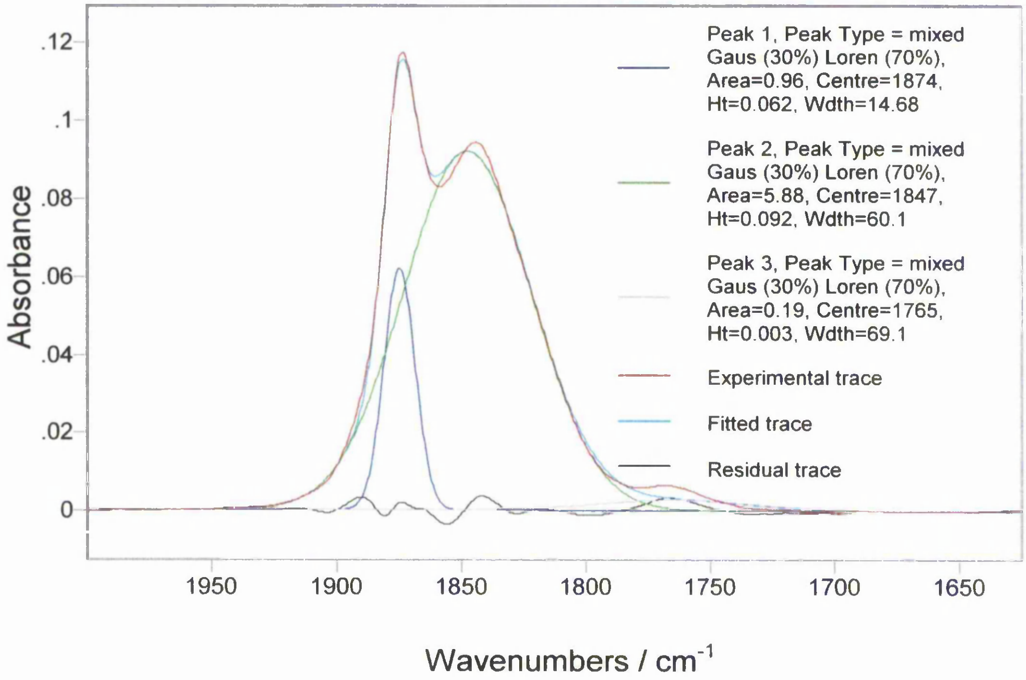

Figure 3.2.3.3 NO adsorption at 10^{-2} mbar.

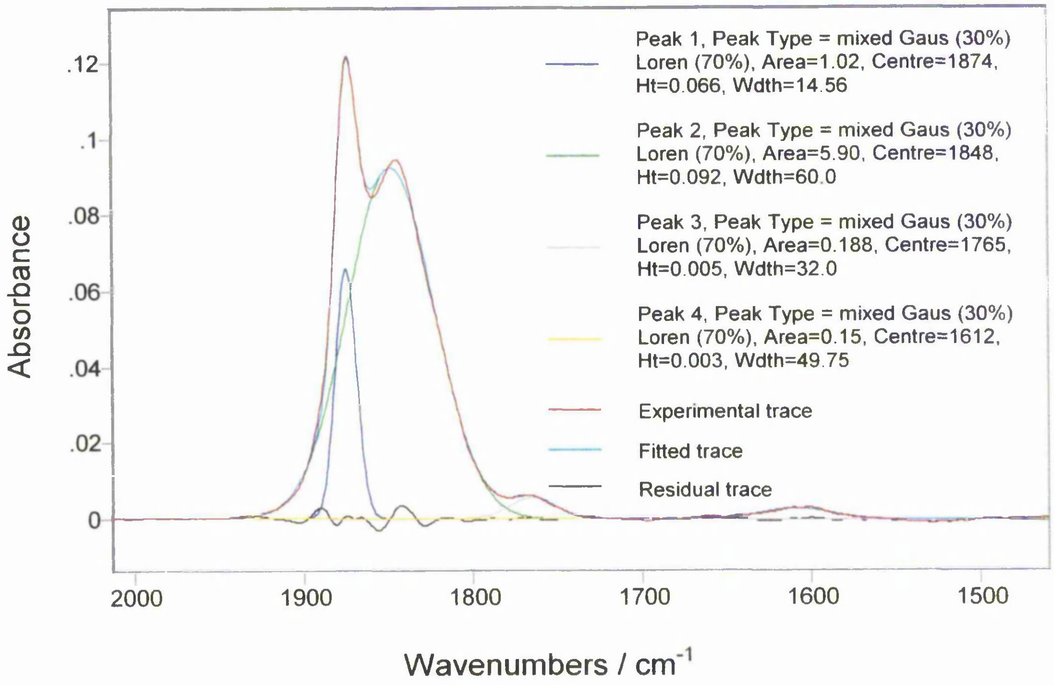

Figure 3.2.3.4 NO adsorption at 10^{-1} mbar.

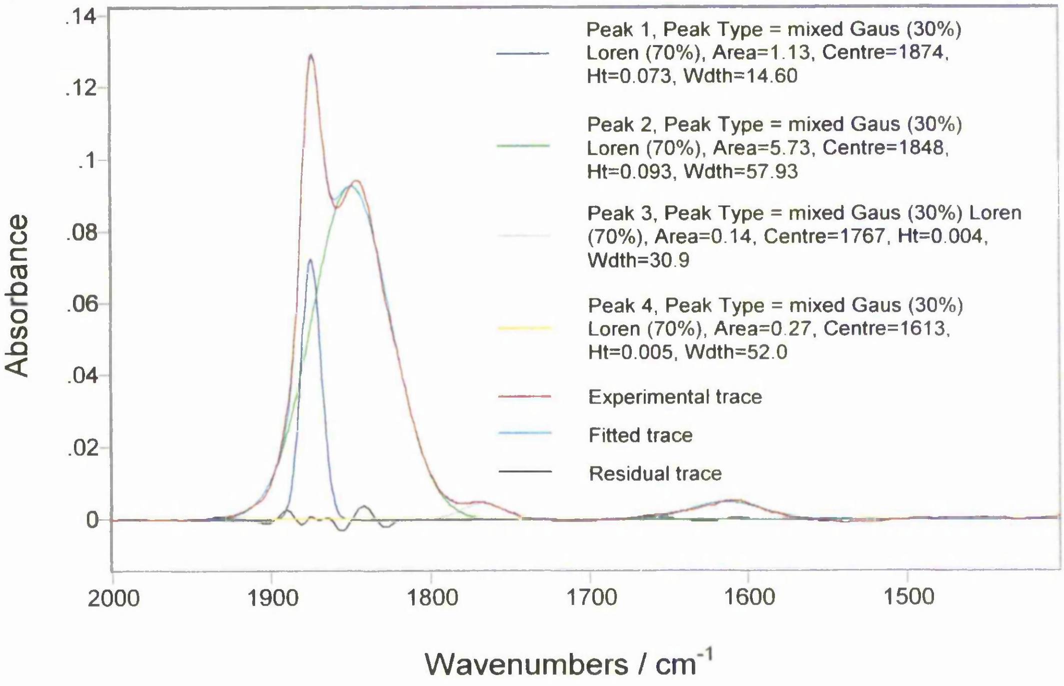

Figure 3.2.3.5 NO adsorption at 1 mbar.

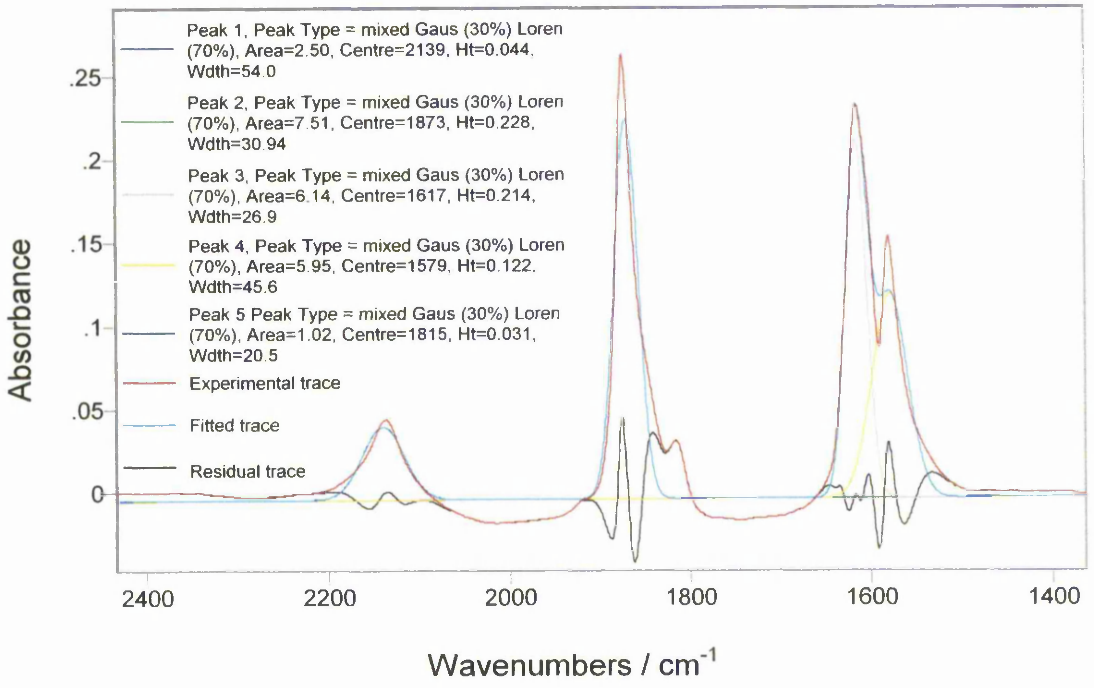

Figure 3.2.3.6 NO adsorption at 5 mbar.

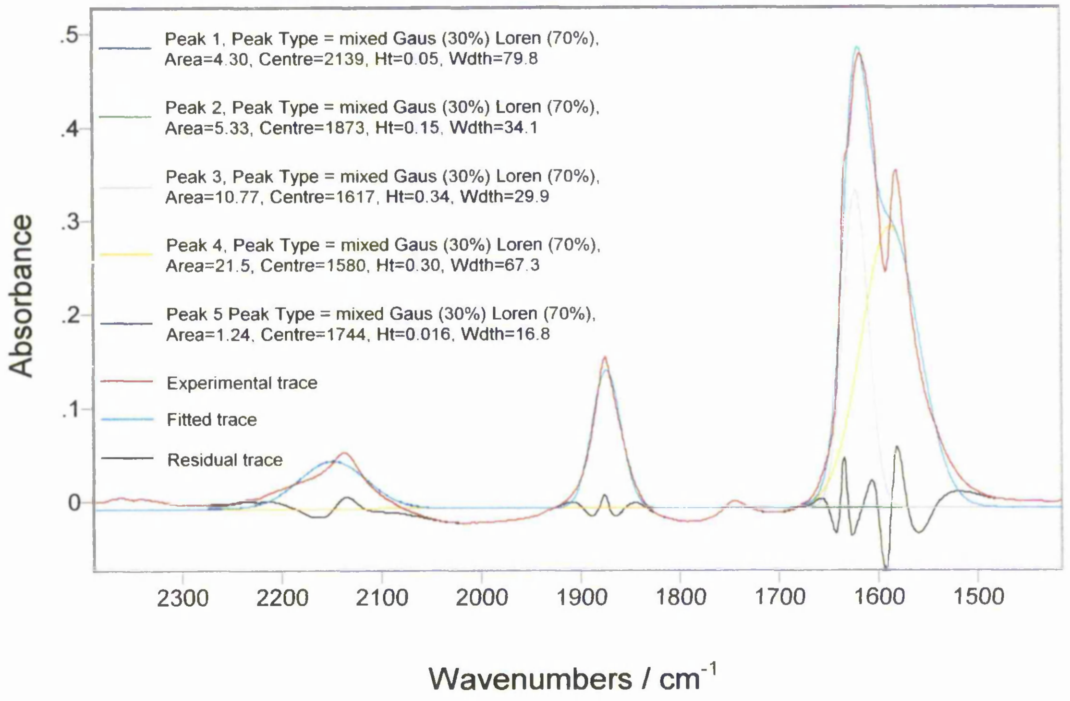

Figure 3.2.3.7 NO adsorption at 10 mbar.

Table 3.2.3.1 Peak fitting data regarding the adsorption of NO on Fe-β-12.5-A-773-1.

Pressure/mbar	Mixed Gaus (30%) Loren (70%) peak fitting after NO adsorption at various pressures ± 2%*									
	Peak 1		Peak 2		Peak 3		Peak 4		Peak 5	
	Centre/cm^{-1}	%	Centre/cm^{-1}	%	Centre/cm^{-1}	%	Centre/cm^{-1}	%	Centre/cm^{-1}	%
10^{-3}	1874	12.0	1846	85.0	1763	3.0	-	-	-	-
10^{-2}	1874	13.0	1846	84.0	1765	3.0	-	-	-	-
10^{-1}	1874	14.0	1846	81.3	1765	2.59	1612	2.11	-	-
1	1874	15.5	1846	78.8	1767	1.90	1613	3.8	-	-
5	2138	11.0	1873	32.5	1617	26.5	1579	25.6	1815	4.4
10	2139	10.0	1873	12.1	1617	25.0	1580	50.0	1744	2.90

* Approximate experimental error expressed as the coefficient of variation.

Table 3.2.3.2 shows the assignment of NO/Fe-ZSM-5 interactions as provided by Joyner *et al.*, [1].

Frequency / cm^{-1}	**Assignment**
1768	Low-spin Fe (II)-NO complex involving isolated Fe(II) ions
1816	Second NO molecule on Fe-oxo nanocluster
1841	NO on isolated Fe^{2+}
1880	NO on Fe cluster
2135	NO^{+} acting as charge compensating cation and/or NO^{2+} species hydrogen bonded to acidic OH groups

XRD RESULTS: *Comparison of Fe-β-12.5-A-773-1 with NH_4^+-β-12.5 -A-773-1.*

Figure 3.2.3.8 shows the XRD profile of Fe-β-12.5-A-773-1 and NH_4^+-β-12.5-A-773-1.

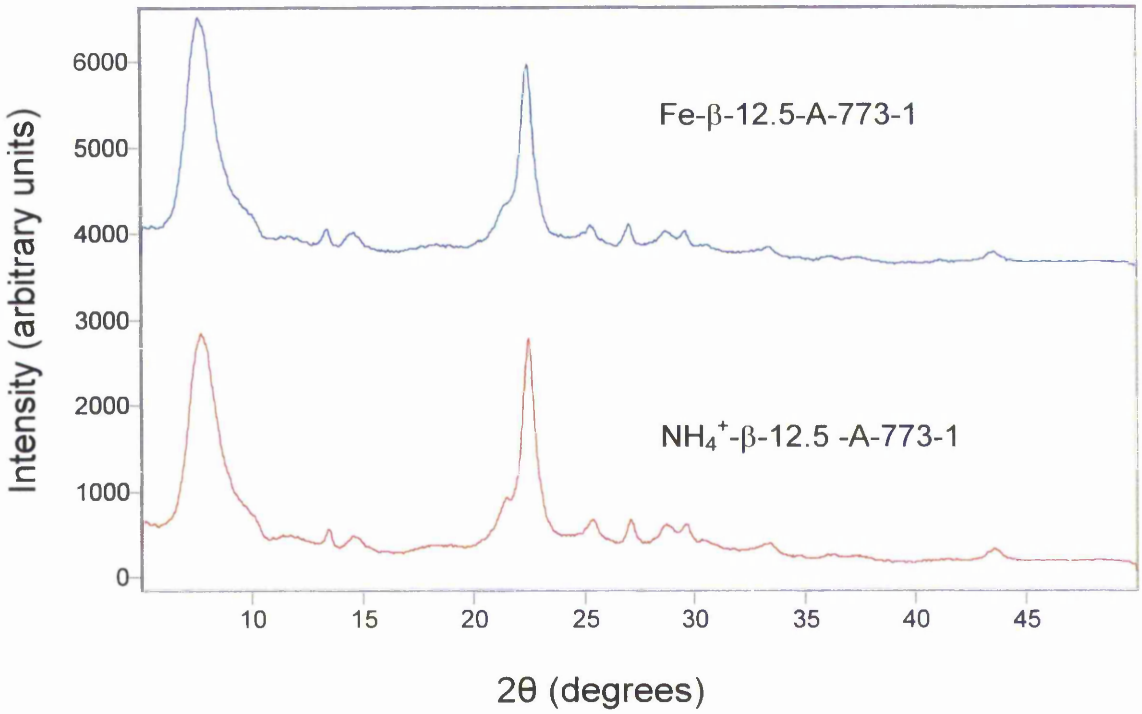

Figure 3.2.3.8 XRD profile of Fe-β-12.5-A-773-1 and NH_4^+-β-12.5 -A-773-1.

TPR RESULTS: Fe-β-12.5-A-773-1.

Figure 3.2.3.9 shows the fitted TPR results for Fe-β-12.5-A-773-1.

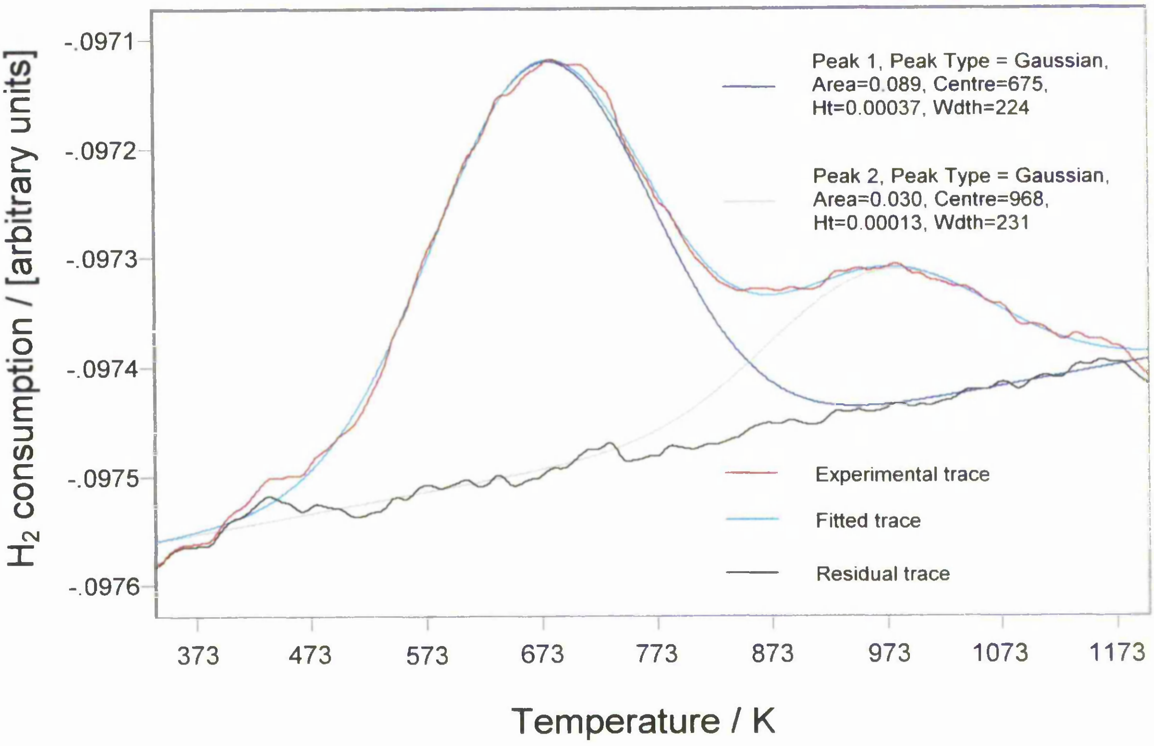

Figure 3.2.3.9 Temperature-programmed reduction results for Fe-β-12.5-A-773-1.

DISCUSSION

The type of iron species deposited on iron-exchanged zeolites is crucial for its catalytic activity. It was suggested by Joyner *et al.*, [1] that large iron oxide species formed in ZSM-5 zeolites exhibit significantly lower turnover numbers for the selective catalytic reduction (SCR) of NO_x compared to iron nanoclusters and more isolated iron cations. From **Figure 3.2.3.8**, the XRD profile of Fe-β-12.5-A-773-1 does not show any peaks due to iron oxide species; in fact, the profile does not show any significant difference when compared with the sample, NH_4^+-β-12.5-A-773-1. In addition, the catalyst, although exhibiting relatively high iron content, was almost colourless. Both of these traits would suggest that extended iron oxide species were not formed during the exchange process, or indeed, after activation.

Figure 3.2.3.1 shows the FTIR spectra of NO adsorbed on Fe-β-12.5-A-773-1 at 303 K at different pressures, and the results of mixed Gaussian (30%) Lorentzian (70%) peak fitting at each pressure are summarised in **Table 3.2.3.1**. At 10^{-3} and 10^{-2} mbar, the main NO adsorptions are found at 1874 and 1846 cm^{-1}. The band at 1846 cm^{-1} accounts for approximately 85% of the total amount of NO adsorbed on Fe-β-12.5-A-773-1 at both pressures, and the band at 1874 cm^{-1} accounts for approximately 12%. From referring to **Table 3.2.3.2**, it can be seen that bands at 1874 and 1846 cm^{-1} correspond to NO adsorbed on isolated Fe^{2+}, and NO on Fe clusters respectively. In addition, a small absorption band at 1765 cm^{-1}, accounting for 3% the total amount of NO adsorbed is present, and can be assigned to a low-spin Fe (II)-NO complex involving isolated Fe (II) ions. At 10^{-1} mbar, in addition to bands at 1874, 1846 and 1765 cm^{-1}, a new band appears at 1612 cm^{-1}, and the band at 1846 cm^{-1} is reduced in intensity at this pressure. The new band at 1612 cm^{-1} accounts for approximately 2% of the total amount of NO adsorbed on Fe-β-12.5-A-773-1. Bands in the region 1500-1680 cm^{-1} can be attributed to nitrite or nitrate species [11-14]. The presence of such species may suggest the possibility of disproportionation reactions induced by multiple NO adsorption at a single cluster or ion such as, $4NO \rightarrow N_2 + 2NO_2$. Raising the pressure to 1 mbar causes only minor changes in the intensity of the bands observed at 10^{-1} mbar, and no new bands are observed. However, raising the pressure to 5 mbar causes some quite significant changes to the FTIR spectrum. The bands at 1844 and 1765 cm^{-1} completely disappear, and the band at 1874 cm^{-1} doubles in intensity. The bands at 1579 and 1617 cm^{-1} increase in intensity, and new bands appear at 1815 and 2138 cm^{-1}. The bands at 1815 and 2138 cm^{-1} have been assigned to the attachment of a second NO molecule on a Fe-oxo nanocluster, and to either NO^{2+} species hydrogen bonded to the acidic OH groups on the zeolite [14], or to NO^{+} species acting as a charge compensating cation [15], respectively. Increasing the pressure to 10 mbar results in a decrease in the band at 1874 cm^{-1}, which is halved in intensity, a doubling in intensity of the band at 1580 cm^{-1}, while the band at 1815 cm^{-1} disappears. A new band appears at 1744 cm^{-1}, which accounts for approximately 2% of the total amount of NO adsorbed on the sample, and this may be due to the reappearance of a low-spin Fe (II)-NO complex involving isolated Fe (II) ions. **Figure 3.2.3.9** shows the temperature-programmed reduction results for Fe-β-12.5-A-773-1. Two peaks are observed; the first, at approximately 675 K, corresponds to the partial reduction of Fe^{3+} to Fe^{2+} species and of Fe_2O_3 aggregates to Fe_3O_4 ($H_2/Fe = 0.51$). The latter species are then reduced to FeO and to Fe^0 clusters at approximately 968 K ($H_2/Fe = 0.17$). It was not possible using the conditions employed in the present study to reduce Fe^{2+} to Fe^0, although temperatures above 1100-1200 K are generally associated with the reduction of Fe^{2+} to Fe^0 with collapse of the zeolite framework [16]. According to Joyner *et al.*, [1], Fe-ZSM-5 samples prepared by aqueous exchange show increased stability against reduction below the +2 oxidation state, and it was suggested by the same authors that iron-oxygen nanoclusters in Fe-ZSM-5 may be responsible for the unexpectedly high stability against reduction, these species have been referred to as ultrastable nanoclusters. It is likely that such species are present in the Fe-Beta prepared in this study, explaining the unusually high resistance to reduction below the +2 oxidation state.

CONCLUSION

Exchange of iron into zeolite Beta leads to the formation of both isolated iron atoms and iron-oxo nanoclusters, the latter species have been referred to as ultrastable nanoclusters, and are associated with the high resistance to reduction below the +2 oxidation state. XRD would suggest that no extended iron oxide species were formed during the exchange process or after activation.

REFERENCES

(1) Joyner, R.; Stockenhuber, M. *J. Phys. Chem. B* 1999, ***103***, 5963.

(2) Morice, J. A.; Rees, L. V. A. *Trans Faraday Soc* 1968, ***64***, 1388.

(3) Delgass, W. N.; Garten, R. L.; Boudart, M. *J. Catal.* 1970, ***18***, 90.

(4) Valyon, J.; Millman, W. S.; Hall, W. K. *Catal. Lett.* 1994, ***24***, 215.

(5) Panov, G. I.; Sobolev, V. I.; Dubkov, K. A.; Kharitonov, A. S. *Stud. Surf. Sci. Catal.* 1996, ***101***, 493.

(6) Ribera, A.; Arends, I. W. C. E.; de Vries, S.; Pérez-Ramírez, J.; Sheldon, R. A. *J. Catal.* 2000, ***195***, 287.

(7) Anderson, J. R.; Tsai, P. *J. Chem. Soc. Chem. Commun.* 1987, 1435.

(8) Feng, X.; Hall, W. K. *Catal. Lett.* 1996, ***41***, 45.

(9) Lazar, K.; Pal-Borbely, G.; Beyer, H. K.; Karge, H. G. *Stud. Surf. Sci. Catal.* 1994, ***91***, 551.

(10) Mauvezin, M.; Delahay, G.; Coq, B.; Kieger, S.; Jumas, J. C.; Olivier-Fourcade, J. *J. Phys. Chem. B* 2001, ***105***, 928.

(11) Hoost, T. E.; Laframboise, K. A.; Otto, K. *Appl. Catal. : B* 1995, ***7***, 79.

(12) Kucherov, A. V.; Slinkin, A. A.; Kondratev, D. A.; Bondarenko, T. N.; Rubinstein, A. M.; Minachev, K. M. *Zeolites* 1985, ***5***, 320.

(13) Aylor, A. W.; Larsen, S. C.; Reimer, J. A.; Bell, A. T. *J. Catal.* 1995, ***157***, 592.

(14) Hoost, T. E.; Laframboise, K. A.; Otto, K. *Catal. Lett.* 1996, ***37***, 153.

(15) Hadjiivanov, K.; Saussey, J.; Freysz, J. L.; Lavalley, J. C. *Catal. Lett.* 1998, ***52***, 103.

(16) Coq, B.; Mauvezin, M.; Delahay, G.; Kieger, S. *J. Catal.* 2000, ***195***, 298.

Chapter 3. Results

3.3 The relationship between zeolite acidity and the catalytic activity of zeolite Beta in the aromatic acylation of anisole with acetic anhydride

3.3.1 Abstract

In **3.1** a number of zeolite Beta samples were presented and discussed, and it was found that calcination, chemical modification, ion exchange, and regeneration all had a profound effect on the zeolites acidic properties. This section deals with the catalytic testing of those materials in the acylation of anisole with acetic anhydride. By correlating catalytic data with acidity data, it is expected to gain further insight into the mechanism of the reaction, and to determine the nature of the active site responsible for the activity of zeolite Beta in the aromatic acylation of anisole with acetic anhydride. For comparative purposes, the catalytic activity of other zeolites including ZSM-5, faujasite, mordenite, and also mesoporous MCM-41 materials are briefly considered.

3.3.2 Background

Attempts to identify the active site in this reaction, and other related reactions, have been made, but despite great efforts there is still considerable debate over this important topic. Derouane *et al.*, [1] observed that the activity of zeolite H-Beta in the acylation of anisole with acetic anhydride was dependent on the concentration of Al in the zeolite. Similarly, Singh *et al.*, [2] found that the yield of benzophenone over zeolite H-Beta decreases with an increase of the Si/Al ratio. Since both of the above studies involved H-forms of zeolite Beta, the correlation between aluminium content and catalytic activity would suggest a Brønsted acid catalysed process. Similarly, Freese *et al.*, [3] found that the presence of Brønsted acid sites in zeolite-Y was a necessary prerequisite for catalytic activity. On the other hand, a study by Bhattacharya *et al.*, [4] found that the activity of Y-Zeolites in the benzoylation of toluene with benzoyl chloride correlates with the degree of Re^{3+}-exchange. Also, Akporiaye *et al.*, [5] in a study of La^{3+}-exchanged zeolite Y found a relationship between the rare-earth cation content and the activity of the solid towards toluene acylation. A study by Isaev *et al.*, [6] regarding thiophene acylation by butyryl chloride found that there was a correlation between the initial rates of reaction and the number of Lewis acid sites, whereas no correlation was found between initial rates and the number of Brønsted sites. More recently, Hutchings *et al.*, [7] reported that Fe-exchanged zeolites act as effective heterogeneous benzoylation catalysts. These previous three studies would suggest that aromatic acylation catalysed by zeolites proceeds *via* a Lewis catalysed process. In fact, taking into consideration all of the named studies, it would seem that aromatic acylation involving zeolites is catalysed by either Brønsted or Lewis acid sites. It has been suggested that Lewis acid zeolite catalysts are preferred when applying acid chlorides and Brønsted acid zeolite catalysts when using acid anhydrides or carboxylic acids as acylating agents [8], [9].

3.3.3 Catalytic activity of zeolite Beta and $AlCl_3$ in the aromatic acylation of anisole with acetic anhydride

CATALYTIC RESULTS:

Figure 3.3.3.1 shows the percentage yield to p-methoxyacetophenone for the entire range of zeolite Beta samples. All samples were subject to the standard reaction conditions, *i.e.* anisole (0.4 M), acetic anhydride (0.2 M), 300 mg activated sample, at 333 K (full details are given in section **2.6**). The selectivity to the para product was > 99% in all cases. **Figure 3.3.3.2** shows the initial rates of reaction for the same range of samples, and the values are summarised in **Table 3.3.3.1**.

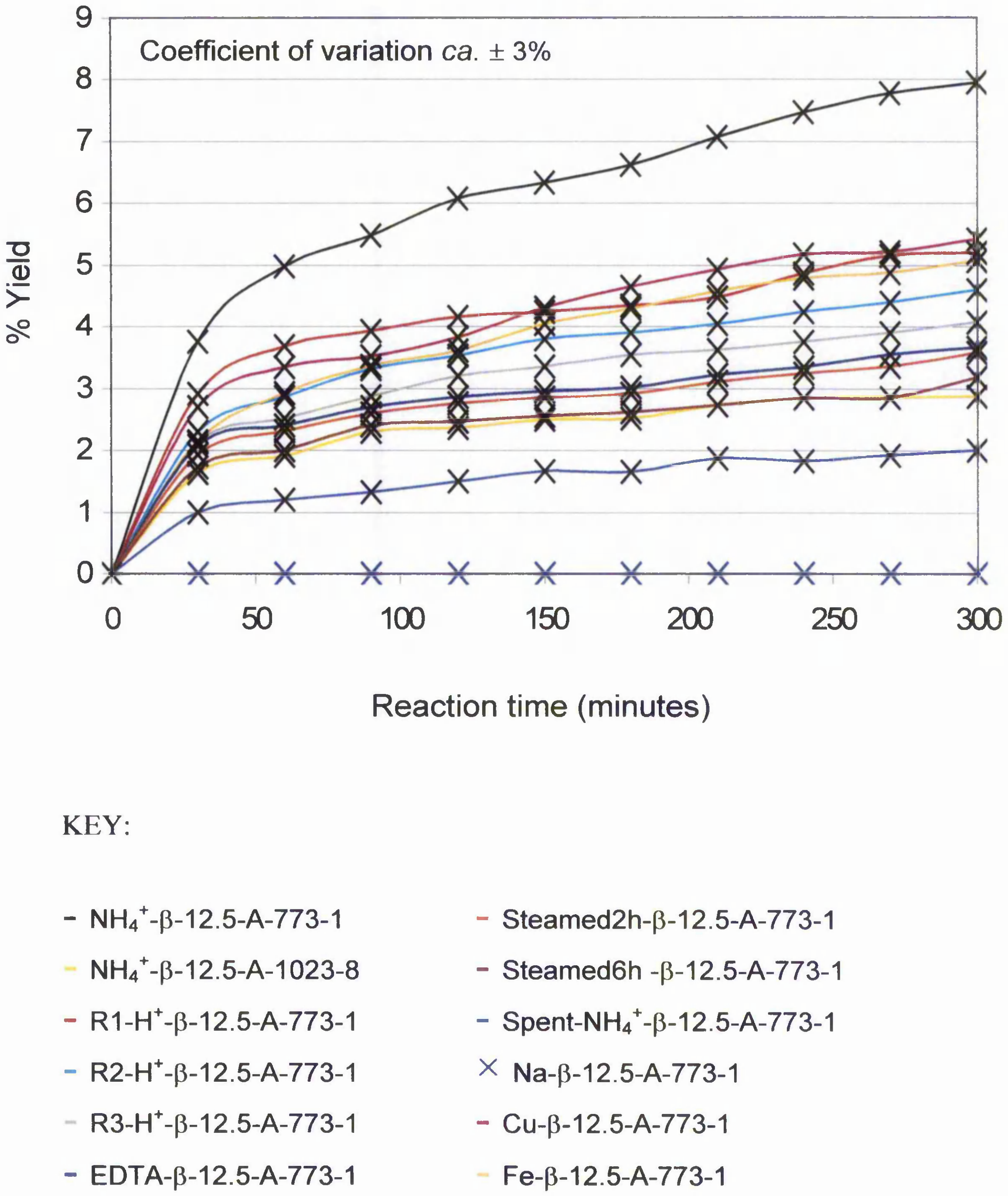

Figure 3.3.3.1 Plot of yield of p-MAP versus reaction time for zeolite Beta samples.

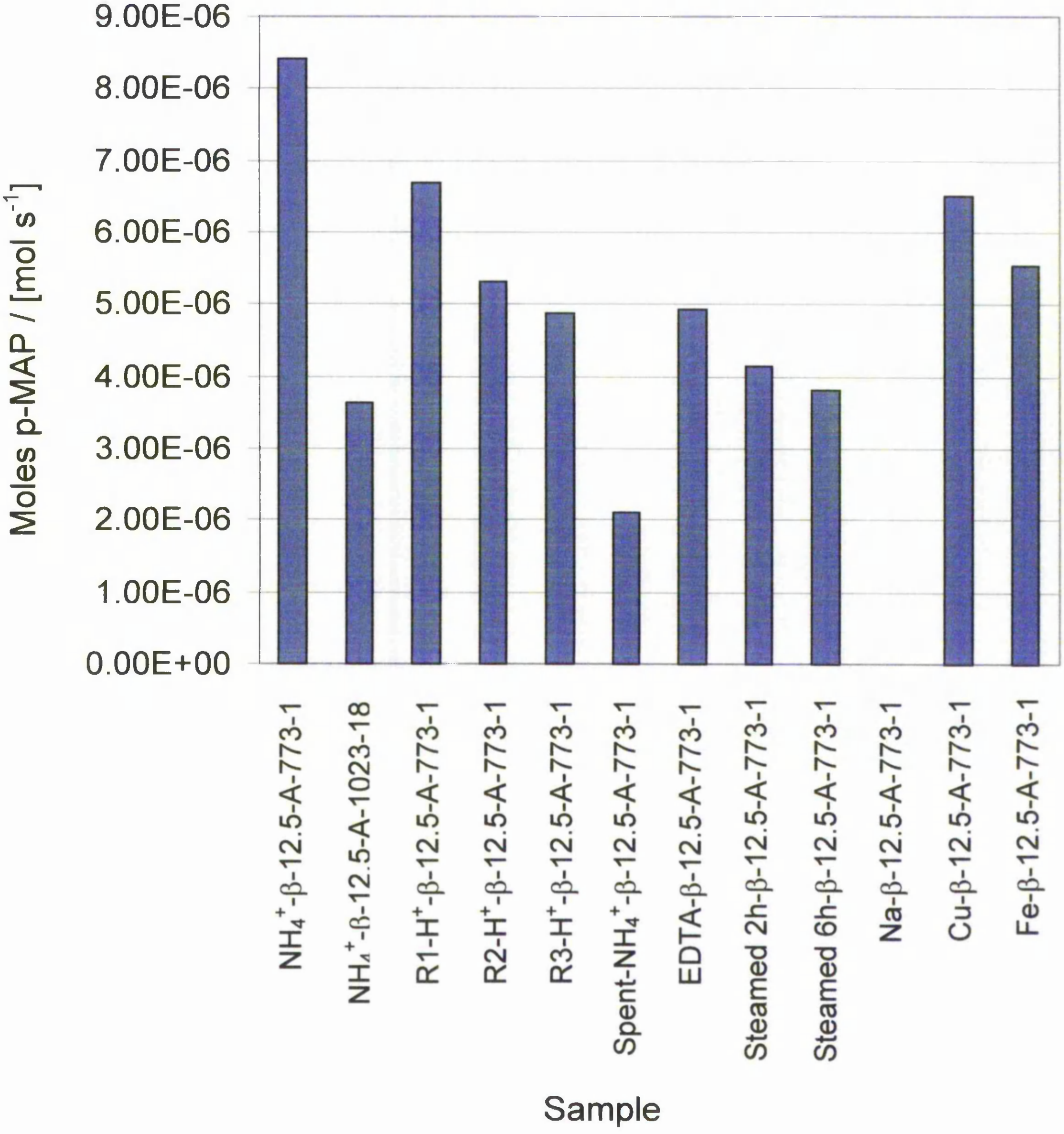

Figure 3.3.3.2 Comparison of initial rates of reaction for zeolite Beta samples.

Sample	Initial rate (mol s^{-1}) ± 3%*
NH_4^+-β-12.5-A-773-1	8.43E-06
NH_4^+-β-12.5-A-1023-18	3.64E-06
R1-H^+-β-12.5-A-773-1	6.69E-06
R2-H^+-β-12.5-A-773-1	5.33E-06
R3-H^+-β-12.5-A-773-1	4.87E-06
Spent-NH_4^+-β-12.5-A-773-1	2.12E-06
EDTA-β-12.5-A-773-1	4.92E-06
Steamed 2h-β-12.5-A-773-1	4.14E-06
Steamed 6h-β-12.5-A-773-1	3.80E-06
Na-β-12.5-A-773-1	0
Cu-β-12.5-A-773-1	6.52E-06
Fe-β-12.5-A-773-1	5.55E-06

* Approximate experimental error expressed as the coefficient of variation.

Table 3.3.3.1 Initial rates of reaction for zeolite Beta samples.

Figure 3.3.3.3 shows the percentage yield to p-methoxyacetophenone for the best performing zeolite Beta sample, NH_4^+-β-12.5-A-773-1, at 398 K, and also the percentage yield to p-methoxyacetophenone and o-methoxyacetophenone over $AlCl_3$.

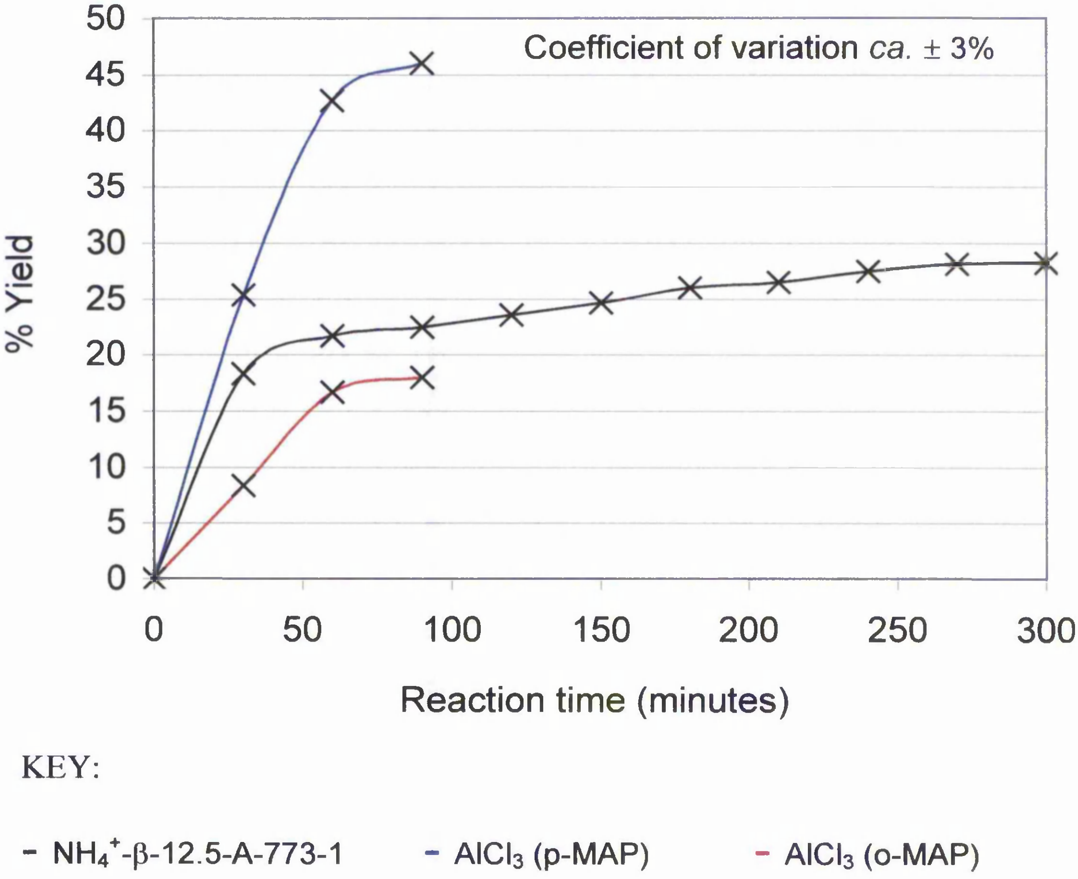

Figure 3.3.3.3 Plot of yield of p-MAP and o-MAP versus reaction time for NH_4^+-β-12.5-A-773-1 and $AlCl_3$.

To determine any correlations existing between the concentration of Brønsted and Lewis sites and the catalytic activity of zeolite Beta, relative concentrations of Brønsted and Lewis acid sites for the whole range of zeolite Beta samples (tabulated in section **3.1**) are plotted against the initial rates of reaction given in **Table 3.3.3.1**. **Figure 3.3.3.4** shows the relative concentration of Brønsted acid sites versus the initial rate of reaction for all zeolite Beta samples with the exception of Cu and Fe Beta; **Figure 3.3.3.5** shows the same plot with the addition of both Fe and Cu Beta samples. **Figure 3.3.3.6** shows the relative concentration of Lewis sites versus the initial rate of reaction for the entire range of zeolite Beta samples.

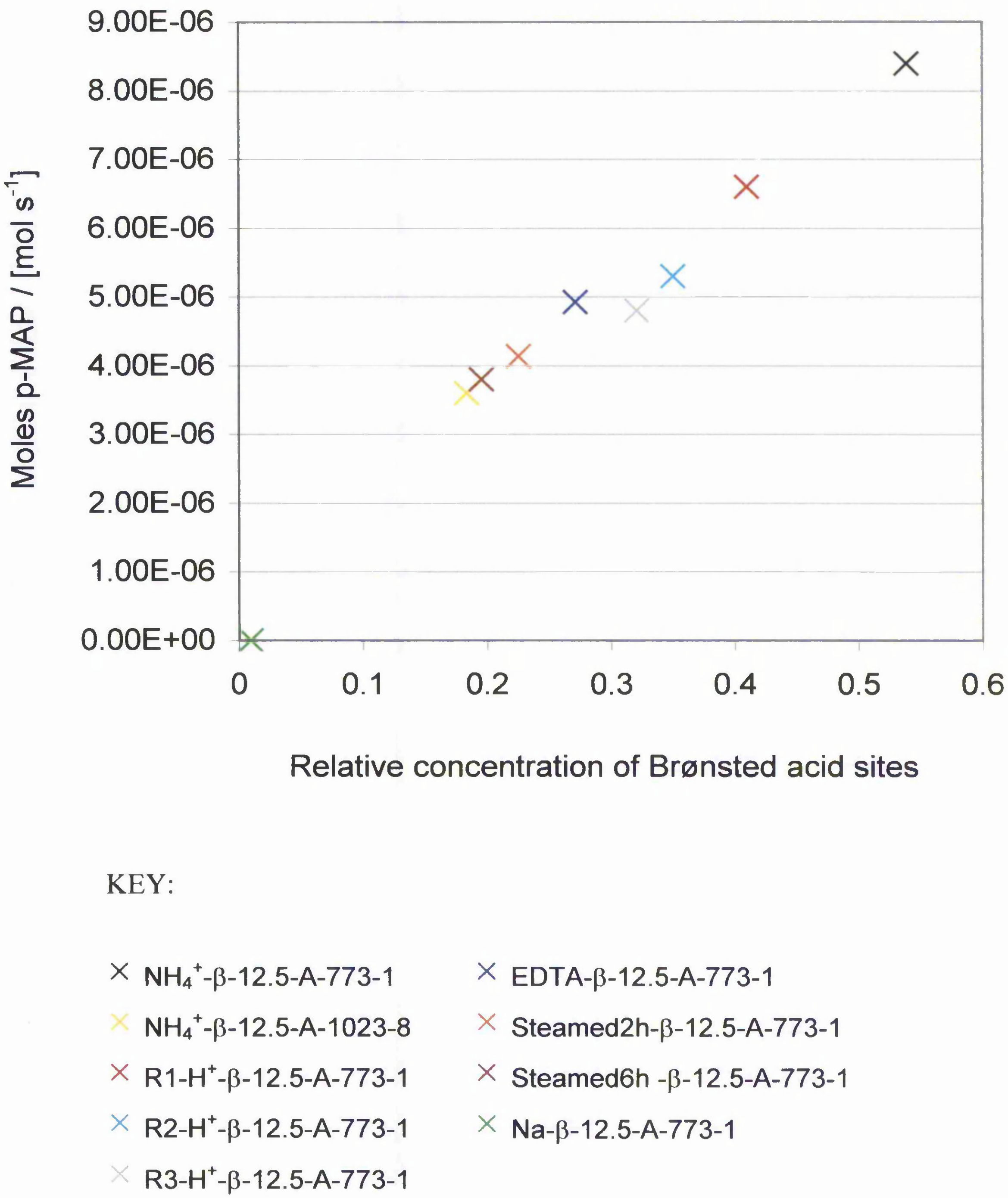

Figure 3.3.3.4 Plot of relative Brønsted acid site concentration versus initial rate of reaction (excluding Cu and Fe Beta).

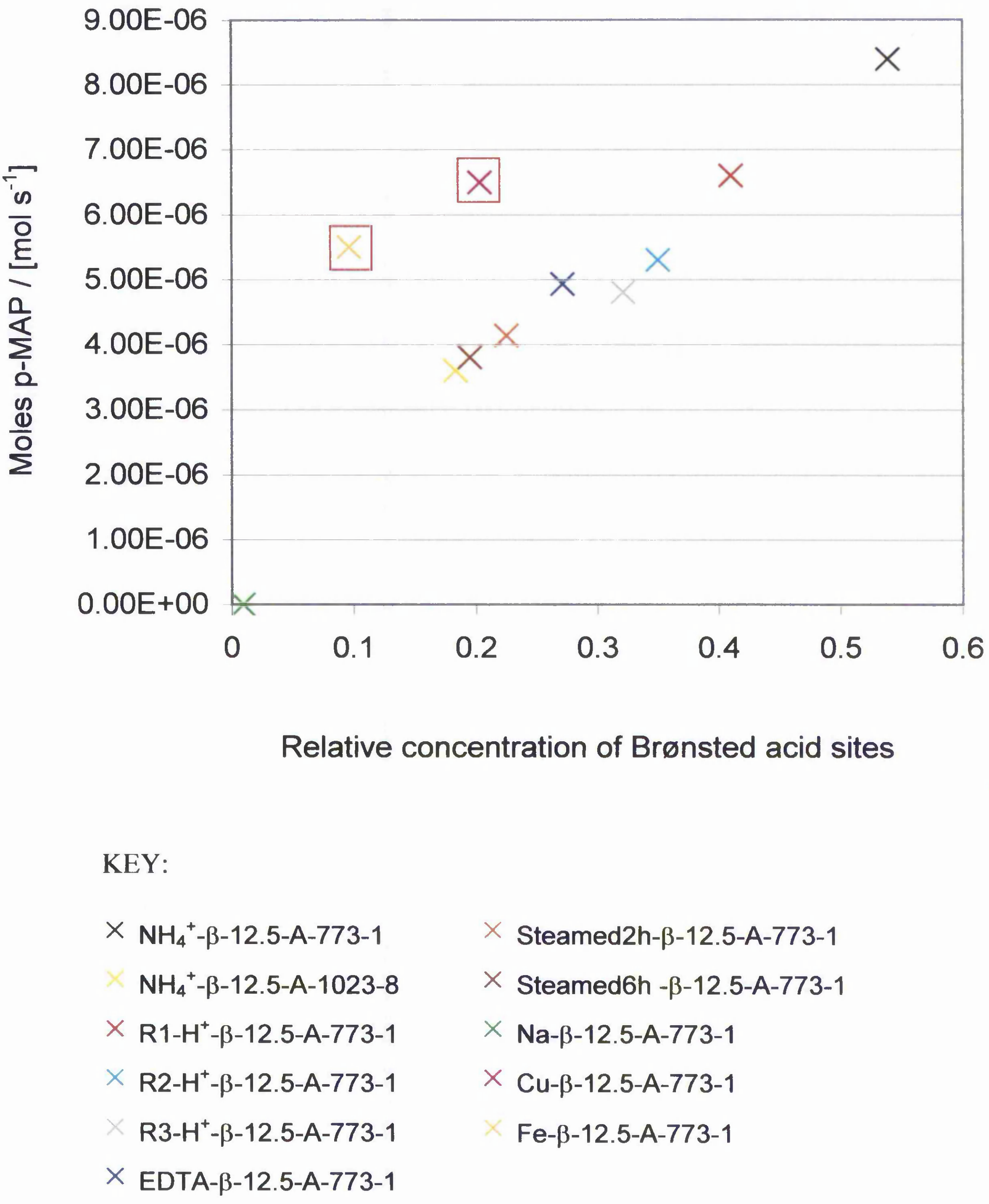

Figure 3.3.3.5 Plot of relative Brønsted acid site concentration versus initial rate of reaction (including Cu and Fe Beta).

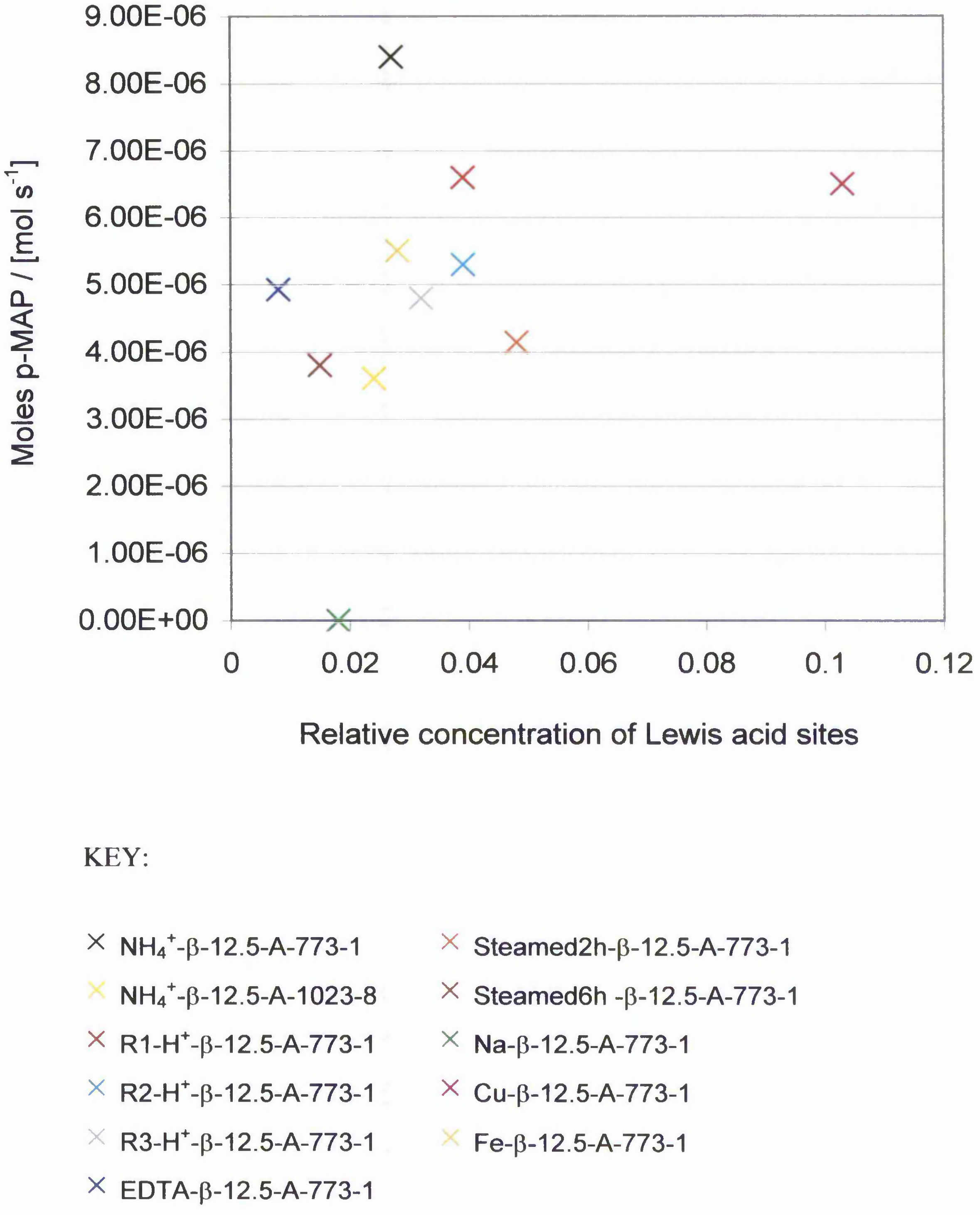

Figure 3.3.3.6 Plot of relative Lewis acid site concentration versus initial rate of reaction for the entire range of zeolite Beta samples.

3.3.4 Catalytic activity of ZSM-5, mordenite, faujasite, and mesoporous MCM-41 in the aromatic acylation of anisole with acetic anhydride

CATALYTIC RESULTS:

Figure 3.3.4.1 shows the percentage yield to p-methoxyacetophenone for ZSM-5, mordenite, faujasite, and mesoporous MCM-41.

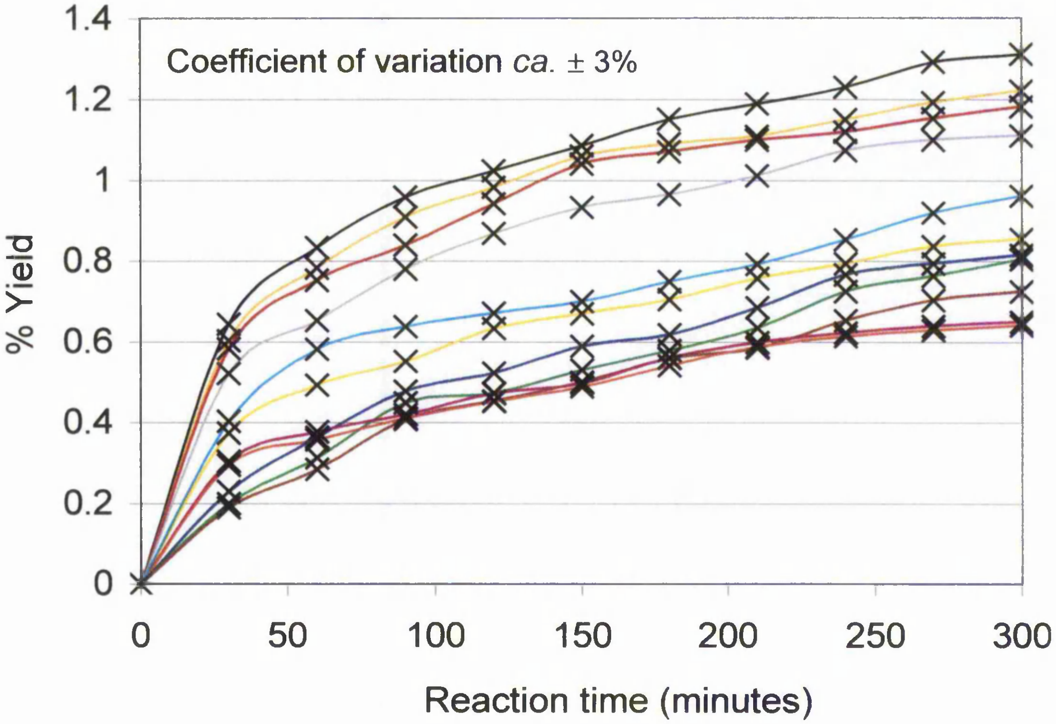

KEY:

- NH_4^+-ZSM-5-25-A-773-1
- Fe-ZSM-5-25-A-773-1
- Cu-ZSM-5-25-A-773-1
- NH_4^+-FAU-2.36-A-573-8
- NH_4^+-MOR-10 -A-823-1
- Fe-MOR-10-A-823-1
- Cu-MOR-10-A-823-1
- 30Al-MCM-41-A-773-1
- 15Al -MCM-41-A-773-1
- 5Al-MCM-41-A-773-1
- 15Al -MCM-41-Fe-5-A-773-1

Figure 3.3.4.1 Plot of yield of p-MAP versus reaction time for various materials.

Figure 3.3.4.2 shows the initial rates of reaction for the same range of samples, and the values are summarised in **Table 3.3.4.1**.

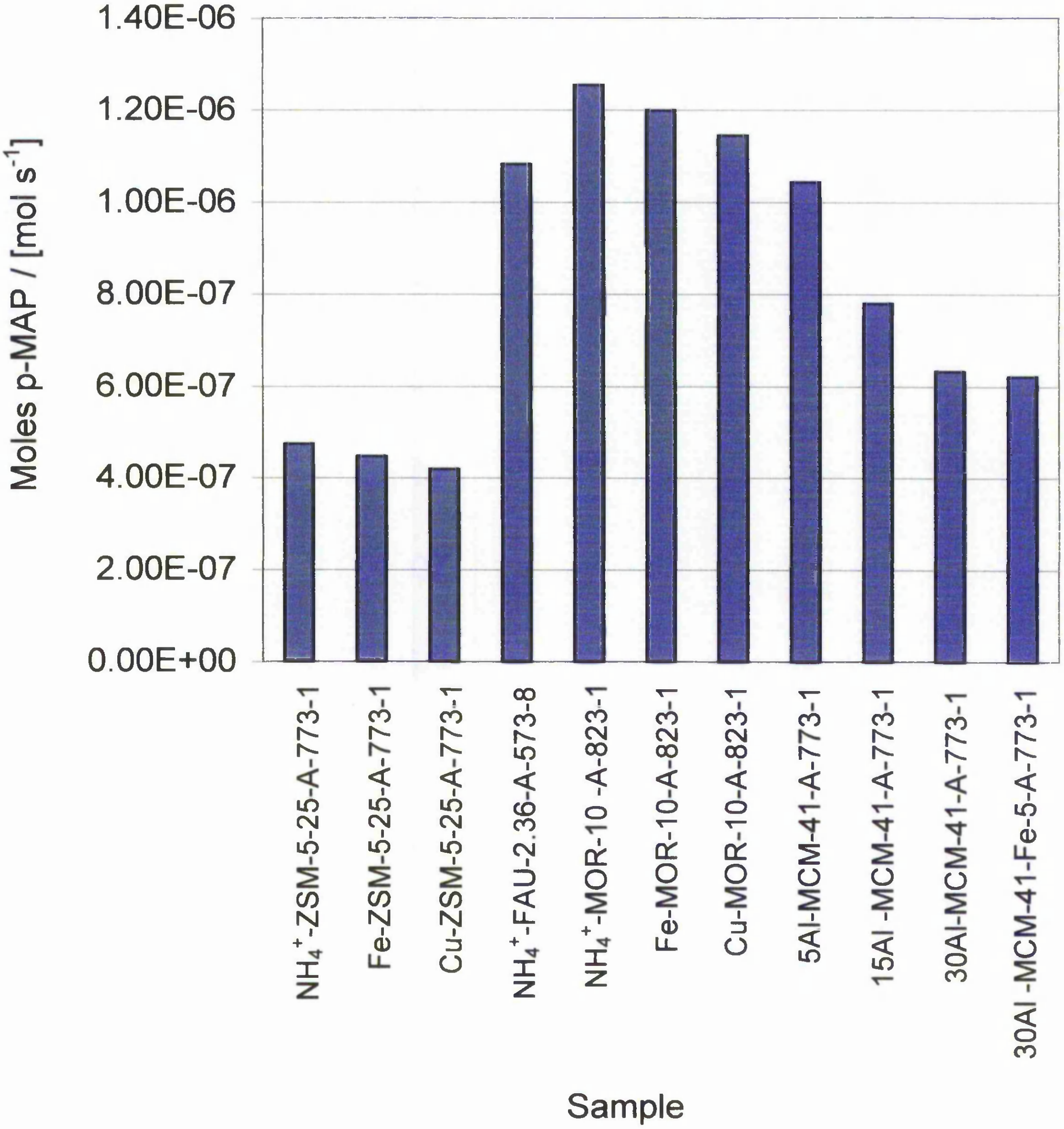

Figure 3.3.4.2 Comparison of initial rates of reaction for various materials.

Sample	**Initial rate (mol s^{-1}) ± 3%***
NH_4^+-ZSM-5-25-A-773-1	4.74E-07
Fe-ZSM-5-25-A-773-1	4.47E-07
Cu-ZSM-5-25-A-773-1	4.19E-07
NH_4^+-FAU-2.36-A-573-8	1.08E-06
NH_4^+-MOR-10 -A-823-1	1.26E-06
Fe-MOR-10-A-823-1	1.20E-06
Cu-MOR-10-A-823-1	1.14E-06
5Al-MCM-41-A-773-1	1.04E-06
15Al -MCM-41-A-773-1	7.80E-07
30Al-MCM-41-A-773-1	6.33E-07
30Al -MCM-41-Fe-5-A-773-1	6.21E-07

* Approximate experimental error expressed as the coefficient of variation.

Table 3.3.4.1 Initial rates of reaction for various materials.

Figure 3.3.4.3 and **Figure 3.3.4.4** show the comparison of yields to p-MAP, and the initial rates of reaction, respectively, between the best performing zeolite Beta sample and the best performing sample from all the other materials tested.

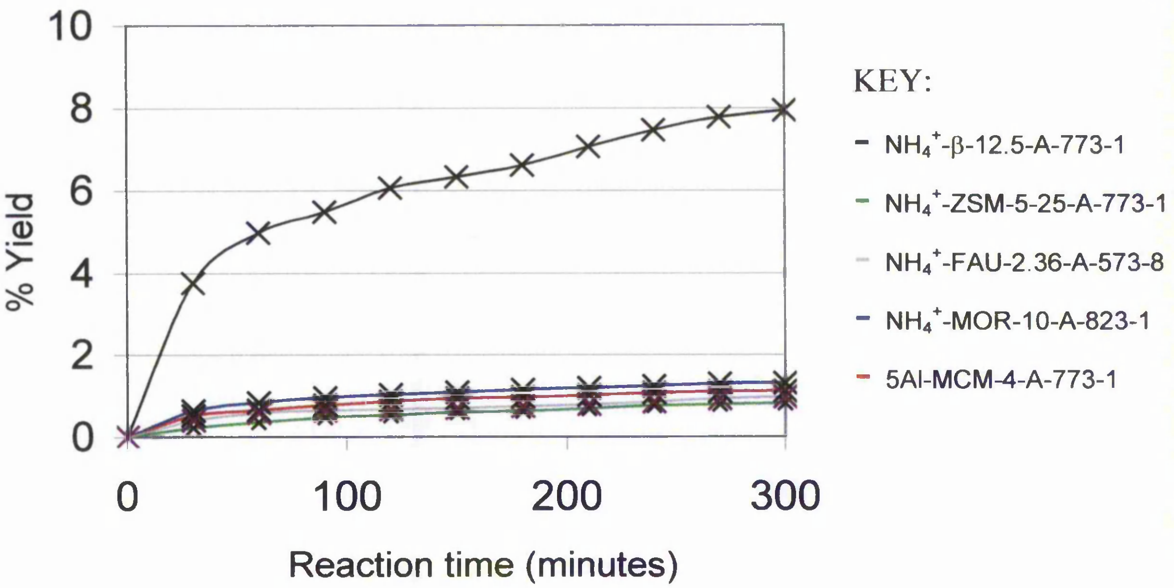

Figure 3.3.4.3 Comparison of yields for best performing samples.

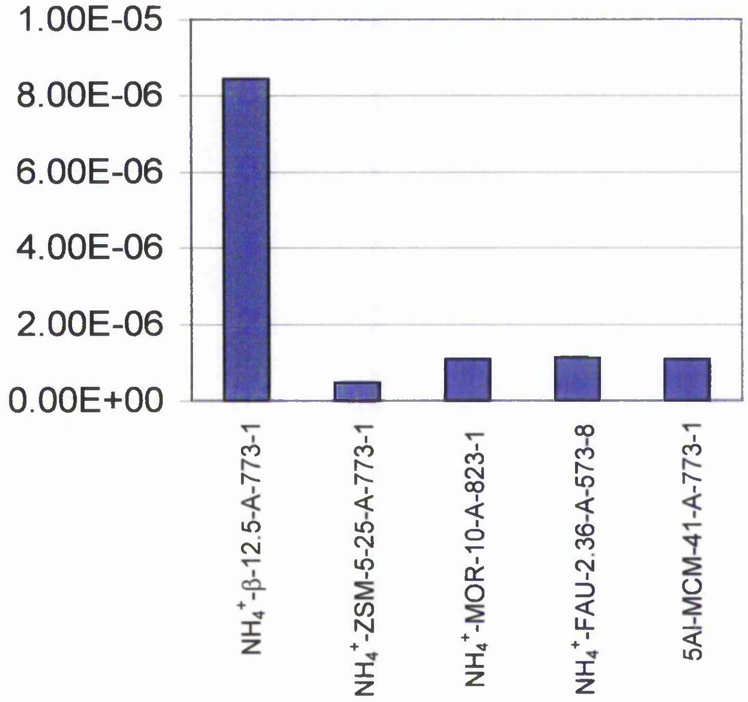

Figure 3.3.4.4 Comparison of initial rates for best performing samples.

DISCUSSION

Figure 3.3.3.1 shows the percentage yields for the entire range of zeolite Beta samples, the initial rates of reaction are shown in **Figure 3.3.3.2** and summarised in **Table 3.3.3.1**. It is apparent that all samples exhibit widely differing catalytic activities. Na-β-12.5-A-773-1 shows no catalytic activity, and NH_4^+-β-12.5-A-773-1 exhibits the highest catalytic activity in terms of both yield and initial rate of reaction. **Figure 3.3.3.3** compares the percentage yield of the best performing zeolite Beta sample, NH_4^+-β-12.5-A-773-1 at 398 K, with the classical homogeneous catalyst, $AlCl_3$. Results show that $AlCl_3$ performs better than NH_4^+-β-12.5-A-773-1, reaching a maximum yield of 45% to the para isomer after 90 minutes, compared with 28% for NH_4^+-β-12.5-A-773-1 after 300 minutes. However, use of $AlCl_3$ also results in the formation of the ortho isomer, which results in a maximum yield of 18% after 90 minutes. Although para substitution generally predominates in classical Friedel Crafts acylation [10], the exclusive formation of the para isomer is rare, and in the case of zeolites, can be explained by shape selectivity operating in the product formation. The ortho isomer would require a greater volume of space within the channels or cavities of the catalyst, and thus the para isomer is preferentially formed. In the present study, zeolite Beta samples exhibit > 99% selectivity to the para isomer, even at higher temperatures, and $AlCl_3$, although showing higher catalytic activity, exhibits approximately 70% selectivity towards the para isomer and 30% selectivity to the ortho isomer. The selectivity observed over $AlCl_3$ agrees well with that reported in the literature for a similar reaction [4]. **Figure 3.3.3.4** shows a plot of initial rate of reaction versus the relative Brønsted acid site concentration for H-forms of zeolite Beta. A very good linear relationship is observed, which would certainly provide good evidence for the operation of a Brønsted acid catalysed process. The plot shows that samples exhibit lower catalytic activity as a result of reduced aluminium content and Brønsted acid site concentration. Many studies point towards a Brønsted acid catalysed process [1-4]. However, no relationship between the initial rate of reaction and the relative Brønsted acid concentration can be observed if transition metal exchanged zeolite Beta samples are included into the plot, as shown in **Figure 3.3.3.5**. Both Cu and Fe exchanged zeolite Beta exhibit unusually high initial rates of reaction despite containing low concentrations of Brønsted acid sites. This finding casts some doubt on the operation of a Brønsted acid catalysed process.

In addition, no relationship between the initial rate of reaction and the relative Lewis acid site concentration can be observed, as shown in **Figure 3.3.3.6**. Despite Cu Beta exhibiting a high concentration of Lewis acid sites, the activity is no greater than that of H-form zeolite Beta samples which contain significantly lower concentrations of Lewis acid sites. In addition, Lewis acid sites that are an inherent part of the zeolite Beta framework as a result of local defects [11], although varying in concentration in different H-Beta samples, seem to have no impact on catalytic reaction.

In order to eliminate the possibility of any homogeneous activity resulting from leaching of transition metal into solution during reaction, the spent reaction solution resulting from the use of Fe and Cu Beta was filtered and new reactants added, however the concentration of p-MAP in this solution was constant over 6 hours reaction time at 333 K, indicating that no homogeneous activity was present.

Figure 3.3.4.1 shows the percentage yields to p-MAP for ZSM-5, mordenite, faujasite, and mesoporous MCM-41, and **Figure 3.3.4.2** shows the initial rates of reaction for the same samples. It is evident that mordenite samples perform best, followed by the MCM-41 sample exhibiting the highest aluminium content, 5Al-MCM-41-A-773-1, and then faujasite and the remaining aluminium containing MCM-41 samples. ZSM-5 samples exhibit the lowest catalytic activity. Interesting, purely siliceous, and Fe-containing MCM-41 did not show any activity in the reaction, indicating that the presence of aluminium is necessary for the acylation reaction to occur. In addition, 30Al-MCM-41-Fe-5-A-773-1 exhibited very similar activity to 30Al-MCM-41-A-773-1 indicating that Fe may only act as a spectator in the reaction. Also, increasing the aluminium content of MCM-41 leads to an increase in catalytic activity. However, catalytic activity over these frameworks is very low compared with zeolite Beta, as shown in **Figure 3.3.4.3**, and **Figure 3.3.4.4**, initial rates and yields are significantly lower for the best performing ZSM-5, mordenite, faujasite, and mesoporous MCM-41 samples compared with the best performing zeolite Beta sample. This result is in line with literature, where zeolite Beta is consistently found to be the best performing zeolite, especially in the acylation of anisole with acetic anhydride [12], [3], however it has also been suggested that faujasite is preferred when applying the bulkier veratrole as a substrate in acylation [13], [14]. Derouane *et al.*, [15] studied the effect of zeolite type on the reaction rate and product yield for the acylation of toluene with acetic anhydride on zeolites H-FAU, H-BEA, H-MOR, and H-MFI. These workers found that H-MOR was the poorest catalyst, and attributed this to its smaller pore size (compared with the other 12 membered ring zeolites, H-FAU and H-BEA) and uni-dimensional pore structure. Both H-MFI and H-FAU exhibited similar activities, but both were significantly less active than H-BEA. In the smaller (10 membered ring) pore MFI structure, mass transport limitations and confinement effects were thought to predominate. In H-FAU a rapid deactivation took place which was attributed to poly-acetylated products that can form in the supercages, but cannot escape due to the smaller size of the supercage windows, preventing access of the reactants to the active sites. They concluded that H-BEA was the superior catalyst due to its large and interconnected channels.

Differences in pore size of the different zeolites are not expected to influence activity since the molecules used should fit into all of the zeolites tested. Zeolite Beta, faujasite, and mordenite all consist of 12-membered rings and MCM-41 has significantly larger pore openings (approximately 29 Å). Only ZSM-5 has smaller pore dimensions than zeolite Beta, consisting of 10-membered rings, however the kinetic diameter of anisole, acetic anhydride, and p-MAP are significantly less than its pore openings [16]. Anisole and p-MAP are expected to have similar kinetic diameters to toluene, which is known to fit into ZSM-5, and acetic anhydride should exhibit a similar diameter to iso-butane and iso-pentane, which also fit into the pores of ZSM-5. However, it is possible that the transition state may not be accommodated in the channels of ZSM-5, which would account for its lower activity.

No clear dependency of the activity from the acid strength can be observed for the acylation reaction. Although the different zeolites studied exhibit significantly different acid strengths, over zeolite Beta yields of p-MAP are significantly larger than over the other frameworks. MCM-41 is generally considered to have sites of lower acid strength than the zeolites [17], while ZSM-5 and mordenite are expected to exhibit higher acidic strength than zeolite Beta.

Finally, it is also interesting to note the change in the percentage yield with time for all samples tested, where a rapid increase in yield is observed for the first 30 minutes, followed by a period where the yield increase slows down dramatically over the remainder of the reaction. Although such a phenomenon is common in batch reactions, since reactants are used up as the reaction progresses, the low yields involved in this particular case suggest that both reactants are still plentiful. As such, the shape of the yield curves may indicate the possibility of two types of active site, a highly active site which deactivates rapidly, and another which is only slightly active but deactivates less readily. Results presented in this section would suggest that the highly active sites present on the catalyst are likely to be Brønsted acid sites, which account for the majority of the catalysts activity. These Brønsted acid sites seem to deactivate rapidly, but the reaction continues to progress, even after 72 hours (data not shown), and since no reaction will occur in the absence of catalyst, this would suggest the possibility of a second type of active site, one which exhibits poor activity and is less susceptible to deactivation. This site is rather enigmatic, but may be a second type of Brønsted acid site, a Lewis acid site, or due to the slightly acidic silanol groups present on the zeolite.

CONCLUSION

A very good linear relationship exists between the initial rate of reaction and the relative Brønsted acid site concentration for H-forms of zeolite Beta, however no such relationship exists when transition metal exchanged zeolite Beta samples are included in the plot. Both Cu and Fe Beta have low concentrations of Brønsted acid sites, but exhibit unusually high initial rates of reaction. This result places some doubt on a mechanism involving Brønsted acid sites. No relationship was observed between the initial rate of reaction and the concentration of Lewis acid sites in zeolite Beta, eliminating them as potential active sites. Zeolite Beta was found to exhibit lower catalytic activity than the homogeneous catalyst, $AlCl_3$, but the zeolite catalyst gave rise exclusively to the desired para product, in contrast to $AlCl_3$, where the selectivity to the para product was 70%. Zeolite Beta was convincingly found to be the best performing zeolite, all other frameworks tested exhibited poor catalytic activity in comparison. It was found, from catalytic testing of MCM-41 materials, that aluminium must be present in order for the acylation reaction to occur. In addition, results would suggest that both pore size and acidic strength effects do not account for the low activity over ZSM-5, mordenite, and faujasite, or indeed, for the high activity of zeolite Beta in the acylation of anisole with acetic anhydride. Catalytic data may suggest the possibility of two types of active site, one of which is highly active and accounts for the majority of the catalysts activity, this site deactivates rapidly. The second site exhibits poor catalytic activity but is less susceptible to deactivation and would explain the gradual increase in product even after 72 hours reaction time.

REFERENCES

(1) Derouane, E. G.; Dillon, C. J.; Bethell, D.; Derouane-Abd Hamid, S. B. *J. Catal.* 1999, ***187***, 209.

(2) Singh, A. P.; Bhattacharya, D. *Catal. Lett.* 1995, ***32***, 327.

(3) Freese, U.; Heinrich, F.; Roessner, F. *Catal. Today* 1999, ***49***, 237.

(4) Singh, A. P.; Bhattacharya, D.; Sharma, S. *J. Mol. Catal. : A* 1995, ***102***, 139.

(5) Akporiaye, D.; Daasvatn, K.; Solberg, J.; Stocker, M. *Stud. Surf. Sci. Catal.* 1993, ***78***, 521.

(6) Isaev, Y.; Fripiat, J. J. *J. Catal.* 1999, ***182***, 257.

(7) Laidlaw, P.; Bethell, D.; Brown, S. M.; Hutchings, G. J. *J. Mol. Catal. : A* 2001, ***174***, 187.

(8) Kouwenhoven, H. W.; van Bekkum, H. *Handbook of Heterogeneous Catalysis*; Ertl, G., Knozinger, H., Weitkamp, J., Eds.; VCH, 1997; Vol. 5; pp 2358.

(9) Spagnol, M.; Gilbert, L.; Alby, D. *Ind. Chem. Lib* 1996, ***8***, 29.

(10) Jensen, F. F.; Goodman, G. *Friedel Crafts and Related Reactions*; Olah, G. A., Ed.; Wiley-Interscience: New York, 1964; Vol. 3; pp 1024.

(11) Jansen, J. C.; Creyghton, E. J.; Njo, S. L.; van Koningsveld, H.; van Bekkum, H. *Catal. Today* 1997, ***38***, 205.

(12) Harvey, G.; Vogt, A. H. G.; Kouwenhoven, H. W.; Prins, R. *Proc. 9th Int. Zeol. Conf.* , Montreal, 1992; pp 363.

(13) Spagnol, M.; Gilbert, L.; Benazzi, E.; Marcilly, C. *Patent PCT, Int. Appl WO 96 35,655* 1996.

(14) Richard, F.; Carreyre, H.; Pérot, G. *J. Catal.* 1996, ***159***, 427.

(15) Derouane, E. G.; Crehan, G.; Dillon, C. J.; Bethell, D.; He, H.; Derouane-Abd Hamid, S. B. *J. Catal.* 2000, ***194***, 410.

(16) Stockenhuber, M.; Paine, G. S.; Apperley, D. C. *Submitted to J. Catal. 2002.*

(17) Meziani, M. J.; Zajac, J.; Jones, D. J.; Partyka, S.; Roziere, J.; Auroux, A. *Langmuir* 2000, ***16***, 2262.

Chapter 3. Results

3.4 The influence of temperature, mass of catalyst, particle size, substrate/acylating agent ratio, and type of substrate/acylating agent on the catalytic activity of zeolite Beta in aromatic acylation

3.4.1 Abstract

This section deals with some parameters that are expected to lead to an increase in the rate of reaction, including temperature, mass of catalyst, particle size of catalyst, substrate/acylating agent ratio, and the type of substrate/acylating agent. The aim of this section is to determine the optimum reaction conditions for the acylation of anisole with acetic anhydride over zeolite Beta.

3.4.2 Background

The primary requirement for a reaction to occur is that the reactant particles must collide and interact with each other in some way. This is the central idea of collision theory, which is used to explain many of the observations made about chemical kinetics. Collision theory states that the rate of a chemical reaction is proportional to the number of collisions between reactant molecules. The more often reactant molecules collide, the more often they will react with one another, and the faster the reaction rate. In reality, only a small fraction of the collisions are effective collisions. Effective collisions are those that result in a chemical reaction. In order to produce an effective collision, reactant particles must possess some minimum amount of energy. This energy, used to initiate the reaction, is called the activation energy. In essence, the three requirements for an effective collision are:

1) The reactants must collide with each other
2) The molecules must have sufficient energy to initiate the reaction (activation energy)
3) The molecules must have the correct orientation

Reaction rate is generally considered to be effected by four parameters including temperature, concentration, surface area, and catalysts, all of which are considered to result in an increase in the number of effective collisions. A study of any reaction would not be complete without investigation of altering such parameters, since such a study is expected to lead to determination of the optimum reaction conditions. Jacob *et al.*, [1] in a study of benzoylation over zeolite catalysts reported an increased conversion of benzoyl chloride when the temperature, and mass of catalyst was increased. A study by Moreau *et al.*, [2] concerning the acetylation of dimethoxybenzenes with acetic anhydride over acidic zeolites found that varying the concentration of acetic anhydride, while keeping that of veratrole constant led to an increase in the initial rate of reaction. The same trend was also observed when the concentration of acetic anhydride was kept constant, while the concentration of veratrole was increased. However in both cases, the initial rate of reaction reached a maximum where increasing one reactant, while the other was kept constant, yielded no further increase in reaction rate. The results of the study suggested that an equimolar mixture of veratrole and acetic anhydride led to the highest initial rate of reaction. A study by De Castro *et al.*, [3] on acylation using α-β-unsaturated organic acids as acylating agents over large pore zeolites found significantly reduced yields when using toluene as substrate compared to xylenes. Such a result was expected since toluene is a less activated aromatic molecule; it is for this reason that aromatic substrates such as anisole and veratrole are chosen for aromatic acylation over zeolites. Ma *et al.*, [4] in a study of Friedel Crafts acylation over zeolite catalysts found that the reactivity of the anhydride was higher than that of the corresponding acid, the authors attributed this to the fact that the protonated carboxylic acid could hardly transform into the acylium cation, since water is a worse leaving group than acid.

3.4.3 The effect of temperature on the catalytic activity of zeolite Beta in the aromatic acylation of anisole with acetic anhydride

Figure 3.4.3.1 shows the percentage yield to p-methoxyacetophenone over the best performing zeolite Beta sample, NH_4^+-β-12.5-A-773-1, at different temperatures.

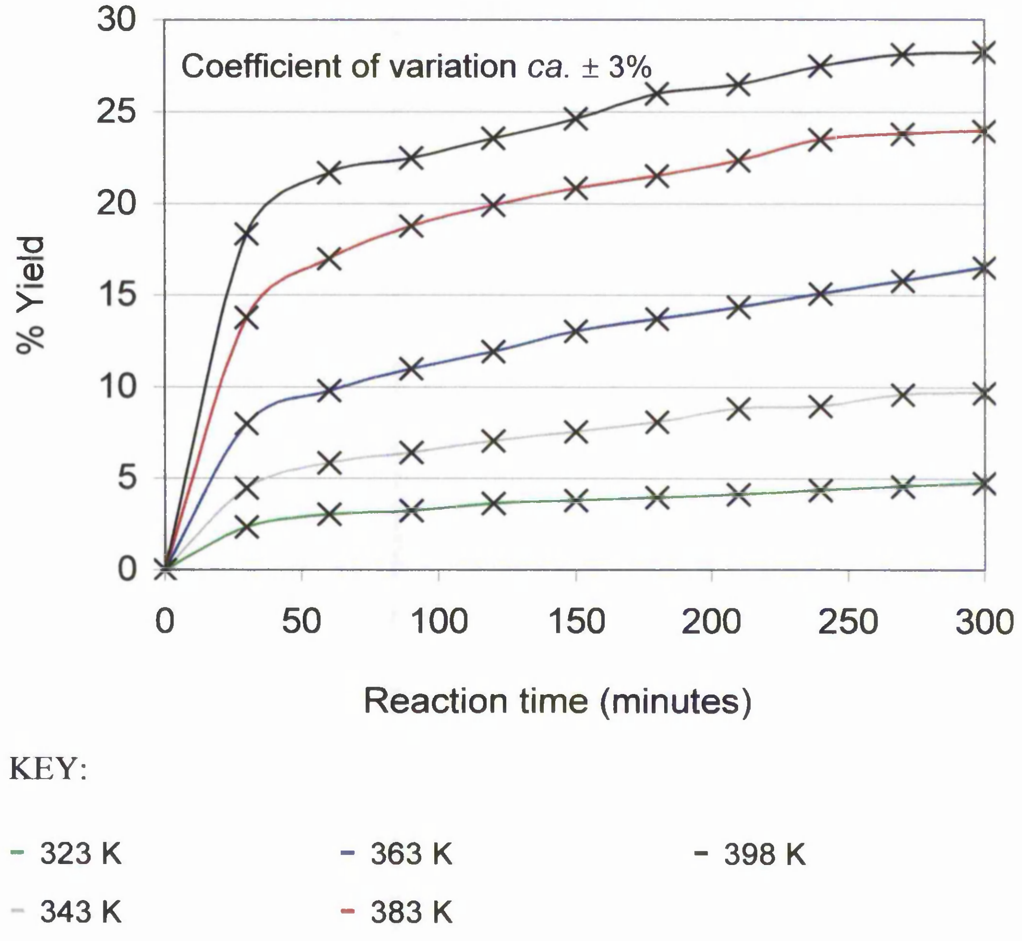

Figure 3.4.3.1 Plot of yield of p-MAP versus reaction time for NH_4^+-β-12.5-A-773-1 at different temperatures.

Figure 3.4.3.2 shows initial rates of reaction for the sample, NH_4^+-β-12.5-A-773-1, at different temperatures, and the values are summarised in **Table 3.4.3.1**.

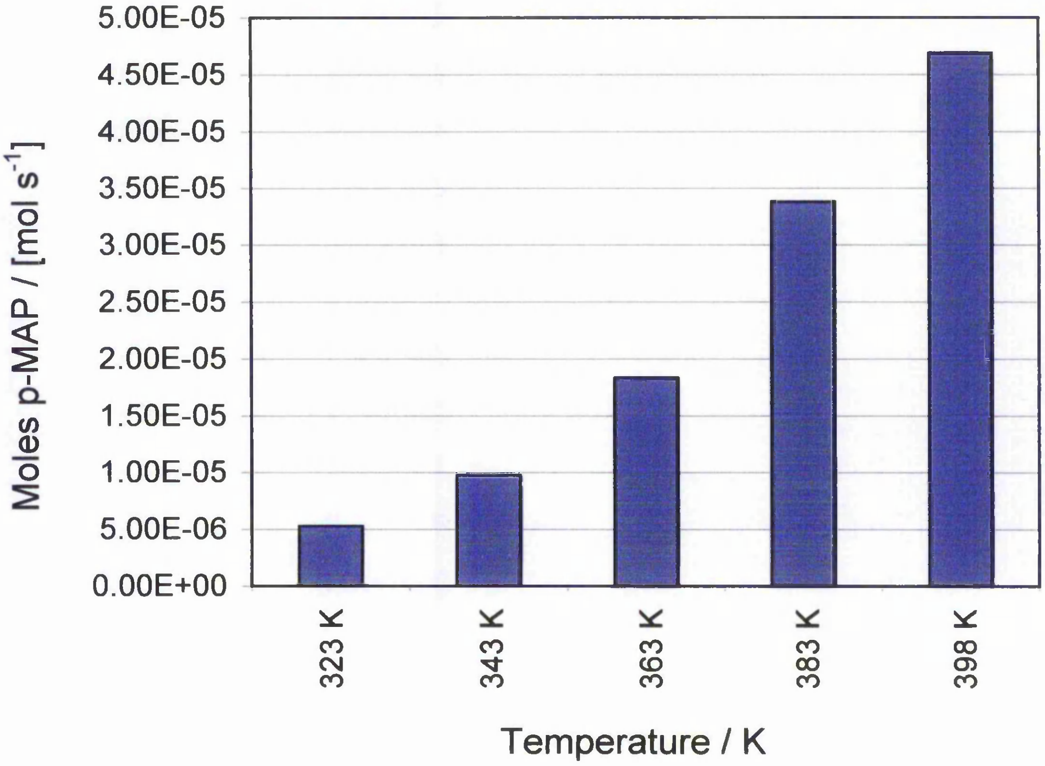

Figure 3.4.3.2 Initial rates of reaction for the sample, NH_4^+-β-12.5-A-773-1, at different temperatures.

Temperature (K) ± 0.5%*	Initial rate (mol s^{-1}) ± 3%*
323	5.29E-06
343	9.75E-06
363	1.83E-05
383	3.38E-05
398	4.69E-05

* Approximate experimental error expressed as the coefficient of variation.

Table 3.4.3.1 Comparison of initial rates of reaction for the sample, NH_4^+-β-12.5-A-773-1, at different temperatures.

Table 3.4.3.2 shows the values of 1/T and ln k for the data tabulated in **Table 3.4.3.1**, and **Figure 3.4.3.3** shows the respective Arrhenius plot.

1/T	ln k
0.00310	-12.1497
0.00292	-11.5387
0.00275	-10.9067
0.00261	-10.2945
0.00251	-9.9685

Table 3.4.3.2 Values of 1/T and ln k.

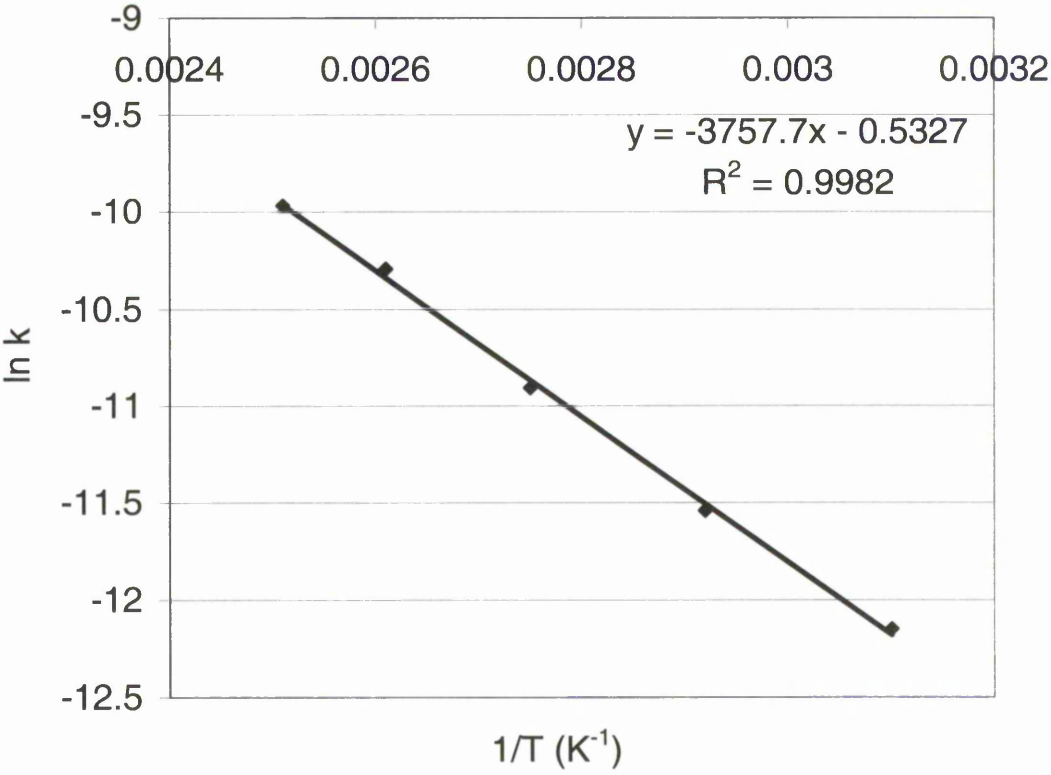

Figure 3.4.3.3 Initial rates of reaction for the sample, NH_4^+-β-12.5-A-773-1, at different temperatures.

Calculation of activation energy

Slope = -3758

Slope = $-\dfrac{E_a}{R}$

E_a = - slope × R

E_a = - (-3758) × 8.314

E_a = 31244 J/mol

E_a = 31 kJ/mol ± 2%

3.4.4 The effect of mass of catalyst on the catalytic activity of zeolite Beta in the aromatic acylation of anisole with acetic anhydride

Figure 3.4.4.1 shows the percentage yield to p-methoxyacetophenone over the best performing zeolite Beta sample, NH_4^+-β-12.5-A-773-1, with varying weight of catalyst.

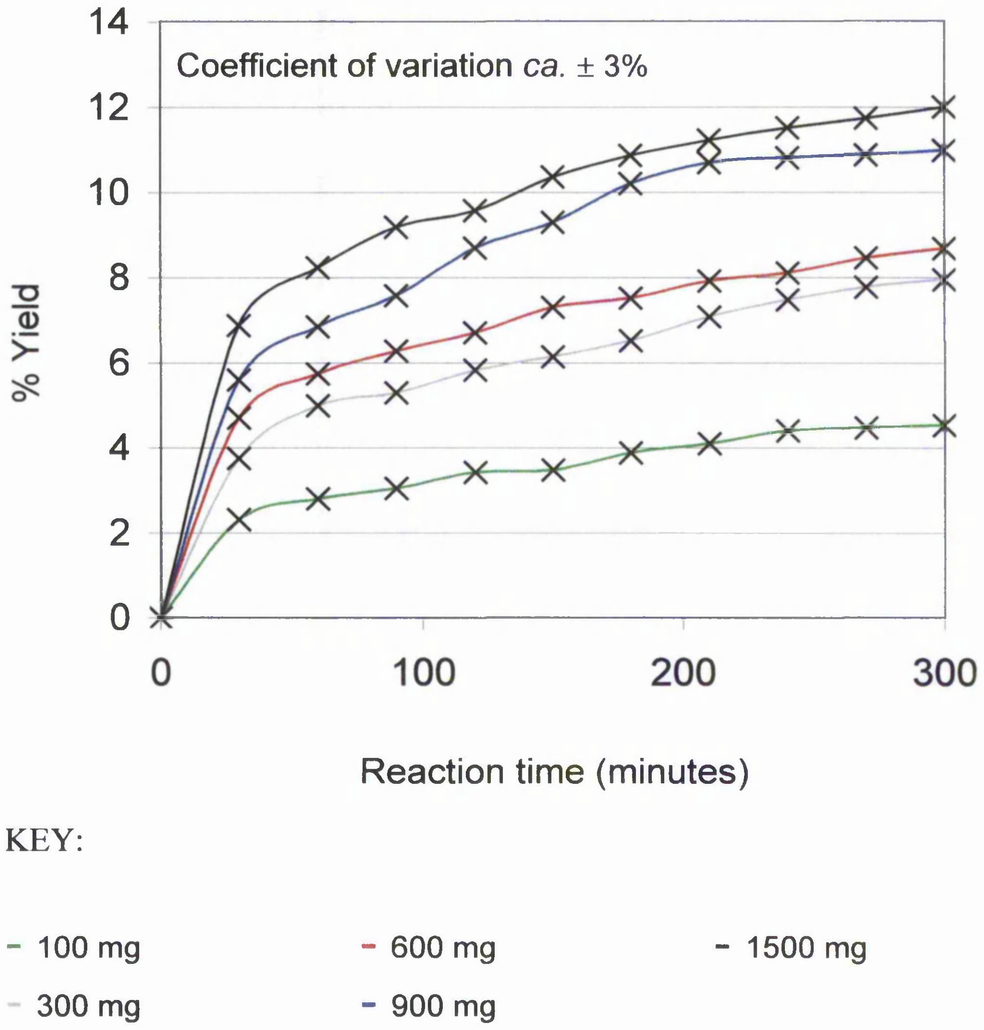

Figure 3.4.4.1 Plot of Yield of p-MAP versus reaction time for NH_4^+-β-12.5-A-773-1 with varying weight of catalyst.

Figure 3.4.4.2 shows initial rates of reaction for the sample, NH_4^+-β-12.5-A-773-1, with varying weight of catalyst, and the values are summarised in **Table 3.4.4.1**.

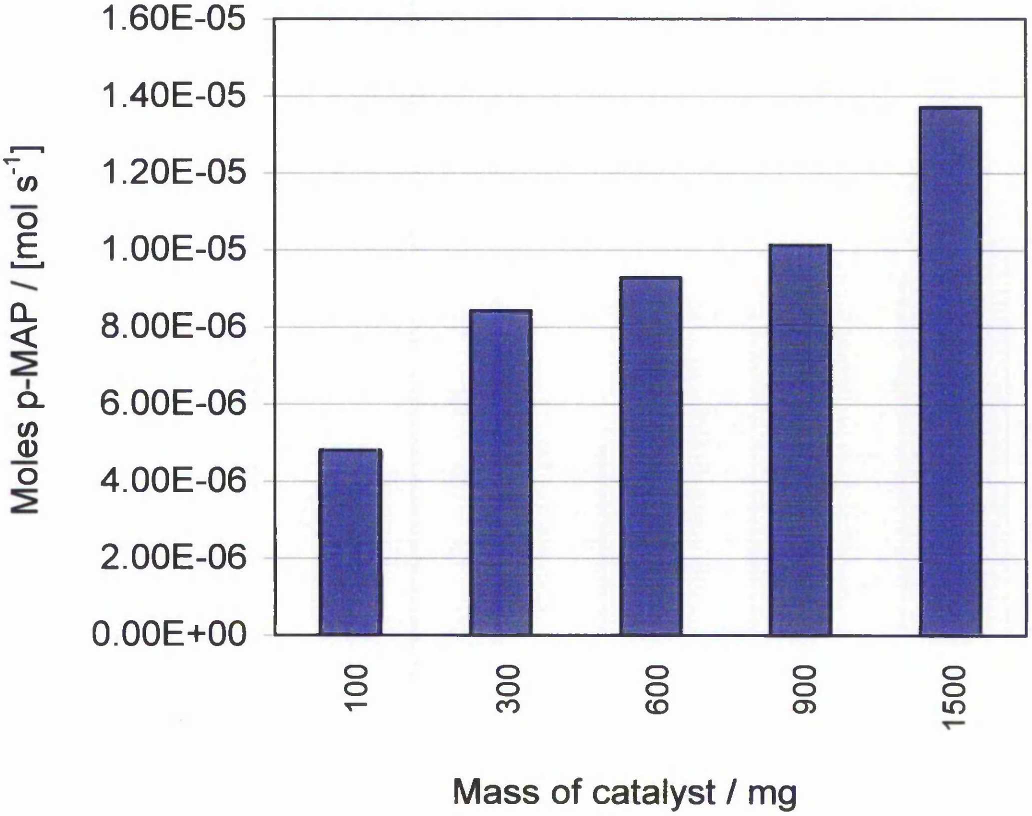

Figure 3.4.4.2 Initial rates of reaction for the sample, NH_4^+-β-12.5-A-773-1, with varying weight of catalyst.

Mass of catalyst (mg)	**Initial rate (mol s^{-1}) ± 3%***
100	4.81E-06
300	8.43E-06
600	9.28E-06
900	1.01E-05
1500	1.37E-05

* Approximate experimental error expressed as the coefficient of variation.

Table 3.4.4.1 Comparison of initial rates of reaction for the sample, NH_4^+-β-12.5-A-773-1, with varying weight of catalyst.

3.4.5 The effect of substrate/acylating agent ratio on the catalytic activity of zeolite Beta in the aromatic acylation of anisole with acetic anhydride

Figure 3.4.5.1 shows the percentage yield to p-methoxyacetophenone over the best performing zeolite Beta sample, NH_4^+-β-12.5-A-773-1, with varying the substrate/acylating agent ratio.

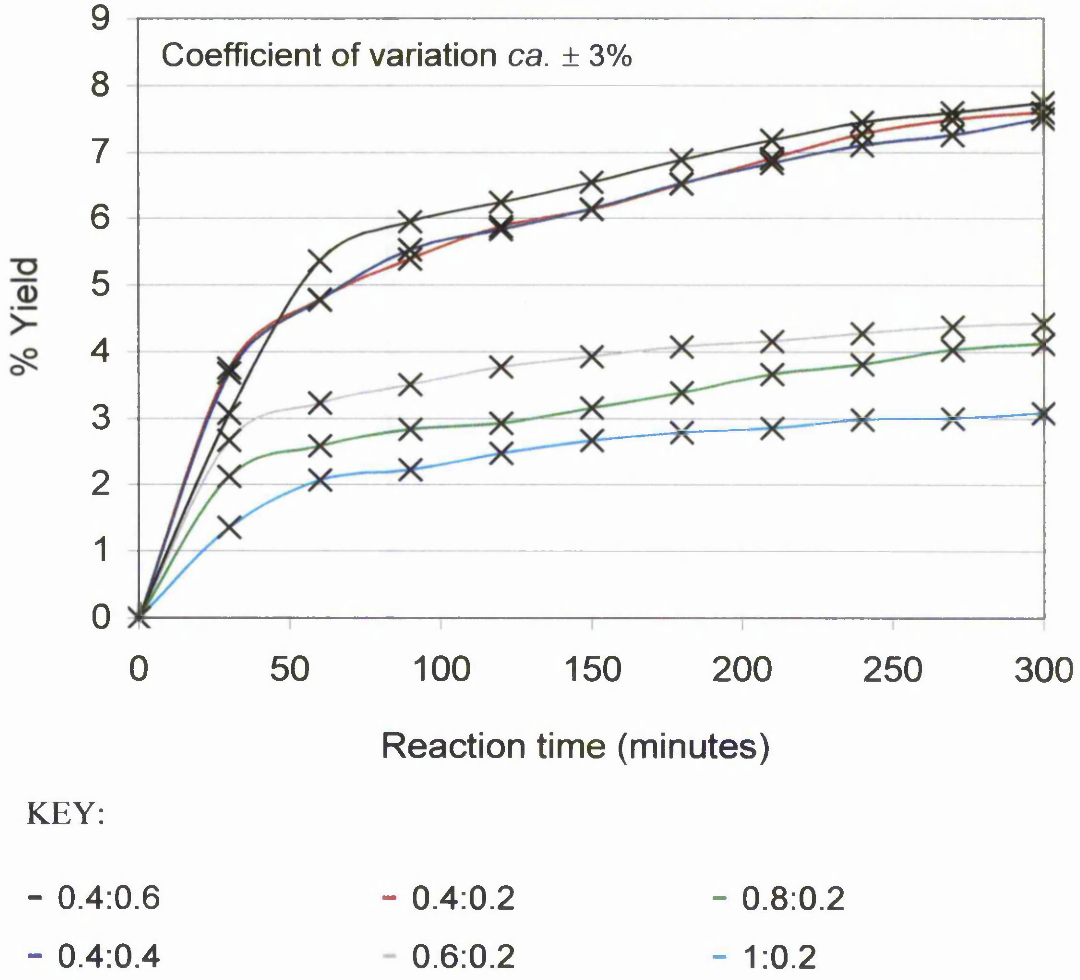

Figure 3.4.5.1 Plot of Yield of p-MAP versus reaction time for NH_4^+-β-12.5-A-773-1 with varying the substrate/acylating agent ratio.

Figure 3.4.5.2 shows initial rates of reaction for the sample, NH_4^+-β-12.5-A-773-1, with varying the substrate/acylating agent ratio, and the values are summarised in **Table 3.4.5.1**.

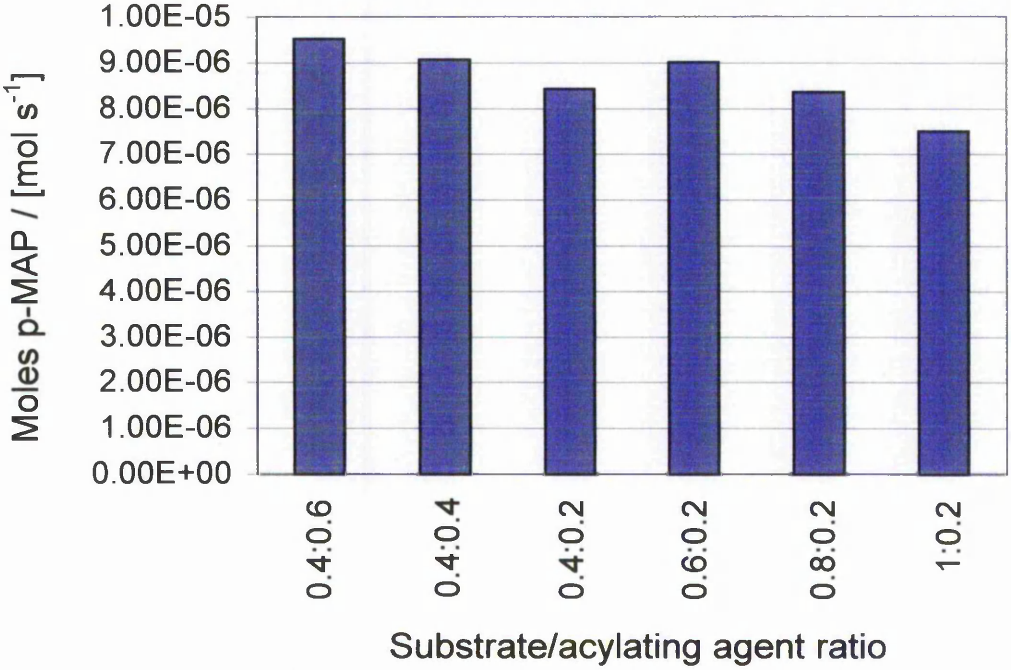

Figure 3.4.5.2 Initial rates of reaction for the sample, NH_4^+-β-12.5-A-773-1, with varying the substrate/acylating agent ratio.

Substrate/acylating agent ratio	**Initial rate (mol s^{-1}) ± 3%***
0.4:0.6	9.52E-06
0.4:0.4	9.07E-06
0.4:0.2	8.43E-06
0.6:0.2	9.01E-06
0.8:0.2	8.36E-06
1:0.2	7.50E-06

* Approximate experimental error expressed as the coefficient of variation.

Table 3.4.5.1 Comparison of initial rates of reaction for the sample, NH_4^+-β-12.5-A-773-1, with varying the substrate/acylating agent ratio.

3.4.6 The effect of particle size, and type of substrate/acylating agent on the catalytic activity of zeolite Beta in the aromatic acylation of anisole with acetic anhydride

Figure 3.4.6.1 shows the percentage yield to p-methoxyacetophenone over the best performing zeolite Beta sample, NH_4^+-β-12.5-A-773-1, with varying the particle size and type of substrate, acylating agent.

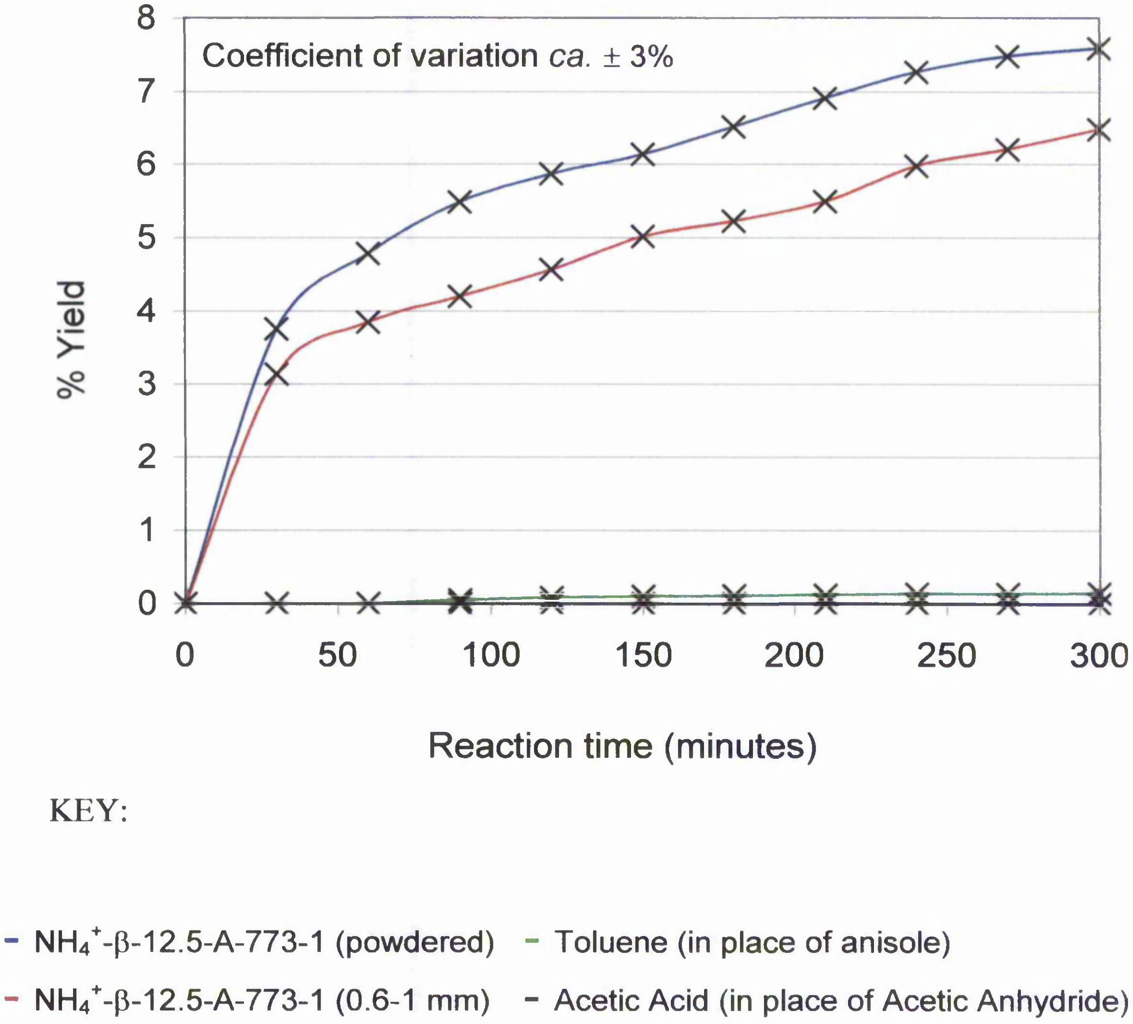

Figure 3.4.6.1 Plot of Yield of p-MAP versus reaction time for NH_4^+-β-12.5-A-773-1 with varying the particle size and type of substrate/acylating agent.

Figure 3.4.6.2 shows initial rates of reaction for the sample, NH_4^+-β-12.5-A-773-1, with varying the particle size and type of substrate/acylating agent, and the values are summarised in **Table 3.4.6.1**.

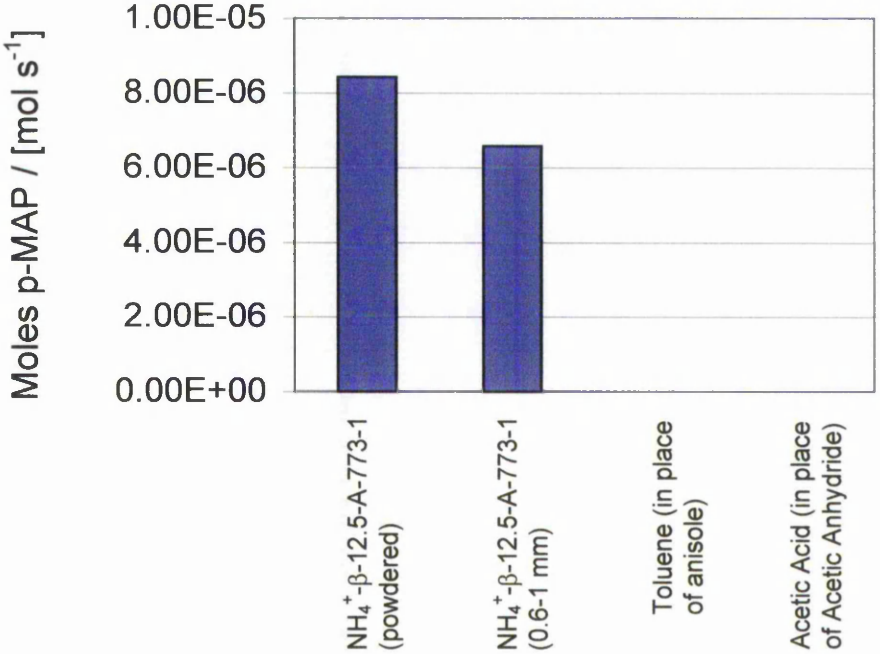

Figure 3.4.6.2 Initial rates of reaction for the sample, NH_4^+-β-12.5-A-773-1, with varying the particle size and type of substrate/acylating agent.

Parameter	Initial rate (mol s^{-1}) ± 3%*
NH_4^+-β-12.5-A-773-1 (powdered)	8.43E-06
NH_4^+-β-12.5-A-773-1 (0.6-1 mm)	6.58E-06
Toluene (in place of anisole)	0
Acetic acid (in place of acetic anhydride)	0

* Approximate experimental error expressed as the coefficient of variation.

Table 3.4.6.1 Comparison of initial rates of reaction for the sample, NH_4^+-β-12.5-A-773-1, with varying the particle size and type of substrate/acylating agent.

DISCUSSION

Effect of reaction temperature

The temperature dependency of the acylation reaction using anisole with acetic anhydride is shown in **Figure 3.4.3.1**, and **Figure 3.4.3.2**, which exhibit the yields and initial rates of reaction respectively. The yields to p-MAP increase from 5% at 323 K to approximately 28% at 398 K over a 300-minute time period, and the initial rate of reaction increases from 5.29×10^{-6} to 4.69×10^{-5} mol s^{-1}. The selectivity to the para-product remains almost constant throughout the range of temperatures studied, although very small traces of ortho-isomer are present at the highest temperature studied, 398 K. From the Arrhenius plot shown in **Figure 3.4.3.3**, the apparent activation energy for the reaction is 31 kJ mol^{-1} ± 2%. Although most of the literature regarding the acylation of anisole with acetic anhydride over zeolite H-Beta does not state a value for the activation energy, Derouane *et al.*, [5] derived an approximate activation energy of 46 kJ mol^{-1}. Singh *et al.*, [6] in a study of benzoylation of toluene with benzoyl chloride over zeolite catalysts derived an apparent activation energy of 48 kJ mol^{-1} over zeolite H-Beta. This value can be compared with activation energies (54 – 63 kJ mol^{-1}) characterising classical aromatic acylation in the homogeneous phase [7]. According to Satterfield *et al.*, [8], apparent activation energies for reactions in zeolites are in the range of 12.5 – 46 kJ mol^{-1}, and when the reaction is diffusion limited, the apparent activation energy is in the range of 8 – 19 kJ mol^{-1}. Thus, the calculated activation energy in the present study would suggest that the reaction is not diffusion controlled. Freese *et al.*, [9] in a study of the acylation of anisole with acetic anhydride over zeolite Beta, faujasite, and ZSM-5, found that the reactions were controlled by mass transfer limitations caused by coke deposition, but no apparent activation energy was stated.

Effect of mass of catalyst

The effect of mass of catalyst on the acylation of anisole with acetic anhydride over zeolite Beta is shown in **Figure 3.4.4.1**, and **Figure 3.4.4.2**, which exhibit the yields and the initial rates of reaction respectively. When the mass of catalyst is increased from 150 mg to 1500 mg, the yield to p-MAP increases from 4% to approximately 12%, and the initial rate of reaction increases by a factor of 4. Product distribution was not influenced by the change in catalyst concentration and para-isomer was the major product (selectivity > 99%) in all experiments.

Effect of substrate/acylating agent ratio

The effect of substrate/acylating agent ratio on the acylation of anisole with acetic anhydride over zeolite Beta is shown in **Figure 3.4.5.1**, and **Figure 3.4.5.2**, which exhibit the yields and the initial rates of reaction respectively. Anisole/acetic anhydride ratios of 0.4:0.6, 0.4:0.4, and 0.4:0.2 show the highest yields with a maximum of approximately 7.5% after 300 minutes. The highest initial rate of reaction is observed for the anisole/acetic anhydride ratio of 0.4:0.6, with a value of 9.52×10^{-6} mol s^{-1}, followed by the equimolar mixture that has a value of to 9.07×10^{-6} mol s^{-1}. Increasing the concentration of anisole, while keeping that of acetic anhydride constant leads to a progressive decrease in both the yield and the initial rate of reaction, so that for an anisole/acetic anhydride ratio of 1:0.2, the yield after 300 minutes is only 3%, and the initial rate of reaction is 7.50×10^{-6} mol s^{-1}. Thus the results would suggest that an equimolar mixture of anisole:acetic anhydride, or a slight excess of either acetic anhydride or anisole lead to the maximum amount of catalytic activity. Increasing the anisole/acetic anhydride ratio beyond 0.4:0.2 leads to a drastic reduction in catalytic activity. The selectivity to the para-isomer remains constant with varying the substrate/acylating agent ratio. In contrast to the present study, Jacob *et al.*, [1], and Singh *et al.*, [6], in a study of the benzoylation of o-xylene and toluene, respectively, with benzoyl chloride, reported that an increase in the substrate/acylating agent molar ratio resulted in increased conversion. In contrast, Moreau *et al.*, [2] in a study of the acylation of veratrole with acetic anhydride found that an equimolar mixture led to the highest initial rate of reaction. The decreased activity observed when applying a high anisole/acetic anhydride ratio is probably due to the lower concentration of acetic anhydride in the zeolite intracrystalline volume compared with anisole.

Effect of particle size, and type of substrate/acylating agent

The effect of particle size and type of substrate/acylating agent on the acylation of anisole with acetic anhydride over zeolite Beta is shown in **Figure 3.4.6.1**, and **Figure 3.4.6.2**, which exhibit the yields and the initial rates of reaction respectively. As expected, increasing the particle size, and thus decreasing the surface exposed to reaction, leads to a decrease in catalytic activity, as observed by a decrease in yield and initial rate of reaction when compared with the powdered sample. This observation would suggest that the reaction is influenced by intra-particle diffusion [10]. A common experimental criterion for diffusion control involves an evaluation of the rate of reaction as a function of particle size. At a sufficiently small particle size the measured rate of reaction will become independent of particle size and the rate of reaction can then be safely assumed to be independent of intra-particle mass transfer effects, if the observed rate is inversely proportional to particle size, the reaction is strongly influenced by intra-particle diffusion.

Changing the substrate from anisole to toluene has a detrimental effect on catalytic activity, and no product is observed for the initial 75 minutes of reaction. It is well established that toluene, being a less activated aromatic substrate, does not perform as well as activated aromatics such as anisole and veratrole [11], and thus many of the more recent studies of acylation over zeolite catalysts employ such molecules in favour of toluene [5] [9] [12]. Changing the acylating agent from acetic anhydride to acetic acid leads to a complete loss of catalytic activity under the conditions employed in the present study.

Bhattacharya *et al.*, [13] in a study of the benzoylation of naphthalene to 2-benzoylnaphthalene over zeolite H-Beta also observed similar results. On changing the acylating agent from benzoic anhydride to benzoic acid, no catalytic activity could be observed. Similarly Moreau *et al.*, [2] in a study of the acylation of veratrole with acetic anhydride over zeolite H-Beta found that changing the acylating agent to acetic acid resulted in loss of catalytic activity. The lack of activity of acetic acid in the acylation reaction over zeolite materials has also been observed by other workers [14-16].

CONCLUSION

The study of the effect of different reaction parameters on the catalytic activity of zeolite Beta in the acylation of anisole with acetic anhydride leads to the determination of the optimum reaction conditions. Higher temperature results in increased catalytic activity with negligible loss of selectivity to the p-isomer. Increasing the mass of catalyst also leads to increased catalytic activity, as does decreasing the particle size. The study suggests that operating with an equimolar mixture, or a slight excess of either acylating agent or substrate results in maximum catalytic activity. Increasing the anisole/acetic anhydride ratio beyond 0.4:0.2 leads to a detrimental loss of activity. A judicious choice of substrate and acylating agent is crucial for obtaining maximal catalytic activity; activated molecules lead to significantly greater yields and initial rates of reaction. The apparent activation energy for the reaction was calculated to be 31 kJ mol^{-1} ± 2%.

REFERENCES

(1) Jacob, B.; Sugunan, S.; Singh, A. P. *J. Mol. Catal. : A* 1999, ***139***, 43.

(2) Moreau, P.; Finiels, A.; Meric, P. *J. Mol. Catal. : A* 2000, ***154***, 185.

(3) De Castro, C.; Primo, J.; Corma, A. *J. Mol. Catal. : A* 1998, ***134***, 215.

(4) Ma, Y.; Wang, Q. L.; Jiang, W.; Zuo, B. *Appl. Catal. : A* 1997, ***165***, 199.

(5) Derouane, E. G.; Dillon, C. J.; Bethell, D.; Derouane-Abd Hamid, S. B. *J. Catal.* 1999, ***187***, 209.

(6) Singh, A. P.; Bhattacharya, D.; Sharma, S. *J. Mol. Catal. : A* 1995, ***102***, 139.

(7) Brown, H. C.; Jensen, F. R. *J. Am. Chem. Soc* 1958, ***80***, 2296.

(8) Satterfield, C. N. *Mass Transfer in Heterogeneous Catalysis*; M.I.T Press, 1970.

(9) Freese, U.; Heinrich, F.; Roessner, F. *Catal. Today* 1999, ***49***, 237.

(10) Thomas, J. M.; Thomas, W. J. *Principles and Practice of Heterogeneous Catalysis*; VCH, 1997.

(11) Venuto, P. B. *Microporous Mater.* 1994, ***2***, 297.

(12) Rohan, D.; Canaff, C.; Fromentin, E.; Guisnet, M. *J. Catal.* 1998, ***177***, 296.

(13) Bhattacharya, D.; Sharma, S.; Singh, A. P. *Appl. Catal. : A* 1997, ***150***, 53.

(14) Chiche, B.; Finiels, A.; Gauthier, C.; Geneste, P.; Graille, J.; Pioch, D. *J. Org. Chem.* 1986, ***51***, 2128.

(15) Richard, F.; Carreyre, H.; Pérot, G. *J. Catal.* 1996, ***159***, 427.

(16) Moreau, P.; Finiels, A.; Pelorgeas, S.; Vigneau, O.; Lasperas, M. *Catal. Lett.* 1997, ***47***, 161.

Chapter 3. Results

3.5 The relationship between the concentration and partial positive charge on aluminium and the initial rate of reaction

3.5.1 Abstract

In this section, the role of tetrahedral aluminium in the acylation of anisole with acetic anhydride over zeolite Beta is introduced. In section **3.3**, it was found that the number of Brønsted acid sites in zeolite H-Beta samples governed the catalytic activity, however, it was also found that for transition metal exchanged materials no such relationship existed, and samples with very low concentrations of Brønsted acid sites led to unexpectedly high initial rates of reaction. This result may cast some doubt on a mechanism involving protonation, thus this section deals with an alternative, and as will be shown, a viable explanation which would explain the activity of both the proton-form of zeolite Beta and transition metal exchanged samples.

3.5.2 Background [1]

When two like atoms share an electron pair in covalence, the electrons are evenly shared, because the two atoms attract them equally. At any one instant, the two electrons may be more closely associated with one nucleus than with the other, but the probability of an opposite condition is equally great, so that on a time average, the bond is electrically symmetrical and has no polarity. If one of the bonded atoms has other attachments that are different from those of the second, or if the two bonded atoms are of different elements, they will probably attract the shared electron pair unevenly. This must result in an electrical dissymmetry, or polarity, in the bond. In this case, on a time average, the two bonding electrons may be considered to spend more than half their time more closely associated with the nucleus that originally attracted them more strongly. This relative attraction for bonding electrons is called electronegativity. Electronegativity is a very subtle property that cannot be satisfactorily defined in a very precise manner, or evaluated by direct experiment. However, the meaning of electronegativity can be stated on a relative basis: that atom is more electronegative which acquires more than half share of the bonding electrons. Despite the inability to evaluate electronegativity from direct measurement, a number of indirect and intuitive methods of evaluation have been successfully applied, and this has led to the development of a table containing a summary of the electronegativity values for the elements, calculated by different methods. The extent of agreement among such different methods is remarkable, and demonstrates quite convincingly that electronegativity is indeed an inherent fundamental quality of atoms, despite the fact that a precise and satisfying definition is unavailable. The electronegativity values of the elements have been used widely as a sort of semi-quantitative supplement or reinforcement to chemical intuition. They can provide, by their relative magnitude, whether a given bond will be very polar or only slightly polar, especially if the bond is in a compound containing only two elements. Electronegativity values are capable of much more useful application than has usually been made. They can be used to estimate quantitatively the polarity of bonds and thus the condition of combined atoms. Pauling defines electronegativity as “the power of an atom in a molecule to attract electrons to itself”. Although this really means the electron attracting power that atom had before it combined, the common, misleading, interpretation implies that the atom in the compound still has this power. A much more reasonable concept is that of electronegativity equalization. In order to attain a state of equal attraction, when initially one atom is more electronegative than the other, it is necessary for an equalization of electronegativity to occur. This is possible through uneven sharing on a time-average basis. By spending more than half their time more closely associated with the atom that originally attracted them more (the more electronegative atom), the electrons simultaneously impart a partial negative charge to that atom and reduce its electronegativity. At the same time they leave the other atom with an electron deficiency and therefore a partial positive charge, simultaneously increasing its electronegativity. This adjustment must cease when the electronegativity has become equalized. Only under such conditions would it seem reasonable to distribute bonding electrons between two atoms either by overlap of two atomic orbitals or by formation of molecular orbitals. The other case is that the bonding electrons would be required to fluctuate continuously in energy from one atom to the other, an impossible scenario, or else they would be forced to remain at all times on the originally more electronegative atom, and all covalent bonds except completely nonpolar bonds would have to be completely polar, or ionic. The principle of electronegativity equalization may be stated as: *When two or more atoms initially different in electronegativity combine chemically, they become adjusted to an equal intermediate electronegativity in the compound.* To determine this intermediate value, it is necessary to assume some basis for estimation. Both the arithmetic and geometric means have been investigated, through a comprehensive study of bond lengths, and the geometric mean was found to be superior. A corollary to the principle of electronegativity equalization is: *The electronegativity of all the atoms in a compound is the geometric mean of the electronegativities of all the atoms before combination.* The geometric mean is easily determined with the help of logarithms. Tabulated data found in related textbooks give the S (electronegativity) and log S values of most of the elements. To determine, for example, the S_m (molecular electronegativity) of H_2O, it is necessary to calculate the cube root of the product $S^2_H S_O$. The log of S_O is added to twice the log of S_H and the sum divided by 3, giving the log of S_m. The antilog is S_m. For water, this is $3\sqrt{(3.55\times3.55\times5.21)} = 4.03$, where $S_H = 3.55$ and $S_O = 5.21$. The process of electronegativity equalization has decreased the electronegativity of oxygen by 5.21 – 4.03, or 1.18, while increasing the electronegativity of hydrogen by 4.03 – 3.55, or 0.48. The next stage is to determine what partial charges on these atoms would account for these electronegativity changes. It was found that there is a linear relationship between the square root of the total ionization energy and the charge, in a sequence of atoms produced from the same atom. A reasonable assumption, therefore, is that the electronegativity of an atom varies linearly with partial charge. If the electronegativity change produced by unit charge (± one electron) is known, it is possible to use this assumption of linearity to compute the partial charge corresponding to any lesser electronegativity change. That is, the partial charge could be defined and determined as the ratio of the actual electronegativity change, produced by the atoms combining with other atoms, to the electronegativity change that would result from acquisition of unit charge:

Equation 3.5.2.1

$$\delta_E = \frac{\Delta S_{E \to m}}{\Delta S_{E \to E\pm}} = \frac{S_m - S_E}{\Delta S_{E \to E\pm}}$$

Unfortunately, no experimental determination of partial charge or bond polarity has been accomplished. An arbitrary choice may be made, however, which can lead to reasonable relative charge values, and these are of great value in comparative chemistry. For this purpose, an isolated molecule of NaF was taken to be 75 per cent ionic. In other words, the charge on sodium was assumed to be 0.75, and that of fluorine –0.75 (electronic charge). The electronegativity of fluorine is 5.75, and that of sodium is 0.70. The value in the NaF molecule is then taken as the geometric mean of 5.75 and 0.70, which calculates to 2.01. In the process of combining with sodium, fluorine has become less electronegative by 5.75 - 2.01, or 3.74. If this is 75% of the change that would have occurred if the fluorine had acquired an electron completely, then the total change corresponding to acquisition of unit charge is 3.74 / 0.75, or 4.99. Similarly, the electronegativity of sodium has increased, by its combining with fluorine, by 2.01 - 0.70, or 1.31. If sodium had lost an electron completely, its electronegativity would have increased by 1.31 / 0.75, or 1.74. These values, 4.99 for fluorine, and 1.74 for sodium, are extremely useful. The partial charge on any combined atom was defined above as the ratio of the electronegativity change it underwent in combining to the electronegativity change it would have undergone had it acquired unit charge. Therefore in any fluoride compound, the partial charge on fluorine can easily be calculated by first determining the electronegativity in the compound, from this determining how much was the decrease from the electronegativity of elemental fluorine, and then dividing this decrease by 4.99. Similarly, in any sodium compound, the partial charge on sodium can be calculated by first determining the electronegativity in the compound, then subtracting from this the value 0.70 for elemental sodium, and then dividing the difference by 1.74. Once these values have been established, 4.99 for fluorine and 1.74 for sodium, similar parameters for all the rest of the chemical elements can be obtained. Thus, the partial charge on the sodium and the fluorine can be calculated as shown below:

$$\delta_{\mathrm{E}} = \frac{S_m - S_E}{\Delta S_{E \rightarrow E\pm}} = \frac{2.01 - 5.75}{4.99} = -0.75$$

$$\delta_{\mathrm{E}} = \frac{S_m - S_E}{\Delta S_{E \rightarrow E\pm}} = \frac{2.01 - 0.70}{1.74} = 0.75$$

3.5.3 Determination of the partial charge on aluminium in ion-exchanged and the H-form of zeolite Beta

Using a similar technique it is possible to determine the partial charge on aluminium in zeolite Beta where the compensating cation is either a proton, sodium, copper, or iron. **Figure 3.5.3.1** shows the fragment taken into consideration when calculating the partial charge.

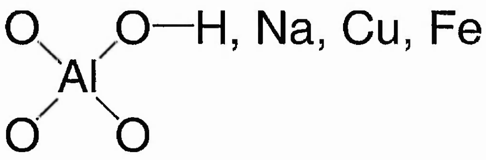

Figure 3.5.3.1 Molecular unit used for calculation of partial charge.

Determination of the partial charge on aluminium in Fe Beta

$$\delta_E = \frac{S_m - S_E}{\Delta S_{E \rightarrow E\pm}}$$

Where: δ_E = Partial charge

S_m = Molecular electronegativity

S_E = Electronegativity of element

$\Delta S_{E \rightarrow E\pm}$ = Electronegativity resulting from acquisition of unit charge

S_m = (Molecular electronegativity) of AlO_4Fe

$S_m = S^4{}_O\, S_{Al}\, S_{Fe}$ where $S_O = 5.21$, $S_{Al} = 2.25$, $S_{Fe} = 2.10$

$S_m = \log 5.21 + \log 5.21 + \log 5.21 + \log 5.21 + \log 2.25 + \log 2.10$

$S_m = 0.7168 + 0.7168 + 0.7168 + 0.7168 + 0.3522 + 0.3222$

$S_m = 3.5416$

$$S_m = \frac{3.5416}{6} = 0.5902$$

S_m = Antilog $0.5902 = \mathbf{3.8928}$

$$\delta_E = \frac{S_m - S_E}{\Delta S_{E \rightarrow E\pm}}$$

$$\delta_E = \frac{3.89 - S_E}{\Delta S_{E \rightarrow E\pm}}$$

$S_E(Al) = 2.25$

$$\delta_E = \frac{3.89 - 2.25}{\Delta S_{E \to E\pm}}$$

$$\Delta S_{E \to E\pm}\ (\mathrm{Al}) = 3.16$$

$$\delta_E = \frac{3.89 - 2.25}{3.16}$$

$$\delta_E = \frac{1.64}{3.16}$$

$$\delta_E = \mathbf{0.520}$$

The partial charge of the proton, sodium, and copper form of zeolite Beta was calculated in the same way and is shown in **Table 3.5.3.1**.

Molecular unit	S_m	S_E (Al)	$\Delta S_{E \to E\pm}$	δ_E (Al)
AlO_4Fe	3.89	2.25	3.16	**0.520**
AlO_4H	4.25	2.25	3.16	**0.633**
AlO_4Cu	4.03	2.25	3.16	**0.565**
AlO_4Na	3.24	2.25	3.16	**0.314**

Table 3.5.3.1 Partial charge of aluminium in various zeolite Beta samples.

3.5.4 Determination of the charge concentration of aluminium in ion-exchanged and the H-forms of zeolite Beta

Now that the partial charge of aluminium in various zeolite Beta samples has been established, the next stage is to work out the 'charge concentration'; this takes into consideration partial charge, and the concentration of tetrahedral aluminium in the various samples. The value for the concentration of tetrahedral aluminium in different samples is taken as the concentration of Brønsted acid sites as determined from ammonia adsorption in the FTIR spectrometer as discussed in section **3.1**. Since each negatively charged aluminium atom in the zeolite lattice must be compensated by a proton in the H-forms of zeolite Beta, then the intensity of the NH_4^+ band normalized to the intensity of the lattice overtones must give a relative value for the number of Brønsted acid sites in each sample, and hence the concentration of tetrahedral aluminium. For ion exchanged samples, depending on the level of exchange, the compensating cation can be either a proton or the cation corresponding to that sample (copper for Cu Beta, iron for Fe Beta and so on), clearly the presence of cations other than protons will not be observed by an increase in intensity of the NH_4^+ band during ammonia adsorption. In this case, the concentration of tetrahedral aluminium is taken as the same value as calculated for NH_4^+-β-12.5-A-773-1, since this is the form from which all ion exchanged samples were prepared, and the activation procedure used in the preparation of this sample was identical to that carried out for ion exchanged samples, it can be assumed that ion exchanged samples contain the same concentration of tetrahedral aluminium as contained within NH_4^+-β-12.5-A-773-1. There is of course the possibility that aluminium has been lost from the framework during successive ion exchange procedures and subsequent activation, however X-ray diffraction data presented in section **3.1** suggest that no aluminium has been lost from the framework in ion exchanged materials. The model calculation below shows how the 'charge concentration' was calculated for NH_4^+-β-12.5-A-773-1, and the 'charge concentration' of all samples are summarized in **Table 3.5.4.1**.

Model calculation for the determination of the 'charge concentration' of Al in NH_4^+-β-12.5 -A-773-1

Step 1. Determination of the relative concentration of tetrahedral aluminium

The relative concentration of Brønsted acid sites present in NH_4^+-β-12.5-A-773-1 as determined by ammonia adsorption and FTIR is **0.539** (see **table 3.1.3.2**), thus the concentration of tetrahedral aluminium is also **0.539**.

Step 2. Subtracting the partial charge of aluminium in Na Beta from the partial charge of aluminium in the sample to be calculated

It was found in section **3.3** that Na Beta is not active in aromatic acylation, thus subtracting the partial charge of aluminium in Na Beta from all other samples gives a value of zero for Na Beta, and hence the charge concentration of Na beta is also zero, in order to normalise for the fact that no activity on Na Beta was observed. This zero point is somewhat arbitrary since it is not possible to access the limiting partial charge where no reaction occurs.

Equation 3.5.4.1 $\delta_E \mathrm{Al(cation)} - \delta_E \mathrm{Al(Na)}$

$$0.633 - 0.314 = 0.319$$

Step 3. Determination of the concentration of active sites in 1g of 'as received' zeolite Beta

SiO_2 / Al_2O_3 mole ratio = 25
Si / Al ratio = 12.5

Relative molecular mass of $(SiO_2)_{12.5}(AlO_2H)$:

25 × O (25 × 15.9994) = **399.99**

12.5 × Si (12.5 × 28.0855) = **351.07**

1 × Al = **26.98**

2 × O (2 × 15.9994) = **32.00**

1 × H = **1.01**

= **811.05**

Number of moles of active sites in 1g of 'as received' zeolite Beta:

$$\frac{1}{811.05} = \mathbf{1.23 \times 10^{-3}\ mol / g}$$

Step 4. Determination of 'charge concentration' by substituting the calculated values into the 'charge concentration' equation

Equation 3.5.4.2 $$\delta_C = \left(\frac{TAC}{TAC_{H\text{ - Beta}}}\right) \times (\delta_E Al(cation) - \delta_E Al(Na)) \times MASZB$$

Where: TAC = Tetrahedral aluminium concentration of sample to be calculated

$TAC_{H\text{-Beta}}$ = Tetrahedral aluminium concentration of NH_4^+-β-12.5 - A-773-1

$\delta_E Al(cation) - \delta_E Al(Na)$ = Partial charge of aluminium in sample to be calculated minus the partial charge of aluminium in Na Beta

MASZB = Moles of active sites in 1 g of 'as received' zeolite Beta

$$\delta_C = \left(\frac{0.539}{0.539}\right) \times 0.319 \times 1.23 \times 10^{-3} = \underline{\mathbf{3.92 \times 10^{-4}\ mol\ g^{-1}}}$$

Table 3.5.4.1 The charge concentration of aluminium in different zeolite Beta samples.

Zeolite Beta Sample	Brønsted acid site concentration (BASC)	Tetrahedral aluminium concentration (TAC)	S_m	δ_EAl	δ_EAl(cation) – δ_EAl(Na)	TAC × δ_EAl	No. moles of active sites in 1g of zeolite Beta (MASZB)	**Charge concentration (δ_C) [mol g^{-1}] ± 2%*** $\left(\frac{\mathrm{TAC}}{\mathrm{TAC}_{\mathrm{H-Beta}}}\right)\times(\delta_E\mathrm{Al(cation)} - \delta_E\mathrm{Al(Na)})\times\mathrm{MASZB}$
NH_4^+-β-12.5-A-773-1	0.539	0.539	4.249	0.633	0.319	0.341	0.00123	0.000392
NH_4^+-β-12.5-A-1023-8	0.183	0.183	4.249	0.633	0.319	0.116	0.00123	0.000133
R1-H^+-β-12.5-A-773-1	0.410	0.410	4.249	0.633	0.319	0.260	0.00123	0.000298
R2-H^+-β-12.5-A-773-1	0.350	0.350	4.249	0.633	0.319	0.222	0.00123	0.000255
R3-H^+-β-12.5-A-773-1	0.321	0.321	4.249	0.633	0.319	0.203	0.00123	0.000231
EDTA-β-12.5-A-773-1	0.271	0.271	4.249	0.633	0.319	0.172	0.00123	0.000197
Steamed2h-β-12.5-A-773-1	0.225	0.225	4.249	0.633	0.319	0.142	0.00123	0.000164
Steamed6h -β-12.5-A-773-1	0.195	0.195	4.249	0.633	0.319	0.123	0.00123	0.000142
Na-β-12.5-A-773-1	0.009	0.539	3.242	0.314	0	0.169	0.00123	0
Cu-β-12.5-A-773-1	0.203	0.539	4.034	0.565	0.251	0.304	0.00123	0.000309
Fe-β-12.5-A-773-1	0.096	0.539	3.893	0.520	0.206	0.280	0.00123	0.000253

* Approximate experimental error expressed as the coefficient of variation.

Figure 3.5.4.1 shows a plot of charge concentration versus the initial rate of reaction for the entire range of zeolite Beta materials.

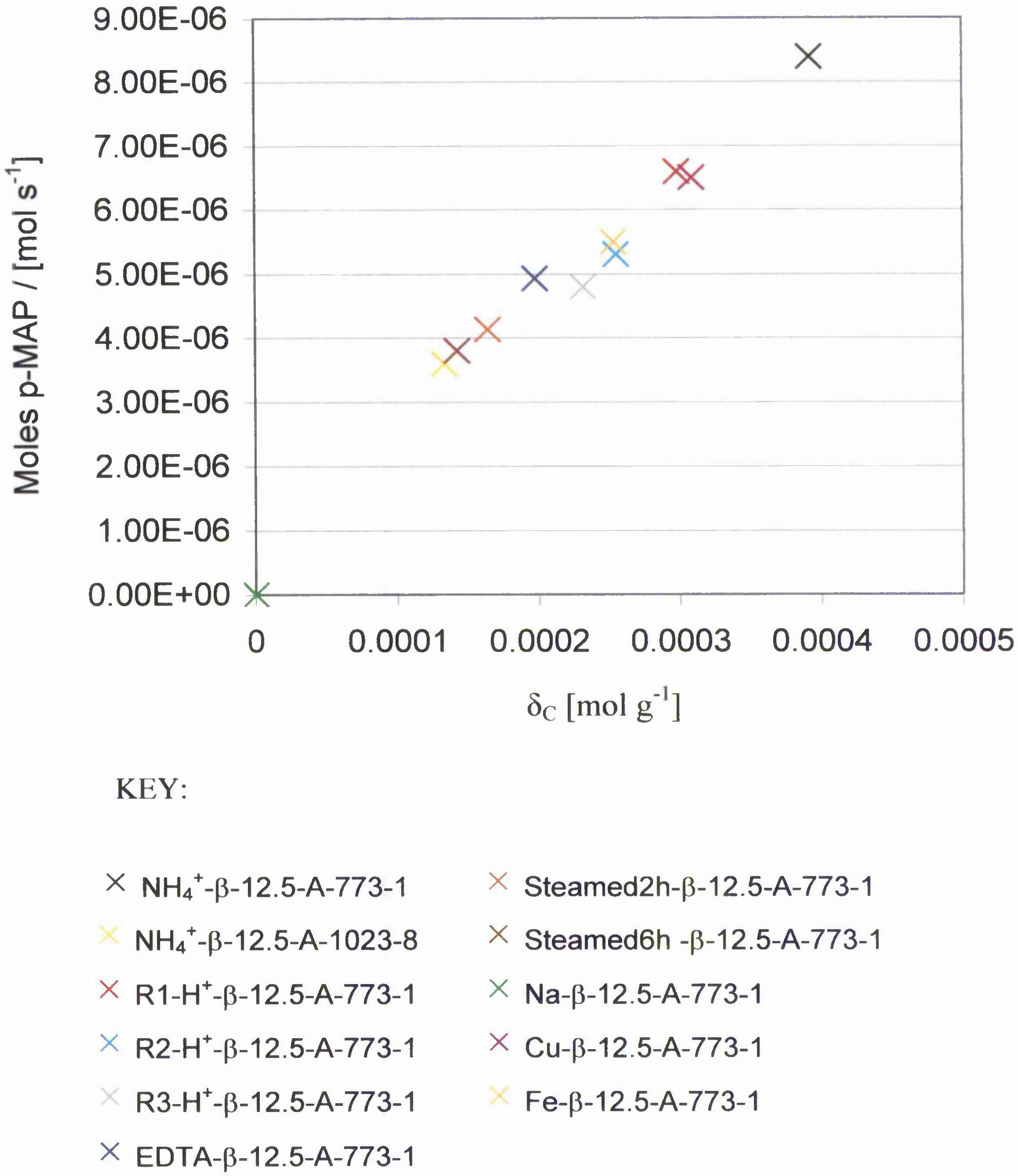

Figure 3.5.4.1 Plot of 'charge concentration' versus initial rate of reaction.

Initial rates of reaction were calculated in section **3.3** and are shown in **Table 3.3.3.1**. For purposes of comparison **Figure 3.5.4.2** shows the plot of Brønsted acid site concentration versus initial rate of reaction, transition metal forms are included.

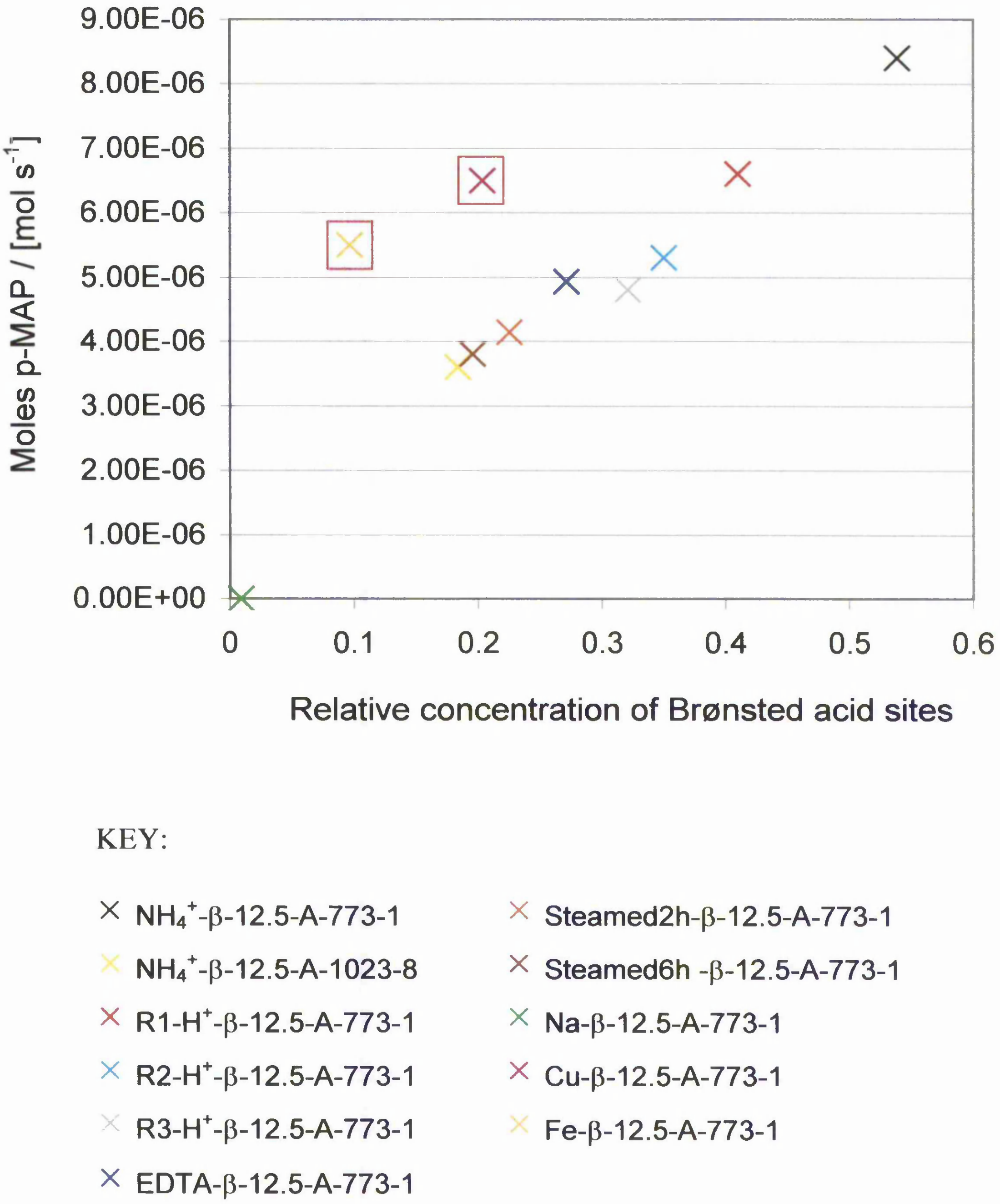

Figure 3.5.4.2 Plot of relative Brønsted site concentration versus initial rate of reaction.

DISCUSSION

It is evident from **Figure 3.5.4.1** that plotting the 'charge concentration' of aluminium versus the initial rate of reaction results in a very reasonable linear relationship. In section **3.3** a linear relationship was found between the relative Brønsted acid site concentration and the initial rate of reaction for H-Beta samples, however the relationship did not hold when transition metal exchanged samples were included in the plot (see **Figure 3.5.4.2**). This cast some doubt on a mechanism involving Brønsted acid sites. However, the strong relationship between the number of Brønsted acid sites and the initial rate of reaction for H-forms of zeolite Beta seemed more than mere coincidence. Since the number of Brønsted acid sites in zeolites approximately equals the number of framework tetrahedral aluminium atoms, it would seem reasonable to consider the latter as potential active species. If the tetrahedral aluminium acts as a Lewis site, both proton and transition metal forms of zeolite Beta could exhibit activity. Under the assumption that the active site for aromatic acylation over zeolite Beta is tetrahedral aluminium acting as a Lewis acceptor, it would expected that the partial charge on the aluminium will have an influence on the reactivity over the catalyst. Indeed, calculating the partial positive charge on aluminium in both the proton and transition metal exchanged forms of zeolite Beta using the Sanderson model outlined above leads to the linear relationship in **Figure 3.5.4.1**, where the points representing both the Cu and Fe-forms of zeolite Beta are shifted into a linear position. If framework aluminium is assumed to be at the centre of the active site, with its activity governed by its partial positive charge, the differences in activity across the full range of zeolite Beta samples can be understood. As already mentioned, in H-Beta, Brønsted acid sites are closely associated with framework aluminium species, and so their concentration parallels the number of tetrahedral aluminium sites present. For these materials, the activity may parallel the number of Brønsted sites present, even if they are not directly involved in the catalytic reaction. In copper and iron-exchanged zeolite Beta, tetrahedral aluminium is of course still present, as evidenced by XRD results in section **3.1**, and thus the active site is still present. The different transition metals, and the zeolite protons in H-Beta, will however, give rise to different partial positive charges on the aluminium, and thus their activities would be expected to differ. In an early report by Chiche *et al.*, [2], dependency of the rate of acylation over zeolites as a function of the partial charge on the aromatic substrate was claimed. By comparison of differently substituted aromatic substrates, it was concluded that in cases where no shape selectivity is observed, the extent of the negative charge on the aromatic carbon determines the reactivity for a given electrophile. If the acylium cation is adsorbed in the transition state (see section **3.8**), this argument of course has to hold true for the electrophile, thus a higher positive partial charge on the electrophile and a larger concentration of these charges induced by the aluminium would be expected to increase the rate.

CONCLUSION

The catalytic performance of all zeolite Beta materials is linearly related to the concentration of tetrahedral framework aluminium, and to its partial positive charge. The unexpectedly high activity of Fe and Cu zeolite Beta, despite having significantly reduced numbers of Brønsted acid sites, can be accounted for under the assumption that framework tetrahedral aluminium acts as the active site. If framework tetrahedral aluminium is the active site, it must act as a Lewis acid site, with the activity being governed by the extent of its partial positive charge.

REFERENCES

(1) Sanderson, R. T. *Inorganic Chemistry*; Reinhold, 1967.

(2) Chiche, B.; Finiels, A.; Gauthier, C.; Geneste, P. *Appl. Catal.* 1987, 365.

Chapter 3. Results

3.6 The influence of the adsorption of reactants and products on the coordination environment of aluminium in zeolite Beta

3.6.1 Abstract

In section **3.5**, a very good linear relationship was observed between the 'charge concentration' of framework tetrahedral aluminium and the initial rate of reaction for the entire range of zeolite Beta samples, suggesting that framework tetrahedral aluminium may be the active site. The possibility of a Brønsted acid catalysed process was thought to be unlikely since the high degree of linearity observed between the Brønsted acid site concentration and the initial rate of reaction for H-forms of zeolite Beta was lost when transition metal exchanged zeolites were included into the plot. The latter materials exhibited unusually high initial rates despite having low concentrations of Brønsted acid site. If framework tetrahedral aluminium is the active site, a study to determine the effect of the adsorption of reactants and products on the coordination environment of aluminium in zeolite Beta employing ^{27}Al MAS NMR may lead to valuable information regarding the interactions occurring at the active site, and yield further insight into the mechanism of reaction. This section deals with the interpretation of those results.

3.6.2 Background

There are several examples in the literature demonstrating that *in situ* solid state MAS NMR is a powerful tool to understand reaction mechanisms based on the study of the nature, dynamics, and reactivity of surface intermediates and active sites in zeolite-catalysed systems [1-3]. The presence of four, five, and sixcoordinate aluminium in zeolites can be ascertained by ^{27}Al MAS NMR. However, aluminium has a half-integer quadrupolar spin complicating the interpretation of ^{27}Al MAS NMR spectra. The second order quadrupolar interaction of the central transition causes resonances to move from their isotropic chemical shift (δ_{ISO}), by the quadrupolar induced shift (δ_{QIS}), and broaden into specific powder line shapes, even under MAS conditions. In some cases, broadening is so severe that it results in some ^{27}Al NMR invisible peaks. In order to make them appear, the sample should be pre-treated with acetylacetone before the ^{27}Al NMR spectrum is measured [4]. The regular framework coordination of aluminium in the zeolite framework is tetrahedral, however, as pointed out by many authors [4-7], octahedral aluminium can be formed quite readily in zeolite Beta by thermal, hydrothermal, and chemical modification. Bourgeat-Lami *et al.*, [4] stated that octahedrally coordinated and NMR invisible aluminium must be regarded as an inherent part of the framework of zeolite Beta, their formation explained by a distortion of aluminium sites caused by the high electron affinity of the proton. The formation of penta-coordinated and/or highly distorted tetrahedral aluminium has also been observed in zeolite Beta samples calcined to high temperature [8]. Several studies point to the flexibility of the coordination sphere of the aluminium atoms in zeolite Beta [2] [6] [7] [9] [10], which facilitate the formation of higher coordination symmetries of the aluminium atoms. The relative amounts of framework tetrahedral and octahedral aluminium in zeolite Beta have been shown to be largely dependent on pretreatment [4] [7]. Kiricsi *et al.*, [7] applied FTIR and MAS NMR to study the changes induced by various calcination conditions, temperature treatments and interactions with molecules such as ammonia, benzene, n-hexane, and water. Bourgeat-Lami *et al.*, [4] studied the influence of cations such as Na^+, K^+, NH_4^+, and protons on the state of aluminium atoms in zeolite Beta. The results from these studies would suggest that framework aluminium adopts a tetrahedral symmetry when protons are not the charge compensating cations. Those aluminium atoms that have adopted another coordination symmetry but are still connected to the framework can revert back to tetrahedral coordination by ion exchange with cations such as Na^+ and K^+, and by adsorption of ammonia [4]. However, not all tetrahedral/octahedral transformations are reversible, as reported by Kuehl *et al.*, [11], when zeolite Beta is severely steamed, a substantial proportion of the framework aluminium is completely hydrolysed, and non-framework aluminium species are formed. More recently, an interesting study by Haouas *et al.*, [2] concerning the nitration of toluene with nitric acid and acetic anhydride yielded some interesting results. The reversible transformation of framework aluminium from a tetrahedral into an octahedral environment was observed by ^{27}Al MAS NMR upon interaction of zeolite H-Beta with different components of the nitrating system. It was suggested, by the same authors, that the narrow width of the ^{27}Al NMR signal of the octahedral framework aluminium complexes formed when nitrate ions interact with the zeolite wall points towards the necessity of the opening of the Si-O-Al bond in the lattice, allowing the accommodation of a very high symmetry environment. The dynamic character of those aluminium atoms that are only partially connected to the framework were thought to play the key role in the catalytic activity and selectivity of nitration over zeolite H-Beta. Thus, framework aluminium was suggested to be the active site in the reaction, where the initial step of nitration occurs through the formation of a framework octahedral complex formed as a result of interaction of the nitric acid with framework tetrahedral aluminium, which would then react with an incoming acetic anhydride molecule to give the adsorbed reactive species, acetylnitrate.

3.6.3 The effect of adsorption of acetic anhydride, anisole, and p-MAP on the coordination environment of aluminium in zeolite Beta samples

Adsorption of acetic anhydride on NH_4^+-β-12.5-V-773-1, Cu-β-12.5-V-773-1, and Na-β-12.5-V-773-1

Figure 3.6.3.1 shows the fitted ^{27}Al MAS NMR spectrum of NH_4^+-β-12.5-V-773-1. **Figure 3.6.3.2** and **Figure 3.6.3.3** show the fitted ^{27}Al MAS NMR spectra of NH_4^+-β-12.5-V-773-1 with acetic anhydride adsorbed at 333 K, and 398 K, respectively. **Figure 3.6.3.4** and **Figure 3.6.3.5** shows the fitted ^{27}Al MAS NMR spectra of Cu-β-12.5-V-773-1 and Na-β-12.5-V-773-1 after adsorption of acetic anhydride at 333 K.

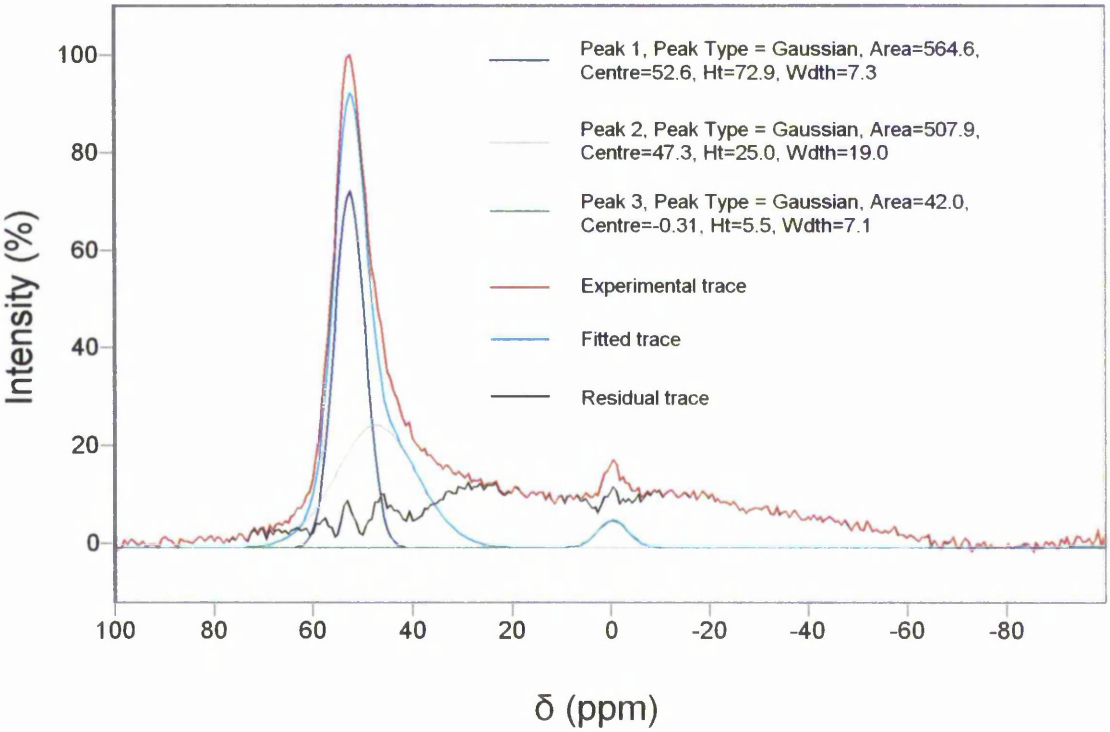

Figure 3.6.3.1 Fitted ^{27}Al MAS NMR spectrum of NH_4^+-β-12.5-V-773-1.

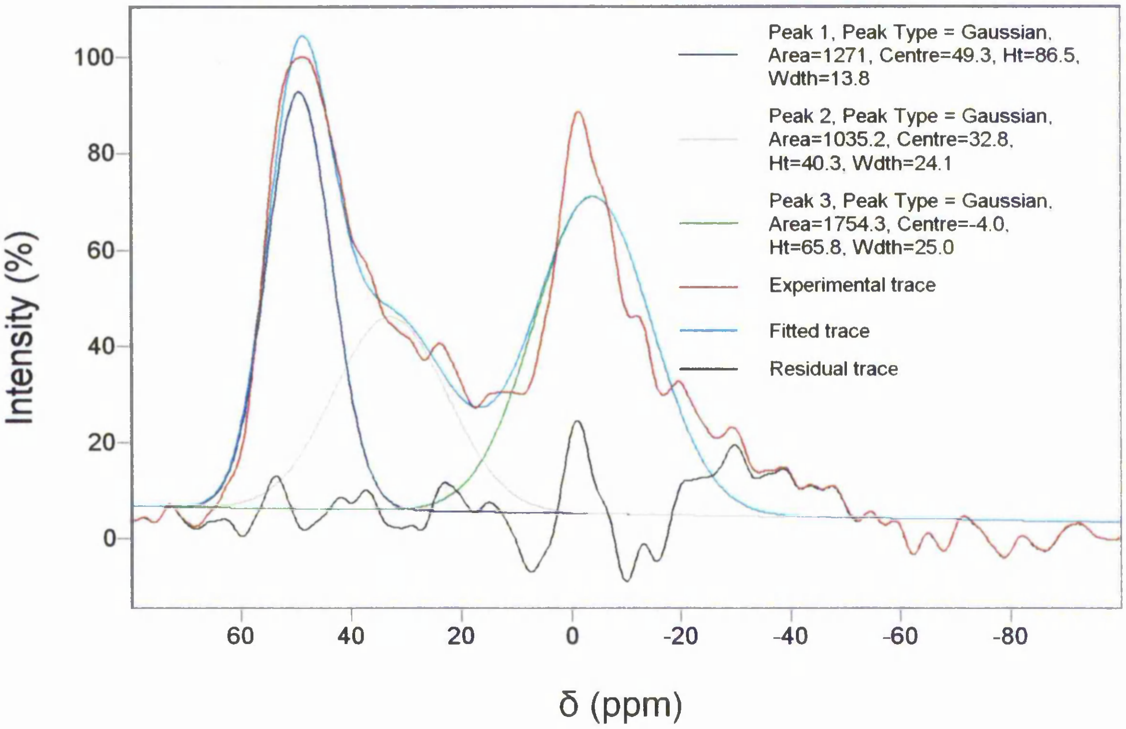

Figure 3.6.3.2 Fitted ^{27}Al MAS NMR spectrum of NH$_4^+$-β-12.5-V-773-1 with acetic anhydride adsorbed at 333 K for 1 h.

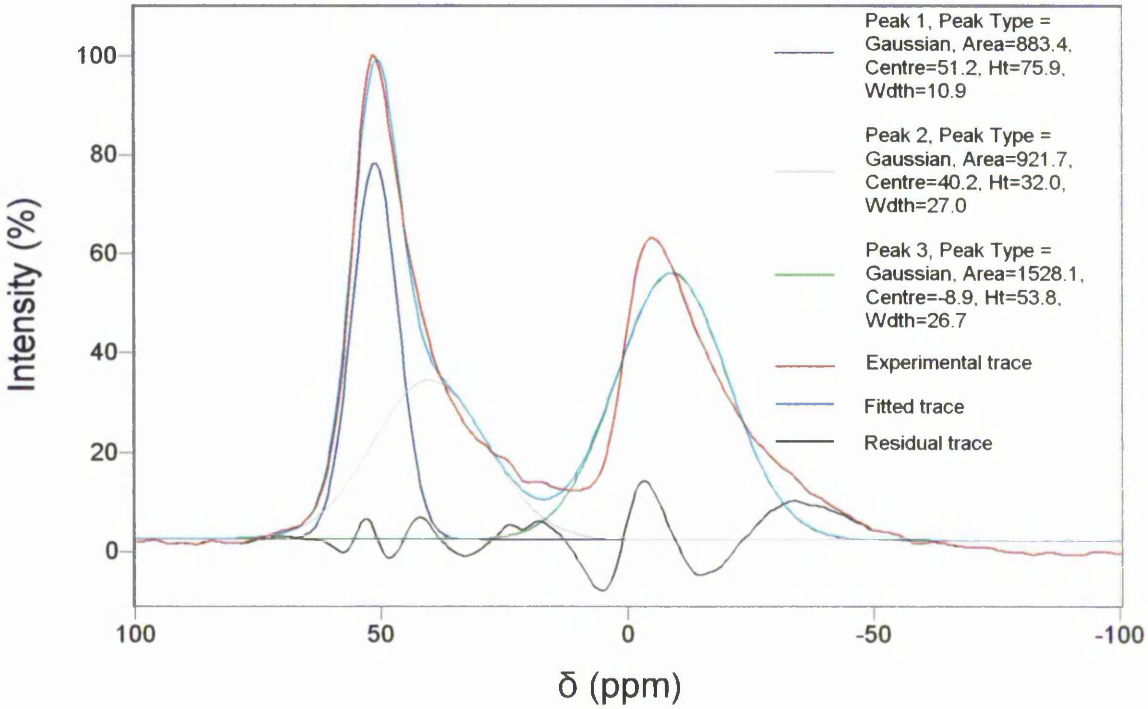

Figure 3.6.3.3 Fitted ^{27}Al MAS NMR spectrum of NH$_4^+$-β-12.5-V-773-1 with acetic anhydride adsorbed at 398 K for 1 h.

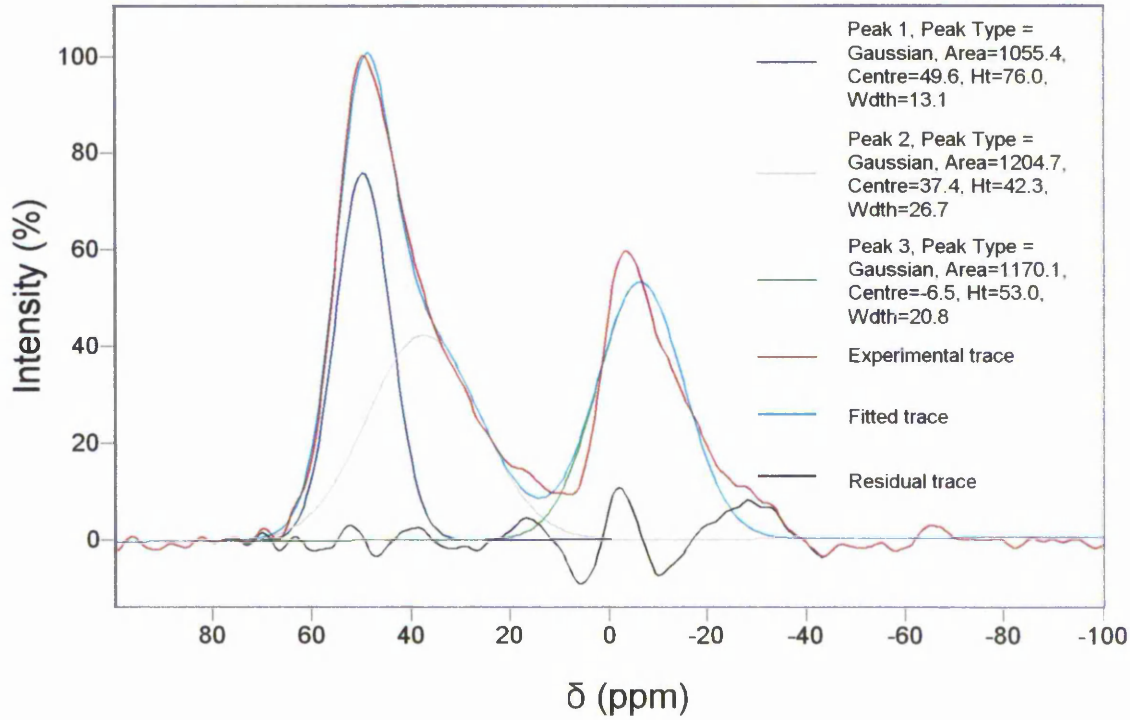

Figure 3.6.3.4 Fitted ^{27}Al MAS NMR spectrum of Cu-β-12.5-V-773-1 with acetic anhydride adsorbed at 333 K for 1 h.

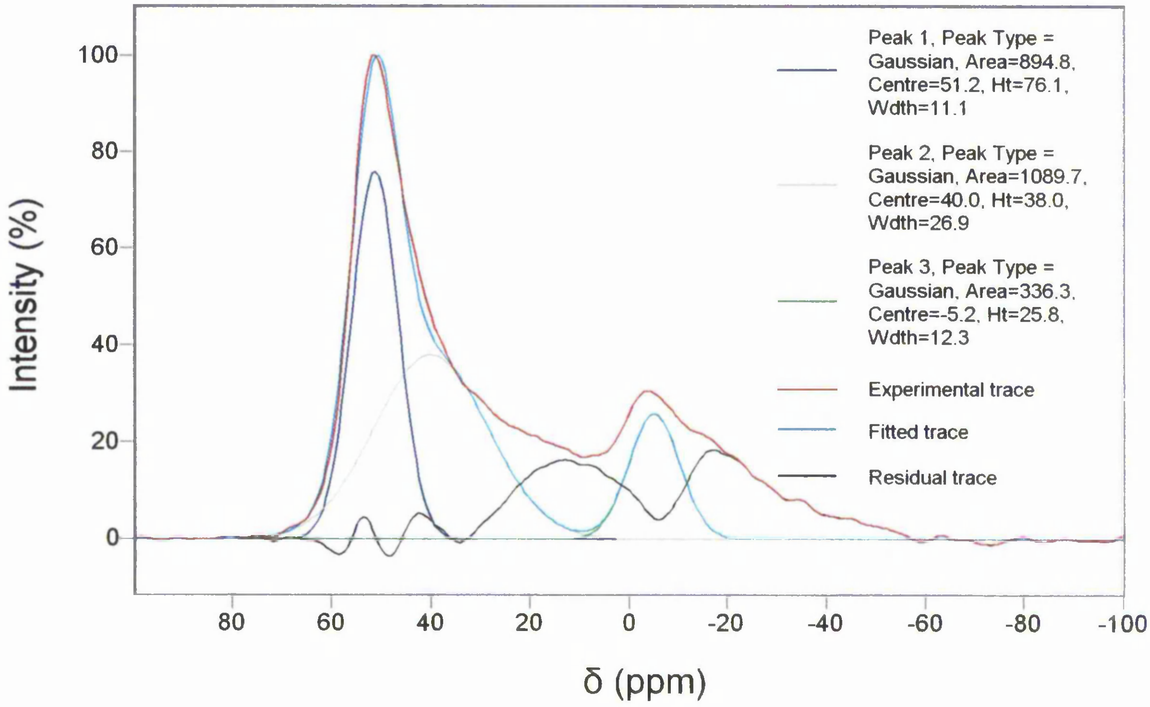

Figure 3.6.3.5 Fitted ^{27}Al MAS NMR spectrum of Na-β-12.5-V-773-1 with acetic anhydride adsorbed at 333 K for 1 h.

Figure 3.6.3.6 shows the fitted ^{27}Al MAS NMR spectrum of NH_4^+-β-12.5-V-773-1 after acetic anhydride adsorption at 333 K, and subsequent desorption at 773 K for 1 h.

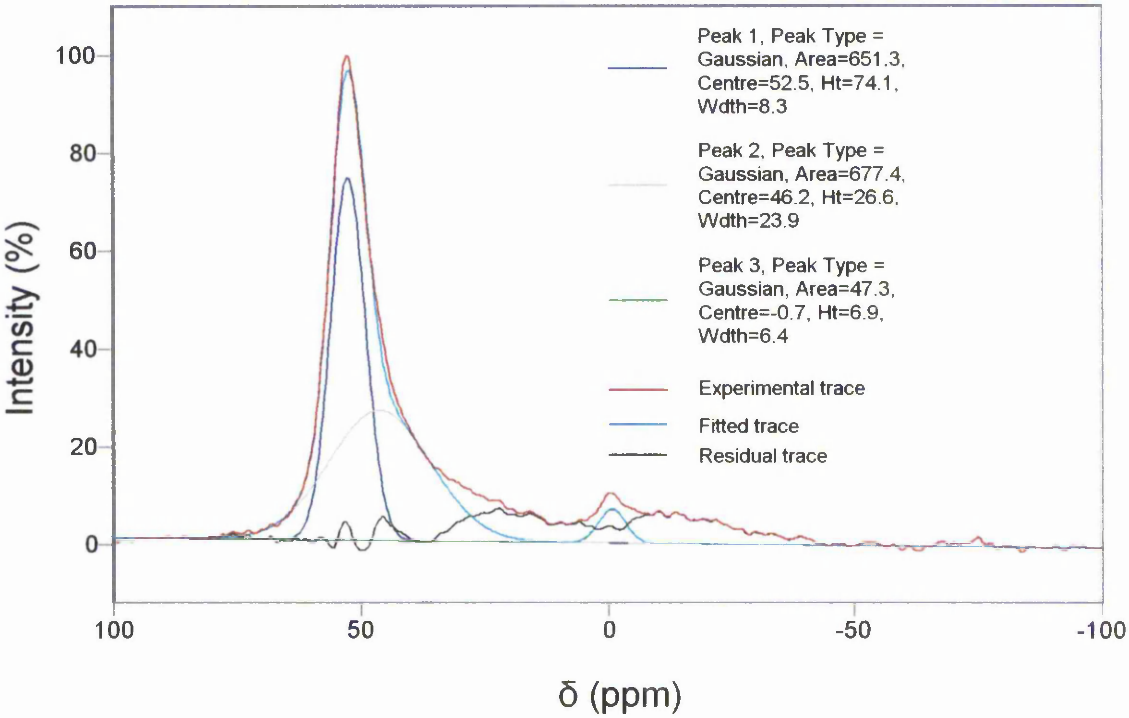

Figure 3.6.3.6 Fitted ^{27}Al MAS NMR spectrum of NH_4^+-β-12.5-V-773-1 after acetic anhydride adsorption at 333 K, and subsequent desorption at 773 K for 1 h.

Adsorption of anisole on NH_4^+-β-12.5-V-773-1

Figure 3.6.3.7 shows the fitted ^{27}Al MAS NMR spectrum of NH_4^+-β-12.5-V-773-1 with anisole adsorbed at 333 K.

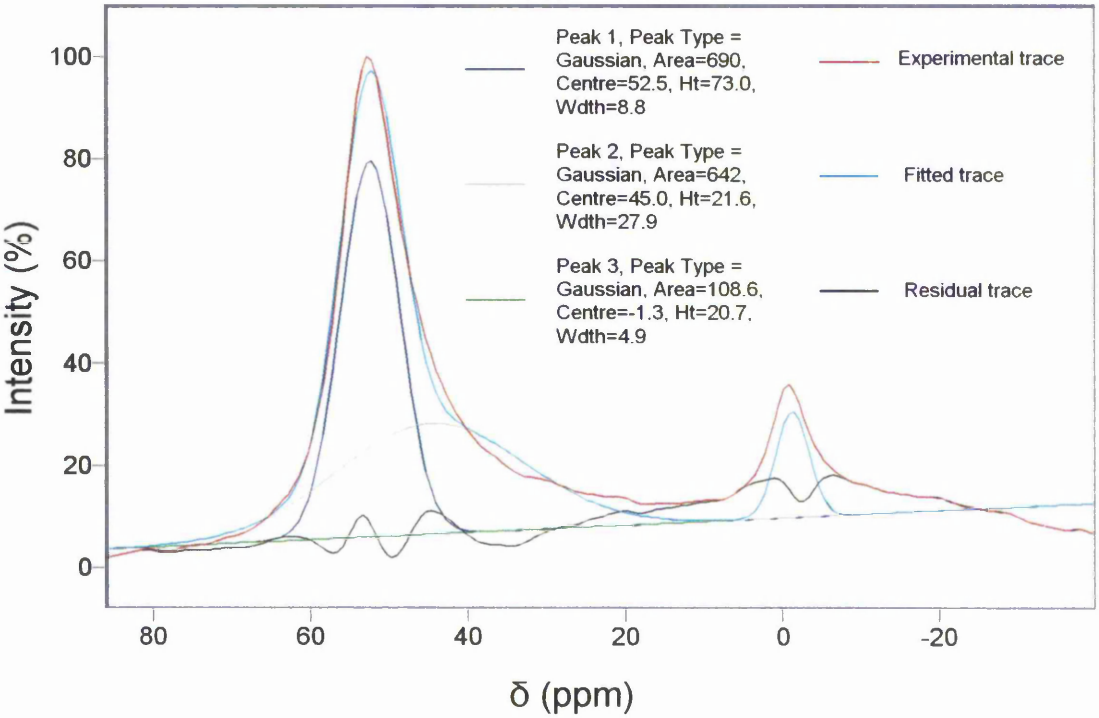

Figure 3.6.3.7 Fitted ^{27}Al MAS NMR spectrum of NH_4^+-β-12.5-V-773-1 with anisole adsorbed at 333 K for 1 h.

Adsorption of p-MAP on NH_4^+-β-12.5-V-773-1

Figure 3.6.3.8 shows the fitted ^{27}Al MAS NMR spectrum of NH_4^+-β-12.5-V-773-1 with p-MAP adsorbed at 333 K.

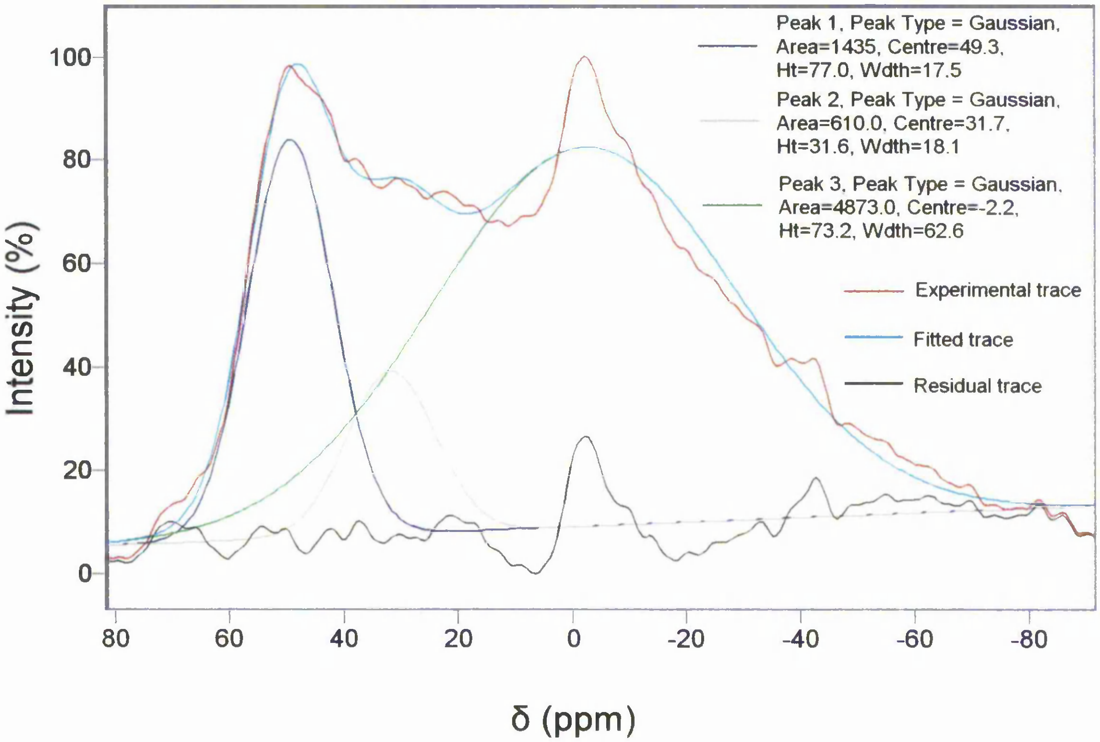

Figure 3.6.3.8 Fitted ^{27}Al MAS NMR spectrum of NH_4^+-β-12.5-V-773-1 with p-MAP adsorbed at 333 K for 1 h.

Table 3.6.3.1 summarises the results obtained from **Figure 3.6.3.1** to **Figure 3.6.3.8**.

Table 3.6.3.1 Relative amounts of tetrahedral, distorted tetrahedral/penta-coordinated, and octahedral aluminium in zeolite Beta samples after adsorption of reactants and products.

Sample	Fitted ^{27}Al MAS NMR spectra					
	Peak 1		Peak 2		Peak 3	
	Position (ppm)	Area %	Position (ppm)	Area %	Position (ppm)	Area %
NH_4^+-β-12.5-V-773-1	52.6	50	47.3	46	-0.31	4
NH_4^+-β-12.5-V-773-1 (Acetic anhydride adsorbed at 333 K)	49.3	31	32.8	26	-4.0	43
NH_4^+-β-12.5-V-773-1 (Acetic anhydride adsorbed at 398 K)	51.2	26	40.2	28	-8.9	46
Cu-β-12.5-V-773-1 (Acetic anhydride adsorbed at 333 K)	49.6	31	37.4	35	-6.5	34
Na-β-12.5-V-773-1 (Acetic anhydride adsorbed at 333 K)	51.2	39	40.0	47	-5.2	14
NH_4^+-β-12.5-V-773-1 (Acetic anhydride desorbed)	52.5	47	46.2	49	-0.7	4
NH_4^+-β-12.5-V-773-1 (Anisole adsorbed at 333 K)	52.5	48.0	45.0	44.4	-1.3	7.6
NH_4^+-β-12.5-V-773-1 (p-MAP adsorbed at 333 K)	49.3	21	31.7	9.0	-2.2	70

DISCUSSION

Figure 3.6.3.1 to **Figure 3.6.3.6** show fitted ^{27}Al MAS NMR spectra of various zeolite Beta samples with and without acetic anhydride adsorbed, and the relative amounts of tetrahedral, distorted tetrahedral/penta-coordinated, and octahedral aluminium are presented in **Table 3.6.3.1**. As was discussed in section **3.1**, peaks at 52, 30-50, and 0 ppm can be attributed to tetrahedral, penta-coordinated or distorted tetrahedral, and octahedral aluminium respectively [12]. The ^{27}Al MAS NMR spectrum of the carefully calcined sample, NH_4^+-β-12.5-V-773-1, was discussed in section **3.1** and exhibits peaks at 52.6, 47.3, and 0 ppm accounting for 50, 46, and 4% of the total amount of aluminium in the sample, and which were assigned to undistorted tetrahedral aluminium, slightly distorted tetrahedral aluminium, and octahedral aluminium respectively. The high proportion of slightly distorted tetrahedral aluminium atoms in NH_4^+-β-12.5-V-773-1 was thought to be due to the presence of nearby defects, which are an inherent characteristic of the structure of zeolite Beta. After adsorption of acetic anhydride at 333 K, some very interesting changes occur in the ^{27}Al MAS NMR spectrum. The most dramatic change is the conversion of approximately 40% of the framework tetrahedral aluminium atoms into framework octahedral symmetry upon adsorption of acetic anhydride. Both undistorted and slightly distorted tetrahedral aluminium atoms were subject to this transformation, with approximately half of each species been converted to octahedral aluminium. In addition, the peak that is indicative of slightly distorted tetrahedral aluminium is shifted from 47.3 ppm in NH_4^+-β-12.5-V-773-1 with no anhydride adsorbed to 32.8 ppm. This result would suggest that the formation of significant amounts of octahedral aluminium results in an increased distortion of those tetrahedral aluminium sites that were only slightly distorted in NH_4^+-β-12.5-V-773-1 with no anhydride adsorbed. Also interesting is the fact that undistorted tetrahedral aluminium does not undergo any such chemical shift, indicating that those undistorted tetrahedral aluminium sites which do not convert to octahedral aluminium do not undergo any distortion. Desorption of acetic anhydride at 773

K for 1 h results in complete restoration of both undistorted and slightly distorted framework tetrahedral aluminium, and a concomitant decrease in octahedral aluminium species, which returns to its original value of 4%. In addition, the distorted tetrahedral aluminium atoms which were shifted towards lower ppm values when acetic anhydride was adsorbed, are shifted back towards higher ppm value upon desorption, indicating that the conversion of octahedral aluminium back to tetrahedral symmetry results in less strain of susceptible tetrahedral aluminium atoms. Thus, the process is fully reversible, and the tetrahedral/octahedral transformation can occur quite readily under appropriate conditions. The adsorption of acetic anhydride on NH_4^+-β-12.5-V-773-1 at higher temperature, 398 K, yielded no significant increase in the amount of framework tetrahedral aluminium that was converted to framework octahedral aluminium. The fact that not all the tetrahedral aluminium can be converted to octahedral aluminium is interesting in itself, and may indicate that not all the aluminium atoms in zeolite Beta can accommodate such high coordination states, or indeed, some tetrahedral aluminium may not be accessible. The adsorption of acetic anhydride on Cu-β-12.5-V-773-1 also leads to the formation of a significant amount of octahedral aluminium (34%), and the same shifting of the peak associated with slightly distorted tetrahedral aluminium is observed, but to a lesser extent (37.4 ppm). This would be consistent with the smaller amount of octahedral aluminium formed, and thus, less straining of susceptible tetrahedral aluminium sites when acetic anhydride is adsorbed on Cu-β-12.5-V-773-1. On Na-β-12.5-V-773-1 contacted with acetic anhydride, only limited transformation of framework tetrahedral to octahedral aluminium is observed (14%). In addition, in section **3.1**, Na-β-12.5-V-773-1 exhibited a small infrared absorption band at 3665 cm^{-1}, indicative of extralattice aluminium, thus the octahedral aluminium peak observed may partially originate from dealumination during the exchange process. It is interesting to note that the extent of interaction of acetic anhydride with framework tetrahedral aluminium in NH_4^+-β-12.5-V-773-1, Cu-β-12.5-V-773-1, and Na-β-12.5-V-773-1, and the amount of octahedral aluminium formed, seems to be related to the partial charge of tetrahedral aluminium as calculated in section **3.5**. The change in the partial charge of tetrahedral aluminium with altering the charge compensating action increases in the order, H>Cu>Na, in line with the extent of conversion of framework tetrahedral to octahedral aluminium as probed by ^{27}Al MAS NMR studies. In addition, it has been shown that catalytic activity is related to the charge concentration of tetrahedral aluminium atoms in various samples. Thus the low partial positive charge of the tetrahedral aluminium atoms in Na-β-12.5-V-773-1 results in negligible interaction with acetic anhydride, no octahedral complex is formed, and no activity is observed. On the other hand, when protons are the charge compensating cations, the partial positive charge on the tetrahedral aluminium is high, resulting in a strong interaction with acetic anhydride, an octahedral complex is formed, and catalytic activity is observed. Thus in this proposal, the formation of an octahedral complex as a result of an interaction of acetic anhydride with tetrahedral aluminium is necessary for the acylation to occur. Indeed, a strong interaction of the oxygen atoms of the carbonyl groups of the anhydride with the partial positive charge on the tetrahedral aluminium would lead to polarisation of the anhydride molecule and thus formation of the active electrophilic cation necessary for the acylation reaction to proceed. This theory is expanded upon in section **3.8** where the mechanism of the reaction is explored in detail. The likely octahedral complex formed as a result of interaction of acetic anhydride with tetrahedral aluminium is depicted in **Figure 3.6.3.9**.

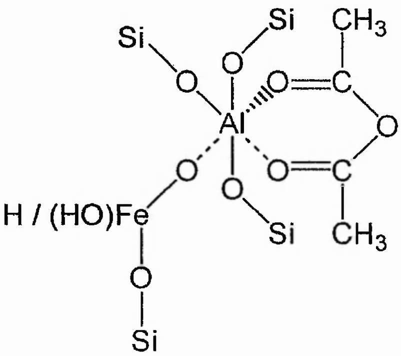

Figure 3.6.3.9 Possible octahedral transition state formed when acetic anhydride interacts with tetrahedral aluminium (zeolite is shown in proton and Fe-exchanged form).

Figure 3.6.3.7 shows the fitted ^{27}Al MAS NMR spectrum of NH_4^+-β-12.5-V-773-1 with anisole adsorbed at 333 K. The adsorption of anisole onto NH_4^+-β-12.5-V-773-1 seems to have little impact on the coordination environment of aluminium in the zeolite lattice, and the percentage of undistorted tetrahedral, slightly distorted tetrahedral, and octahedral aluminium is similar to that observed in the sample NH_4^+-β-12.5-V-773-1 with nothing adsorbed, and there is no shift in the position of the band indicative of slightly distorted aluminium. In contrast, **Figure 3.6.3.8** shows the fitted ^{27}Al MAS NMR spectrum of NH_4^+-β-12.5-V-773-1 with p-MAP adsorbed at 333 K. In this case, the adsorption of p-MAP onto NH_4^+-β-12.5-V-773-1 has a dramatic impact on the coordination environment of aluminium in the lattice, where a significant decrease in the amount of undistorted, and slightly distorted tetrahedral aluminium is observed along with a concomitant increase in the amount of framework octahedral aluminium. The octahedral peak formed is very broad and this would suggest an octahedral aluminium species of highly distorted symmetry. This octahedral peak accounts for 70% of the total amount of aluminium in the framework, which would suggest a strong interaction of p-MAP with framework tetrahedral aluminium, which may be expected due to its high polarity [13-15]. In addition to a significant decrease in the amount of slightly distorted tetrahedral aluminium upon p-MAP adsorption, the position of the peak associated with slightly distorted tetrahedral aluminium shifts to 32 ppm indicating increased distortion of these sites when octahedral aluminium is formed, and as observed with samples with acetic anhydride adsorbed, the position of the peak indicative of undistorted tetrahedral aluminium remains unaffected.

CONCLUSION

Adsorption of acetic anhydride onto the proton and Cu-forms of zeolite Beta leads to the reversible transformation of framework tetrahedral aluminium to framework octahedral aluminium. Only limited transformation was observed on the inactive Na-Beta. It is proposed that the partial positive charge on tetrahedral aluminium determines the extent of interaction with acetic anhydride, and thus the extent of formation of an octahedral complex. The latter species is thought to determine the catalytic activity, since the anhydride molecule becomes polarised when the octahedral complex is formed, this forms the active electrophilic cation. The adsorption of anisole was found to have little impact on the coordination environment of aluminium in zeolite Beta, however adsorption of p-MAP led to the transformation of a significant amount of framework tetrahedral aluminium into framework octahedral aluminium, even more pronounced than in samples with acetic anhydride adsorbed. This high degree of interaction of p-MAP with framework tetrahedral aluminium may be linked to the deactivation of zeolite Beta in the acylation of anisole with acetic anhydride, especially if it hinders the adsorption of acetic anhydride onto framework tetrahedral aluminium.

REFERENCES

(1) Derouane, E. G.; He, H.; Derouane-Abd Hamid, S. B.; Ivanova, I. I. *Catal. Lett.* 1999, ***58***, 1.

(2) Haouas, M.; Kogelbauer, A.; Prins, R. *Catal. Lett.* 2000, ***70***, 61.

(3) Hunger, M.; Horvath, T. *Catal. Lett.* 1997, ***49***, 95.

(4) Bourgeat-Lami, E.; Massiani, P.; Di Renzo, F.; Espiau, P.; Fajula, F.; Courieres, T. D. *Appl. Catal.* 1991, ***72***, 139.

(5) van Bokhoven, J. A.; Koningsberger, D. C.; Kunkeler, P. J.; van Bekkum, H.; Kentgens, A. P. M. *J. Am. Chem. Soc.* 2000, ***122***, 12842.

(6) Kunkeler, P. J.; Zuurdeeg, B. J.; van der Waal, J. C.; van Bokhoven, J. A.; Koningsberger, D. C.; van Bekkum, H. *J. Catal.* 1998, ***180***, 234.

(7) Kiricsi, I.; Flego, C.; Pazzuconi, G.; Parker, W. O.; Millini, R.; Perego, C.; Bellussi, G. *J. Phys. Chem.* 1994, ***98***, 4627.

(8) Trombetta, M.; Busca, G.; Storaro, L.; Lenarda, M.; Casagrande, M.; Zambon, A. *Phys.Chem.Chem.Phys.* 2000, ***2***, 3529.

(9) Zhidomirov, G. M.; Kazansky, V. B. *Adv. Catal.* 1986, ***34***, 131.

(10) Jia, C.; Massiani, P.; Barthomeuf, D. *J. Chem. Soc. Faraday Trans.* 1993, ***89***, 3659.

(11) Kuehl, G. H.; Timken, H. K. C. *Microporous Mater.* 2000, ***35-36***, 521.

(12) Müller, M.; Harvey, G.; Prins, R. *Microporous Mater.* 2000, ***34***, 281.

(13) Rohan, D.; Canaff, C.; Fromentin, E.; Guisnet, M. *J. Catal.* 1998, ***177***, 296.

(14) Derouane, E. G.; Dillon, C. J.; Bethell, D.; Derouane-Abd Hamid, S. B. *J. Catal.* 1999, ***187***, 209.

(15) Derouane, E. G.; Crehan, G.; Dillon, C. J.; Bethell, D.; He, H.; Derouane-Abd Hamid, S. B. *J. Catal.* 2000, ***194***, 410.

Chapter 3. Results

3.7 Deactivation of zeolite Beta in the aromatic acylation of anisole with acetic anhydride

3.7.1 Abstract

In section **3.1.5** it was found that multiple cycle regeneration of spent zeolite H-beta resulted in dealumination of the zeolite framework, and catalytic data in section **3.3** showed that the lower catalytic activity of regenerated Zeolite H-Beta was due to its reduced aluminium content. In addition, the catalytic activity of Spent-NH_4^+-β-12.5-A-773-1, which was not subject to oxidative regeneration exhibited particularly poor catalytic activity, indicating the inhibiting effect of coke on the reaction. This section deals with the identification of coke species on zeolite H-Beta, in particular, it explores the possibility of deactivation due to the strong adsorption of either reactants and/or products at the catalytically active sites.

3.7.2 Background

It is clear that zeolites present many advantages over classical Friedel Crafts catalysts such as $AlCl_3$, however they are not without their drawbacks. One of the major problems to be solved in the use of zeolites in the synthesis of organic compounds is their deactivation by deposition of heavy reaction products within the pores or on the outer surface of the crystallites. Such factors can have a detrimental affect on catalytic activity, and unfortunately, deactivation seems to be inevitable when applying zeolites in organic reactions. The problem is highlighted in the catalytic cracking process. Silica-alumina gels served as the main catalytic cracking catalysts until they were supplanted by zeolites in the mid 1960's. Nowadays, cracking in industrial practice is carried out with mainly faujasite type zeolites (typically H^+, Re^{3+}, and La^{3+}-Y). Despite their superiority over silica-alumina gels, in addition to the desired catalytic conversion of reactant paraffin and other components of gas oil into smaller paraffins and olefins, many side reactions also occur. Important side reactions are isomerisation, disproportionation, and the formation of high-molecular weight products called coke. Solid deposits of coke accumulate in the catalyst; the deposits clog the pores and cover the catalytically active sites. Coke is a catalyst poison, and its formation is extremely fast under conditions of industrial cracking of gas oil. The catalyst is therefore deactivated rapidly in an industrial reactor, and it is separated from the oil after only about 3 seconds of contact and is sent to a separate reactor (a regenerator), where the coke is burned off with air. After which the catalyst returns back to the main reactor to be mixed with gas oil (and some steam to disperse and rehydroxylate the zeolite). As the catalyst structure is slowly degraded in the process, catalyst is continually removed and replaced with fresh particles. This example highlights the major drawback in the use of zeolite catalysts in organic reactions. In most industrial processes that utilise zeolites as catalysts, regeneration in air is usually sufficient to restore catalytic activity. However, reactions in which catalytic activity is governed by Al concentration may exhibit lower catalytic activity after progressive regenerations, since dealumination and loss of crystallinity are known to occur after regeneration cycles. The use of zeolite Beta in the acylation of anisole with acetic anhydride is no exception to this dealumination affect, and many studies have been devoted to the understanding of the origin of deactivation in this reaction [1-3]. Rohan *et al.*, [1] made an extensive study of the deactivation of zeolite H-Beta in the acylation of anisole with acetic anhydride. The authors suggested that the p-methoxyacetophenone (P-MAP) that is selectively and rapidly formed on the fresh catalyst inhibits its own production. Catalyst samples were recovered after various times and the organic material that was retained on the zeolite was analysed by GC and GC-MS. The major part of this material consisted of P-MAP, and was recovered by soxhlet extraction in methylene chloride. The minor part consisted of di- and tri-acetylated anisole entrapped in the zeolite micropores, and could only be recovered after dissolution of the zeolite in a hydrofluoric acid solution. These species were shown to cause pore blockage, and were considered to be responsible for part of the catalyst deactivation, the other part being due to P-MAP located in the mesopores. These workers concluded that use of an excess of anisole enhanced catalyst stability since it limits both the retention of P-MAP and the formation of poly-acetylated anisoles. For the same reaction, Freese *et al.*, [2] reported that two types of coke (extractable and non-extractable) were responsible for the deactivation of the catalyst, however the nature of the coke was not identified. A study by Derouane *et al.*, [3], also for the same reaction found, in agreement with Rohan *et al.*, [1] that P-MAP was most likely responsible for part of the catalyst deactivation, the other part being due to acetic acid, which was shown to cause partial dealumination of the zeolite framework at long retention times. Such dealumination was shown to be irreversible. However, contrary to the proposal of Rohan *et al.*, these workers concluded that P-MAP was retained in the micropores and not the mesopores of the catalyst and that obstruction of the micropores by larger molecules resulting from multiple acetylation was unlikely. Product inhibition by P-MAP was suggested to occur because the equilibrium constant for the adsorption of P-MAP in the micropores of the H-Beta catalyst was calculated to be much larger than that of the reactants, acetic anhydride and anisole. It was thus concluded that catalyst deactivation as conversion increases was mainly due to product inhibition, i.e. the competitive adsorption of the reactants and products in the zeolite intracrystalline volume.

3.7.3 Determination of the nature of coke species on spent zeolite Beta

In order to determine the nature of coke species deposited on spent zeolite Beta, the best performing zeolite Beta sample, NH_4^+-β-12.5-A-773-1, was subject to the standard reaction conditions, filtered, left to dry at room temperature, and then analysed by FTIR spectroscopy. **Figure 3.7.3.1** shows the FTIR spectra of

Spent-NH_4^+-β-12.5-A-773-1 prior to and after evacuation in the FTIR cell at room temperature, after activation to 823 K for 1 h under vacuum, and after oxidative regeneration in air at 823 K overnight. The major absorptions are numbered, and assigned in **Table 3.7.3.1**.

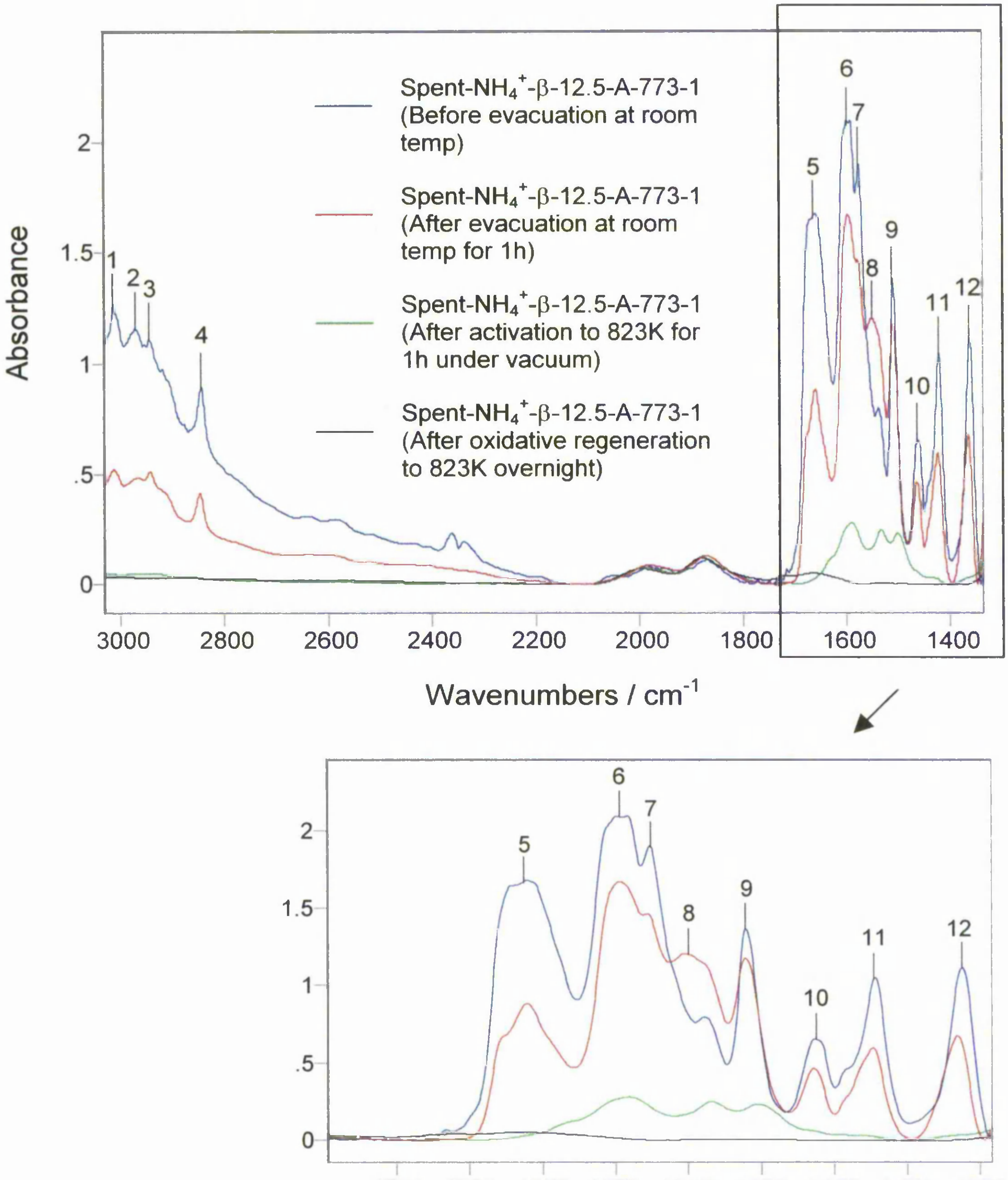

Figure 3.7.3.1 FTIR spectra of coke on Spent-NH_4^+-β-12.5-A-773-1, and peak markings showing the major absorption bands.

Peak number	Position / cm^{-1}	Assignment
1	3010	Aryl-H
2	2970	O-H stretching
3	2944	O-H stretching
4	2845	Aryl-O-CH_3 (Ether)
5	1663	Aryl-C=O (Ketone)
6	1595	Benzene ring
7	1578	Benzene ring
8	1550	Benzene ring
9	1510	Benzene ring
10	1462	O-H bending
11	1424	O-H bending
12	1362	-CH_3 symmetrical deformation

Table 3.7.3.1 Assignment of coke absorption IR bands.

In order to determine the relative amount of reactant and product adsorbed onto NH_4^+-β-12.5-A-773-1 at the standard reaction temperature of 333 K, and to determine the strength of interaction with the zeolite, a series of experiments were carried out where each of the reactants and products were adsorbed on to the zeolite and monitored by FTIR spectroscopy. After adsorption, and subsequent evacuation to remove physisorbed species, Temperature Programmed Desorption was carried out. In addition to NH_4^+-β-12.5-A-773-1, Na-β-12.5-A-773-1 was also subject to the same set of experiments in order to compare the best performing zeolite Beta sample with one which showed no activity at all. The fitted TPD curves are shown in **Figure 3.7.3.2** and **Figure 3.7.3.3** for desorption of reactants and products from NH_4^+-β-12.5-A-773-1 and Na-β-12.5-A-773-1 respectively.

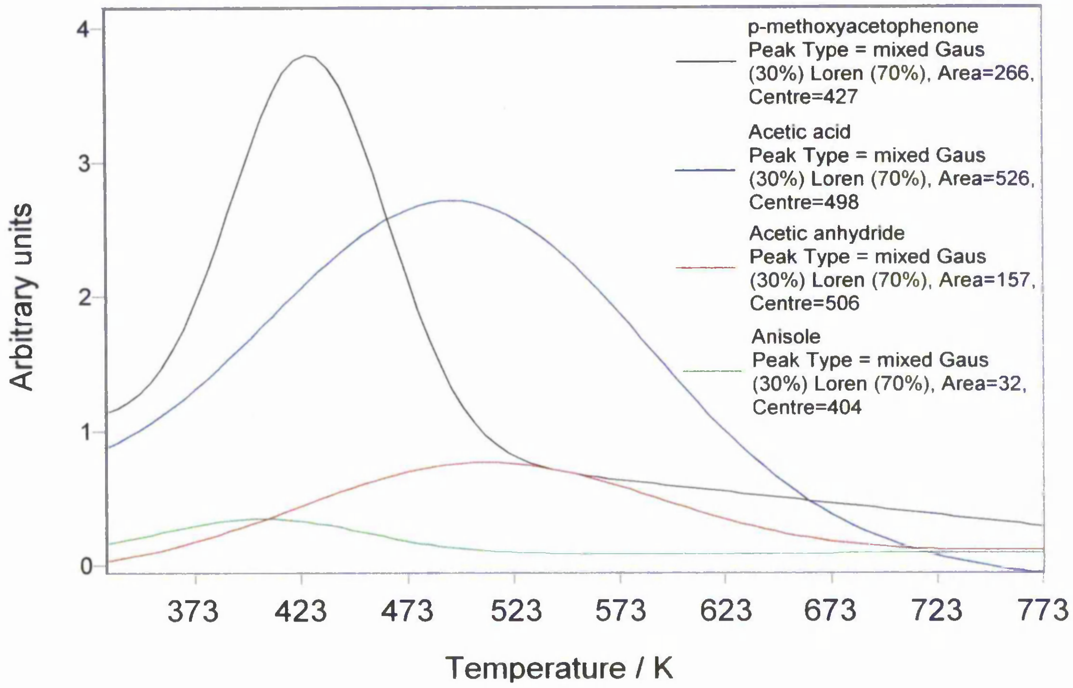

Figure 3.7.3.2 TPD trace of anisole (1414-1536 cm^{-1}), acetic anhydride (1713-1794 cm^{-1}), p-MAP (1475-1721 cm^{-1}), and acetic acid (1526-1818 cm^{-1}) for NH_4^+-β-12.5-A-773-1.

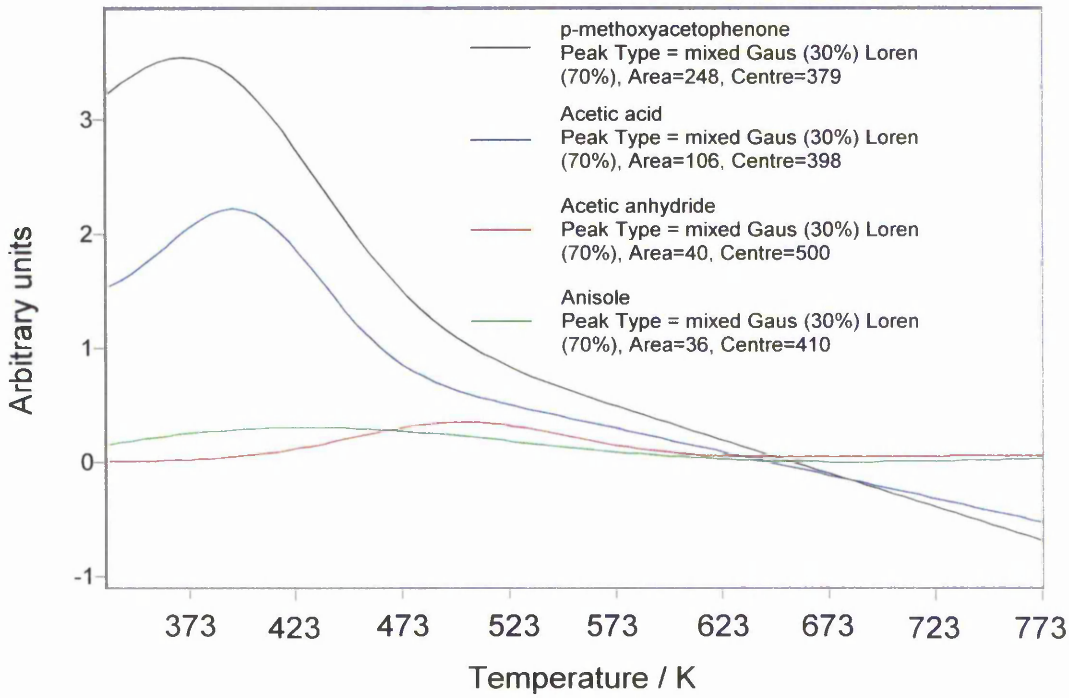

Figure 3.7.3.3 TPD trace of anisole (1414-1536 cm^{-1}), acetic anhydride (1713-1794 cm^{-1}), p-MAP (1475-1721 cm^{-1}), and acetic acid (1526-1818 cm^{-1}) for Na-β-12.5-A-773-1.

3.7.4 The effect on the catalytic activity of adding p-MAP to the initial reaction mixture

If it is assumed that p-methoxyacetophenone is the major contributor to the deactivation of zeolite H-Beta, then adding this molecule to the initial reaction mixture should lead to decreased catalytic activity. **Figure 3.7.4.1** and **Figure 3.7.4.2** show the percentage yield and initial rate of reaction, respectively, with and without the addition of p-MAP to the reaction mixture for the acylation of anisole with acetic anhydride over NH_4^+-β-12.5-A-773-1 under standard reaction conditions. The catalytic activity of Spent-NH_4^+-β-12.5-A-773-1 is also included.

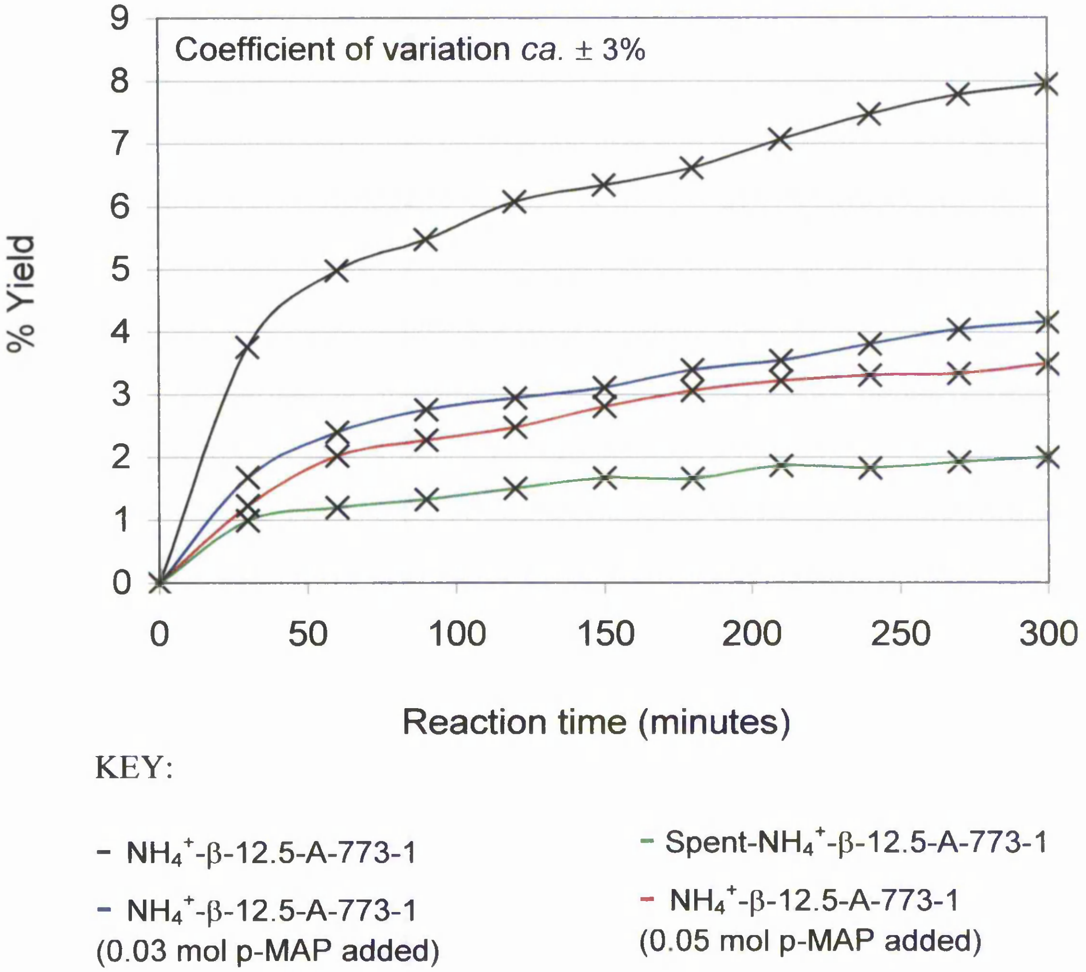

Figure 3.7.4.1 Plot of yield of p-MAP versus reaction time after addition of 0.03 and 0.05 mol of p-MAP to the initial reaction mixture.

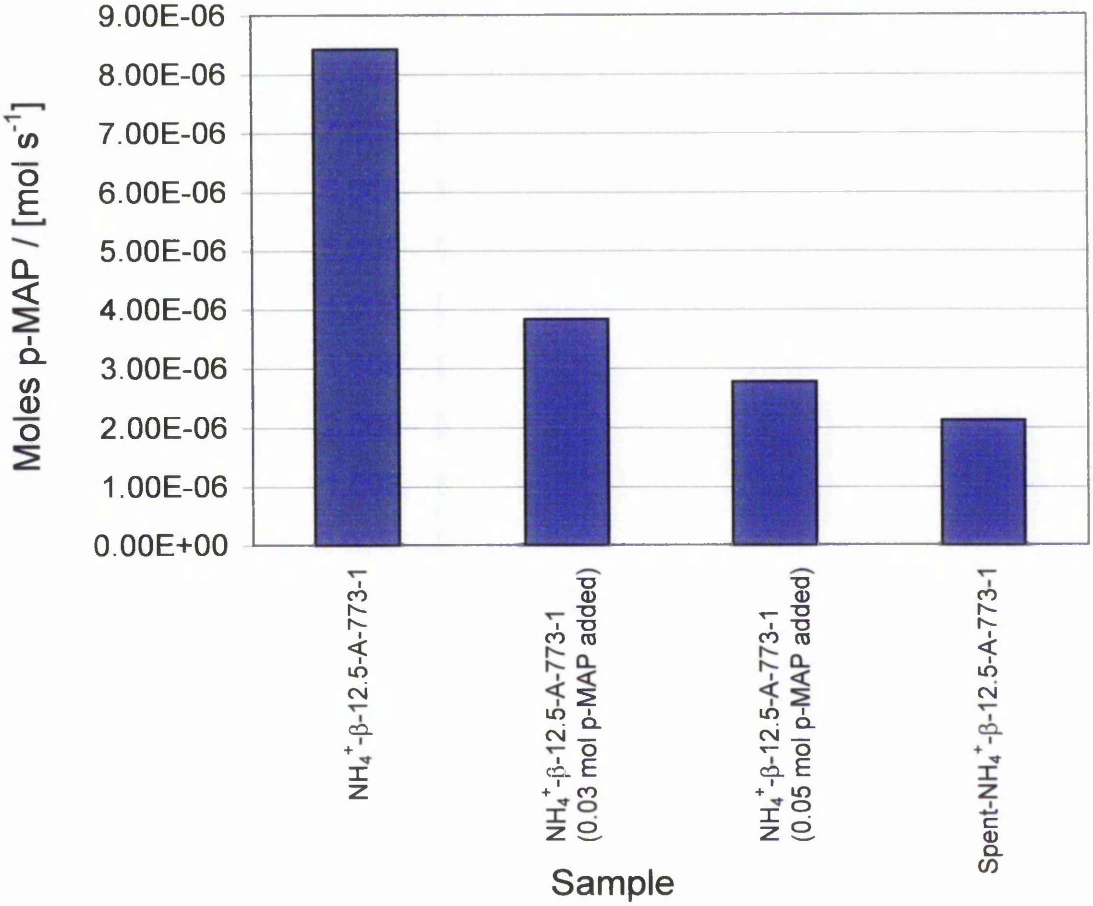

Figure 3.7.4.2 Comparison of initial rates of reaction after addition of 0.03 and 0.05 mol p-MAP.

Sample	Initial rate (mol s^{-1}) ± 3%*
NH_4^+-β-12.5-A-773-1	8.43E-06
NH_4^+-β-12.5-A-773-1 (0.03 mol p-MAP added)	3.84E-06
NH_4^+-β-12.5-A-773-1 (0.05 mol p-MAP added)	2.78E-06
Spent-NH_4^+-β-12.5-A-773-1	2.12E-06

* Approximate experimental error expressed as the coefficient of variation.

Table 3.7.4.1 Initial rates of reaction after addition of 0.03 and 0.05 mol p-MAP.

3.7.5 Soxhlet extraction with methylene chloride

Spent-NH_4^+-β-12.5-A-773-1 was subject to Soxhlet extraction with methylene chloride to reflux temperature for 24 h, and the resulting solution analysed by GC. **Figure 3.7.5.1** shows the GC trace obtained, and the retention times are assigned in **Table 3.7.5.1**.

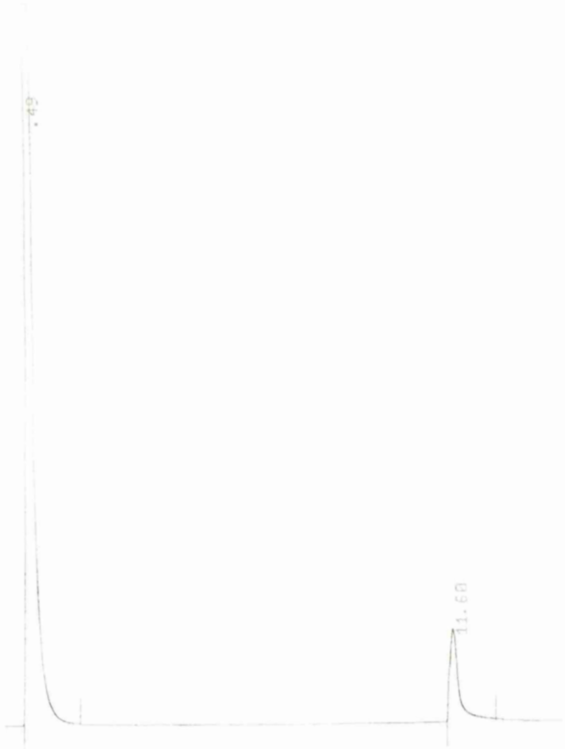

Figure 3.7.4.2 GC trace obtained after Soxhlet extraction of Spent-NH_4^+-β-12.5-A-773-1 with methylene chloride.

Retention time / mins	Assignment
0.49	Methylene chloride
11.60	p-methoxyacetophenone

Table 3.7.5.1 Assignment of GC peaks.

DISCUSSION

Before discussing the main findings of this section, it is interesting to point out the change in the catalyst colour from white to pale yellow, to brown, to dark brown as the reaction proceeds. Other workers have also commented on this [1-3]. Freese *et al.*, [2] suggested that the colour change, from white to dark brown, was an indication of coking. Interestingly, Derouane *et al.*, [4] observed that the colour of zeolite H-Beta becomes yellow-brown when the catalyst is contacted with acetic anhydride, even in the absence of any aromatic substrate, and that this colourisation disappears upon addition of water. These workers concluded that some reaction occurs between zeolite Beta and the acylating agent, and that the species formed is destroyed by water, although no identification of the species was attempted. It would seem plausible to accept both of these theories, in the first instance, the change in catalyst colour from white to pale yellow, may, as suggested by Derouane *et al.*, [4], be due to some species formed between zeolite H-Beta and the acylating agent, however, the further change in colour to brown, and later in the reaction, dark brown, would be more an indication of coking as the reaction proceeds.

Figure 3.7.3.1 shows the FTIR spectra of coke species deposited on Spent-NH_4^+-β-12.5-A-773-1, and the assignment of the absorption bands is given in **Table 3.7.3.1**. It can be seen that significant coking of the catalyst has taken place during the reaction. Spent-NH_4^+-β-12.5-A-773-1 (before evacuation at room temp) exhibits the largest amount of coke, some of which is removed after evacuation to 10^{-6} mbar at room temp, indicating that some physisorbed species may have been present. After activation to 823 K under vacuum (10^{-6} mbar), a significant proportion of coke is removed, however traces of coke are still present from the FTIR spectra, and in addition, the catalyst still exhibited a brown colour after this treatment. Oxidative regeneration to 823 K overnight resulted in complete removal of coke from zeolite H-Beta, and the catalyst was restored to its original white colour following this procedure. Assignment of the bands in the FTIR spectra of Spent-NH_4^+-β-12.5-A-773-1 samples indicates the presence of methoxyacetophenone and acetic acid. Intense bands are observed at 1595, 1578, and 1510 cm^{-1}, which are indicative of a benzene ring system [5]. In addition, the band at 3010 cm^{-1} would indicate the presence of aryl-H [5]. The bands at 2845 and 1663 cm^{-1} are due to aryl-O-CH_3 and aryl-C=O respectively [5]. Clearly the presence of all of these bands would be evidence for the presence of methoxyacetophenone on Spent-NH_4^+-β-12.5-A-773-1. The bands at 2970 and 2944 cm^{-1} are indicative of O-H stretching bands, and more specifically carboxylic acids [5], suggesting that the second product of the reaction between anisole and acetic anhydride, namely acetic acid, is also retained on the zeolite to some extent. The band at 1362 cm^{-1} can be assigned to the –CH_3 symmetrical deformation vibration [5] and would also be associated with the acetic acid molecule. No absorption bands are observed between 1740-1790 and 1800-1850 cm^{-1} which would be indicative of acid anhydrides [5], thus acetic anhydride does not seem to be retained in Spent-NH_4^+-β-12.5-A-773-1 to any large degree.

Figure 3.7.3.2 and **Figure 3.7.3.3** show fitted TPD traces for desorption of reactants and products from NH_4^+-β-12.5-A-773-1, and Na-β-12.5-A-773-1, respectively. It can be seen that the relative amount of p-MAP and acetic acid retained on NH_4^+-β-12.5-A-773-1 are much greater than that of acetic anhydride and anisole. Unexpectedly, p-MAP desorbs at lower temperatures (427 K) compared with acetic acid (498 K). Anisole desorbs at approximately 404 K, and acetic anhydride has a maximum desorption peak centred at 506 K, similar to that of acetic acid. Interestingly, for Na-β-12.5-A-773-1, the position of the desorption peak for p-MAP and acetic acid are shifted towards lower temperatures when compared with NH_4^+-β-12.5-A-773-1. In addition, the relative amounts of acetic acid and acetic anhydride retained on Na-β-12.5-A-773-1 are significantly reduced in comparison with NH_4^+-β-12.5-A-773-1. To summarise, both reactants and products are retained to a much lesser extent on Na-β-12.5-A-773-1. In addition, acetic acid and p-MAP are present on both samples to a much greater extent than acetic anhydride and anisole, which would suggest that the majority of the latter two molecules were removed during evacuation prior to the TPD experiment.

Figure 3.7.4.1 and **Figure 3.7.4.2** show the percentage yield to p-MAP, and the initial rate of reaction, respectively, for NH_4^+-β-12.5-A-773-1 under standard reaction conditions, and with the addition of 0.03 and 0.05 mol of p-MAP to the initial reaction mixture. Clearly, adding p-MAP to the initial reaction mixture leads to a significant decrease in both yield and the initial rate of reaction, which is most evident when a higher concentration of p-MAP is added to the initial reaction mixture. The yield and the initial rate are reduced to half of that obtained using the standard reaction mixture. Both Rohan *et al.*, [1] and Derouane *et al.*, [3] observed similar results.

Figure 3.7.5.1 shows the results of Soxhlet extraction on Spent-NH_4^+-β-12.5-A-773-1 with methylene chloride for 24 h. The only molecule present in the extracted solution, with the exception of methylene chloride, was p-MAP. It is important to note that soxhlet extraction would be unable to remove any species that are clogged in the zeolite pores, but according to Derouane *et al.*, [3] obstruction of the micropores by larger molecules resulting from multiple acetylation is unlikely.

Taking into consideration all of the findings in this section, and the finding in section **3.6** that adsorption of p-MAP onto zeolite Beta leads to a significant transformation of framework tetrahedral aluminium (the active site) to octahedral aluminium, it would seem that, in agreement with others [3] [1], p-MAP is the major contributor of catalyst deactivation, despite its unexpectedly low desorption temperature. Due to its high polarity, p-MAP is strongly retained in the zeolite channel system, interacting directly with the catalytically active site, framework tetrahedral aluminium. In addition, the intracrystalline volume of the zeolite is rapidly consumed by p-MAP in the early stages of reaction, thus limiting the access of reactants into the zeolite pores. In addition to p-MAP, acetic acid is also retained on spent zeolite H-Beta samples. It was suggested by Derouane *et al.*, [3] that acetic acid produced in the course of the reaction accumulates in the product mixture when the reaction is performed under batch conditions, resulting in irreversible partial dealumination at long retention times. The same authors also suggested that acetic acid might react with the silanol defects of the zeolite.

CONCLUSION

Results show comprehensively that p-MAP contributes significantly to the deactivation of zeolite H-Beta in the acylation of anisole with acetic anhydride, however not exclusively, acetic acid also seems to be retained on spent zeolite H-Beta samples, and may be associated with some dealumination of the zeolite framework. If acetic acid reacts with the silanol defects in zeolite Beta, TPD results would suggest that this interaction is quite strong. In contrast, it is likely that the highly polar p-MAP interacts with the catalytically active framework tetrahedral aluminium, attracted towards its partial positive charge, and covering the active site.

REFERENCES

(1) Rohan, D.; Canaff, C.; Fromentin, E.; Guisnet, M. *J. Catal.* 1998, ***177***, 296.

(2) Freese, U.; Heinrich, F.; Roessner, F. *Catal. Today* 1999, ***49***, 237.

(3) Derouane, E. G.; Dillon, C. J.; Bethell, D.; Derouane-Abd Hamid, S. B. *J. Catal.* 1999, ***187***, 209.

(4) Derouane, E. G.; Crehan, G.; Dillon, C. J.; Bethell, D.; He, H.; Derouane-Abd Hamid, S. B. *J. Catal.* 2000, ***194***, 410.

(5) Williams, D. H.; Fleming, I. *Spectroscopic Methods in Organic Chemistry*, 5 ed.; McGraw-Hill Education, 1995.

Chapter 3. Results

3.8 Possible mechanism

3.8.1 Abstract

In this section, all the results from previous sections are tied together in order to propose a suitable mechanism for the acylation of anisole with acetic anhydride over zeolite Beta.

3.8.2 Background

As briefly mentioned in the introduction, Friedel Crafts acylation is an electrophilic aromatic substitution. In the broadest sense, electrophilic aromatic substitution involves attack of an electron-deficient species, E^+, on an aromatic, Ar-H to form a larger aromatic product, Ar-E.

Equation 3.8.2.1

$$E^+ + \text{Ar-H} \rightarrow \text{Ar-E} + H^+$$

In this context, the aromatic ring may also be viewed as a nucleophile:

Equation 3.8.2.2

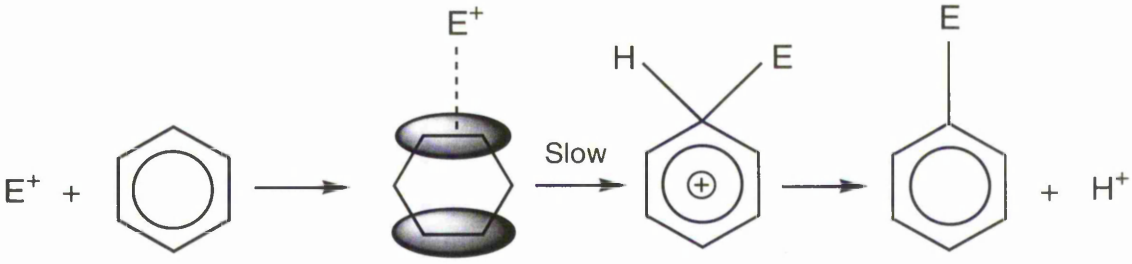

3.8.2.2.a **3.8.2.2.b** **3.8.2.2.c**

In classical organic chemistry, the first phase of this process may sometimes be interaction of the approaching electrophile with the π orbitals of the aromatic to form a π complex (**Equation 3.8.2.2, 3.8.2.2.a**). The next stage involves localised attack of the electrophile on a ring carbon to form a carbocation (**Equation 3.8.2.2, 3.8.2.2.b**), often termed a σ complex, Wheland intermediate, or arenium ion, in which the positive charge is delocalised over the five remaining nuclear carbon atoms, and the H atom and E group are in a plane perpendicular to that of the ring carbocation. The step **3.8.2.2.a** to **3.8.2.2.b** is frequently but by no means always rate-determining, depending upon the nature of the system. C-H bond breakage and expulsion of a proton in the last step complete the substitution process and provide stabilisation by restoration of ring-aromaticity [1]. Electrophiles (E^+) capable of attacking aromatic rings have been generated in zeolite-catalysed systems from precursors varying considerably in size and chemical properties. The electron-deficient species can be generated by diverse mechanisms, e.g. from olefins and carbonyl compounds by protonation, from alkyl halides, alcohols, ethers, aryl halides and anhydrides by C-X or C-O heterolysis, from alkyl aromatics by hydride transfer, and from paraffins via carbocations generated by β-scission, among others. In many situations, the actual rate-determining step may not be the **3.8.2.2.a** to **3.8.2.2.b** stage shown in **Equation 3.8.2.2**, particularly if the operation of these chemical processes within zeolite micropores is impacted by adsorption/diffusion effects [1]. Aromatic ring systems are generally arranged in approximate order of ease of substitution by an electrophile, and tables containing such data can be found in most organic textbooks. In the important set of mono-substituted benzene nuclei, the effects of each group on the relative reactivity of the ring, and on the positional orientation (ortho, meta, para) in a given ring may be explained on the basis of resonance and field effects on the stability of the intermediate arenium ion (**3.8.2.2.b**). In brief, electron-withdrawing groups such as $-NO_2$ will tend to destabilise σ complexes such as **3.8.2.2.b**, while electron donating groups such as $-CH_3$ or $-OH$ will tend to stabilise them. By referring to such data, it is evident that toluene is more reactive than benzene, and anisole, phenol, and aniline are considerably more reactive, while nitrobenzene is highly resistant to attack. The order of reactivity in substituted aromatics can vary with the nature of the electrophile, E^+ [2]. The mechanism of aromatic acylation over zeolite catalysts has been well documented [1], [3-14]. For the acylation of anisole, Corma *et al.*, [11] provide a reasonable argument for operation of an Eley-Rideal type mechanism. A pure Eley-Rideal mechanism corresponds to a process where the reaction proceeds through attack of the acylium ion on the aromatic substrate in the liquid phase, in such a case, first order is observed, whatever the initial substrate concentration. According to Moreau *et al.*, [4] the acylation of veratrole (dimethoxybenzene) in the presence of acidic zeolites occurs via a modified Eley-Rideal type process, where a molecule of acetic anhydride reacts with veratrole in the liquid phase, but in which the veratrole is also adsorbed on the active sites of the catalyst, which acts in a certain way as a poison and leads to an experimentally observed levelling off (zero order). However, in contrast, Derouane *et al.*, [15] suggested that a Langmuir-Hinshelwood model would best describe the kinetics of reaction catalysed by zeolites in the liquid phase as it accounts for the competition of the reactants and products for the intracrystalline volume of the zeolite. In a Langmuir-Hinshelwood process, the acylating agent is adsorbed onto the Brønsted acidic sites of the zeolite, but the aromatic substrate is also adsorbed, competitively, on equivalent Brønsted acid sites on the surface. All of the references sited here do agree on one point, the formation of the active acylating species, the acylium cation, is generated from the acylating agent by an acidic zeolite, most commonly by a protonation process, this species then attacks the aromatic ring resulting in the formation of a Wheland intermediate. The formation of the Wheland intermediate (or Brown σ-complex) is considered to be the rate determining step. C-H bond breakage and the expulsion of a proton complete the exchange process and restores ring aromaticity, the proton released in the breakdown of the Wheland intermediate constitutes to the restoration of the proton-form of the zeolite. Spagnol *et al.*, [8] showed that Brønsted acid sites activate more strongly acetic anhydride than Lewis acid sites; they also showed that Lewis acids exhibit a higher complexation affinity with acylchloride compared with Brønsted acid sites. Similarly, van Bekkum *et al.*, [16] also suggested that Lewis acid catalysts are preferred when applying acid chlorides and Brønsted acid catalysts when using acid anhydrides or carboxylic acids as acylating agents. In the specific case of the aromatic acylation of anisole with acetic anhydride, the generally accepted mechanism seems to involve protonation of the acylating agent and subsequent formation of the acylium cation. **Figure 3.8.2.1** shows such a mechanism.

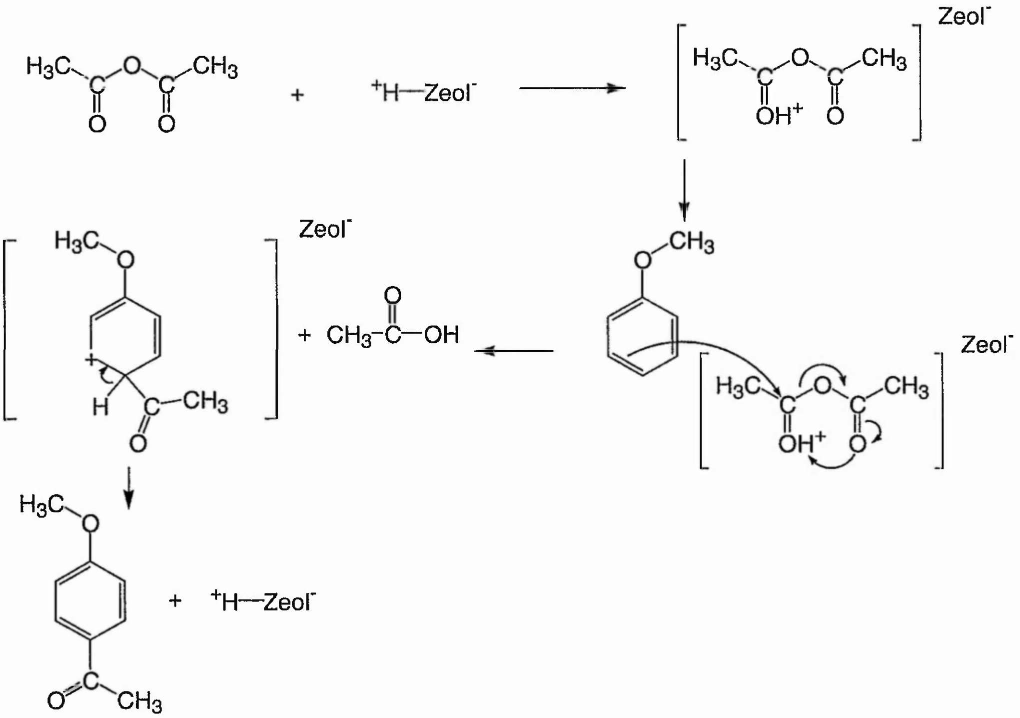

Figure 3.8.2.1 Plausible mechanism for aromatic acylation over an H-form zeolite.

DISCUSSION

In section **3.3**, a clear relationship was found between the relative concentration of Brønsted acid sites and the initial rate of reaction, which would certainly indicate a Brønsted acid catalysed process, and thus be in agreement with the generally accepted mechanism. Such a relationship would be in agreement with the findings of Derouane *et al.*, [15] who observed that the activity of zeolite H-Beta is dependent on the concentration of aluminium atoms, and thus Brønsted sites. However, also in section **3.3**, it was found that there was no relationship between the relative Brønsted acid site concentration and the initial rate of reaction for transition metal exchanged zeolites. In fact, despite having very low numbers of Brønsted sites, these materials exhibited significant initial rates of reaction when compared with the best performing H-form Beta. This finding casts some doubt on a mechanism involving protonation. Section **3.5** described in some detail the role of tetrahedral aluminium in aromatic acylation over zeolites. It was found that by calculating the 'charge concentration' of aluminium in different zeolite Beta samples, and plotting this value against the initial rate of reaction led to a very reasonable linear relationship. Before proposing a suitable mechanism for the aromatic acylation of anisole with acetic anhydride over zeolite Beta, it is important to note a few significant points. The first of which was discussed in section **3.5**, namely the clear relationship between the 'charge concentration' of aluminium and the initial rate of reaction. The second point, described in section **3.6**, is the reversible conversion of framework tetrahedral aluminium to framework octahedral aluminium upon adsorption of the acylating agent (acetic anhydride). This phenomenon occurred in both the copper and proton forms of zeolite Beta, whereas only limited transformation was observed with Na-Beta. The third point concerns the catalytic data regarding MCM-41 samples described in section **3.3**. It was found that aluminium must be present for the acylation reaction to proceed. Under the conditions employed in this study, Fe-MCM-41 and purely siliceous MCM-41 did not show any activity, although the iron site in the former is expected to act as a Lewis site. However, both Al-

MCM-41 and aluminium containing Fe-MCM-41 exhibited some activity. Additionally, increasing the concentration of aluminium in Al-MCM-41 led to an increase in activity. The fourth and final point is that no clear dependency of the activity from the acid strength can be observed for the acylation reaction. Although the different zeolites studied exhibit significantly different acid strength, over zeolite Beta yields of p-MAP are an order of magnitude higher than over the other frameworks. MCM-41 is generally considered to have sites of lower acidic strength than the zeolites [17], while ZSM-5 and mordenite are expected to exhibit higher acidic strength than zeolite Beta. The explanation for the increased activity over zeolite Beta could very likely be due to its unusual amount of framework 'flexibility', which has been remarked upon in numerous papers [12], [18-21]. This 'flexibility' would allow zeolite Beta to accommodate higher coordination environments more easily, facilitating the formation of an octahedral complex with the acylating agent. This explanation would certainly account for the much higher activities observed over zeolite Beta materials. Taking into account all of these points, and others discussed throughout the investigation, it is proposed that tetrahedral aluminium acts as a Lewis acceptor site, attracting the acylating agent (acetic anhydride) and forming an octahedral complex, in which the electrons on the oxygen atoms of the carbonyl groups of the anhydride are attracted towards the partial positive charge on the Al atom (the Lewis acceptor), this polarises the anhydride molecule, producing a positive charge on one of the carbon atoms, thus producing the electrophilic cation intermediate. The nucleophilic attack of the aromatic (anisole) on the stabilised electrophilic cation forms the Wheland type intermediate. A concerted decomposition of the intermediate to acetic acid and p-MAP completes the process. Such a process as described would be consistent with an Eley-Rideal type mechanism whereby an adsorbed molecule of anhydride reacts with a molecule of anisole impinging from the liquid phase. The universally found very high selectivity to the para-product over zeolites is also supported by such a mechanism, since steric hindrance would favour the formation of the para isomer, in addition to thermodynamic preference. In the present study, the selectivity to the para isomer was > 99% in all cases. The series of events is summarised in **Figure 3.8.2.2** and **Figure 3.8.2.3** for the proton form of zeolite Beta, and in **Figure 3.8.2.4** for transition metal exchanged forms. In the mechanism involving the proton from of zeolite Beta, two feasible mechanisms are possible. In the first of these mechanisms, depicted in **Figure 3.8.2.2**, the proton is merely a spectator in the reaction, although it is crucial in that it bestows the partial positive charge on the aluminium atom allowing it to attract the anhydride molecule, but it is not directly involved in the reaction. In this mechanism, the acetate ion formed when the aromatic substrate (anisole) attacks the stabilised electrophilic cation reacts with the proton given off by the Wheland intermediate to produce acetic acid. In the second mechanism, depicted in **Figure 3.8.2.3**, the acetate ion formed reacts immediately with the proton of the Brønsted acid site to form acetic acid, and the proton given off by the Wheland intermediate interacts with the negatively charged aluminium atom of the zeolite lattice, restoring the Brønsted acid site.

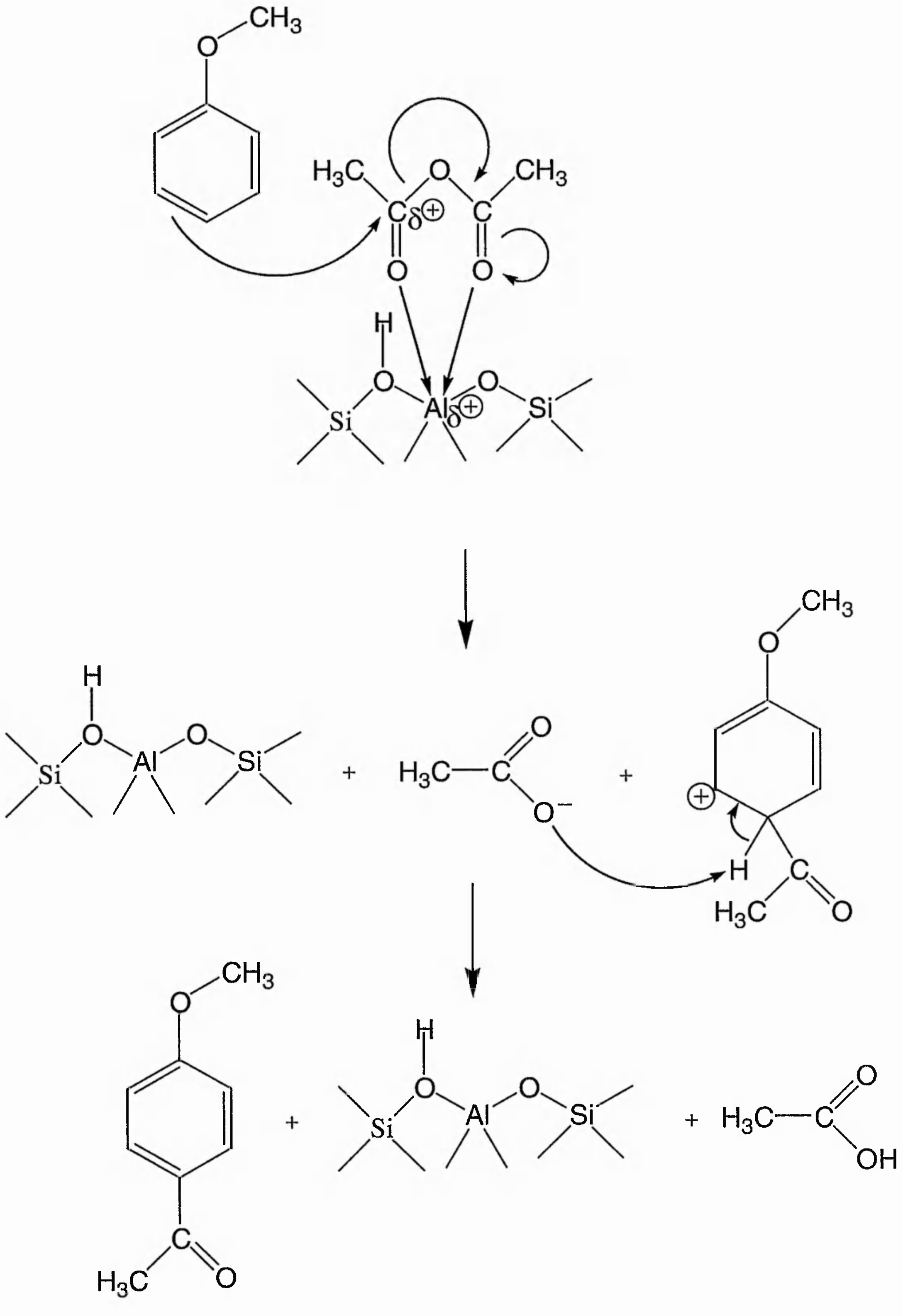

Figure 3.8.2.2 Plausible mechanism for aromatic acylation over an H-form zeolite.

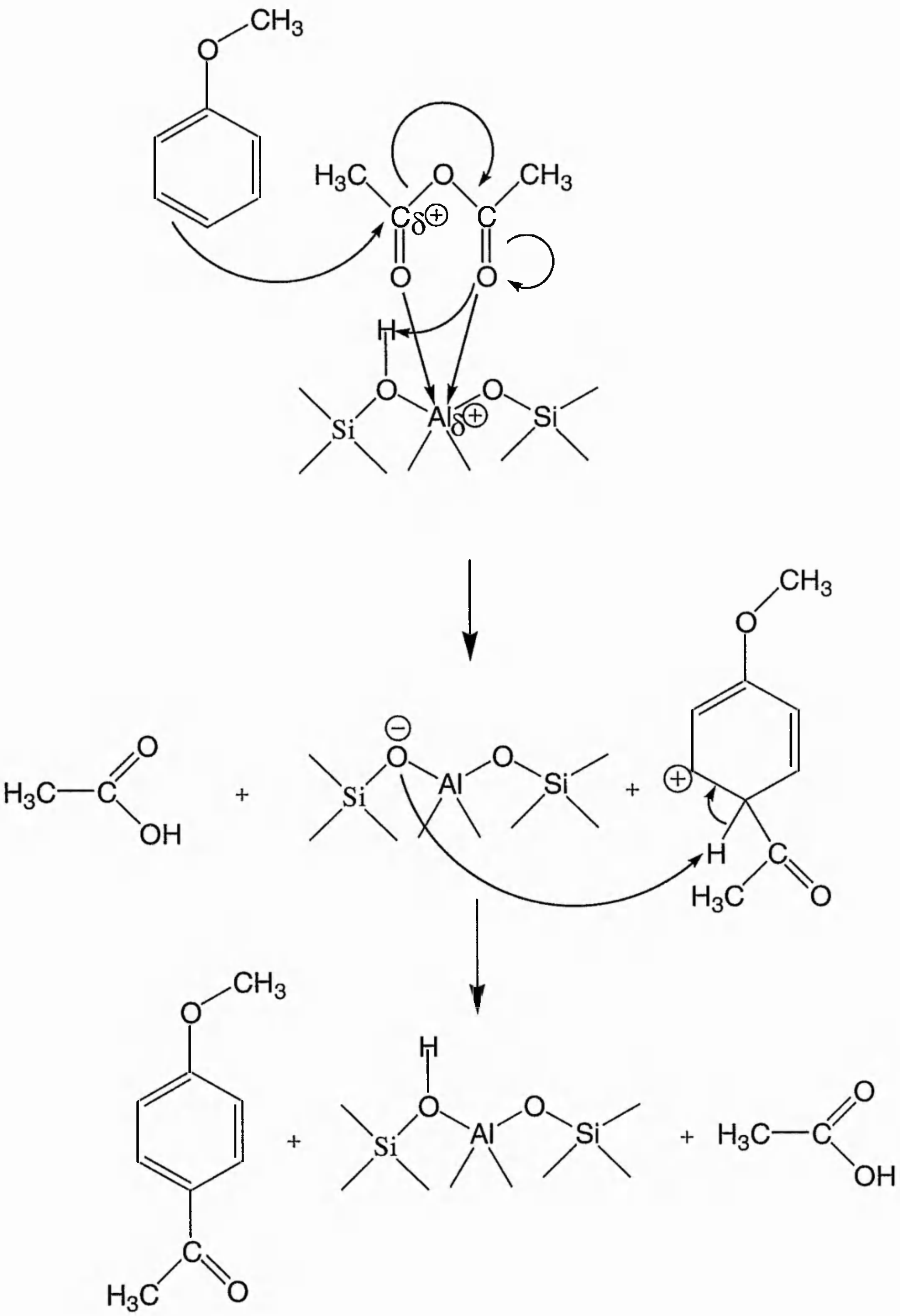

Figure 3.8.2.3 Plausible mechanism for aromatic acylation over an H-form zeolite.

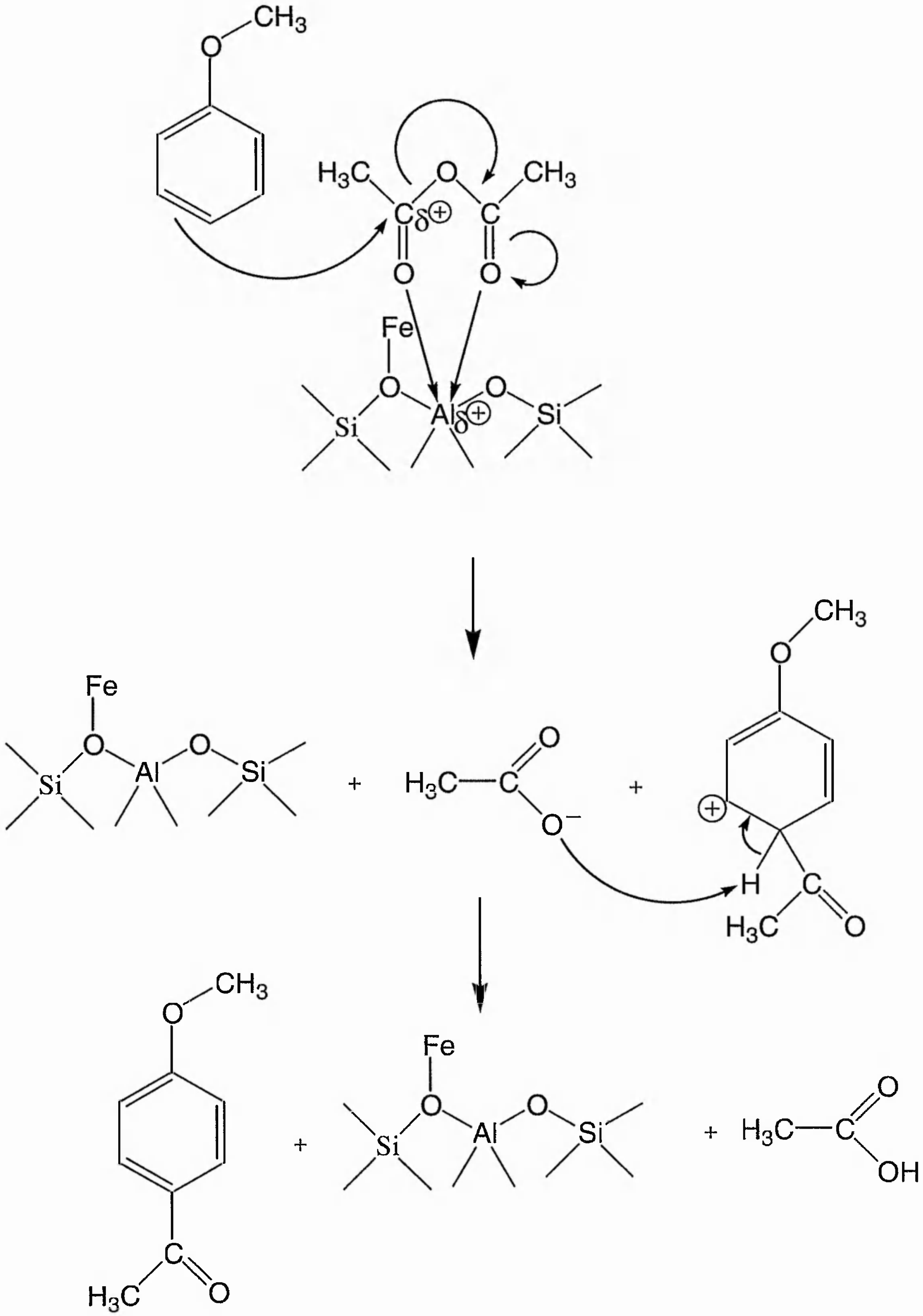

Figure 3.8.2.4 Plausible mechanism for aromatic acylation over Fe Beta.

It is the first time that such a mechanism has been proposed, with the exception of Haouas *et al.*, [12] who observed the reversible transformation of framework aluminium from a tetrahedral into an octahedral environment upon interaction with nitric acid. This octahedral complex was suggested to play a key role in the nitration of toluene. More recently, van Bokhoven *et al.*, [22] in a study of the interaction of aromatic molecules with the acid sites in zeolite Beta proposed that the acceptor site might be the Al atom. The authors suggested that the benzene molecule interacts with the tetrahedral aluminium via overlap of the diffuse 3p orbitals on the Al with the π^* molecular orbital on the benzene molecule.

It is also important to reiterate at this stage a finding from section **3.3**, it was proposed that two types of active site may be involved in aromatic acylation over zeolites, one which is highly active and accounts for the majority of the catalysts activity, but which deactivates rapidly. This site is proposed to be tetrahedral aluminium as discussed above. However the catalytic data presented in **3.3** would suggest the possibility of a second type of active site, which is far less active, but less susceptible to deactivation, and accounts for the gradual increase in product yield over longer periods of time. If this were indeed the case, then two mechanisms would be required to account for the two types of active site. However, the catalytic activity of this site is negligible, and its nature was not identified during this investigation, so further studies would be required to prove its existence and elucidate its nature.

CONCLUSION

A mechanism that takes into account all of the observations and findings in previous results sections is proposed. In essence, the mechanism is of the Eley-Rideal form, where an adsorbed molecule of acetic anhydride reacts with an anisole molecule impinging from the liquid phase. Eley-Rideal mechanisms are frequently observed in catalysis by solid acids, although the proposed mechanism in the present study differs from that of other authors. The major difference being the absence of protonation to form the electrophilic cation, instead, the electrophilic cation is formed by interaction of the acylating agent with tetrahedral framework aluminium, which acts as a Lewis acceptor, forming an octahedral framework complex which polarises the anhydride molecule, forming the electrophilic cation intermediate. The formation of the Wheland intermediate is most likely to be the rate-determining step. Such a mechanism as described would account for the catalytic activity of both proton and transition metal forms of zeolite Beta, with the catalytic activity been primarily determined by both the concentration and the partial positive charge of tetrahedral aluminium atoms in the sample.

REFERENCES

(1) Venuto, P. B. *Microporous Mater.* 1994, ***2***, 297.

(2) Sykes, P. *A guidebook to Mechanism in Organic Chemistry*; John Wiley and Sons: New York, 1986.

(3) Ma, Y.; Wang, Q. L.; Jiang, W.; Zuo, B. *Appl. Catal. : A* 1997, ***165***, 199.

(4) Moreau, P.; Finiels, A.; Meric, P. *J. Mol. Catal. : A* 2000, ***154***, 185.

(5) Bhattacharya, D.; Sharma, S.; Singh, A. P. *Appl. Catal. : A* 1997, ***150***, 53.

(6) Jacob, B.; Sugunan, S.; Singh, A. P. *J. Mol. Catal. : A* 1999, ***139***, 43.

(7) Pandey, A. K.; Singh, A. P. *Catal. Lett.* 1997, ***44***, 129.

(8) Spagnol, M.; Gilbert, L.; Alby, D. *Ind. Chem. Lib* 1996, ***8***, 29.

(9) Chiche, B.; Finiels, A.; Gauthier, C.; Geneste, P. *Appl. Catal.* 1987, 365.

(10) De Castro, C.; Primo, J.; Corma, A. *J. Mol. Catal. : A* 1998, ***134***, 215.

(11) Corma, A.; Climent, M. J.; García, H.; Primo, J. *Appl. Catal.* 1989, ***49***, 109.

(12) Haouas, M.; Kogelbauer, A.; Prins, R. *Catal. Lett.* 2000, ***70***, 61.

(13) Corma, A.; Garcia, H. *Catal. Today* 1997, ***38***, 257.

(14) Stockenhuber, M.; Paine, G. S.; Apperley, D. C. *Submitted to J. Catal. 2002*.

(15) Derouane, E. G.; Crehan, G.; Dillon, C. J.; Bethell, D.; He, H.; Derouane-Abd Hamid, S. B. *J. Catal.* 2000, ***194***, 410.

(16) Kouwenhoven, H. W.; van Bekkum, H. *Handbook of Heterogeneous Catalysis*; Ertl, G., Knozinger, H., Weitkamp, J., Eds.; VCH, 1997; Vol. 5; pp 2358.

(17) Meziani, M. J.; Zajac, J.; Jones, D. J.; Partyka, S.; Roziere, J.; Auroux, A. *Langmuir* 2000, ***16***, 2262.

(18) Zhidomirov, G. M.; Kazansky, V. B. *Adv. Catal.* 1986, ***34***, 131.

(19) Kunkeler, P. J.; Zuurdeeg, B. J.; van der Waal, J. C.; van Bokhoven, J. A.; Koningsberger, D. C.; van Bekkum, H. *J. Catal.* 1998, ***180***, 234.

(20) Kiricsi, I.; Flego, C.; Pazzuconi, G.; Parker, W. O.; Millini, R.; Perego, C.; Bellussi, G. *J. Phys. Chem.* 1994, ***98***, 4627.

(21) Jia, C.; Massiani, P.; Barthomeuf, D. *J. Chem. Soc. Faraday Trans.* 1993, ***89***, 3659.

(22) van Bokhoven, J. A.; Koningsberger, D. C.; Ramaker, D. E. *J. Phys. Condens. Matter.* 2001, ***13***, 10383.

Chapter 4. Overall Conclusion

Thermal, hydrothermal, chemical modification, ion exchange, and oxidative regeneration were all found to have a dramatic effect on the acidic properties of zeolite Beta. In the entire range of zeolite Beta samples, catalytic activity was found to be related to the concentration of framework tetrahedral aluminium, and to its partial positive charge. The coordination environment of aluminium in active zeolite Beta samples was found to change from framework tetrahedral to framework octahedral symmetry upon adsorption of the acylating agent (acetic anhydride). Only very limited transformation was observed on the inactive Na-Beta. A mechanism is proposed, whereby a molecule of acetic anhydride interacts with framework tetrahedral aluminium, forming a framework octahedral complex, which polarises the anhydride molecule, forming the active electrophilic cation intermediate. Following an Eley-Rideal type mechanism, a molecule of aromatic substrate (anisole) impinges from the liquid phase, reacting with the polarised anhydride molecule and forming a Wheland type intermediate. The decomposition of the Wheland intermediate to p-MAP and acetic acid completes the process. The desired product, p-MAP, is rapidly and selectively formed on all zeolite Beta samples. The two major products of the reaction, p-MAP and acetic acid were found to be the major contributors to catalyst deactivation. Zeolite Beta was found to be far superior in the acylation of anisole with acetic anhydride compared with ZSM-5, faujasite, mordenite, and the mesoporous MCM-41. Pore size and acidic strength seem to play no significant role in the activity of various materials in this reaction.

Chapter 5. Future Work

It becomes evident from the content of this thesis that zeolite catalysed reactions are extremely complex. Despite the availability and use of highly informative characterisation techniques, there is still considerable debate over the precise mechanism regarding the acylation of aromatic molecules over zeolite catalysts, as well as the nature of the active site. Some of the theories proposed throughout this thesis cast some doubt on currently accepted ideas, particularly regarding the nature of the active site and the mechanism of reaction. As such, it is vitally important that further studies be carried out in order to support these theories. In particular, further ^{27}Al MAS NMR studies probing the extent of acetic anhydride adsorption onto partially and fully exchanged Cu, Na, Li and K exchanged zeolite Beta would be necessary. This, in combination with FTIR and catalytic reaction studies, would provide further evidence regarding the role of tetrahedral aluminium in aromatic acylation. In addition, *in situ* FTIR studies following the reaction through its entirety would provide valuable data regarding the interactions occurring on the zeolite surface. It was proposed in the thesis that two types of active site may be responsible for the catalytic activity of zeolites in aromatic acylation, one of which is highly active, but deactivates rapidly, and accounts for the majority of the catalysts activity. This was identified and proposed to be tetrahedral framework aluminium. The other, which is far less active and is less susceptible to deactivation, seems to play a more prominent role in the latter stages of reaction, and accounted for the long-term activity of the catalyst. This site was not identified and studies to investigate its existence and elucidate its nature would be interesting.